UNIVERSITÄT BONN

Finite density chiral effective field theory in nuclear physics

Dissertation in Physik
von
André Lacour
aus Frechen

HISKP-TH-10-18 **Juli 2010**

Helmholtz-Institut für Strahlen- und Kernphysik

Nußallee 14–16 · D–53115 Bonn · Germany

Finite density chiral effective field theory in nuclear physics

Dissertation

zur

Erlangung des Doktorgrades (Dr. rer. nat.)

der

Mathematisch–Naturwissenschaftlichen Fakultät

der

Rheinischen Friedrich–Wilhelms–Universität

vorgelegt von

André Lacour

aus

Frechen

Bonn Juli 2010

Angefertigt mit Genehmigung der Mathematisch-Naturwissenschaftlichen Fakultät der Rheinischen Friedrich-Wilhelms-Universität Bonn

1. Gutachter: Prof. Dr. U.-G. Meißner
2. Gutachter: Prof. Dr. J. A. Oller

Tag der Promotion: 27. August 2010

Finite density chiral effective field theory in nuclear physics

In the present work, we develop an Effective Field Theory for nuclear matter at zero temperature that is valid up to about twice the nuclear matter saturation density. For that, a novel in-medium power counting will be derived with explicit nucleonic and pionic degrees of freedom coupled to external sources. It allows for a systematic expansion taking into account short- and long-range multi-nucleon interactions, which are mediated by nucleon contact-terms and pion exchanges, respectively. In order to implement the in-medium power counting in actual calculations we develop non-perturbative methods based on Unitary Chiral Perturbation Theory for performing required resummations. Employing our framework, we find that the main trends for symmetric nuclear matter and pure neutron matter are already reproduced at next-to-leading order. In particular, we are able to reproduce the empirical saturation point and the compressibility of nuclear matter, while the energy per nucleon as a function of density agrees with so-called sophisticated many-body calculations from the literature. Interestingly, we also find cancellations of nucleon-nucleon contributions for the in-medium pion self-energy, the in-medium chiral quark condensate and the in-medium pion decay consant. This actually explains the successful applications of previous approaches employing Effective Field Theories.

Chirale Effektive Feld Theorie für endliche Dichte in Kernphysik

In dieser Dissertation erarbeiten wir eine effektive Feldtheorie für Kernmaterie am absoluten Nullpunkt mit Gültigkeit bis ungefähr zur zweifachen Sättigungsdichte derselben. Dafür leiten wir ein neuartiges Zählschema für Rechnungen im Medium her, das auf Nukleonen und Pionen als expliziten Freiheitsgraden sowie deren Kopplung an externe Quellen beruht. Es erlaubt eine systematische Entwicklung unter der Berücksichtigung kurz- und langreichweitiger Wechselwirkungen zwischen Nukleonen, welche durch Kontaktwechselwirkungen und Pionaustäusche vermittelt werden. Um dieses Zählschema in Rechnungen anwenden zu können, entwickeln wir zusätzlich benötigte nicht-störungstheoretische Methoden, beruhend auf unitärer chiraler Störungstheorie, um geforderte Resummierungen durchführen zu können. Mit Hilfe unserer neu erarbeiteten Theorie sind wir in der Lage, tendenziell die Kurvenverläufe von symmetrischer Kernmaterie und reiner Neutronenmaterie schon bei nächstführender Ordnung im Zählschema zu reproduzieren. Insbesondere können wir den empirischen Sättigungspunkt und die Kompressibilität der Kernmaterie reproduzieren, wobei die Energie pro Nukleon als Funktion der Dichte gut mit sogenannten ausgeklügelten Vielteilchenrechnungen aus der Literatur überein stimmt. Interessanterweise finden wir für die Mediumkorrekturen der Pion Selbstenergie, des chiralen Quarkkondensates und der Pion Zerfallskonstante jeweils eine paarweise Aufhebung von derartigen Beiträgen, die der Nukleon-Nukleon Wechselwirkung zugrunde liegen. Dies erklärt, warum bisherige Ansätze, die auch auf effektiven Feldtheorien beruhten, relativ gut Ergebnisse von Beobachtungen reproduzieren können.

Contents

Introduction

Nuclear matter, by definition, refers to an infinite uniform system of nucleons interacting by means of the strong force without electromagnetic interactions. Such a hypothetical system is assumed to approximate conditions in the interior of heavy nuclei. It is also of real physical interest since neutron matter in fact exists in neutron stars. Renewed interest in this problem is fueled by experiments at rare isotope facilities, which open the door to new domains of unstable nuclides that are not all accessible in the lab. One of the long-standing issues in nuclear physics is the calculation of atomic nuclei and nuclear matter properties from microscopic inter-nucleon forces in a systematic and controlled way.

The theoretical models which make prediction on properties of nuclear matter can roughly be devided in the following three classes: Phenomenological *density functionals*, so-called *ab–initio* calculations and *Effective Field Theory* approaches. Phenomenological density functionals are based on effective density-dependent interactions with usually between six and fifteen parameters. Ab initio – or sophisticated many-body – calculations, such as the Brueckner-Hartree-Fock and the Dirac-Brueckner-Hartree-Fock approach, are based on high-precision free space nucleon-nucleon interactions and the nuclear many-body problem is treated macroscopically. Effective Field Theory approaches lead to a systematic expansion in powers of the Fermi momentum ξ_F, respectively in the density ρ_F, with a small number of free parameters. The parameters of these models are typically adjusted to reproduce the properties of normal nuclei or nuclear matter. Therefore extrapolations outside the valley of stable nuclei must be considered with some scepticism. In particular a reliable calculation of nuclear matter should contain as little phenomenological input as possible to allow extrapolation from finite nuclei to nuclear matter without readjustment of the parameters or introduction of new ones. In those approaches relativistic field theories of nuclear phenomena featuring manifest Lorentz covariance are widely used to describe properties of nuclear matter and finite nuclei. Typically nucleons are described as point Dirac-particles moving in by self-consistency generated large isoscalar Lorentz-scalar and Lorentz-vector mean fields [Wa74]. The scalar mean field drives a strong attraction of order 300-400 MeV at nuclear density and an almost equally strong vector mean field drives a repulsion. This is a benchmark characteristic of the so-called Quantum Hadrodynamics [SW86, Se92, SW00, FS00]. As discussed in [Se92], when the empirical low-energy nucleon-nucleon scattering is described in a Lorentz-covariant fashion, it contains strong scalar and four-vector amplitudes [Cl83, MSW83]. Applications are calculated with different degrees of refinement since the $\sigma\omega$ mean-field model of [Wa74], including more vector and scalar fields and additional renormalizable scalar meson self-couplings [Se92] with adjustable parameters.

In the last decades *Effective Field Theory* (EFT) [We79] has been applied to an increasingly wider range of phenomena, for instance in condensed matter, nuclear and particle physics. Effective Field Theories build on a basic physical principle that underlies every low-energy effective model or theory.

A high-energy probe sees details down to scales comparable to the wavelength. Thus, by way of example, an electron scattering at sufficiently high energies reveals the quark structure of nucleons in a nucleus. But at lower energies details are not resolved, so one can replace short-distance structure with something simpler. This means for example that at low energies the interactions of quarks and gluons, the fundamental particles of the strong interaction, can effectively be described by interactions of hadrons. In applying an Effective Field Theory Lagrangian one must confront in a controlled way the behavior of excluded short-distance physics. Quantum mechanics implies that sensitivity to short-distance physics is always present in a low-energy theory, but in a field theory it is made manifest through dependence on a regulator. Removing this regulator dependence requires a well-defined renormalization scheme. An Effective Field Theory is based on a power counting that establishes a hierarchy between the infinite amount of contributions. At a given order in the expansion only a finite amount of them has to be considered, the others are suppressed and constitute higher order contributions. *Chiral Perturbation Theory* (χPT) [GL84, GL85] is understood as the low-energy Effective Field Theory of *Quantum Chromodynamics* (QCD), the theory of strong interactions. χPT is related to QCD in the way that it shares the same symmetries, their breaking and low-energy spectrum. Pions play a unique role in the physics of the strong interactions: QCD is known to undergo a spontaneous breakdown of the $SU(2)_L \otimes SU(2)_R$ chiral symmetry in the limit of massless u and d quarks. In the approach of χPT, the pions are identified as the Goldstone bosons associated with this spontaneous breakdown of chiral symmetry. They finally acquire a finite mass because of the small but non-vanishing masses of the lightest quarks u and d, which explicitly break chiral symmetry. In this manner Chiral Perturbation Theory allows to take pions as degrees of freedom.

Chiral Perturbation Theory can be extended to include also one-nucleon states as degrees of freedom [GSS88, BKM95]. In the multi-nucleon sector things become more involved. The nucleon-nucleon scattering length in the S-wave channel is known to be much larger than the effective interaction range. This fact implies that expanding the scattering amplitude in powers of the momentum is not useful and we have to keep powers of the scattering length times the momentum to all orders. Resumming those orders gives a correct result, but the power counting of individual diagrams is not manifest. As a consequence, individual diagrams diverge in the limit of a large scattering length, even though the sum of all diagrams up to all orders rising from the Lagrangian is finite. For the lightest nuclear systems with two, three and four nucleons [We90, We91], Chiral Effective Field Theory (χEFT) in nuclear systems has been successfully applied [ORK96, Ko99, EGM00, Ep01, EM03, EGM05, Ep06, EHM09]. Nonetheless, still some issues are raised concerning the full consistency of the approach and variations of the power counting have been suggested [KSW98a, KSW98b, FMS00a, FMS00b, BBSK02, PR04, NTK05, EM06, ST08, EG09].

A common technique for heavier nuclei is to employ the chiral nucleon-nucleon potential delivered by Chiral Perturbation Theory in standard many-body algorithms [SKEM08, MLEA10], sometimes supplied with renormalization group techniques [FRS08, BFS09]. One of the most pressing issues of interest is the consistent inclusion of multi–nucleon interactions involving three or more nucleons in nuclear matter and nuclei, see e.g. [KFW05, BFS05, BFS06, KMW07, Na07, SKEM08, EHM09, BFS09]. In this work such a theory is established. It will be shown that it is possible to construct a chiral power counting for nuclear matter that is bound from below and treats systematically the inclusions of multi-nucleon interactions taking into account their non-perturbative nature. A particular technique for taking non-perturbative effects into account is given by the methods of Unitary Chiral Perturbation Theory (UχPT), which perform resummations partial wave by partial wave in the scattering amplitude [OO99, OM01, LOMb]. We will present those methods and show that the free parameter, which will enter our calculations, occurs in the evaluation of the free part

and its range of values will be determined. Having obtained a complete theoretical framework by the in-medium chiral power counting and the non-perturbative methods, we can apply this to calculations in the nuclear medium. As first applications we will calculate the nuclear matter energy density, the in-medium (scalar) chiral quark condensate and the in-medium pion self-energy each up-to-and-including next-to-leading order. As it will become clear from the power counting, at this order nucleon-nucleon interactions start to contribute and their impact on the results will be discussed in detail.

Several publications have been released during the work on this thesis. There are three publications [LOMa, LOMb, LOMd] actually covering topically the work at hand. All excerpts of those publications are indicated by footnotes. Also there have been elaborated two conference proceedings [LOMc, LOMe] summarizing the progress.

This work is organized as follows: After this introduction we will summarize the empirical features of the nuclear forces and of nuclear matter in chapter 1. Chapter 2 will be a short introduction into Chiral Perturbation Theory originating from the spontaneous breakdown of chiral symmetry in Quantum Chromodynamics. The application of Chiral Perturbation Theory to calculations in the nuclear medium will be shown in chapter 3. Also in chapter 3 there will be introduced the new in-medium power counting which allows to take into account multi-nucleon interactions, simultaneous to the well established framework. In chapter 4 we will present the non-perturbative methods of Unitary Chiral Perturbation Theory, which we are going to apply for our in-medium calculations. We will present this for the two-nucleon sector and will examplify its use to nucleon-nucleon scattering in the vacuum. After chapter 4 we will apply the established framework to several examples. First in chapter 5 we will sketch the nucleon self-energy in the nuclear medium. This will be useful, because we will need intermediate results over and over in subsequent chapters. Chapter 6 deals with the ground state energy density of nuclear matter. We will calculate and evaluate the energy per particle for symmetric nuclear and neutron matter. The pion self-energy in asymmetric nuclear matter will be calculated in chapter 7, the in-medium corrections to the chiral quark condensate for symmetric nuclear and neutron matter in chapter 8 and the in-medium corrections to the pion decay constant in chapter 9. In chapter 10 we will make first attempts to include the strange quantum number in the calculations. As a first step, we will skip the extensive baryon-baryon interaction. Most chapters will separately be provided with an abstract, an introduction as well as a summary with conclusions. Optionally there will also be given results and discussions thereof. A global summary and outlook will be given following chapter 10. The appendices A and B will deal with the partial wave decomposition of the nucleon-nucleon amplitudes and the Lorentz transformation of the nuclear medium, respectively. In appendices C and D we give the derivations and results of all for the calculations necessary scalar and tensor integrals, respectively. Finally, in appendix E the nucleon-nucleon interaction kernels, which are needed in chapters 5–9, are presented, including their derivations. An elaborated bibliography will be provided at the end of this thesis.

Chapter 1

Nuclear forces and nuclear matter

In this chapter we want to recall some basic features of the nuclear forces and nuclear matter. First we summarize the basic properties of the nucleon-nucleon interactions. Then we will sketch general empirical properties of the nucleus like its density distribution and its binding energy. That will finally lead us to the definition of *nuclear matter*.

1.1 Empirical properties of nucleon-nucleon interactions

The stability of nuclear matter (to be defined later) excludes the possibility of completely attractive ordinary forces between pairs of nucleons. If such existed and could be approximated by a square potential of range b and depth V_0, a system of a nucleons would collapse to a sphere of radius $b/2$ and the energy per particle would be proportional to the number of particles A for large values. The collapsed state has such low energy because the potential energy in the collapsed state is proportional to the number of pairs $A(A-1)/2$. This is not compensated by the kinetic energy since the exclusion principle forces the kinetic energy at the constant radius $b/2$ to rise only with powers of $A^{5/3}$. Hence, a system of A nucleons with purely attractive pair forces would not give rise to nuclear matter; there must be a repulsive force. We wish now to summarize the empirical key features of the nucleon-nucleon interaction. The following list is adapted from [FW03].

Attraction: The existence of the deuteron with total angular momentum $J = 1$ and even parity indicates that the force between proton and neutron is basically attractive, at least in the spin-triplet ($^3S_1$) state. Furthermore the interference between Coulomb and nuclear scattering in the proton-proton system shows that the nuclear force between any two nucleons is essentially attractive.

Finite range: For incident nucleon energies just above the elastic threshold ($\leq$ 10 MeV in the center-of-mass frame) the differential cross section for proton-neutron scattering is isotropic. We therefore conclude that scattering for these energies occurs basically in the relative S-wave state. This result allows a rough estimate of the range r of the nucleon-nucleon force from the classical limit on the maximum angular momentum p by $rp = \hbar l_{max}$, that can contribute to the scattering amplitude. Substituting the relation between energy and momentum gives

$$\hbar l_{max} = r\sqrt{2mE} \ , \tag{1.1}$$

where m represents the reduced mass here and $\hbar = 197.33\,\text{MeV fm}$. Since $l_{max} < 1$ for energies up to 10 MeV, the range of the nuclear force is a few Fermi ($\doteq$ femtometer $= 10^{-15}$m).

Spin-dependence: At very low energies the proton-neutron cross section $\sigma_{pn}(0) = 20.4\,\text{barn}$ is much too large to arise from a potential chosen to fit the properties of the deuteron. Since the measured proton-neutron cross section is the statistical average of the singlet and triplet cross section

$$\sigma_{pn} = \frac{1}{4}\,\sigma(^1S_0) + \frac{3}{4}\,\sigma(^3S_1)\ , \tag{1.2}$$

the singlet potential must differ from the triplet potential of the deuteron. A low-energy scattering experiment measures only two parameters of the potential. These can be taken as the scattering length a_l and the *effective range* r_l and are related to the *phase shift* δ_l by the *effective range expansion* via

$$k\cot\delta_l(k) \overset{k\to 0}{\longrightarrow} -\frac{1}{a_l} + \frac{1}{2}r_l k^2 + \mathcal{O}(k^4)\ , \tag{1.3}$$

where l denotes the l^{st} partial wave. For low energies of the scattering particles the details of the scattering potential are unimportant, what matters is how the potential looks from far away. This is because at low energies the particle is not going to actually touch the object producing the scattering potential. The scattering length is therefore a measure of how far from the potential those details become important. (This is similar to multipole expansion in electrodynamics. Two positive charges from far away will look like a single particle with twice the charge.) An extensive analysis of low-energy proton-neutron scattering yields the following parameters for the S-wave [EGM04] (see also references therein)

$$\begin{aligned} a_0(^1S_0) &= -23.593 \pm 0.071\ \text{fm} \\ a_0(^3S_1) &= 5.427 \pm 0.003\ \text{fm} \\ r_0(^1S_0) &= 2.645 \pm 0.025\ \text{fm} \\ r_0(^3S_1) &= 1.730 \pm 0.005\ \text{fm}\ . \end{aligned} \tag{1.4}$$

The spin-singlet state has a very large negative scattering length, which means it fails to have a bound state. A large positive scattering length signals the presence of a shallow (binding energy near zero) bound state. The spin-triplet system has one bound state, the deuteron, with a binding energy of 2.2 MeV. Although there is a large difference in scattering lengths and cross sections at zero energy, the singlet and triplet potentials are in fact rather similar.

Non-centrality: Since the deuteron has a quadrupole moment, the orbital angular momentum l cannot be a constant of the motion. In fact the ground state of the deuteron must contain both $l = 0$ and $l = 2$ to yield a nonvanishing quadrupole moment (the even parity forbids $l = 1$). Hence the nucleon-nucleon potential cannot be invariant under rotation of the spatial coordinates alone. The most general velocity-independent nucleon-nucleon potential for spin-$\frac{1}{2}$ particles that is invariant under total rotations generated by $\mathbf{J} = \mathbf{L} + \mathbf{S}$ and under spatial reflections is given by

$$V(x) = V_C(x) + S_{12}(x)\,V_T(x)\ , \tag{1.5}$$

where $\vec{x} \doteq \vec{x}_2 - \vec{x}_1$ and $x \doteq |\vec{x}|$. The central potential $V_C(x)$ and the tensor potential $V_T(x)$ can be further decomposed into various spin-isospin channels, e.g.

$$V_C(x) = V_C^0(x) + \vec{\sigma}_1\cdot\vec{\sigma}_2\,V_C^\sigma(x) + \vec{\tau}_1\cdot\vec{\tau}_2\,V_C^\tau(x) + (\vec{\sigma}_1\cdot\vec{\sigma}_2)(\vec{\tau}_1\cdot\vec{\tau}_2)\,V_C^{\sigma\tau}(x)\ . \tag{1.6}$$

The tensor operator is defined as

$$S_{12}(x) \doteq 3(\vec{\sigma}_1 \cdot \hat{x})(\vec{\sigma}_2 \cdot \hat{x}) - \vec{\sigma}_1 \cdot \vec{\sigma}_2 \ , \tag{1.7}$$

with $\hat{x} = \vec{x}/x$. Any higher powers of the spin operators can be reduced to the form of eq. (1.5) through the properties of the Pauli matrices. The total spin of the nucleon-nucleon system is given by $\mathbf{S} = \frac{1}{2}(\vec{\sigma}_1 \cdot \vec{\sigma}_1)$, and the square of this relation yields

$$\vec{\sigma}_1 \cdot \vec{\sigma}_2 = \begin{cases} -3 & , \ S = 0 \text{ (singlet state)} \\ +1 & , \ S = 1 \text{ (triplet state)} \ . \end{cases} \tag{1.8}$$

The total Hamiltonian constructed with eq. (1.5) is symmetric under the interchange of the particles' spins, which means that the wave function must be either symmetric ($S = 1$) or antisymmetric ($S = 0$) under this operation. As a result, the total spin S is a good quantum number for the two-nucleon system. Since the singlet wave function ${}^1\chi$ is annihilated by the spin operator ($\mathbf{S}\,{}^1\chi = 0$), it follows from eq. (1.7) that $S_{12}\,{}^1\chi = 0$. Thus the tensor operator annihilates the singlet state and acts only on the triplet state.

Charge Independence: The nucleon-nucleon force is approximately charge independent, which means that any two nucleons is a given two-body state always experience the same force. The Pauli principle, however, limits the neutron-neutron and proton-proton systems to overall antisymmetric states, because they are composed of identical fermions. A complete set of state vectors for two noninteracting nucleons is obtained by specifying the momentum of each nucleon and the spin projection $|\mathbf{p}_1 s_1 \mathbf{p}_2 s_2\rangle$. In the interacting system there are still eight good quantum numbers, which can be taken to be the energy E, the total angular momentum J and its z-projection M_J, the spin S, the parity π, and the three components of the center-of-mass momentum $\mathbf{p}_{cm}$, $|EJM_JS\pi\mathbf{p}_{cm}\rangle$. The parity of the various states arises from the behavior under spatial and spin interchange, which need not be the same as the behavior under particle interchange (which means combined spatial and spin interchange). Charge independence implies that the forces are equal in those states that can be occupied by all three kinds of pairs: nn, pp and pn. It is important to realize that charge independence does not imply the equality of scattering amplitudes and scattering cross sections for various pairs, since the states available are restricted by the Pauli principle. For example at low energies we have

$$\begin{aligned} \left(\frac{d\sigma}{d\Omega}\right)_{pn} &= \frac{1}{4}|f({}^1S_0)|^2 + \frac{3}{4}|f({}^3S_1)|^2 \\ \left(\frac{d\sigma}{d\Omega}\right)_{nn} &= \ |f({}^1S_0)|^2 \ , \end{aligned} \tag{1.9}$$

and charge independence merely requires

$$f({}^1S_0)_{pn} = f({}^1S_0)_{pp} = f({}^1S_0)_{nn} \ . \tag{1.10}$$

Exchange character: As the energy increases, more partial waves contribute to the scattering amplitude. One might expect that at sufficiently high energies, the Born approximation supplied a useful description of the differential cross section:

$$\frac{d\sigma}{d\Omega} \sim \left| \int d^3x \, e^{i\mathbf{q}\cdot\mathbf{x}} V(x) \right|^2 \ , \tag{1.11}$$

with the momentum transfer squared $\mathbf{q}^2 = 4k^2 \sin^2(\theta/2)$. In the Born approximation for large momentum transfer, the integrand oscillates rapidly and the Fourier transform tends to zero. From this one would expect that the scattering from a potential $V(x)$ should yield a differential cross section that falls off with increasing scattering angle θ. In contrast, measurements of proton-neutron scattering yielded that there is a great deal of backwards scattering and that there is an apparent approximate symmetry around $\theta = 90°$. If the symmetry was exact only even angular momenta would contribute to the scattering amplitude, for the odd ones distort the cross section. To explain this behavior, the concept of an exchange force has been introduced, that depends on the symmetry of the wave function. For a naive description one may introduce a so-called *Serber force* defined by

$$V = V(x)\frac{1}{2}(1 + P_M) \ , \tag{1.12}$$

with the *Majorana space-exchange operator* P_M defined by $P_M \phi(\mathbf{x}_i, \mathbf{x}_j) \doteq \phi(\mathbf{x}_j, \mathbf{x}_i)$. Phase shift analyses confirmed that the nuclear force has roughly a Serber exchange nature and is weakly repulsive in the odd angular momentum states.

Strongly repulsive core: Differential cross section data of proton-proton scattering yield an isotropy for $\theta > 10°$ (the forward peak is due to Coulomb scattering), which might suggest that only S-waves contribute even to higher energies. This conclusion can be ruled out considering the unitarity limit on the cross section which gives smaller results than observed. Higher partial waves must therefore interfere to give a flat angular distribution. In particular it was predicted, that a repulsive core in the singlet potential would change the sign of the S-wave phase shift at higher energies. The ${}^3S_1 - {}^3D_1$ interference term could then produce a nearly uniform distribution [Ja51]. Modern nucleon-nucleon potentials (CD-Bonn [Ma01], Reid93 [SKRS93, SKTS94], AV18 [WSS95]) suggest a hard core radius of $r_c = 0.6 - 0.7$ fm for the ${}^1S_0$-channel. Qualitatively the repulsion can be understood in the way, that the wave functions are prohibited to overlap because of the Pauli exclusion principle. Although the origin of the repulsive core must be closely related to the quark-gluon structure of the nucleon, it has been a long-standing open question in Quantum Chromodynamics. In an Effective Field Theory the picture of a hard core is obsolete, since the short-distance physics is not accessible and is therefore encoded in low-energy constants. The short range repulsion can also be dynamically modelled by vector meson exchange. The strongly repulsive core is essential not only for describing nucleon-nucleon scattering data, but also for the stability and saturation of atomic nuclei, for determining the maximum mass of neutron stars, and for igniting the Type II supernova explosions.

Spin-orbit force: Large polarizations of scattered nucleons are observed perpendicular to the plane of scattering. These effects are difficult to explain with just central and tensor forces, and an additional spin-orbit force of the type

$$V = \mathbf{L} \cdot \mathbf{S}\, V_{LS}(x) \ , \tag{1.13}$$

is generally introduced to understand these polarizations. The spin-orbit operators can be written as $\mathbf{L} \cdot \mathbf{S} = \frac{1}{2}[J(J+1) - l(l+1) - S(S+1)]$. It is obvious that the spin-orbit force vanishes in singlet states ($S = 0$, $l = J$) and also in S-wave states ($l = 0$, $S = J$). The usual phenomenological V_{LS} has a very short range and is due to vector mesons exchange. Thus the spin-orbit force is effective only at high energies, for it vanishes in S-wave states, and the centrifugal barrier tends to keep the high partial waves away from the potential.

Range expansion of the forces: Phenomenological nucleon-nucleon potentials are thought to be characterized by three distinct regions [MS01]. The long range part ($r \gtrsim 2$ fm) is well understood and is dominated by the one-pion exchange. The medium range part (1 fm$\lesssim r \lesssim 2$ fm) receives significant contributions from the exchange of multi-pions and heavy mesons ($\rho, \omega, \sigma \ldots$). The short range part ($r \lesssim 1$ fm) is empirically known to have a strongly repulsive core (see the corresponding paragraph).

1.2 Some properties of nuclei

The charge distribution of a nucleus is obtained by phase shift analyses of elastic scattering with charged particles (e^-, p, α). Note that Coulomb scattering experiments measure the charge distribution, and the matter distribution needs not be identical. For instance in heavy nuclei the mass distribution differs from the charge distribution due to neutron excess and sub structures. The nuclear force extends outside of the charge distribution; therefore, purely nuclear measurements generally yield slightly larger mean-square radii. Provided a suitable form factor, the *radius* R and the *average nucleon spacing* r_0 can be derived from such scattering data. The *mass density distribution* can be empirically estimated to

$$\rho(r) = \frac{\rho_0}{1 + e^{\frac{r-R}{a}}} \ , \tag{1.14}$$

where the parameter a is a measure for the surface thickness and the radius R is the point where $\rho(R) = \rho_0/2$. The parameters show the following systematic behavior:

1. the *central nuclear density* ρ_0 is a constant from nucleus to nucleus:

$$\rho_0 \frac{A}{Z} = const. \ , \tag{1.15}$$

   with *nucleon number* A and *atomic-* or *proton number* Z.

2. the radius of a nucleus behaves like [Bl80]

$$\begin{aligned} R &= r_0 A^{\frac{1}{3}} \ , \\ \text{with} \quad r_0 &= 1.128 \pm 0.059 \text{ fm} \ . \end{aligned} \tag{1.16}$$

   We shall estimate the *volume* V of a nucleus as $4\pi R^3/3$. As an immediate consequence, the particle density in nuclear matter [Bl80]

$$\rho_0 \doteq \frac{A}{V} = \frac{3}{4\pi r_0^3} = 0.166 \pm 0.027 \text{ nucleons/fm}^3 \tag{1.17}$$

   is a constant independent of the size of the nucleus. (This is e.g. not true in atoms.)

3. The root-mean-square *proton charge radius* is $r_p^e = 0.877$ fm [PDG08] (note that the *proton matter radius* r_p^m differs from that value), while the *mean interparticle distance* d in nuclei may be characterized by

$$d = \rho_0^{-\frac{1}{3}} \approx 1.82 \text{ fm} \ . \tag{1.18}$$

   Since $d > 2r_p$ one might hope to understand the properties of nuclei by examining the behavior of a collection of nucleons interacting through two-nucleon potentials. Nowadays it is well-known that three-nucleon forces yield essential contributions. Nontheless, the above inequality may justify an expansion in multi-nucleon interactions.

4. The *surface thickness* t, the region in which the density drops from 0.9 to 0.1 of the total density ρ_0, is found to be

$$t = 2a \ln 9 \approx 2.6 \text{ fm} . \tag{1.19}$$

for a broad range of nuclei (from Mg^{24} to Pb^{208}).

The *binding energy* E of a nucleus containing A nucleons, N neutrons and Z protons was first suggested bei Weizsäcker [We35], considering the nucleus as a *liquid drop*. The *semi-empirical mass formula* formally known as *Bethe-Weizsäcker mass formula* reads

$$E = -a_V A + a_S A^{\frac{2}{3}} + a_C \frac{Z(Z-1)}{A^{\frac{1}{3}}} + a_A \frac{(N-Z)^2}{A} + a_P \frac{\varepsilon_P}{A^{\frac{1}{2}}} , \tag{1.20}$$

where the best-fit parameters vary from source to source, we state in the following those of [St00]

$$\begin{array}{llllll} a_V & = 15.85 \text{ MeV} & a_S & = 18.34 \text{ MeV} & a_C & = 0.71 \text{ MeV} \\ a_A & = 23.22 \text{ MeV} & a_P & = 11.46 \text{ MeV} . & & \end{array} \tag{1.21}$$

The terms are described in the following.

Volume term: The first term is a consequence of the short range of nuclear forces. Hence a given nucleon may only interact strongly with its nearest neighbors and next-to-nearest neighbors. Therefore, the number of pairs of particles that actually interact is roughly proportional to A, giving the volume term its form. The coefficient a_V is smaller than the binding energy of the nucleons to their neighbors, which is of order of 40 MeV. This is because the larger the number of nucleons in the nucleus, the larger their kinetic energy is, due to Pauli's exclusion principle.

Surface term: The second term is a correction to the volume term. The volume term suggests that each nucleon interacts with a constant number of nucleons, independent of A. While this is very nearly true for nucleons deep within the nucleus, those nucleons on the surface of the nucleus have fewer nearest neighbors, justifying this correction. This can also be thought of as a surface tension term, and indeed a similar mechanism creates surface tension in liquids. If the volume of the nucleus is proportional to A, then the surface area should be proportional to $A^{\frac{2}{3}}$. It can also be deduced that a_S should have a similar order of magnitude as a_V.

Coulomb term: The source of the third term is the electrostatic repulsion between protons. To a very rough approximation, the nucleus can be considered a sphere of uniform charge density. The term is derived from the Coulomb potential, given that the radius is proportional to $A^{\frac{1}{3}}$. Because electrostatic repulsion will only exist for more than one proton, Z^2 becomes $Z(Z-1)$.

Asymmetry term: The fourth term takes into account that small nuclei are more stable for $N = Z$ due to the Pauli exclusion principle. The term is suppressed with $1/A$, so that its role becomes less significant for larger nuclei.

Pairing term: The last term captures the effect of spin-coupling and is a purely empirical correction. It takes into account that two neutrons or protons can form a pair with total spin $S = 0$. Such a system with even numbers of each nucleon is quantum mechanically favoured in comparison to those with odd numbers. The factor ε_P takes this into account

$$\varepsilon_P = \begin{cases} +1 & N, Z \text{ odd} \\ 0 & A \text{ odd} \\ -1 & N, Z \text{ even} \end{cases} . \tag{1.22}$$

1.3 Nuclear matter

We are now able to define a substance known as *nuclear matter*. Nuclear matter is a hypothetical configuration, where we let $A \to \infty$ in eq. (1.20), set $N = Z$ and turn off the Coulomb repulsion between the protons. Its properties are supposed to be independent of the number of constituents A, if A is so large that surface effects can be neglected. Of course, nuclear matter does not exist in reality. The Coulomb effects increase with the square of the proton number Z, and they become important before the nucleon number A is large enough to neglect surface effects. In fact, the Coulomb force prevents the formation of any stable or metastable nucleus when A is considerably higher than 200. However it is possible to understand some of the properties of complex nuclei by assuming that they consist in first approximation of this hypothetical nuclear matter and by introducing the effects of the surface and the Coulomb field as a subsequent step. Nuclear matter has a constant *binding energy per particle* given by [Bl80]

$$\bar{E} \doteq \frac{E}{A} = -16.0 \pm 1.0 \text{ MeV} . \tag{1.23}$$

This value therefore represents the energy per particle of an infinite nucleus with equal numbers of neutrons and protons but with no Coulomb effects. The binding energy per particle, eqs. (1.23), and nuclear density, eq. (1.17), exhibit the *saturation of nuclear forces*, because they are both constant; in particular independent of A. We regard nuclear matter as a uniform degenerate *Fermi system* that may be characterized by its *Fermi momentum* ξ_F. For $N = Z$ and unpolarized nuclear matter we have a degeneracy factor of 4 (proton, neutron $\times$ spin-up, spin-down) the particle density becomes

$$\rho_F = \frac{A}{V} = \frac{1}{V} \sum_{\lambda;|\mathbf{k}|\leq\xi_F} 1 = 4 \int \frac{d^3\mathbf{k}}{(2\pi)^3}\, \theta(\xi_F - |\mathbf{k}|) = \frac{2\xi_F^3}{3\pi^2} , \tag{1.24}$$

where λ is a place holder for quantum numbers. Using eq. (1.17) and the experimental value for the nucleon spacing r_0, eq. (1.16), we can write down the *saturation Fermi momentum* [Bl80]

$$\xi_0 = \sqrt[3]{\frac{9\pi}{8}} \frac{1}{r_0} = 1.35 \pm 0.07 \text{ fm}^{-1} = 266.4 \pm 13.8 \text{ MeV} . \tag{1.25}$$

Let us now define a few more properties of nuclear matter. From the Fermi momentum we obtain straightforwardly the quantities *Fermi energy* $\epsilon_F = \xi_F^2/(2m_N^*)$, *Fermi velocity* $v_F = \xi_F/m_N^*$ (with m_N^* the effective nucleon mass) and *Fermi wavelength* $\lambda_F = d(2/(3\pi^2))^{1/3}$. The *total energy* E_{tot} is given by

$$E_{tot}(\rho) = A[m_N^* + \bar{E}(\rho)] . \tag{1.26}$$

A quantity of special interest is the *nuclear compressibility* κ, since it can be related to many other properties like the velocity of sound. The compressibility is defined via

$$\kappa \doteq -\frac{1}{V}\left(\frac{\partial V}{\partial P}\right)_A = \frac{1}{\rho}\left(\frac{dP}{d\rho}\right)^{-1} , \tag{1.27}$$

where the *pressure* P is related to the *energy density* $\mathcal{E} = \bar{E}\rho$ by

$$P \doteq -\left(\frac{\partial E_{tot}}{\partial V}\right)_A = \rho^2 \frac{d\bar{E}}{d\rho} = \rho\frac{d\mathcal{E}}{d\rho} - \mathcal{E} . \tag{1.28}$$

It is sometimes convenient to express the compressibility κ in terms of the *chemical potential* μ

$$\mu \doteq \left(\frac{\partial E_{tot}}{\partial A}\right)_V - m_N = \left(\frac{\partial E}{\partial A}\right)_V = \frac{d\mathcal{E}}{d\rho} , \tag{1.29}$$

so that

$$\kappa = \frac{1}{\rho^2}\left(\frac{d\mu}{d\rho}\right)^{-1} . \tag{1.30}$$

The *saturation density* ρ_0 is manifestly defined by

$$\left.\frac{d\bar{E}}{d\rho}\right|_{\rho_0} = 0 . \tag{1.31}$$

From eq. (1.31) it is accessible that the following relations hold

$$\begin{aligned} P|_{\rho_0} &= 0 , \\ \left.\frac{dP}{d\rho}\right|_{\rho_0} &= \rho_0^2 \left.\frac{d^2\bar{E}}{d\rho^2}\right|_{\rho_0} , \\ \mu|_{\rho_0} &= \bar{E}\big|_{\rho_0} . \end{aligned} \tag{1.32}$$

Another interesting quantity is the *compression modulus* or ***in****compressibility* K defined by

$$K \doteq \xi_0^2 \left.\frac{d^2\bar{E}}{d\xi_F^2}\right|_{\xi_0} = 9\rho_0^2 \left.\frac{d^2\bar{E}}{d\rho^2}\right|_{\rho_0} . \tag{1.33}$$

This quantity is regularly misquoted in the literature as the compressibility. In fact it is related to the compressibility by

$$K = 3\xi_0 \left.\frac{d\mu}{d\xi_F}\right|_{\xi_0} = \frac{9}{\rho_0\kappa} . \tag{1.34}$$

It is worth keeping in mind that the compression modulus is defined only at the saturation density ρ_0, in particular its relation to the compressibility expressed in eq. (1.34) is true only for $\rho = \rho_0$. Indeed, the general relation is

$$\rho^2\frac{d^2\bar{E}}{d\rho^2} = \frac{1}{\rho}\left(\frac{1}{\kappa} - 2P\right) . \tag{1.35}$$

Chapter 2

Chiral perturbation theory

In this chapter we give a brief introduction to the basic features of Chiral Perturbation Theory (χPT). We will start with Quantum Chromodynamics (QCD), the gauge theory of the strong interaction, and will describe the spontaneous breakdown of chiral symmetry. Then we will expound the CCWZ formalism which provides the transformation rules for Goldstone bosons emerging from spontaneously symmetry breakdown. Since we are working with an expansion in low momenta we will introduce Weinberg's power counting scheme for effective Lagrangians. With that we will formulate χPT as an effective low-energy field theory which shares all symmetry properties with QCD. We will construct the basic structured for building an effective Lagrangian and will introduce the method of external fields into the framework. Finally, we will provide the explicit $SU(2)_f$ chiral Lagrangian in its heavy baryon formulation (HBχPT) which we will use throughout this work.

2.1 Quantum Chromodynamics and chiral symmetry

The gauge principle associates a gauge field with each independent continuous parameter of the gauge group. The underlying gauge group of QCD is color $SU(3)_c$ [Gr64, FGL73]. The matter fields are the quarks which are spin-1/2 fermions, with six different flavors – up, down, strange, charm, bottom (or beauty) and top (or truth) – in addition to their three possible colors. The QCD Lagrangian has the form

$$\mathcal{L}_{QCD} = \bar{q}\big(i\not{D} - \mathcal{M}\big)q - \frac{1}{4}G^a_{\mu\nu}G^{a,\mu\nu} + \frac{\theta\, g^2}{64\pi^2}\epsilon^{\mu\nu\rho\sigma}G^a_{\mu\nu}G^a_{\rho\sigma} \ . \tag{2.1}$$

The Dirac-Spinor $q = (u, d, s, c, b, t)^T$ comprises all quark flavors chosen in a way that the mass matrix is diagonal, $\mathcal{M} = \mathrm{diag}(m_u, m_d, m_s, m_c, m_b, m_t)$. The covariant derivative of the quark field is given by

$$D_\mu q = \big(\partial_\mu - igT^aG^a_\mu\big)q \ , \tag{2.2}$$

where g is the strong coupling constant and G^a_μ are the eight gauge boson fields called gluons. The generators T^a satisfy the Lie algebra

$$[T^a, T^b] = if^{abc}T^c \ , \tag{2.3}$$

with the totally antisymmetric structure constants f^{abc}. For $SU(3)_c$ the generators are represended by the Gell-Mann matrices by $T^a = \lambda^a/2$. Whereas quarks belong to the fundamental represen-

tation of the $SU(3)_c$, i.e. they form a color triplet, gluon fields form the adjoint representation of that gauge group (color octet).

The field strength tensors $G^a_{\mu\nu}$ in eq. (2.1) are defined by $[D_\mu, D_\nu] = -igG^a_{\mu\nu}T^a$ which gives

$$G^a_{\mu\nu} = \partial_\mu G^a_\nu - \partial_\nu G^a_\mu + g f^{abc} G^b_\mu G^c_\nu \ . \tag{2.4}$$

The last term in eq. (2.1) is called the θ-term. It is allowed by gauge invariance and implies an explicit P and CP violation of the strong interaction. The present empirical information indicates that the effects from the θ-term are tiny, so we shall drop this term in everything that follows. Furthermore we have not written gauge fixing terms altogether in eq. (2.1).

The six quark flavors may commonly be divided into three light quarks u, d and s and three heavy quarks c, b and t, [PDG06]

$$\left(\begin{array}{c} m_u \approx 1.5 \text{ to } 3.0\,\text{MeV} \\ m_d \approx 3.0 \text{ to } 7.0\,\text{MeV} \\ m_s \approx 95 \pm 25\,\text{MeV} \end{array}\right) \ll 1\text{GeV} \leq \left(\begin{array}{c} m_c \approx 1.25 \pm 0.09\,\text{GeV} \\ m_b \approx 4.20 \pm 0.07\,\text{GeV} \\ m_t \approx 174.2 \pm 3.3\,\text{GeV} \end{array}\right) \ , \tag{2.5}$$

where the scale of 1 GeV is associated with the masses of the lightest hadrons containing light quarks, that are not identified to be Goldstone bosons resulting from spontaneous symmetry breaking. The scale of spontaneous symmetry breaking, $4\pi f_\phi \approx 1170\,\text{MeV}$, is of the same order of magnitude, where f_ϕ is the meson decay constant in the chiral limit and will be defined later on.

In the limit of N_f massless quark flavors, the left– and right–handed components of the N_f quark fields decouple according to

$$\mathcal{L}^0_{QCD} = \bar{q}_L \, i\not{D} \, q_L + \bar{q}_R \, i\not{D} \, q_R - \frac{1}{4} G^a_{\mu\nu} G^{a,\mu\nu} \ , \tag{2.6}$$

where we defined the left– and right–handed fields using projection operators $P_{L/R}$,

$$q_{L/R} = P_{L/R}\, q = \frac{1}{2}(1 \mp \gamma_5)\, q \ . \tag{2.7}$$

We find that the Lagrangian eq. (2.6) displays an additional global $U(N_f)_L \times U(N_f)_R$ symmetry. Decomposing the symmetry group into irreducible subgroups yields

$$\underbrace{SU(N_f)_L \times SU(N_f)_R}_{\text{chiral group}} \times U(1)_V \times U(1)_A \ , \tag{2.8}$$

where $U(1)_A$ is anomalously broken and therefore no symmetry of QCD [tHo76]. The $U(1)_V$ subgroup generates conserved baryon number since the isosinglet vector current counts the number of quarks minus antiquarks in a hadron. The chiral symmetry is of course only approximate in the real world as there are small but non-vanishing quark masses.

Two empirical facts in the hadron spectrum suggest that the chiral symmetry is broken. First in the Wigner-Weyl mode we should expect parity doubling of the hadrons, e.g. baryons with $J^P = \frac{1}{2}^-$ quantum numbers should be degenerate in mass with the $J^P = \frac{1}{2}^+$ ones. But such a degeneracy is not observed, the parity counterparts are much heavier. Second, the masses of the pseudoscalar octet mesons are small in comparison to all other mesons. These are strong indications that the symmetry is spontaneously broken, yielding Nambu-Goldstone bosons that carry the same parity

quantum number as the broken generators. In this way the chiral group is broken to its vectorial subgroup

$$SU(N_f)_L \times SU(N_f)_R \stackrel{SSB}{\longrightarrow} SU(N_f)_V \ , \tag{2.9}$$

where SSB abbreviates *spontaneous symmetry breaking*. There have to occur $N_f^2 - 1$ pseudoscalar Goldstone bosons, that share the parity assignment with the broken subgroup. For $N_f = 2$ these can be identified with the pions, for $N_f = 3$ with the pions, kaons, and the eta. In the low energy regime one should be able to describe the properties of these Nambu-Goldstone bosons and their interactions in the framework of effective Lagrangians.

2.2 Construction of the chiral Lagrangian

2.2.1 CCWZ formalism

The formalism to deal with effective Lagrangians for spontaneously broken symmetries was worked out by Callan, Coleman, Wess and Zumino [CCWZ69, CWZ69] in 1969. The presentation used here is based on [Ma96]. Consider a symmetry group G spontaneously broken down to a subgroup H. For the fields $\psi(x)$ one chooses the vacuum ground state ψ_0, which is invariant under H, such that it fulfills the transformation rule

$$\psi(x) = \Xi(x)\psi_0 \ , \quad \text{with} \quad \Xi(x) \in G \ . \tag{2.10}$$

Notice that $\Xi(x)$ is not unique as $\Xi(x)\psi_0 = \Xi(x)h(x)\psi_0$ for any $h(x) \in H$. In the CCWZ formalism, one picks a set of broken generators X^a and writes

$$\Xi(x) = e^{i\phi^a(x)X^a} \ , \tag{2.11}$$

with the Nambu-Goldstone fields $\phi^a(x)$. Under a global symmetry transformation $\psi(x) \to g\,\psi(x)$ with $g \in G$, $\Xi(x)$ behaves according to

$$\Xi(x) \to g\,\Xi(x) = \tilde{\Xi}(x)\,h \tag{2.12}$$

in general, for some $h \in H$ and a $\tilde{\Xi}(x) \in G$ of the form (2.11), different from $\Xi(x)$. Hence the transformation of $\Xi(x)$ can be written as

$$\Xi(x) \to g\,\Xi(x)\,h^{-1}\big(g, \Xi(x)\big) \ , \tag{2.13}$$

where h^{-1} is a nonlinear function of g and $\Xi(x)$, the so-called compensator field.

G is the chiral group, $H = SU(N_f)_V$ the unbroken vector subgroup and the Goldstone boson manifold is the coset space G/H which is isomorphic to $SU(N_f)$. The generators of G are T_L^a and T_R^a, which act on left– and right–handed fields respectively, those of the unbroken subgroup H are the flavor generators $T^a = T_L^a + T_R^a$. $SU(N_f)_L \times SU(N_f)_R$ transformations may be represented by block diagonal matrices

$$g = \begin{pmatrix} R & 0 \\ 0 & L \end{pmatrix} \ , \tag{2.14}$$

with $L \in SU(N_f)_L$ and $R \in SU(N_f)_R$. The unbroken transformations are of the form $R = L = K$,

$$h = \begin{pmatrix} K & 0 \\ 0 & K \end{pmatrix} \ . \tag{2.15}$$

One chooses the broken symmetry operators to be $X^a = T^a_L - T^a_R$. The resulting Ξ-field, according to the general CCWZ prescription (2.11), is now

$$\Xi(x) = \exp\left[\frac{i\phi^a(x)X^a}{2f_\phi}\right] = \exp\left[\frac{i}{2f_\phi}\begin{pmatrix} \phi^a(x)T^a & 0 \\ 0 & -\phi^a(x)T^a \end{pmatrix}\right] \equiv \begin{pmatrix} u(x) & 0 \\ 0 & u^\dagger(x) \end{pmatrix} , \quad (2.16)$$

where f_ϕ is a constant with the dimension of mass, introduced in order to make the exponent of the last equation dimensionless, and the factor of $1/2$ is just convention for our choosen basis. The transformation rule (2.13) for $\Xi(x)$ now reads

$$\begin{pmatrix} u(x) & 0 \\ 0 & u^\dagger(x) \end{pmatrix} \to \begin{pmatrix} R & 0 \\ 0 & L \end{pmatrix} \begin{pmatrix} u(x) & 0 \\ 0 & u^\dagger(x) \end{pmatrix} \begin{pmatrix} K^{-1}(g,u) & 0 \\ 0 & K^{-1}(g,u) \end{pmatrix} , \quad (2.17)$$

yielding

$$u(x) \to R\,u(x)\,K^{-1}(g,u) = K(g,u)\,u(x)\,L^\dagger , \quad (2.18)$$

which defines $K(g,u)$ in terms of L, R and $u(x)$. The field $\phi = \phi^a T^a$ transforms in a complicated nonlinear way. Notice that there are other possible bases, we just introduced the one used in this thesis.

2.2.2 Chiral power counting

In order for chiral perturbation theory to be a predictive effective field theory, there has to be a way to organize the perturbative expansion, which can be consistently truncated to describe low-energy processes to a certain desired accuracy. The prerequisite for the construction of effective field theories was introduced by Weinberg [We79]. He stated that a perturbative description in terms of the most general effective Lagrangian containing all possible terms compatible with assumed symmetries yields the most general S–matrix consistent with the fundamental principles of quantum field theory and the assumed symmetries. The corresponding effective Lagrangian will contain an infinite number of terms with an infinite number of free parameters. Turning Weinberg's theorem into a practical tool requires first some scheme to organize the effective Lagrangian and second a systematic method of assessing the "importance of diagrams" generated by the interaction terms of the effective Lagrangian when calculating physical matrix elements.

In the framework of χPT the most general chiral Lagrangian describing the dynamics of the Goldstone bosons and their interaction with other hadronic states is organized as a string of terms with increasing number of momenta (or derivatives) and quark mass terms,

$$\mathcal{L}_{\text{eff}} = \sum_{n=1}^{\infty} \mathcal{L}^{(n)} , \quad (2.19)$$

where the superscripts refer to the order in the momentum and quark mass expansion. In the context of Feynman rules, derivatives generate four-momenta, being of chiral order one. The chiral order of a quantity will in the following be noted by $\mathcal{O}(p^n)$, where p generically denotes a small expansion parameter.

Weinberg's power counting scheme analyzes the behavior of a given diagram when applying the aforementioned counting values to momenta, quark and meson masses (with use of the on-shell condition $k^2 = m_\pi^2$). In a mass-independent renormalization scheme, such as dimensional regularization, the only dimensional parameters are the momenta p. This works fine as long as heavy

particles are integrated out, e.g. only Goldstone bosons are considered. In order to include baryons in our theory – whose masses are somewhere in the range of the scale of spontaneous symmetry breaking – one has to invent a suitable renormalization scheme, which obeys the power counting. Finding a suitable renormalization condition will allow to apply the following power counting to loop diagrams: a loop integration in d dimensions counts as $\mathcal{O}(p^d)$, meson and fermion propagators count as $\mathcal{O}(p^{-2})$ and $\mathcal{O}(p^{-1})$, respectively, vertices derived from the mesonic Lagrangian $\mathcal{L}_\phi^{(2k)}$ and the baryonic Lagrangian $\mathcal{L}_{\phi\Psi}^{(k)}$ count as $\mathcal{O}(p^{2k})$ and $\mathcal{O}(p^k)$, respectively. The chiral dimension D of a diagram with amplitude

$$\mathcal{M} \;\sim\; p^D \;\sim\; \int (d^4p)^{N_L} \frac{1}{p^{2I_\phi}} \frac{1}{p^{I_\Psi}} \prod_k^\infty (p^k)^{N_k^\Psi} \prod_k^\infty (p^{2k})^{N_{2k}^\phi} \;, \tag{2.20}$$

is thus given by

$$D = 4N_L - 2I_\phi - I_\Psi + \sum_{k=1}^\infty 2kN_{2k}^\phi + \sum_{k=1}^\infty kN_k^\Psi \;, \tag{2.21}$$

where N_L, I_ϕ, I_Ψ, N_{2k}^ϕ and N_k^Ψ denote the number of independent loop momenta, internal meson propagators, internal baryon propagators, meson vertices originating from $\mathcal{L}_\phi^{(2k)}$, and baryon vertices originating from $\mathcal{L}_{\phi\Psi}^{(k)}$, respectively. We make use of the topological relation

$$N_L = I_\phi + I_\Psi - \sum_{k=1}^\infty N_{2k}^\phi - \sum_{k=1}^\infty N_k^\Psi + 1 \tag{2.22}$$

and consider only processes containing exactly one baryon in the initial and final state, respectively, such that $\sum_{k=1}^\infty N_k^\Psi = I_\Psi + 1$. Finally we obtain

$$D = 2N_L + 1 + \sum_{k=1}^\infty 2(k-1)N_{2k}^\phi + \sum_{k=1}^\infty (k-1)N_k^\Psi \;. \tag{2.23}$$

All the terms on the right hand side are positive because of $k \geq 1$, and for fixed D there is always just a finite number of combinations of N_L, N_{2k}^ϕ, N_k^Ψ that obey the condition (2.23). Clearly, for small enough momenta and masses diagrams with small D should dominate. Loop diagrams are always suppressed due to the term $2N_L$ in eq (2.23).

2.2.3 Lowest order meson Lagrangian

If not explicitely mentioned otherwise, $SU(N)$ will always refer to flavor $SU(N)$ throughout this work. According to the usual procedure for low-energy effective theories, we now want to construct the most general Lagrangian, invariant under chiral symmetry transformations, as an expansion in terms of small momenta, with the Nambu-Goldstone bosons representing the degrees of freedom. Since derivatives yield the momenta we will speak of derivatives in the following. Additionally we require Lorentz invariance, and symmetry under parity, time and charge conjugation. Lorentz invariance demands that all four-vectors are contracted and derivatives of the pseudoscalar bosons have to occur in even numbers, due to the lack of a structure that could contract single derivatives. So we write:

$$\mathcal{L}_\phi = \sum_{n=1}^\infty \mathcal{L}_\phi^{(2n)} \;, \tag{2.24}$$

where the superscripts denote the number of derivatives in the respective terms. The terms with zero derivatives have been neglected, because such terms are just constant (and only play a role when gravity is involved.) So the effective chiral meson Lagrangian starts at order two. In order to write down the lowest order effective meson Lagrangian in our chosen basis we introduce the chiral vielbein

$$u_\mu = i\left(u^\dagger \partial_\mu u - u \partial_\mu u^\dagger\right) = i\{u^\dagger, \partial_\mu u\} \ , \tag{2.25}$$

which behaves according to $u_\mu \to K u_\mu K^\dagger$ under chiral transformations. With that the lowest order effective meson Lagrangian may be written as

$$\mathcal{L}_\phi^{(2)} = \frac{f_\phi^2}{4}\langle u_\mu u^\mu \rangle \ , \tag{2.26}$$

where $\langle \ldots \rangle$ indicates the trace in flavor space. The explicit expression for the field u in exponential gauge in $SU(N_f)$ reads:

$$u = \exp\left(\frac{i\phi}{2f_\phi}\right), \quad \phi = \phi^a T^a \ , \tag{2.27}$$

where T^a are the generators of the $SU(N_f)$ group. When expanding eq. (2.26) in terms of the meson fields,

$$\mathcal{L}_\phi^{(2)} = \frac{f_\phi^2}{4}\frac{\langle \partial_\mu \phi \, \partial^\mu \phi \rangle}{f_\phi^2} + \mathcal{L}_{int} = \frac{1}{2}\partial_\mu \phi^a \, \partial^\mu \phi^a + \mathcal{L}_{int} \ , \tag{2.28}$$

we see that the coefficient in (2.26) has been chosen such as to reproduce the standard normalization for the kinetic terms. $\mathcal{L}_{int}$ denotes terms of higher power in the meson fields, i.e. contact interactions of mesons. We note that the meson fields are derivatively coupled, so the amplitude vanishes in the low-energy limit. In order to determine the quantity f_ϕ, we have to calculate the two-point function of the axial-vector current

$$A_\mu^a = \bar{q}\gamma_\mu\gamma_5 \frac{T^a}{2} q \ , \tag{2.29}$$

where T^a are again the generators of the underlying group. We find

$$\langle 0|A_\mu^a|\phi^b(p)\rangle = i\delta^{ab} f_\phi \, p_\mu \{1 + \mathcal{O}(m_q)\} \ , \tag{2.30}$$

from which we immediately read off that f_ϕ is the decay constant of the Goldstone bosons [GL84, GL85].

2.2.4 Baryon fields

We have seen how to construct the chirally invariant effective Lagrangian for the Goldstone bosons. Now, we would like to include fields for other low-lying hadrons, i.e. for the ground state baryon fields with spin one half ($S = \frac{1}{2}$) and no excitations ($\ell = n = 0$). The first occurrence of Chiral Perturbation Theory including baryons – or being more precise nucleons – as explicit degrees of freedom was in [GSS88]. We will proceed in a similar way as for the mesons: choose a suitable representation and construct the most general Lagrangian allowed by symmetries. The Lagrangian for baryons is not restricted to even powers in the chiral counting scheme, so the effective Lagrangian analogue to the expressions of (2.24) for baryons reads:

$$\mathcal{L}_{\phi\Psi} = \sum_{n=1}^{\infty} \mathcal{L}_{\phi\Psi}^{(n)} \ . \tag{2.31}$$

In the following we give the prescription for an arbitrary number of flavors N_f. We want the baryon fields to transform in any way under $SU(N_f)_L \times SU(N_f)_R$ that reduces to the adjoint representation of $SU(N_f)_V$ after spontaneous symmetry breakdown. We choose the baryon multiplet to transform according to $\Psi \to K\Psi K^\dagger$, which is indeed the transformation law for adjoint representations. It is convenient for the construction of the baryon Lagrangian to introduce the chiral connection

$$\Gamma_\mu = \frac{1}{2}\left(u^\dagger \partial_\mu u + u \partial_\mu u^\dagger\right) = \frac{1}{2}[u^\dagger, \partial_\mu u] \ , \tag{2.32}$$

and use the chiral vielbein u_μ defined in eq. (2.25). The transformation properties of (2.32) under chiral transformations are $\Gamma_\mu \to K\Gamma_\mu K^\dagger - (\partial_\mu K)K^\dagger$. Using these, we can construct a covariant derivative of the baryon field according to

$$[D_\mu, \Psi] = \partial_\mu \Psi + [\Gamma_\mu, \Psi] \ , \tag{2.33}$$

transforming in the well-known way $[D_\mu, \Psi] \to K[D_\mu, \Psi]K^\dagger$.

Note that for $SU(2)_f$, which we will employ in this work, the derivation simplifies a bit, since the nucleon fields can be described in the fundamental representation rather than the adjoint. To first order in derivatives, the most general pion-nucleon Lagrangian is given by

$$\mathcal{L}^{(1)}_{\pi N} = \bar{N}(i\not{D} - m)N + \frac{g_A}{2}\bar{N}\not{u}\gamma_5 N \ , \tag{2.34}$$

with the chiral covariant derivative $D_\mu = \partial_\mu + \Gamma_\mu$, the average nucleon mass m and the axial pion-nucleon coupling g_A. The nucleon fields N contain four components of Lorentz space times two components of isospin space. The pion fields $\vec{\pi}(x)$ enter in the matrix $u = \exp(i\vec{\tau}\cdot\vec{\pi}/2f_\pi)$, with the weak pion decay constant f_π whose empirical value is $f_\pi \approx 92.4\,\mathrm{MeV}$.

2.2.5 External sources

A convenient way to calculate matrix elements from chiral Lagrangians is to use external sources in the path integral formalism, a method well-known from other quantum field theories. For application to χPT see [GL84, GL85]. For this purpose we introduce vector v_μ, axial–vector a_μ, scalar s and pseudoscalar p sources. These are coupled to the QCD Lagrangian according to

$$\mathcal{L} = \mathcal{L}_{QCD} + \bar{q}\,\gamma^\mu\big(v_\mu + \gamma_5\, a_\mu\big)q - \bar{q}\,\big(s - i\gamma_5\, p\big)q \ . \tag{2.35}$$

The effective generating functional is then of the form

$$\exp\big(i\,\mathcal{Z}[v_\mu, a_\mu, s, p]\big) = \int \mathcal{D}u \exp\left(i \int d^4x\ \mathcal{L}_{eff}[u, v_\mu, a_\mu, s, p]\right) \ , \tag{2.36}$$

and matrix elements can be obtained by functional derivation with respect to the external sources. Generalizing the chiral symmetry transformation to local gauge transformation, the left– and right–handed vector currents have the chiral transformation behavior

$$l_\mu = v_\mu - a_\mu \quad \longrightarrow \quad L l_\mu L^\dagger + iL\partial_\mu L^\dagger \ , \tag{2.37}$$

$$r_\mu = v_\mu + a_\mu \quad \longrightarrow \quad R r_\mu R^\dagger + iR\partial_\mu R^\dagger \ . \tag{2.38}$$

These can be coupled to the chiral Lagrangian as gauge fields, in the form of covariant derivatives

$$\nabla_\mu u = \partial_\mu u - i[v_\mu, u] - i\{a_\mu, u\} \ , \tag{2.39}$$

which can be included in the chiral vielbein eq. (2.25) and the chiral connection eq. (2.32) by

$$u_\mu \doteq i\left(u^\dagger(\partial_\mu - ir_\mu)u - u(\partial_\mu - il_\mu)u^\dagger\right) = i\{u^\dagger, \nabla_\mu u\} - 2a_\mu \ , \tag{2.40}$$

$$\Gamma_\mu \doteq \frac{1}{2}\left(u^\dagger(\partial_\mu - ir_\mu)u + u(\partial_\mu - il_\mu)u^\dagger\right) = \frac{1}{2}[u^\dagger, \nabla_\mu u] - iv_\mu \ . \tag{2.41}$$

The scalar and pseudoscalar sources can be combined into the field χ,

$$\chi = 2B(s + i\,p) \ , \tag{2.42}$$

which has to transform according to $\chi \to R\,\chi\,L^\dagger$. The parameter B is related to the strength of the vacuum chiral quark condensate in the chiral limit and the weak meson decay constant f_ϕ in the same limit via

$$\langle 0|\bar{q}_i q_j|0\rangle = -\delta_{ij} B f_\phi^2\big(1 + \mathcal{O}(m_q)\big) \ , \tag{2.43}$$

where $|0\rangle$ refers to the vacuum state. Note that B, proportional to the quark condensate, is only real if CP is conserved. For standard χPT (which means $B/f_\phi \gg 1$) the quark masses are counted as $\mathcal{O}(p^2)$. Note that B is a scale-dependent quantity. χ may further be combined into the fields

$$\chi_\pm = u^\dagger\,\chi\,u^\dagger \pm u\,\chi^\dagger\,u \ , \tag{2.44}$$

that obey the required transformation rule $\chi_\pm \to K\,\chi_\pm\,K^\dagger$. Field-strength tensors can also be included. We define the left– and right–handed chiral field-strength tensor via

$$R_{\mu\nu} = \partial_\mu r_\nu - \partial_\nu r_\mu - i[r_\mu, r_\nu] \ , \tag{2.45}$$

$$L_{\mu\nu} = \partial_\mu l_\nu - \partial_\nu l_\mu - i[l_\mu, l_\nu] \ . \tag{2.46}$$

They transform according to $R_{\mu\nu} \to R\,R_{\mu\nu}\,R^\dagger$ and $L_{\mu\nu} \to L\,L_{\mu\nu}\,L^\dagger$. These may be combined to

$$F^\pm_{\mu\nu} = u^\dagger\,R_{\mu\nu}\,u \pm u\,L_{\mu\nu}\,u^\dagger \ , \tag{2.47}$$

which again obey the mandatory transformation rule $F^\pm_{\mu\nu} \to K\,F^\pm_{\mu\nu}\,K^\dagger$.

2.3 Heavy baryon expansion of chiral Lagrangians

The first systematic calculations of pion-nucleon scattering have been performed in [GSS88]. The nucleons have been treated fully relativistically in this approach. However in a naive formulation, like *dimensional regularization* with a *minimal subtraction renormalization* scheme, one looses the one-to-one correspondence between the number of loops and the power of small external momenta. In this way, the chiral power counting is disobeyed. The origin of this unwanted trait is that the inclusion of nucleons unavoidably introduced a new mass scale to the problem, the nucleon mass m. The nucleon mass cannot be regarded as a small paramater and does not vanish in the chiral limit.

Nowadays, there are several methods available to avoid the problem of spoiling the chiral power counting. On the side of relativistic approaches there are renormalization methods like *infrared renormalization* [BL99] and *on-mass-shell renormalization* [FGJS03], which are both typically used with a dimensional regulator (and also still the $\overline{MS}$ renormalization scheme to handle ultraviolet divergencies). The method we will comprehend here is the heavy baryon formulation HBχPT [JM91, BKKM92], which essentially corresponds to a non-relativistic treatment of the nucleons.

2.3.1 Heavy baryon formalism

The idea is to use a simultaneous expansion in powers of $q/\Lambda_\chi \sim q/(4\pi f_\pi)$ and q/m, where m is the nucleon mass. Let us now briefly explain how such an expansion may be performed. The four-momentum p_μ for a heavy particle like the nucleon is conveniently parameterized as

$$p_\mu = m v_\mu + k_\mu \ , \tag{2.48}$$

where v_μ is the four-velocity satisfying $v^2 = 1$ and k_μ is a small residual momentum $v \cdot k \ll m$. The advantage of such a parameterization is that the trivial kinematic dependence of p_μ on the large term $m v_\mu$ is now explicit. In the rest frame with $v_\mu = (1, 0, 0, 0)$ the three-momentum is entirely given by $\mathbf{k}$ and $p_\mu = (\sqrt{m^2 + \mathbf{k}^2}, \mathbf{k})$. Note that in the limit $m \to \infty$ the nucleon four-velocity becomes a conserved quantum number since its change by a finite amount would lead to an infinite momentum transfer between the incoming and outgoing nucleons [Ge90]. To get rid of the nucleon mass term in the Lagrangian for the free Dirac field one can introduce the eigenstates H and h of the velocity operator $\not{v}$ via

$$H = P_v^+ e^{imv\cdot x}\Psi \ , \qquad h = P_v^- e^{imv\cdot x}\Psi \ , \tag{2.49}$$

with the projection operators $P_v^\pm$ onto the eigenstates of the four-velocity operator v corresponding to the eigenvalue ± 1, which are given by

$$P_v^\pm = \frac{1 \pm \not{v}}{2} \ . \tag{2.50}$$

The exponential factor in eq. (2.49) eliminates the trivial kinematic dependence of the nucleon field on the momentum $m v_\mu$. H and h are usually called the *large* and the *small components*, respectively. The free Lagrangian can be expressed in term of the fields H and h as

$$\mathcal{L} = \bar\Psi(i\not{\partial} - m)\Psi = \bar H (iv\cdot\partial) H - \bar h (iv\cdot\partial + 2m) h + \bar H i\not{\partial} h + \bar h i\not{\partial} H \ . \tag{2.51}$$

This leads to the following equations of motions for H and h

$$\begin{aligned} (v\cdot\partial) H &= -P_v^+ i\not{\partial} h \ , \\ (v\cdot\partial) h &= \ \ P_n^- i\not{\partial} H + 2im h \ . \end{aligned} \tag{2.52}$$

From the second equation one sees that

$$h = \frac{i}{2m} P_v^- \not{\partial} H + \mathcal{O}\big(m^{-2}\big) \ . \tag{2.53}$$

Therefore, the large component field H obeys the free equation of motion

$$(v\cdot\partial) H = 0 \ , \tag{2.54}$$

up to $1/m$ corrections. The nucleon mass does not enter this equation of motion to leading order. Note that in the nucleon rest-frame, H and h can be identified with the usual upper and lower components of a Dirac spinor modulo the factor e^{imt}. The small component field h can now be completely eliminated from the Lagrangian eq. (2.51) using the equations of motion eqs. (2.52). A more elegant path integral formulation of this non-relativistic reduction can be found in [MRR92].

For the case of nucleons interacting with pions one can proceed in a similar way as for the free nucleons to eliminate h. The equations of motion eqs. (2.52) are then modified by terms including

pion and nucleon fields, with an infinte chain of higher order corrections. Since the chiral symmetry only allows for derivative pion-nucleon and pion-pion couplings (and quark mass insertions and external sources etc. pp.), these additional terms can be regarded as small corrections of order $1/\Lambda_\chi$ to the leading order equations of motion eqs. (2.52). One important problem of this approach is that time derivatives of the nucleon fields contribute large factors of order m. But using the equation of motion $(i\partial\!\!\!/ - m)\Psi = \ldots$, one can eliminate the derivatives of the nucleon field by replacing them with higher order terms of the effective Lagrangian. Such terms are anyway present in the effective Lagrangian, which contains all possible chiral invariant interactions. In other words, one can simply drop time derivatives acting on the nucleon field in all interaction terms, leaving a single time derivative in the free Lagrangian term. For a more detailed discussion on that approach as well as for concrete examples see [FMS98]. Proceeding with the elimination of h from the pion-nucleon effective Lagrangian then yields additional terms, which have coefficients of $(1/m)^n$, so-called recoil corrections. Equivalently, the effective Lagrangian can be derived in terms of non-relativistic nucleon fields from the beginning.

2.3.2 Heavy baryon flavor $SU(2)$ Lagrangian

In the following we skip a detailed derivation, which can be found in [BKM95, BKM97], and just give the chiral Lagrangian terms which we will employ in this work. The leading and next-to-leading order contributions from the two-flavor Lagrangian of Heavy Baryon Chiral Perturbation Theory read

$$\begin{aligned}
\mathcal{L}_{\pi N}^{(1)} &= \bar{N}\Big(iD_0 - \frac{g_A}{2}\vec{\sigma}\cdot\vec{u}\Big)N \ , \\
\mathcal{L}_{\pi N}^{(2)} &= \bar{N}\bigg(\frac{1}{2m}\vec{D}\cdot\vec{D} + i\frac{g_A}{4m}\Big\{\vec{\sigma}\cdot\vec{D}, u_0\Big\} + c_1\langle\chi_+\rangle + \Big(c_2 - \frac{g_A^2}{8m}\Big)u_0^2 + c_3 u_\mu u^\mu \\
&\quad + \frac{i}{2}\Big(c_4 + \frac{1}{4m}\Big)\vec{\sigma}\cdot(\vec{u}\times\vec{u}) + c_5\Big(\chi_+ - \frac{\langle\chi_+\rangle}{2}\Big) \\
&\quad - \frac{i}{4m}[S^\mu, S^\nu]\Big((1+c_6)F_{\mu\nu}^+ + c_7\langle F_{\mu\nu}^+\rangle\Big) + \ldots\bigg)N
\end{aligned} \tag{2.55}$$

where the ellipses represent terms that are not needed here. It was chosen the frame with $v_\mu = (1,0,0,0)$. We use the standard notation of the commutator and anti-commutator relations $[\cdot,\cdot]$ and $\{\cdot,\cdot\}$, respectively. The c_i are chiral low-energy constants whose values are fitted from phenomenology [BKM95]. The spin operator is given by $S^\mu = (0,\vec{\sigma})^T$. We will also need the chiral effective pion-pion Lagrangian to leading order, which is given by

$$\mathcal{L}_{\pi\pi}^{(2)} = \frac{f_\pi^2}{4}\langle u_\mu u^\mu + \chi_+\rangle \ , \tag{2.56}$$

with definitions given in section 2.2. The generators $T^a = \tau^a$ are the Pauli matrices.

Chapter 3

Theory for nuclear matter

This chapter serves to introduce the reader into the topic of in-medium Effective Field Theory. First we will motivate the need of a new power counting scheme for nuclear matter. Then we present some fundamentals which have to be considered for in-medium calculations in contrast to those in the vacuum. After that a new improved in-medium chiral power counting scheme will be derived, that allows for a systematic expansion taking into account both local as well as pion-mediated inter–nucleon interactions. Based on this power counting, one can identify classes of non-perturbative diagrams that require a resummation.

3.1 Introduction

Many-body field theory was derived from quantum field theory by considering nuclear matter as a finite density system of free nucleons at asymptotic times in [Ol02]. The generating functional of Chiral Perturbation Theory (χPT) in the presence of external sources was deduced, similarly as in the pion and pion-nucleon sectors [GL84, GSS88]. Based on these results the authors of [MOW02] derived a chiral power counting in the nuclear medium. This approach was later generalized to finite nuclei and e.g. applied to the calculation of the pion-nucleus optical potential up to $\mathcal{O}(p^5)$ [GRW04]. However, only nucleon interactions due to pion exchanges were considered so far, the local nucleon-nucleon and multi-nucleon interactions were neglected. It is common in present applications of Chiral Perturbation Theory to nuclei and nuclear matter [Ro89, OGN95, MOW02, KFW02, KFW03, KFW05, KMW07, DO08] to consider only meson-baryon chiral Lagrangians, while ignoring constraints from free nucleon-nucleon scattering. Others, like [LFA00], include local multi-nucleon interactions but loose contact to the vacuum by fitting parameters to nuclear matter properties.

All these calculations share the assumption that spontaneous chiral symmetry breaking still holds for finite density nuclear systems. This assumption can be cross-checked by calculating the temporal pion decay constant f_t in the nuclear medium [MOW02]. Let us consider the axial-vector current $A^i_\mu = \bar{q}(x)\gamma_\mu\gamma_5(\tau^i/2)q(x)$, with $q(x)$ a two-dimensional vector corresponding to the light quarks fields and τ^i the Pauli matrices. Spontaneous chiral symmetry breaking results because the axial charge, $Q^i_A(x) = \int d^3x A^i_0(x)$, does not annihilate the ground state, denoted by $|\Omega\rangle$. As long as the matrix element $\langle\Omega|Q^b_A(0)|\pi^a(\mathbf{p})\rangle = i(2\pi)^3 f_t p_0 \delta^{(3)}(\mathbf{p})\delta^{ab}$ is not zero, the vacuum is not left invariant by the action of the axial charge and spontaneous chiral symmetry breaking happens. In

the previous equation $|\pi^a(\mathbf{p})\rangle$ denotes a pion state with Cartesian coordinate a, three-momentum $\mathbf{p}$, energy p_0 and f_t is the temporal weak pion decay coupling. (Mathematically one can obtain meaningful results from $i\delta^{(3)}(\mathbf{p})p_0$ in the chiral limit by considering wave packets [MOW02], $\int d\mathbf{p}|\mathbf{p}|^{-1}f(\mathbf{p}^2)|\pi^a(\mathbf{p})\rangle$ with $f(0)$=const. [GSW62].) Note that due to the presence of the nuclear medium one should distinguish between the spatial and temporal couplings of the pion to the axial-vector current. The calculations in [MOW02] indicate a linear decreasing of f_t with density, $f_t = f_\pi(1-(0.26\pm0.04)\rho/\rho_0)$, where $f_\pi = 92.4$ MeV is the weak pion decay constant in vacuum and ρ_0 is the nuclear matter saturation density. This result clearly indicates that it makes sense to use chiral Lagrangians in the nuclear medium up to central nuclear densities. On the other hand, the form of the chiral Lagrangians changes depending whether the quark condensate $\langle\Omega|\bar{u}u+\bar{d}d|\Omega\rangle$ is large or small. In the former case we have *standard* χPT [We79, GL84, GL85] and in the latter the so-called *generalized* χPT would result [FSS91, FSS93]. In SU(2) χPT it has been shown that the first case holds [CGL01]. [TW95, WT95, KW96, KW97, MOW02] obtain that the in-medium quark condensate decreases linearly with density as $1-(0.35\pm0.09)\rho/\rho_0$ [MOW02]. Thus, the standard χPT scenario holds up to nuclear matter saturation density. The authors of [KHW08] calculated higher order corrections to this result and found the same linear trend for symmetric nuclear matter up to $\rho \simeq \rho_0$. For higher densities, the linear decreasing is softened and frozen to a reduction of 40% with respect to the vacuum value. For the pure neutron matter the higher order corrections calculated in [KW09] do not spoil the linear decrease of the quark condensate even for densities $\rho > \rho_0$.

Since the seminal works of Weinberg [We90, We91] it is known that the nucleon propagators do not always count as $1/k$, with k a typical nucleon three-momentum. Rather they often do as the inverse of a nucleon kinetic energy, m_N/k^2 (with the nucleon mass m_N). We could also say, they are unnaturally large or *enhanced*. This fact exposes the straightforward application of the pion-nucleon power counting valid in the vacuum, which is applied e.g. in [MOW02, PJM02, KFW02, KFW03, KFW05], as incomplete. As we already know from chapter 1, the long-range and the medium-range parts of the nuclear force are characterized by an interaction that is mediated by pions. The short-range force can effectively be described by local multi-nucleon interactions. In this chapter we derive an extended and newly organized power counting that takes into account all those multi-nucleon interactions simultaneous with the pion-nucleon dynamics from the nucleons' self-interactions (the so-called pion-cloud). In the following approach the important nucleon-nucleon dynamics are generated by applying Chiral Effective Field Theory to systems with nucleons and pions. No explicit mean fields are included, but this is not at odds with the mean-field models. Instead this approach is dynamical which should reproduce the physical effects of such mean fields in terms of the self-interactions of the included explicit degrees of freedom.

After this introduction we first wish to sketch the principles of quantized field theory in the nuclear medium, in particular for Chiral Perturbation Theory, in section 3.2. Then, in section 3.3, we derive the announced novel in-medium chiral power counting scheme for in-medium chiral effective field theory with explicit nucleonic and pionic degrees of freedom coupled to external sources. A summary and conclusions are given in section 3.4.

3.2 In-medium theory

We consider the ground state of nuclear matter which, under the action of any time dependent operator at asymptotic times, behaves as Fermi seas of nucleons. Since the Pauli exclusion principle allows only two fermions (one with spin-up and one with spin-down) in each momentum eigenstate, the normalized ground state $|\Omega\rangle$ is obtained by filling the momentum states up to a maximum value, the limiting *Fermi momentum* ξ_F, also called *Fermi limit* or *Fermi surface*

$$|\Omega\rangle = \prod_{\lambda;|\mathbf{k}|\leq\xi_F} a^\dagger(\mathbf{k}_\lambda)|0\rangle \ , \tag{3.1}$$

where λ is a place holder for additional quantum numbers like spin and isospin. In the limit that the volume of the system becomes infinite, we can replace sums over states by integrals

$$\rho_F = \frac{A}{V} = \frac{1}{V}\sum_{\lambda;|\mathbf{k}|\leq\xi_F} 1 = 4\int \frac{d^3\mathbf{k}}{(2\pi)^3}\,\theta(\xi_F - |\mathbf{k}|) = \frac{2\xi_F^3}{3\pi^2} \ . \tag{1.24}$$

Let us now generalize eq. (1.24) optionally to asymmetric and polarized matter. The *density* of a certain nucleon flavor $N = \{p, n\}$ with certain spin $s = \{\uparrow, \downarrow\}$ is just given by the sum of all states with the certain quantum numbers

$$\rho_{N,s} = \int \frac{d^3k}{(2\pi)^3}\theta(\xi_{N,s} - |\mathbf{k}|) = \frac{\xi_{N,s}^3}{6\pi^2} \ . \tag{3.2}$$

The sum over both spins gives the *nucleon density*

$$\rho_N = \rho_{N,\uparrow} + \rho_{N,\downarrow} \overset{u.m.}{=} \frac{\xi_N^3}{3\pi^2} \ , \tag{3.3}$$

with the last equality only holding for *u*npolarized *m*atter. The *nuclear matter density* is then given by the sum of both nucleon densities

$$\rho = \rho_p + \rho_n \ . \tag{3.4}$$

In the language of second quantization nuclear matter is described in terms of particles and holes [FW03]. The fermion field is given by

$$\hat{\psi}(\mathbf{x}) = \sum_{\lambda;\mathbf{k}} \psi_{\lambda;\mathbf{k}}(\mathbf{x})\, c_{\lambda;\mathbf{k}} \ , \tag{3.5}$$

where the fermion operator is defined by

$$c_{\lambda;\mathbf{k}} = \begin{cases} a_{\lambda;\mathbf{k}} & |\mathbf{k}| > \xi_F, \quad \text{particles} \\ b^\dagger_{\lambda;-\mathbf{k}} & |\mathbf{k}| < \xi_F, \quad \text{holes} \end{cases} \ . \tag{3.6}$$

The absence of a particle with momentum $+\mathbf{k}$ inside the Fermi sea implies that the system possesses a momentum $-\mathbf{k}$. Eq. (3.6) preserves the commutation and anticommutation rules

$$\{a_\mathbf{k}, b^\dagger_{\mathbf{k}'}\} = \{b_\mathbf{k}, a^\dagger_{\mathbf{k}'}\} = 0 \ , \qquad \{a_\mathbf{k}, a^\dagger_{\mathbf{k}'}\} = \{b_\mathbf{k}, b^\dagger_{\mathbf{k}'}\} = \delta_{\mathbf{k}\mathbf{k}'} \ . \tag{3.7}$$

The $a^\dagger$ and a operators create and destroy particles above the Fermi limit, while $b^\dagger$ and b operators create and destroy holes inside the Fermi sea. Correspondingly, the *free Hamilton operator* reads

$$\begin{aligned}\hat{H}_0 &= \sum_{\lambda;|\mathbf{k}|} \hbar\omega_k \, c^\dagger_{\lambda;\mathbf{k}} c_{\lambda;\mathbf{k}} \\ &= \underbrace{\sum_{\lambda;|\mathbf{k}|\geq\xi_F} \hbar\omega_k \, a^\dagger_{\lambda;\mathbf{k}} a_{\lambda;\mathbf{k}}}_{\text{particles}} - \underbrace{\sum_{\lambda;|\mathbf{k}|\leq\xi_F} \hbar\omega_k \, b^\dagger_{\lambda;\mathbf{k}} b_{\lambda;\mathbf{k}}}_{\text{holes}} + \underbrace{\sum_{\lambda;|\mathbf{k}|\leq\xi_F} \hbar\omega_k}_{\text{filled Fermi sea}} \ . \end{aligned} \tag{3.8}$$

Note, from now on we set $\hbar = 1$. In the absence of particles and holes, the energy is that of the filled Fermi sea. Creating a hole lowers the energy, whereas creating a particle raises the energy. If the total number of fermions is fixed particles and holes necessarily occur in pairs. Each particle-hole pair then has a net positive energy, showing that the filled Fermi sea represents indeed the ground state.

In order to obtain realistic results, one has to go beyond the free Fermi gas approximation. A field theoretical approach seems appropriate to calculate correlations between particles/holes. In particular, corrections beyond the linear density approximation arise from nucleon-nucleon correlations which transform the nucleonic Fermi gas into a nuclear Fermi liquid and therefore create a binding of nuclear matter. Also it enables access to the realm of calculating properties involving external sources in a well-established framework. For practical calculations in a quantum field theory the essential change while switching from vacuum to in-medium calculations is the propagator. A free particle in nuclear matter is only able to propagate above the Fermi surface while its momenta below are blocked, which is known as Fermi blocking. On the other hand, inside the momentum region of the Fermi sea a defect or *hole* is allowed to propagate freely. In this way, the full in-medium nucleon propagator consists of a particle propagating above the Fermi surface and a hole propagating below [FW03],

$$G_0(k)_{i_3} = \frac{\theta(|\mathbf{k}| - \xi_{i_3})}{k^0 - E(\mathbf{k}) + i\epsilon} + \frac{\theta(\xi_{i_3} - |\mathbf{k}|)}{k^0 - E(\mathbf{k}) - i\epsilon} \ . \tag{3.9}$$

The subscript i_3 refers to the third component of isospin of the nucleon, with $i_3 = +1/2$ for the proton and $-1/2$ for the neutron, and ξ_{i_3} is the corresponding Fermi momentum. Using the Cauchy principal value method we can write

$$\begin{aligned}&\theta(|\mathbf{k}| - \xi_{i_3}) \left[\frac{\mathcal{P}}{k^0 - E(\mathbf{k})} - i\pi\,\delta(k^0 - E(\mathbf{k}))\right] + \theta(\xi_{i_3} - |\mathbf{k}|) \left[\frac{\mathcal{P}}{k^0 - E(\mathbf{k})} + i\pi\,\delta(k^0 - E(\mathbf{k}))\right] \\ &= \frac{\mathcal{P}}{k^0 - E(\mathbf{k})} + i\pi\,\delta(k^0 - E(\mathbf{k}))\Big[2\,\theta(\xi_{i_3} - |\mathbf{k}|) - 1\Big] \ , \end{aligned} \tag{3.10}$$

and obtain a representation that contains a *free-space* and a *density-dependent* (or *Fermi sea insertion*) part

$$G_0(k)_{i_3} = \frac{1}{k^0 - E(\mathbf{k}) + i\epsilon} + 2\pi i\,\delta(k^0 - E(\mathbf{k}))\theta(\xi_{i_3} - |\mathbf{k}|) \ . \tag{3.11}$$

Both notations, eq. (3.9) and eq. (3.11), are useful and will be employed. We consider that isospin symmetry is conserved so that all the nucleon and pion masses are equal. The proton and neutron propagators can be combined in a common expression

$$G_0(k) = \sum_{i_3} \Big(\frac{1}{2} + i_3\tau_3\Big) G_0(k)_{i_3} \ , \tag{3.12}$$

where τ^i correspond to the Pauli matrices in isospin space.

In an expansion in terms of Feynman diagrams an interaction with the nucleons is represented by a nucleon line that is closed by a Fermi sea insertion. This leads to nucleonic closed loops, where the integration range in momentum space is limited to spheres due to the appearing Heaviside step functions (examples are given in appendix C.1.1). In this way, the framework of Chiral Perturbation Theory can be applied straightforwardly with a change of the free nucleon propagator to the full in-medium nucleon propagator. However, in order to obtain a fully systematic description we must take into account nucleon-nucleon interactions systematically, which is the topic of the next section.

3.3 Chiral power counting for nuclear matter[#1]

The effective chiral pion Lagrangian was determined in the nuclear medium in the presence of external sources in [Ol02]. For that the Fermi seas of protons and neutrons were integrated out making use of functional techniques. This approach was similar to that used in [GSS88] which was for the case of only one nucleon. In this way it is manifestly shown that pion or nucleon field redefinitions do not affect physical observables also in nuclear matter because they appear as integration variables in a functional. Nonetheless, in [Ol02] only the meson-baryon chiral Lagrangian is employed. More precisely, if we write a general chiral Lagrangian in terms of an increasing number of nucleon fields ψ,

$$\mathcal{L}_{\text{eff}} = \mathcal{L}_{\pi\pi} + \mathcal{L}_{\bar{\psi}\psi} + \mathcal{L}_{\bar{\psi}\bar{\psi}\psi\psi} + \dots \ , \tag{3.13}$$

only the contributions from $\mathcal{L}_{\pi\pi}$ and $\mathcal{L}_{\bar{\psi}\psi}$ were retained. Based on these results, the authors of [MOW02] derived a chiral power counting in the nuclear medium.

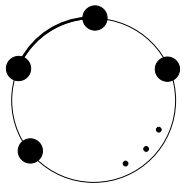

Figure 3.1: Representation of an "in-medium generalized vertex" (IGV). See the text for further details.

[Ol02] also establishes the concept of an "in-medium generalized vertex" (IGV). Such type of vertices result because one can connect several bilinear vacuum vertices through the exchange of baryon propagators with the flow through the loop of one unit of baryon number, contributed by the nucleon Fermi seas. This is schematically shown in fig. 3.1 where the thick arc segment indicates an insertion of a Fermi sea. At least one is needed because otherwise we would have a vacuum closed nucleon loop that in a low energy effective field theory is buried in the higher order chiral counterterms. On the other hand, a filled large circle in fig. 3.1 indicates a bilinear nucleon vertex from $\mathcal{L}_{\pi N}$, while the dots refer to the insertion of any number of them. It was also stressed in [MOW02] that within a nuclear environment a nucleon propagator could have a "standard" or "non-standard" chiral counting. To see this note that a soft momentum $Q \sim p$, related to pions or external sources attached to the bilinear vertices in fig. 3.1, can be associated to any of the vertices.

[#1] The contents of this section have been published in [LOMa]

Denoting by k the on-shell four-momenta associated with one Fermi sea insertion in the IGV, the four-momentum running through the j^{th} nucleon propagator can be written as $p_j = k + Q_j$. In this way,

$$i\frac{\not{k} + \not{Q}_j + m}{(k+Q_j)^2 - m^2 + i\epsilon} = i\frac{\not{k} + \not{Q}_j + m}{Q_j^2 + 2Q_j^0 E(\mathbf{k}) - 2\mathbf{Q}_j\mathbf{k} + i\epsilon} \ , \tag{3.14}$$

where $E(\mathbf{k}) = \mathbf{k}^2/2m$, with m the physical nucleon mass (not the bare one), and Q_j^0 is the temporal component of Q_j. We have just shown in the previous equation the free part of an in-medium nucleon propagator because this is enough for our present discussion. Two different situations occur depending on the value of Q_j^0. If $Q_j^0 = \mathcal{O}(m_\pi) = \mathcal{O}(p)$ one has the standard counting so that the chiral expansion of the propagator in eq. (3.14) is

$$i\frac{\not{k} + \not{Q}_j + m}{2Q_j^0 m + i\epsilon}\left(1 - \frac{Q_j^2 - 2\mathbf{Q}_j\cdot\mathbf{k}}{2Q_j^0 m} + \mathcal{O}(p)\right) \ . \tag{3.15}$$

Thus, the baryon propagator counts as a quantity of $\mathcal{O}(p^{-1})$. But it could also occur that Q_j^0 is of the order of a kinetic nucleon energy in the nuclear medium or that it even vanishes. The dominant term in eq. (3.14) is then

$$-i\frac{\not{k} + \not{Q}_j + m}{\mathbf{Q}_j^2 + 2\mathbf{Q}_j\cdot\mathbf{k} - i\epsilon} \ , \tag{3.16}$$

and the nucleon propagator should be counted as $\mathcal{O}(p^{-2})$, instead of the previous $\mathcal{O}(p^{-1})$. This is referred to as the "non-standard" case in [MOW02]. We should stress that this situation also occurs already in the vacuum when considering the two-nucleon reducible diagrams in nucleon-nucleon scattering. This is indeed the reason advocated in [We90] for solving a Lippmann-Schwinger equation with the nucleon-nucleon potential given by the two-nucleon irreducible diagrams. In the present investigation, we extend the results of [Ol02, MOW02] in a twofold way. i) We are able to consider chiral Lagrangians with an arbitrary number of baryon fields (bilinear, quartic, etc). First only bilinear vertices like in [Ol02, MOW02] are considered, but now the additional exchanges of heavy meson fields of any type are allowed. The latter should be considered as merely auxiliary fields that allow one to find a tractable representation of the multi-nucleon interactions that result when the masses of the heavy mesons tend to infinity. Such methods are also used in nuclear lattice simulations, see e.g. [Bo07]. These heavy meson fields are denoted in the following by H, see fig. 3.2, and a heavy meson propagator is counted as $\mathcal{O}(p^0)$ due to their large masses. ii) We take the non-standard counting from the start and any nucleon propagator is considered as $\mathcal{O}(p^{-2})$. In this way, no diagram whose chiral order is actually lower than expected if the nucleon propagators were counted assuming the standard rules is lost. This is a novelty in the literature.

In the following $m_\pi \sim k_F \sim \mathcal{O}(p)$ are taken of the same chiral order, and are considered much smaller than a hadronic scale Λ_χ of several hundreds of MeV that results by integrating out all other particle types, including nucleons with larger three-momentum, heavy mesons and nucleon isobars [We91]. The chiral order of a given diagram is represented by ν and is given by

$$\nu = 4L_H + 4L_\pi - 2I_\pi + \sum_{i=1}^{V} d_i - \sum_{i=1}^{V_\rho} 2m_i + \sum_{i=1}^{V_\pi} \ell_i + \sum_{i=1}^{V_\rho} 3 \ . \tag{3.17}$$

From left to right, L_H is the number of loops due to the internal heavy mesonic lines, L_π that of pionic loops and I_π is the number of internal pionic lines. Each loop introduces a factor of four in the power counting, because of the integration over the free four-momentum, and a pion propagator

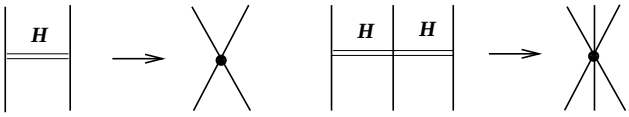

Figure 3.2: Representation of multi-nucleon interactions through the multiple exchange of heavy mesons H as described in the text.

reduces the order in two units. The quantity d_i is the chiral order of the i^{th} bilinear vertex in the baryonic fields and V is the total number of such vertices. V_ρ is the number of IGVs and m_i is the number of nucleon propagators in i^{th} IGV minus one, where every one of the latter reduces the chiral counting by two units according to the Weinberg counting. The definition of m_i contains the removal of one baryon propagator because there is always at least one Fermi sea insertion for each IGV that increases the chiral counting in three units because of the associated integration over a Fermi sea, $\int d^3k\,\theta(\xi_{i_3} - |\mathbf{k}|)$, with ξ_{i_3} the corresponding Fermi momentum. The last sum in the previous equation then results. Other symbols that appear are the chiral order ℓ_i of a vertex without baryons (only pions and external sources), and their total number V_π. In eq. (3.17) we have not included any contribution from π-H vertices without baryons, because in the limit where the mass of the H fields go to infinity, the H propagators are contracted to a point and the pions will always be attached to baryons.

Let us note that associated with the bilinear vertices in an IGV one has four-momentum conserving Dirac delta functions that can be used to fix the momentum of each of the baryonic lines joining them, except one for the running three-momentum due to the Fermi sea insertion. Let us now introduce another symbol, V_Φ. Here, we take as a whole any set of IGVs that are joined through *heavy* mesonic lines H, whose total number is I_H. The number of these clusters of in-medium generalized vertices is denoted by V_Φ. In this way, we can write

$$L_H = I_H - \sum_{i=1}^{V_\Phi} (V_{\rho,i} - 1) = I_H - V_\rho + V_\Phi \ , \tag{3.18}$$

where $V_{\rho,i}$ is the number of IGVs within the i^{th} set of generalized vertices connected by heavy mesonic lines. Additionally, they could be connected between them or with other IGVs belonging to other clusters by pionic lines. Since there is a total four-momentum conserving delta function associated to every of these clusters it follows that

$$L_\pi = I_\pi - V_\pi - V_\Phi + 1 \ . \tag{3.19}$$

These relations are illustrated in fig. 3.3 where a possible arrangement of IGVs is shown. On the other hand,

$$2I_H + 2I_\pi + E = \sum_{i=1}^{V} v_i + \sum_{i=1}^{V_\pi} n_i \ . \tag{3.20}$$

Here, v_i is the number of mesonic lines attached to the i^{th} bilinear vertex, n_i is the number of pions in the i^{th} mesonic vertex and E is the number of external pions. Taking into account eqs. (3.18), (3.19) and (3.20), eq. (3.17) reads ,

$$\nu = 2I_H - E + 4 - 4V_\pi + \sum_{i=1}^{V_\pi} (\ell_i + n_i) + \sum_{i=1}^{V} (d_i + v_i) - 2m - V_\rho \ , \tag{3.21}$$

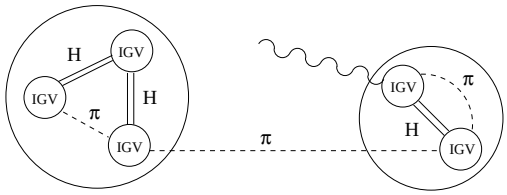

Figure 3.3: Representation of a possible arrangement of IGVs separated in two clusters. In this figure $V_\rho = 5$, $V_\Phi = 2$, $I_\pi = 3$, $I_H = 3$ and $E = 1$. The pions are indicated by the dashed lines and the external source by a wavy line. Eqs. (3.19) and (3.18) imply that $L_\pi = 2$ and $L_H = 0$ as it should.

with $m = \sum_{i=1}^{V_\rho} m_i$. We now employ in eq. (3.21) that $V_\rho + m = V$, and $2I_H = \sum_{i=1}^{V} w_i$, where w_i is the number of heavy meson internal lines for the i^{th} bilinear vertex. Then, we arrive at our final equation

$$\nu = 4 - E + \sum_{i=1}^{V_\pi}(n_i + \ell_i - 4) + \sum_{i=1}^{V}(d_i + w_i - 1) + \sum_{i=1}^{m}(v_i - 1) + \sum_{i=1}^{V_\rho} v_i \ . \tag{3.22}$$

Note that ν given in eq. (3.22) is bounded from below because $n_i + \ell_i - 4 \geq 0$, as $\ell_i \geq 2$ and $n_i \geq 2$, except for a finite number of terms that could contain only one pion line but always having external sources attached to them. Similarly $d_i + w_i - 1 \geq 0$. For the pion-nucleon Lagrangians this is always true as $d_i \geq 1$. For those bilinear vertices mediated by heavy lines $d_i \geq 0$ but then $w_i \geq 1$. For the term before the last one in eq. (3.22) $v_i - 1 \geq 0$, except for the higher-order nucleon-mass renormalization counter terms or the finite number of terms which would not have pionic lines but only external sources from $\mathcal{L}_{\pi N}$. The former terms have $d_i \geq 2$ and then $(d_i + w_i - 1) + (v_i - 1) \geq 0$. For $d_i = 2$ the chiral order does not increase but these terms can be absorbed in the physical nucleon mass. For the last term in eq. (3.22) $v_i \geq 0$ and then it is positive. It is worth stressing that adding a new IGV to a connected diagram increases the counting at least by one unit because then $v_i \geq 1$. Using again that $V_\rho + m = V$ eq. (3.22) can be rewritten as

$$\nu = 4 - E + \sum_{i=1}^{V_\pi}(n_i + \ell_i - 4) + \sum_{i=1}^{V}(d_i + w_i + v_i - 2) + V_\rho \ . \tag{3.23}$$

The number ν given in eq. (3.22) represents a lower bound for the actual chiral power of a diagram, μ, so that $\mu \geq \nu$. The actual chiral order of a diagram might be higher than ν because the nucleon propagators are counted always as $\mathcal{O}(p^{-2})$ to obtain eq. (3.22), while for some diagrams there could be propagators that follow the standard counting. Eq. (3.22) implies the following conditions for augmenting the number of lines in a diagram without increasing the chiral power by:

1. adding pionic lines attached to mesonic vertices, $\ell_i = n_i = 2$.
2. adding pionic lines attached to meson-baryon vertices, $d_i = v_i = 1$.
3. adding heavy mesonic lines attached to bilinear vertices, $d_i = 0$, $w_i = 1$.
4. adding nucleon mass renormalization terms, $d_i = 2$, $v_i = 0$.

There is no way to decrease the order. Only by adding vertices with $\ell_i = 2$ and $n_i < 2$ or $d_i = 1$ and $v_i = 0$. However, its number is bounded from above by the necessarily finite number of external sources. We apply eq. (3.22) by increasing step by step V_ρ up to the order considered. For each V_ρ we look for those diagrams that do not increase the order according to the previous list. Some of these diagrams are indeed of higher order and one can refrain from calculating them by establishing which of the nucleon propagators scale as $\mathcal{O}(p^{-1})$.

3.4 Summary and conclusions

We have motivated the necessity of a systemic power counting scheme for nuclear matter in section 3.1 and have reviewed some basic principles for field-theoretical calculations in a medium in section 3.2.

In section 3.3 we have developed a promising scheme for an Effective Field Theory in the nuclear medium that combines both short-range and pion-mediated inter-nucleon interactions. It is based on the development of a new chiral power counting which is bounded from below and at a given order it requires the calculation of a finite number of contributions. The latter could eventually involve infinite strings of two-nucleon reducible diagrams with the leading $\mathcal{O}(p^0)$ two-nucleon χPT amplitudes. As a result, our power counting accounts for non-perturbative effects to be resummed, which e.g. give rise to the generation of the deuteron in vacuum nucleon-nucleon scattering. The power counting from the onset takes into account the presence of enhanced nucleon propagators and it can also be applied to multi-nucleon forces.

For sure, calculations of physical processes at sufficiently high orders are needed to assess the realm of applicability of the present approach. In the following chapter there will be developed non-perturbative methods for the just mentioned necessary resummations. Then, in the subsequent chapters, some of the fundamental quantities of and in nuclear matter will be calculated up to next-to-leading order.

Chapter 4

Chiral effective theory for nucleon-nucleon interactions[#2]

To implement the power counting of the last chapter in actual calculations we will develop in this chapter non-perturbative methods based on Unitary Chiral Perturbation Theory that allow us to perform the required resummations. Simplifying our in-medium chiral power counting to the case of free interactions, it reduces to an analog of the well-known Weinberg power counting [We90, We91]. The difference is, that in our case the counting is directly applied to the physical amplitudes, while the original Weinberg counting applies to the potential only.

4.1 Introduction

In the last chapter we have derived a novel chiral power counting scheme for an effective field theory of nuclear matter with nucleons and pions as degrees of freedom. It allows for a systematic expansion taking into account both local (short-range) as well as pion-mediated (long-range) multi-nucleon interactions simultaneously. Notice that many present applications of Chiral Perturbation Theory to nuclei and nuclear matter [Ro89, OGN95, KW97, KFW02, MOW02, KFW03, KFW05, KOV06, KMW07, DO08] only consider meson-baryon Lagrangians. For instance, in [KFW02] (and subsequent activities) local nucleon-nucleon interactions were not explicitly included, instead they were accounted for by a fine-tuning of the cut-off parameter. On the other hand, in [LFA00] the in-medium local nucleon-nucleon interactions were explicitly included and fitted in terms of just one free parameter, in order to reproduce the saturation properties of symmetric nuclear matter. In all those approaches the free parameters were adjusted to fit to nuclear matter properties, while short-range interactions are included without being fixed from vacuum nucleon-nucleon scattering.

We implement here non-perturbative methods to perform actual calculations employing the power counting of eq. (3.23), which requires the resummation of some series of in-medium two-nucleon reducible diagrams. We employ the techniques of Unitary Chiral Perturbation Theory (UχPT), which were successfully applied to meson-meson [OO97, OO99] and meson-baryon [Ol00, OM01] systems. We extend those methods to the nuclear medium systematically in a way consistent with the chiral power counting of eq. (3.23).

[#2]The contents of this chapter have been published in [LOMb].

After this introduction we first consider nucleon-nucleon scattering in the vacuum in section 4.2 while developing our new non-perturbative methods. In section 4.3 we extend the framework to in-medium nucleon-nucleon interactions and will give some technical issues in section 4.4. We also provide a summary in section 4.5.

4.2 Free nucleon-nucleon interactions

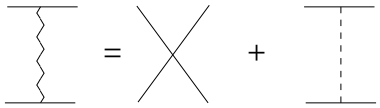

Figure 4.1: The exchange of a wiggly line between two nucleons corresponds to the sum of the local and the one-pion exchange contributions, eqs. (4.2) and (4.3), respectively.

The lowest order tree-level amplitudes for nucleon-nucleon scattering, $\mathcal{O}(p^0)$, are given by the one-pion exchange, with the lowest order pion-nucleon coupling, and local terms from the quartic nucleon Lagrangian without quark masses or derivatives

$$\mathcal{L}_{NN}^{(0)} = -\frac{1}{2}C_S(\bar{N}N)(\bar{N}N) - \frac{1}{2}C_T(\bar{N}\vec{\sigma}N)(\bar{N}\vec{\sigma}N) \ . \tag{4.1}$$

The fact that these are the leading tree-level contributions is a consequence of our counting eq. (3.23), which determines that the lowest order diagrams are those with $(d_i = 0, v_i = 1, \omega_i = 1)$ and $(d_i = 1, v_i = 1, \omega_i = 0)$. The former arises from the contact interaction Lagrangian, eq. (4.1), and the latter corresponds to the lowest order one-pion exchange. The tree-level scattering amplitude for $N_{s_1,i_1}(\mathbf{p}_1)N_{s_2,i_2}(\mathbf{p}_2) \to N_{s_3,i_3}(\mathbf{p}_3)N_{s_4,i_4}(\mathbf{p}_4)$ from eq. (4.1) is

$$\begin{aligned} T_{NN}^{c} = &- C_S\left(\delta_{s_3s_1}\delta_{s_4s_2}\,\delta_{i_3i_1}\delta_{i_4i_2} - \delta_{s_3s_2}\delta_{s_4s_1}\,\delta_{i_3i_2}\delta_{i_4i_1}\right) \\ &- C_T\left(\vec{\sigma}_{s_3s_1}\cdot\vec{\sigma}_{s_4s_2}\,\delta_{i_3i_1}\delta_{i_4i_2} - \vec{\sigma}_{s_3s_2}\cdot\vec{\sigma}_{s_4s_1}\,\delta_{i_3i_2}\delta_{i_4i_1}\right) \ , \end{aligned} \tag{4.2}$$

where s_m is a spin label and i_m an isospin one. Obviously, this amplitude only contributes to the nucleon-nucleon S-waves. The one-pion exchange tree-level amplitude is

$$T_{NN}^{1\pi} = \frac{g_A^2}{4f_\pi^2}\left[\frac{(\vec{\tau}_{i_3i_1}\cdot\vec{\tau}_{i_4i_2})(\vec{\sigma}\cdot\mathbf{q})_{s_3s_1}(\vec{\sigma}\cdot\mathbf{q})_{s_4s_2}}{\mathbf{q}^2 + m_\pi^2 - i\epsilon} - \frac{(\vec{\tau}_{i_4i_1}\cdot\vec{\tau}_{i_3i_2})(\vec{\sigma}\cdot\mathbf{q}')_{s_4s_1}(\vec{\sigma}\cdot\mathbf{q}')_{s_3s_2}}{\mathbf{q}'^2 + m_\pi^2 - i\epsilon}\right] \ , \tag{4.3}$$

with $\mathbf{q} = \mathbf{p}_3 - \mathbf{p}_1$ and $\mathbf{q}' = \mathbf{p}_4 - \mathbf{p}_1$. The corresponding nucleon-nucleon partial waves due to one-pion exchange can be calculated using eq. (A.28). Instead, we first take the one-pion exchange between nucleon-nucleon states with definite spin and isospin, so that eq. (A.28) simplifies to

$$N_{JI}^{1\pi}(\ell,\bar{\ell},S) = \frac{Y_{\bar{\ell}}^0(\hat{\mathbf{z}})}{2J+1}\sum_{\sigma_i,\sigma_f=-S}^{S}(0\sigma_i\sigma_i|\bar{\ell}SJ)(m\sigma_f\sigma_i|\ell SJ)\int d\hat{p}\,T_{\sigma_f\sigma_i}^{1\pi}(S,I)Y_\ell^m(\hat{p})^* \ , \tag{4.4}$$

where ℓ and $\bar{\ell}$ are the final and initial orbital angular momentum in the two-nucleon rest frame, respectively. Explicit expressions for $N_{JI}^{1\pi}(\ell,\bar{\ell},S)$ are given in appendix B. The sum of the local vertex, eq. (4.2), and the one-pion exchanges, eq. (4.3), is represented diagrammatically in the following by the exchange of a wiggly line, fig. 4.1.

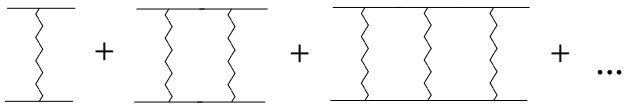

Figure 4.2: Resummation of the two-nucleon reducible diagrams. This is referred in the text as a resummation of the right-hand cut or unitarity cut.

Weinberg [We90, We91] argued that the two-nucleon reducible diagrams should be resummed because they are infrared enhanced (by large factors $\sim m/|\mathbf{p}_i|$) due to the large nucleon mass. This resummation, depicted in figure 4.2, is required by our power counting, eq. (3.23), when the latter is applied to the vacuum case as discussed at the end of section 3.3. Notice that every two-nucleon reducible loop in the string is connected by adding $\mathcal{O}(p^0)$ local interactions and the exchange of pionic-lines at the lowest order. As pointed out in the conditions 2) and 3) of section 3.3 the counting does not increase then. Rephrasing the discussion of this section to the present case, the nucleon propagators in a two-nucleon reducible loop follow the non-standard counting and each of them is $\mathcal{O}(p^{-2})$, so that altogether are $\mathcal{O}(p^{-4})$. The leading wiggly line exchange is $\mathcal{O}(p^0)$. When these two factors are multiplied by the $\mathcal{O}(p^4)$ contribution from the measure of the loop integrals, associated with the running momenta of the wiggly lines, an $\mathcal{O}(p^0)$ contribution results.The latter does not increase the chiral order and the series of diagrams in figure 4.2 must be resummed. One could argue that if the nucleon propagator is taken as $\mathcal{O}(p^{-2})$ for the two-nucleon reducible loops, then the measure could be taken as $\mathcal{O}(p^5)$, counting dp^0 as $\mathcal{O}(p^2)$. If this counting is followed, a suppression by an extra power of p seems to arise. However, this factor is multiplied by the large nucleon mass, so that mp finally results, which is then multiplied by local interactions. If the latter count as $\sim 1/mm_\pi$, the resummation would be required as well within this point of view. We show below that this is the case in our approach.

4.2.1 The methods of Unitary Chiral Perturbation Theory

We follow the techniques of UχPT [OO97, OO99, OM01] that performs this resummation partial wave by partial wave. Many recent nucleon-nucleon scattering analyses using χPT [ORK96, Ko99, EGM00, EM03, EGM05] follow [We90, We91] and solve the Lippmann-Schwinger equation in order to accomplish such resummation. UχPT has been applied with great success in meson-meson [OO99, OOR00, AO08] and meson-baryon scattering [OR98, OM01, BNW05, OPV05, BMN06, Ol06]. The master equation for UχPT is

$$T_{JI}(\ell,\bar{\ell},S) = \left[I + N_{JI}(\ell,\bar{\ell},S)\cdot g\right]^{-1}\cdot N_{JI}(\ell,\bar{\ell},S)\ . \tag{4.5}$$

This equation, derived in detail in [OO99, OM01, Ol03], results by performing a once-subtracted dispersion relation of the inverse of a partial wave amplitude. The function g is defined as follows. Let us denote by $\mathbf{p}$ the center-of-mass (CM) three-momentum of the nucleon-nucleon system. A nucleon-nucleon partial wave amplitude has two cuts [MS70], the right hand-cut for $\infty > \mathbf{p}^2 > 0$, due to unitarity, and the left-hand cut for $-\infty < \mathbf{p}^2 < -m_\pi^2/4$, due to the crossed channel dynamics. The upper limit for the latter interval is given by the one-pion exchange, as the pion is the lightest particle that can be exchanged. These cuts are represented in figure 4.3. Because of unitarity, a partial wave satisfies in the CM frame

$$\mathrm{Im}T_{JI}(\ell,\bar{\ell},S)^{-1}_{\ell,\bar{\ell}} = -\frac{m|\mathbf{p}|}{4\pi}\delta_{\ell\bar{\ell}}\ , \tag{4.6}$$

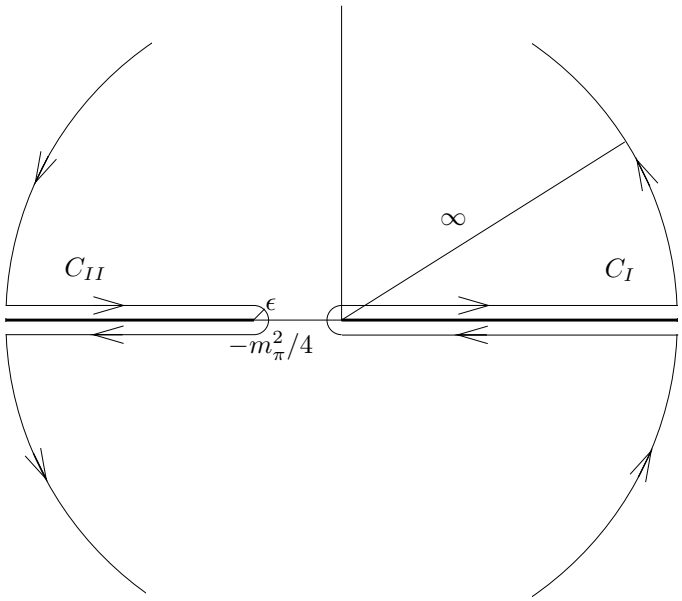

Figure 4.3: Right- and left-hand cuts of $T_{JI}(\ell,\bar{\ell},S)(\mathbf{p}^2)$, for $\mathbf{p}^2>0$ and $\mathbf{p}^2<-m_\pi^2/4$, in order. We have also indicated the integration contours C_I and C_{II} used for calculating $g(\mathbf{p}^2)$ and $N_{JI}(\ell,\bar{\ell},S)(\mathbf{p}^2)$, eqs. (4.7) and (4.16), respectively. The union of both contours $C_I\cup C_{II}$ is the one used for $T_{JI}^{-1}(\ell,\ell,S)(\mathbf{p}^2)$, eq. (4.19). In the calculation $\epsilon\to 0^+$.

above the elastic threshold and below the pion production one. The function g in eq. (4.5) only has a right-hand cut and its discontinuity along this cut is $2i$ times the right hand side of eq. (4.6). A once-subtracted dispersion relation can be written down given the degree of divergence of eq. (4.6) for $\mathbf{p}^2\to\infty$. The integration contour taken is a circle of infinite radius centered at the origin that engulfs the right-hand cut, as shown in fig. 4.3 by C_I. In this way

$$\begin{aligned} g(A) =& g(D)-\frac{m(A-D)}{4\pi^2}\int_0^\infty dk^2\frac{k}{(k^2-A-i\epsilon)(k^2-D-i\epsilon)}\\ =& g(D)-\frac{im}{4\pi}\left(\sqrt{A}-i\sqrt{|D|}\right)\\ \equiv& g_0-i\frac{m\sqrt{A}}{4\pi}\ . \end{aligned} \tag{4.7}$$

One subtraction has been taken at $D<0$ so that the integral is convergent. Note that the subtraction constant $g(D)$ is the value of $g(A)$ at $A=D$, in particular, $g_0=g(0)$. Since $g(\mathbf{p}^2)=\mathcal{O}(p^0)$, as discussed above, it follows that

$$g_0=g(0)=\mathcal{O}(p^0)\ . \tag{4.8}$$

The function $g(A)$ corresponds to the divergent integral

$$g(A)\to -m\int\frac{d^3k}{(2\pi)^3}\frac{1}{k^2-A-i\epsilon}\ . \tag{4.9}$$

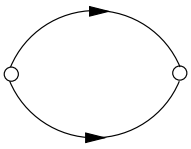

Figure 4.4: Unitarity loop corresponding to the function $g(A)$, eq. (4.9).

The previous integral, depicted in fig. 4.4, is linearly divergent although it shares the same analytical properties as eq. (4.7). In dimensional regularization with $D \to 3$ one has, $g(A) = -im\sqrt{A}/4\pi$. This result is purely imaginary above threshold, $A > 0$, and it corresponds to the imaginary part of eq. (4.7). However, this is just a specific characteristic of the regularization method employed, since, as it is explicitly shown in eq. (4.7), there is an undetermined constant g_0. For $A = 0$ the integral in eq. (4.9) is (infinitely-)negative, so that it is quite natural to assume that $g_0 < 0$. Another more fundamental reason for taking $g_0 < 0$, required by the consistency of the approach, is given below. In the following, we regularize any two-nucleon reducible loop in terms of the subtraction constant g_0, taking into account eqs. (4.7) and (4.8). This regularization method will be shown up-to-and-including next-to-leading order in the calculations performed in this chapter. For explicit calculations of loop integrals apart from $g(A)$ within this scheme see appendix C.3 and the calculation of the energy per nucleon, E/A in chapter 6.

Next, we discuss how to fix $N_{JI}(\ell, \bar{\ell}, S)$ in eq. (4.5). This function has only a left-hand cut, due to the exchange of pions in the chiral EFT (of course, in a meson-exchange calculation it would include further exchanges of other heavier mesons like ρ, ω, etc). It has no right-hand cut since it is fully incorporated in the function $g(A)$ by construction. As a result, N_{JI} should not be infrared enhanced since the effects of the large nucleon mass, associated with the two-nucleon reducible diagrams that give rise to the unitarity cut, are taken into account by eq. (4.5). Note that the latter results by integrating over the two-nucleon intermediate states at the level of the inverse of a partial wave, eq. (4.7). In a plain perturbative chiral calculation of a nucleon-nucleon partial wave the right-hand cut is not resummed and the convergence of the perturbative series is spoilt due to the infrared enhancement of the two-nucleon reducible loops. However, since the right-hand cuts are resummed in eq. (4.5), the idea is to match this general equation with a perturbative calculation within χPT up to the same number of two-nucleon reducible loops. The number must be the same to guarantee that N_{JI} is real along the physical region and fulfills the requirement of not having a right-hand cut. We can make use of the geometric series in powers of g of T_{JI}, eq. (4.5),

$$\begin{aligned} T_{JI}(\ell, \bar{\ell}, S) = {} & N_{JI}(\ell, \bar{\ell}, S) - N_{JI}(\ell, \bar{\ell}, S) \cdot g \cdot N_{JI}(\ell, \bar{\ell}, S) \\ & + N_{JI}(\ell, \bar{\ell}, S) \cdot g \cdot N_{JI}(\ell, \bar{\ell}, S) \cdot g \cdot N_{JI}(\ell, \bar{\ell}, S) + \dots \end{aligned} \tag{4.10}$$

where we have used the matrix notation $N_{JI} \cdot g$ for the case with coupled channels. Here, g just corresponds to the identity matrix times eq. (4.7), because the latter is the same for all partial waves. Together with the previous geometric series one also has the standard chiral expansion

$$N_{JI} = \sum_{m=0}^{n} N_{JI}^{(m)} \ , \tag{4.11}$$

with the chiral order indicated by the superscript. Now, for the determination of the different $N_{JI}^{(m)}$, $m \leq n$, the matching between eq. (4.10) is performed with a perturbative chiral calculation for which the reducible part of every two-nucleon reducible (or unitarity) loop is counted as $\mathcal{O}(p)$.

It is important to stress that this counting is applied for calculating N_{JI} not T_{JI}, for the latter each two-nucleon reducible loop counts as $\mathcal{O}(p^0)$, eq. (3.23). In this way, the matching up to a chiral order n automatically comprises at most n two-nucleon unitarity loops. In addition, the chiral order of the vertices employed will also make that no spurious imaginary parts are left since one is handling in the matching with perturbative unitarity up to order n.

A few examples will clarify this process of matching and why it makes sense to take as $\mathcal{O}(p)$ the reducible part of a two-nucleon reducible loop for calculating N_{JI} within UχPT. At lowest order, $n = 0$, there are no two-nucleon reducible loops and $N^{(0)}_{JI}(\ell, \bar{\ell}, S) = L^{(0)}_{JI}(\ell, \bar{\ell}, S)$, where the latter is the tree-level calculation in χPT at $\mathcal{O}(p^0)$ given by the sum of T^c_{NN}, eq. (4.2), and $T^{1\pi}_{NN}$, eq. (4.3), projected in the appropriate partial wave. This is the wiggly line at the far left of fig. 4.2. At $\mathcal{O}(p)$, $n = 1$, the only new contribution is the two-nucleon reducible part of the second diagram in fig. 4.2, denoted by $L^{(1)}_{JI}(\ell, \bar{\ell}, S)$ for a given partial wave. Writing $N_{JI} = N^{(0)}_{JI} + N^{(1)}_{JI} + \mathcal{O}(p^2)$, and matching eq. (4.10) with the sum of the first two diagrams of fig. 4.2 one has

$$N^{(0)}_{JI} + N^{(1)}_{JI} - N^{(0)}_{JI} \cdot g \cdot N^{(0)}_{JI} + \mathcal{O}(p^2) = L^{(0)}_{JI} + L^{(1)}_{JI} + \mathcal{O}(p^2) \ , \tag{4.12}$$

with the result

$$N^{(1)}_{JI} = L^{(1)}_{JI} + N^{(0)}_{JI} \cdot g \cdot N^{(0)}_{JI} \ . \tag{4.13}$$

Notice that in the expansion of eq. (4.10) each factor of the kernel $N_{JI}(\ell, \bar{\ell}, S)$ multiplies the loop function g with its value on shell. This is why in eq. (4.12) we have $-N^{(0)}_{JI} \cdot g \cdot N^{(0)}_{JI}$ for one iteration of g, which is then subtracted from the function $L^{(1)}_{JI}$ in eq. (4.13).

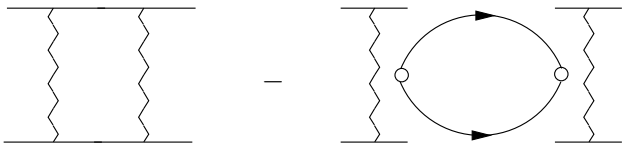

Figure 4.5: Diagrammatic representation of the next-to-leading order contribution to the interaction kernel, $N^{(1)}_{JI} = L^{(1)}_{JI} - \left(-N^{(0)}_{JI} \cdot g \cdot N^{(0)}_{JI}\right)$. Both diagrams share the same cut structure, therefore $N^{(1)}_{JI}$ is real below the pion threshold.

Eq. (4.13) shows explicitly that the simultaneous expansion in chiral powers and number of loops for fixing $N^{(n)}_{JI}$ implies that UχPT really takes as $\mathcal{O}(p)$ the difference between a full calculation of *one* two-nucleon reducible loop and the result obtained by factorizing the vertices on-shell, eq. (4.10). Ultimately this relies on the fact that the difference has no right-hand cut, which is the one associated with the infrared enhanced two-nucleon reducible loops, and it has only a left-hand cut. The latter is incorporated perturbatively in the interaction kernel $N_{JI}(\ell, \bar{\ell}, S)$, which is improved order by order. This is the reason why we have treated the expansion in two-nucleon reducible loops on the same foot as the chiral expansion. This procedure is repeated up to any desired order. E.g. at $\mathcal{O}(p^2)$ new contributions would arise that require the calculation of the irreducible part of the box diagram in fig. 4.2 and the reducible parts of the last diagram of fig. 4.2 with the wiggly line exchange iterated twice [Ka06]. In addition, there are also local interaction terms from the quartic nucleon Lagrangian and two-nucleon irreducible pion loops [Ka00, EGM00, EM03, EGM05, KMW07]. If we denote all these new contributions projected onto the corresponding partial wave by $L^{(2)}_{JI}(\ell, \bar{\ell}, S)$, the following equation results

$$N^{(2)}_{JI} = L^{(2)}_{JI} + N^{(1)}_{JI} \cdot g \cdot N^{(0)}_{JI} + N^{(0)}_{JI} \cdot g \cdot N^{(1)}_{JI} - N^{(0)}_{JI} \cdot g \cdot N^{(0)}_{JI} \cdot g \cdot N^{(0)}_{JI} \ . \tag{4.14}$$

The N_{JI} calculated up to some given order in the chiral expansion eq. (4.11) is then substituted in eq. (4.5). On the other hand, one can formally match eq. (4.5) with a perturbative chiral calculation of $T_{JI}(\ell, \bar{\ell}, S)$ for any value of the S-wave nucleon-nucleon scattering lengths because they enter parametrically in the calculation. This procedure gives rise to values of the low-energy constants C_S and C_T that are consistent with their ascribed $\mathcal{O}(p^0)$ scaling, see eq. (4.28) below. It is worth pointing out that eq. (4.5) is algebraic, so that the numerical burden for in-medium calculations is reduced tremendously.

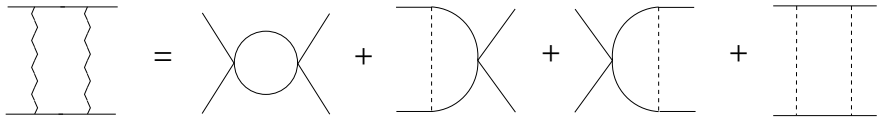

Figure 4.6: Box diagram, $L_{JI}^{(1)}$, originating from the first iteration of a wiggly line. It consists of the diagrams shown on the right-hand side of the figure with zero, one or two local vertices and/or one-pion exchange amplitudes.

4.2.2 On the subtraction constant g_0

The dependence on the parameter g_0 arises because of the infrared enhanced two-nucleon reducible loops. This has made necessary to resum the right-hand cut, which requires the presence of one subtraction constant, g_0, eq. (4.7). Indeed, for a fixed chiral order, according to the application of eq. (3.23) to nucleon-nucleon scattering in vacuum, the dependence on g_0 becomes smaller as higher powers of g are considered for calculating N_{JI}, eq. (4.11). To show this, we need to take advantage of the analytical properties of N_{JI}, eq. (4.5). As discussed above, this quantity has only the left-hand cut, shown in fig. 4.3. For the following discussion we take the case of one uncoupled channel to simplify the writing. Its generalization to coupled channels is straightforward employing a matrix notation. The imaginary part of N_{JI} along the left-hand cut is given by,

$$\mathrm{Im}N_{JI} = \frac{|N_{JI}|^2}{|T_{JI}|^2}\mathrm{Im}T_{JI} = |1 + gN_{JI}|^2\mathrm{Im}T_{JI} \ , \ |\mathbf{p}|^2 < -\frac{m_\pi^2}{4} \ . \tag{4.15}$$

Note that g is real along the left-hand cut. We employ this result to write down a once-subtracted dispersion relation for N_{JI}. The integration contour is shown in fig. 4.3 as C_{II} and consists of a circle of infinite radius centered at the origin that engulfs the left-hand cut.

$$N_{JI}(A) = N_{JI}(D) + \frac{A-D}{\pi}\int_{-\infty}^{-m_\pi^2/4} dk^2 \frac{\mathrm{Im}T_{JI}(k^2)\,|1 + g(k^2)N_{JI}(k^2)|^2}{(k^2 - A - i\epsilon)(k^2 - D)} \ , \tag{4.16}$$

We have taken one subtraction in the dispersion relation because the one-pion exchange amplitude, eq. (4.3), tends to a constant for $\mathbf{k}^2 \to \infty$. Then, we have for T_{JI}, eq. (4.5),

$$T_{JI}(A) = \left(\left[N_{JI}(D) + \frac{A-D}{\pi}\int_{-\infty}^{-m_\pi^2/4} dk^2 \frac{\mathrm{Im}T_{JI}\,|1 + gN_{JI}|^2}{(k^2 - A - i\epsilon)(k^2 - D)} \right]^{-1} + g(A) \right)^{-1} \ . \tag{4.17}$$

In order to solve eq. (4.16) one needs $\mathrm{Im}T_{JI}$ as input along the left-hand cut. χPT could be used, since this imaginary part is due to multi-pion exchanges. As a result one could afford its calculation perturbatively because the infrared enhancements associated with the right-hand cut are absent

in the discontinuity along the left-hand cut. The reason is because this discontinuity, according to Cutkosky's theorem [La59, Cu60], implies to put the pionic lines on-shell so that within loops the pion poles are picked up. Therefore, the energy along nucleon propagators now is of $\mathcal{O}(p)$, instead of a nucleon kinetic energy. In this way, the order of the diagram rises compared to that of the reducible parts and it becomes a perturbation. E.g., let us take as illustration the last diagram on the right hand side of fig. 4.6, corresponding to the twice iterated one-pion exchange. Its reducible part is infrared enhanced, which has been calculated by us in the presence of the nuclear medium, in agreement with [KBW97] when reduced to the vacuum case. However, its discontinuity across the left-hand cut arises by putting on-shell the two intermediate pion lines. Its leading contribution to ImT in a $1/m$ expansion in the t-channel CM frame is given by

$$\mathrm{Im}T = -\mathcal{N}\frac{(t/4-m_\pi^2)^{5/2}}{4\pi t^{3/2}}\ ,\ t>4m_\pi^2\ , \tag{4.18}$$

with $t=-2\mathbf{p}^2(1-\cos\theta)$, $\cos\theta\in[-1,1]$ and $\mathcal{N}$ is a numerical factor due to the spin algebra. No factor m appears in the numerator and it follows the standard chiral counting. In this way, the leading contribution to ImT_{JI} along the left-hand cut is given by the one-pion exchange. The latter can then be inserted in eq. (4.16), once projected in a given partial wave. The solution of this equation would correspond to the leading result for N_{JI} in the chiral expansion of eq. (3.23), without involving the expansion in the number of two-nucleon reducible loops. This interesting exercise will be left for future consideration.

Pion exchange amplitudes are treated perturbatively in the Kaplan-Savage-Wise (KSW) power counting [KSW98a, KSW98b, FMS00a, FMS00b]. This is done for any energy region and, in particular, along both the right- and left-hand cuts. On the other hand, the dispersive treatment offered here only needs as input the discontinuity (imaginary part) of a nucleon-nucleon partial wave along the left-hand cut, see eq. (4.17). This discontinuity arises due to pion exchanges which, as discussed in the previous paragraph, could be calculated perturbatively in χPT. Differences with respect to KSW arise due to the resummation of the right-hand-cut in eq. (4.17), including both local and pion-exchange contributions. This would correspond to higher orders in KSW power counting [FMS00a, FMS00b]. Notice also that while KSW is a strict perturbation theory calculation in quantum field theory (QFT) ours merges inputs from perturbative QFT and S-matrix theory, see e.g. ref. [Ba65] for a pedagogical account of first application of the similar N/D method to nucleon-nucleon scattering.

Two subtraction constants appear in eq. (4.17), $N_{JI}(D)$ from eq. (4.16) and g_0 from the function $g(A)$, eq. (4.7). We are going to show that they are not independent, however. The two constants have appeared due to the splitting between the functions N_{JI} and g when expressing $T_{JI}^{-1}=N_{JI}^{-1}+g$, eq. (4.5). This is analogous to the standard fact that in any renormalization scheme there is an exchange of contributions between local parts in loops and local counterterms. In order to proceed with the demonstration that the resulting T_{JI}, eq. (4.17), does not depend on the subtraction constant $g(D)$, let us write directly a dispersion relation for T_{JI}^{-1} taking the contour $C_I\cup C_{II}$ in fig. 4.3

$$\begin{aligned}T_{JI}^{-1}(A) = T_{JI}^{-1}(D) &- \frac{m(A-D)}{4\pi^2}\int_0^\infty dk^2\frac{k}{(k^2-A-i\epsilon)(k^2-D)}\\ &- \frac{(A-D)}{\pi}\int_{-\infty}^{-m_\pi^2/4}dk^2\frac{\mathrm{Im}T_{JI}/|T_{JI}|^2}{(k^2-A-\epsilon)(k^2-D)} - \frac{A-D}{(\ell-1)!}\frac{d^{\ell-1}}{d(k^2)^{\ell-1}}\frac{f_{JI}(k^2)}{(k^2-A)(k^2-D)}\Big|_{k^2=0}\ ,\end{aligned} \tag{4.19}$$

where $f_{JI}(\mathbf{p}^2) = |\mathbf{p}|^{2\ell} T_{JI}^{-1}(\mathbf{p}^2)$. The last term in the previous equation gives contribution for $\ell \geq 1$ and arises due to the behaviour at threshold of a partial wave, vanishing as $|\mathbf{p}|^{2\ell}$. Two-body unitarity is assumed all the way along the right-hand cut in the first integral. This is not essential for the discussion that follows and we could have written directly $\mathrm{Im}T_{JI}^{-1}$ along the right-hand cut, as done for the left-hand one. In eq. (4.19) we could use different subtraction points for the two integrals, e.g. B and D, respectively. One then has

$$T_{JI}^{-1}(A) = T_{JI}^{-1}(D) + \frac{m(D-B)}{4\pi^2}\int_0^\infty dk^2 \frac{k}{(k^2-D)(k^2-B)} - \frac{m(A-B)}{4\pi^2}\int_0^\infty dk^2 \frac{k}{(k^2-A-i\epsilon)(k^2-B)} - \frac{A-D}{\pi}\int_{-\infty}^{-m_\pi^2/4} dk^2 \frac{\mathrm{Im}T_{JI}/|T_{JI}|^2}{(k^2-A-i\epsilon)(k^2-D)} - \frac{A-D}{(\ell-1)!}\frac{d^{\ell-1}}{d(k^2)^{\ell-1}}\frac{f_{JI}(k^2)}{(k^2-A)(k^2-D)}\bigg|_{k^2=0} . \tag{4.20}$$

As discussed above the input for solving N_{JI} in eq. (4.16) is $\mathrm{Im}T_{JI}$ along the left-hand cut. This can also be shown explicitly from eq. (4.19) by writing $1/|T_{JI}|^2 = |N_{JI}^{-1} + g|^2$, as follows from eq. (4.5). Subtracting g from T_{JI}^{-1} we then arrive to the following equation for N_{JI}^{-1},

$$N_{JI}^{-1}(A) = T_{JI}^{-1}(D) - g(D) - \frac{(A-D)}{\pi}\int_{-\infty}^{-m_\pi^2/4} dk^2 \frac{\mathrm{Im}T_{JI}\,|N_{JI}^{-1}+g|^2}{(k^2-A-\epsilon)(k^2-D)} - \frac{A-D}{(\ell-1)!}\frac{d^{\ell-1}}{d(k^2)^{\ell-1}}\frac{f_{JI}(k^2)}{(k^2-A)(k^2-D)}\bigg|_{k^2=0} , \tag{4.21}$$

In the following we omit the last term in the previous equation for simplicity, since it does not depend on $g(D)$. The reader could include it straightforwardly if desired. If eq. (4.21) is solved by iteration, it is straightforward to show that T_{JI} does not depend on g_0 at any order in the iteration. The zeroth iterated solution is $N_{JI;0}^{-1} = T_{JI}^{-1}(D) - g(D)$, which yields $T_{JI;0}^{-1}(D) = T_{JI}^{-1}(D) - g(D) + g(A)$. Obviously, the sum $-g(D) + g(A)$ is independent of $g(D)$. For the first iterated solution one has

$$N_{JI;1}^{-1}(A) = T_{JI}^{-1}(D) - g(D) - \frac{A-D}{\pi}\int_{-\infty}^{-m_\pi^2/4} dk^2 \frac{\mathrm{Im}T_{JI}\,|T^{-1}(D) - g(D) + g(k^2)|^2}{(k^2-A-i\epsilon)(k^2-D)} . \tag{4.22}$$

Notice that only the combination $-g(D) + g(k^2)$ appears in the integral, which is independent of $g(D)$. However, $N_{JI;1}^{-1}$ depends explicitly on $g(D)$ due to the term before the integral. Nevertheless, given that $T_{JI;1}^{-1}(A) = N_{JI;1}^{-1}(A) + g(A)$, the first $g(D)$ on the right hand side of eq. (4.22) is accompanied again with $g(A)$ so that no dependence on $g(D)$ is left. This process can be straightforwardly generalized to any order. For the j^{th} iteration the combination $T^{-1}(D) - g(D)$ that appears in $N_{JI;j}^{-1}(A)$ before the integral is added to $g(A)$ for calculating $T_{JI;j}(A)$, so that no dependence on $g(D)$ arises from this fact. In addition, under the integration sign we have repeatedly j times the same term $T_{JI}^{-1}(D) - g(D) + g(k^2)$, which does not depend on $g(D)$.

From the previous discussion, one concludes quite confidently that no $g(D)$-dependence is left because this was the case for $T_{JI}(A)$ evaluated at any order in the iterative solution of $N_{JI}^{-1}(A)$, eq. (4.21). In this way, it is clear that one could interpret the constant $g(D)$, eq. (4.7), and the subtraction point D in close analogy with renormalization theory. The latter corresponds to the "renormalization scale" and the former fixes the "renormalization scheme". For a given $g(D)$ then $N_{JI}(D)$ is fixed so as to reproduce $T_{JI}(D)$ at the point $|\mathbf{p}^2| = D$. The dependence on $g(D)$ is then transmuted into the experimental input $T_{JI}(D)$. The final result should be independent of $g(D)$,

which in turn, by taking the derivative of T_{JI}^{-1}, eq. (4.17), with respect to this parameter implies the equation

$$\frac{\partial N_{JI}(D)}{\partial g(D)} = N_{JI}^2 - \frac{2(A-D)}{\pi}\int_{-\infty}^{-m_\pi^2/4} dk^2 \frac{\mathrm{Im}T_{JI}\,\mathrm{Re}\big[(g\partial N_{JI}/\partial g(D) + N_{JI})(1+N_{JI}^* g)\big]}{(k^2-A-i\epsilon)(k^2-D)} \ . \quad (4.23)$$

This discussion also shows that one always has the freedom to take g_0 to be the same for all the partial waves, as we have done.[#3] For higher partial waves it is convenient to derive the dispersion relation for $N_{JI}/|\mathbf{p}|^{2\ell}$ instead of eq. (4.17). In this way, the low energy behaviour of a partial wave as $|\mathbf{p}|^{2\ell}$ for $|\mathbf{p}| \to 0$ is ensured, independently of the approximation for $\mathrm{Im}T_{JI}$ [BGKT60]. The resulting expression is

$$N_{JI}(A) = \frac{A^\ell}{D^\ell} N_{JI}(D) + \frac{A^\ell(A-D)}{\pi}\int_{-\infty}^{-m_\pi^2/4} dk^2 \frac{\mathrm{Im}T_{JI}(k^2)\,|1+g(k^2)N_{JI}(k^2)|^2}{k^{2\ell}(k^2-A-i\epsilon)(k^2-D)} \ . \quad (4.24)$$

Note also that for $\ell \geq 1$ no subtraction is needed if $\mathrm{Im}T \sim const.(\mathrm{mod}\ log)$ for $k^2 \to \infty$, as in the one-pion exchange. Then, one could also rewrite the previous equation for $\ell \geq 1$ as

$$N_{JI}(A) = \frac{A^\ell}{\pi}\int_{-\infty}^{-m_\pi^2/4} dk^2 \frac{\mathrm{Im}T_{JI}(k^2)\,|1+g(k^2)N_{JI}(k^2)|^2}{k^{2\ell}(k^2-A-i\epsilon)} \ . \quad (4.25)$$

The degree of divergence of $\mathrm{Im}T_{JI}$ for $|\mathbf{p}| \to \infty$ increases by including higher order loop contributions, see e.g. eq. (4.18). As a result, more subtractions should be taken and the resulting subtraction constants could be related with higher order chiral counterterms.

We have proposed to consider g as $\mathcal{O}(p)$ in order to fix N_{JI}. Indeed, g is suppressed along the left-hand cut, vanishing in the low momentum region of the dispersive integral of eq. (4.16), which dominates its final value for low energy nucleon-nucleon scattering. On the physical Riemann sheet $|\mathbf{k}| = +i\kappa$, with $\kappa = \sqrt{-k^2} > 0$, and since g_0 is negative and of natural size $\sim -mm_\pi/4\pi$, it tends to cancel with $-im|\mathbf{k}|/4\pi = m\kappa/4\pi > 0$ and becomes zero for $\kappa = -4\pi g_0/m \sim m_\pi$. This is an important reason for having taken $g_0 < 0$ above. Proceeding along these lines, so that g is treated as relatively small along the left-hand cut, eq. (4.16) would simplify at leading order. On the one hand, $|1+gN_{JI}|^2$ is replaced by 1 and, on the other, $\mathrm{Im}T_{JI}$ is given by the one-pion exchange. Hence, one obtains for $N_{JI}^{(0)}$ in S-wave the sum of a constant plus one-pion exchange (resulting from the dispersive integral), precisely the content of the wiggly lines, fig. 4.1. For $\ell \geq 1$ let us take directly eq. (4.25). In this way, when neglecting gN_{JI}, the dispersive integral just gives rise to the one-pion exchange, as was the case for our previously calculated $N_{JI}^{(0)}$. One could continue further in this way, and solve eq. (4.16) in a power series expansion of g along the left-hand cut at each chiral order in the calculation of $\mathrm{Im}T_{JI}$. The truncation of such expansion leaves a residual g_0 dependence. We have followed the same point of view in order to determine N_{JI} through the matching process discussed above. Indeed, alternatively to performing the geometric series expansion of eq. (4.10),

[#3] There is an infinity of solutions of eq. (4.19) differing between each other in the number of zeros of T_{JI}. Each of these zeros is a pole of T_{JI}^{-1} so that it brings altogether as free parameters the position of the pole and its residue. They are the so-called Castillejo-Dalitz-Dyson (CDD) poles [CDD56]. The CDD poles are typically associated with resonances [Ma58, CDD56]. Notice that a pole in T_{JI}^{-1} typically makes its real part to vanish if the remnant is a smooth function of energy around the pole. In low energy S-wave meson-meson scattering the Adler zeros correspond to CDD poles [OO99]. However, for nucleon-nucleon scattering there is no evidence for a low energy zero in the partial waves (apart from the trivial one at threshold for $\ell \geq 1$.) In the pionless EFT for nucleon-nucleon interactions the third integration on the right hand side of eq. (4.19) is absent. The infinity tower of chiral counterterms in this EFT can be accounted for by adding CDD poles, see [OO99] where this is shown explicitly for a similar problem.

we could consider directly the inverse of T_{JI}, similarly as done in order to obtain eq. (4.15). Then, it follows from eq. (4.5) that

$$\begin{aligned}\frac{1}{T_{JI}} &= \frac{1}{N_{JI}} + g \ , \\ \frac{T^*_{JI}}{|T_{JI}|^2} &= \frac{N^*_{JI}}{|N_{JI}|^2} + g \ , \\ N_{JI} &= T_{JI}|1 + gN_{JI}|^2 - |N_{JI}|^2 g^* \ . \end{aligned} \tag{4.26}$$

The first method discussed above for determining N_{JI} is the perturbative solution of eq. (4.26) in a chiral series of powers of g. The solutions of eqs. (4.26) and (4.16) employing the perturbative method are equivalent because N_{JI} from eq. (4.26) has only a left-hand cut, being its imaginary part along this cut the same as eq. (4.15), and it is analytical, so that it satisfies the perturbative version in power of g of the dispersion relation eq. (4.16). We have shown this equivalence explicitly for $N^{(0)}_{JI}$. It is also straightforward to show it for $N^{(1)}_{JI}$. The following remark is in order. The perturbative solution in the chiral expansion of powers of g of eq. (4.26) has the advantages over solving eq. (4.16) that it is algebraic and the chiral counterterms in T_{JI} are taken into account in the solution N_{JI} in a straightforward manner. It is also versatile: it be straightforwardly be corrected by initial and final state interactions and extended to the nuclear medium. Notice that eq. (4.26) can only be solved perturbatively since the input T_{JI} is calculated in CHPT and only fulfills unitarity perturbatively. However, the exact solution of the integral equation eq. (4.16) has the advantage of not requiring the expansion in powers of g but just the chiral series on $\mathrm{Im}T_{JI}$ along the left-hand cut, and the latter expansion rests in a sound basis as discussed above.

4.2.3 Fixing low-energy constants

We now concentrate on fixing the constants C_S and C_T from the local quartic nucleon Lagrangian, eq. (4.1). These constants and g_0, eq. (4.8), are the only free parameters that enter in the evaluation of the nucleon-nucleon scattering amplitudes from eq. (4.5) up to $\mathcal{O}(p)$. We first discuss the leading order result and then the next-to-leading order one. C_S and C_T are fixed by considering the S-wave nucleon-nucleon scattering lengths a_t and a_s for the triplet and singlet channels, respectively. At $\mathcal{O}(p^0)$ we have at threshold

$$\begin{aligned} T_{01}(0,0,0) &= \frac{-(C_S - 3C_T)}{1 - g_0(C_S - 3C_T)} \ , \\ T_{10}(0,0,1) &= \frac{-(C_S + C_T)}{1 - g_0(C_S + C_T)} \ . \end{aligned} \tag{4.27}$$

The triplet S-wave is elastic at this energy, without mixing with the ${}^3D_1$ partial wave, because of the vanishing of the three-momentum. The resulting expressions for the scattering lengths from eq. (4.27) imply that

$$\begin{aligned} C_S &= \frac{m}{16\pi} \frac{16\pi g_0/m + 3/a_s + 1/a_t}{(g_0 + m/(4\pi a_s))(g_0 + m/(4\pi a_t))} \ , \\ C_T &= \frac{m}{16\pi} \frac{1/a_s - 1/a_t}{(g_0 + m/(4\pi a_s))(g_0 + m/(4\pi a_t))} \ . \end{aligned} \tag{4.28}$$

One of the benchmark characteristics of nucleon-nucleon scattering are the large absolute values of the S-wave scattering lengths $a_s = -23.758 \pm 0.04$ fm and $a_t = 5.424 \pm 0.004$ fm, so that

$m_\pi \gg |1/a_s|, 1/a_t$. Given the expression for the imaginary part of $g(A)$ above threshold in eq. (4.7) one can estimate that $g_0 \sim -mm_\pi/4\pi \sim -0.54\ m_\pi^2$, as explicitly shown in the second line of eq. (4.7) one can trade between the subtraction constant and $-im\sqrt{A}/4\pi$ just by changing the subtraction point. In a natural way, both should be taken of similar size for estimations. g_0 is then much larger in absolute value than $m/(4\pi|a_s|)$ and $m/(4\pi a_t)$, although there is a difference because a_t is smaller by around a factor 4 than $|a_s|$. As a result, it follows from eq. (4.28) that $|C_S| \sim 1/|g_0| \gg |C_T| = \mathcal{O}(m/16\pi a_t g_0^2)$. In this way, the low-energy constants C_S and C_T do not diverge for a_s, $a_t \to \infty$ and after iteration it is still consistent to treat $\mathcal{L}_{NN}^{(0)}$, eq. (4.1), as $\mathcal{O}(p^0)$. Notice as well that the one loop iteration of the contact terms compared in absolute value with the tree level goes like $-m|\mathbf{p}|(C_S - (4S-1)C_T)/4\pi$, taking into account the expression for $g(A)$ given in eq. (4.7). The three-momentum is divided by the scale $\sim -4\pi/mC_S \sim m_\pi$, considering the just given estimates for $C_S \sim 1/g_0$ and $g_0 \sim -mm_\pi/4\pi$. This justifies to iterate these diagrams for $|\mathbf{p}| = \mathcal{O}(p)$ as discussed above. For the case of the once-iterated pion exchange one would have the factor $m|\mathbf{p}|g_A^2/16\pi f_\pi^2$ as compared with the tree level one-pion exchange. Then $|\mathbf{p}|$ is divided by the scale $16\pi f_\pi^2/mg_A^2 \sim 2m_\pi = \mathcal{O}(p)$, and the one-pion exchange should be as well iterated together with the lowest order contact terms. The issue of iterating potential pions is analyzed in detail in [FMS00a, FMS00b], in order to understand the failure of Kaplan-Savage-Wise (KSW) power counting in some triplet channels, particularly, for the ${}^3S_1$-${}^3D_1$ and ${}^3P_{0,2}$ channels. The authors of [FMS00a, FMS00b] conclude that for some spin triplet channels the summation of potential pion diagrams is necessary to reproduce observables, while for the singlet channels this iteration does not seem to be a significant improvement over treating pion exchanges perturbatively.

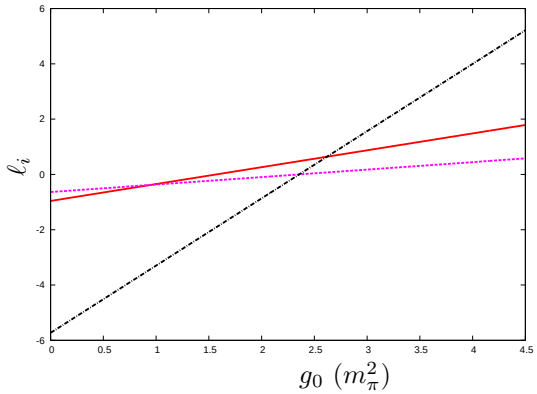

Figure 4.7: Values for ℓ_1 (red solid line), $\ell_2({}^1S_0)$ (magenta dashed line) and $\ell_2({}^3S_1)$ (cyan dot-dashed line) as a function of g_0. ℓ_2 is expressed in units of m_π^{-2}.

Only local terms and one-pion exchange contributions enter in the calculation of $N_{JI}^{(0)}(\ell, \bar{\ell}, S)$. This is rather simplistic in order to describe properly the nucleon-nucleon interactions as a function of energy soon above threshold. Let us now consider eq. (4.5) with N_{JI} up to $\mathcal{O}(p)$. At this order, $\mathrm{Im}T_{JI}$ along the left-hand cut is still given by the one-pion exchange, so that the exact solution of eq. (4.16) for N_{JI} would be the same. The differences observed in the results at $\mathcal{O}(p^0)$ and $\mathcal{O}(p)$ are then due to keep a one more factor g in the perturbative solution of eq. (4.16). This discussion shows clearly the mixed nature of the chiral expansion in powers of g for obtaining N_{JI}.

We employ the ${}^1S_0$ and ${}^3S_1$ scattering lengths for evaluating C_S and C_T at $\mathcal{O}(p)$. We denote by a any of these scattering lengths and apply eq. (4.5) at threshold. We obtain

$$a = -\left.\frac{1}{k}\frac{\mathrm{Im}T_{JI}}{\mathrm{Re}T_{JI}}\right|_{k\to 0} = -\frac{m}{4\pi}\frac{N_{JI}}{1+g_0 N_{JI}}\ . \tag{4.29}$$

Taking eq. (4.13) at threshold we rewrite $N_{JI}^{(0)} = -C$ and express $L_{JI}^{(1)} \equiv -C^2 g_0 + C\ell_1 + \ell_2$ because the box diagram $L_{JI}^{(1)}$, fig. 4.6, consists of four contributions with two, one and zero local vertices. The first contribution is given by $-C^2 g_0$, the second by $C\ell_1$ and the last one by ℓ_2, respectively. The coefficients ℓ_1 and ℓ_2 are given in terms of g_0 and the known parameters m, g_A and m_π. ℓ_1 is the same for the partial waves ${}^1S_0$ and ${}^3S_1$ while ℓ_2 is different. The values of ℓ_1 and ℓ_2 as a function of g_0 are shown in fig. 4.7. Substituting these expressions in eq. (4.29)

$$C = \frac{C^{(0)} + \ell_2}{1 - \ell_1} \,, \tag{4.30}$$

with $C^{(0)} = 1/(\frac{m}{4\pi a} + g_0)$ the $\mathcal{O}(p^0)$ result.

4.2.4 Phase shifts in free nucleon-nucleon scattering

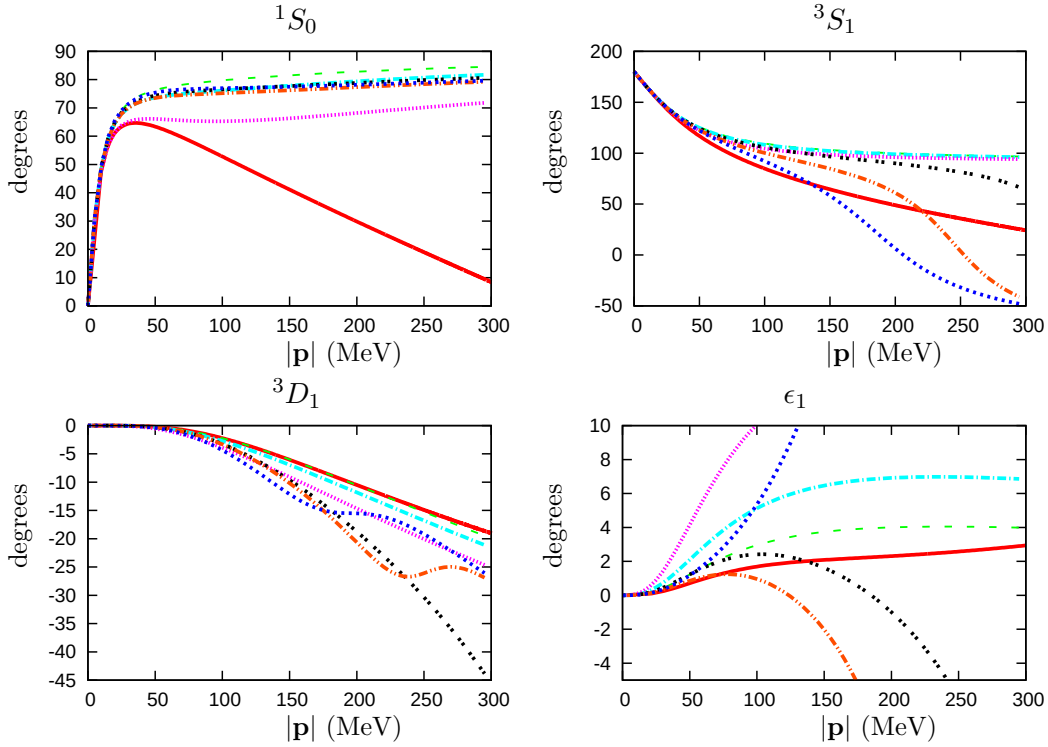

Figure 4.8: ${}^1S_0$, ${}^3S_1$, ${}^3D_1$ phase shifts and the mixing angle ϵ_1 as a function of $|\mathbf{p}|$. The (red) solid lines correspond to the Nijmegen data [SKRS93, SKTS94, NNO]. For the rest of the lines three values of $g_0 = -(1/4)m_\pi^2$, $-(1/3)m_\pi^2$ and $-(1/2)m_\pi^2$ are employed. For the leading order these lines are the (green) dashed,(cyan) dot-dashed and (magenta) dotted lines, respectively. While to next-to-leading order these are the (black) double-dotted, (orange) double-dot-dashed and (blue) short-dashed lines, in that order.

In figs. 4.8, 4.9 and 4.10 we show the leading and next-to-leading order results for the nucleon-nucleon scattering data (phase shifts and mixing angles) up to $|\mathbf{p}| = 300$ MeV making use of eq. (4.5). Since C_S at leading order is close to $1/g_0$, as explained above, we show the results for the values $g_0 = -(1/4)m_\pi^2$, $-(1/3)m_\pi^2$ and $-(1/2)m_\pi^2$ because its inverses are $-4m_\pi^{-2}$, $-3m_\pi^{-2}$ and $-2m_\pi^{-2}$, respectively. In this way, the resulting C_S at leading order is of order m_π^{-2}, a natural size. E.g. employing the estimation for $g_0 \simeq -0.54 m_\pi^{-2}$, given below eq. (4.28), one would obtain

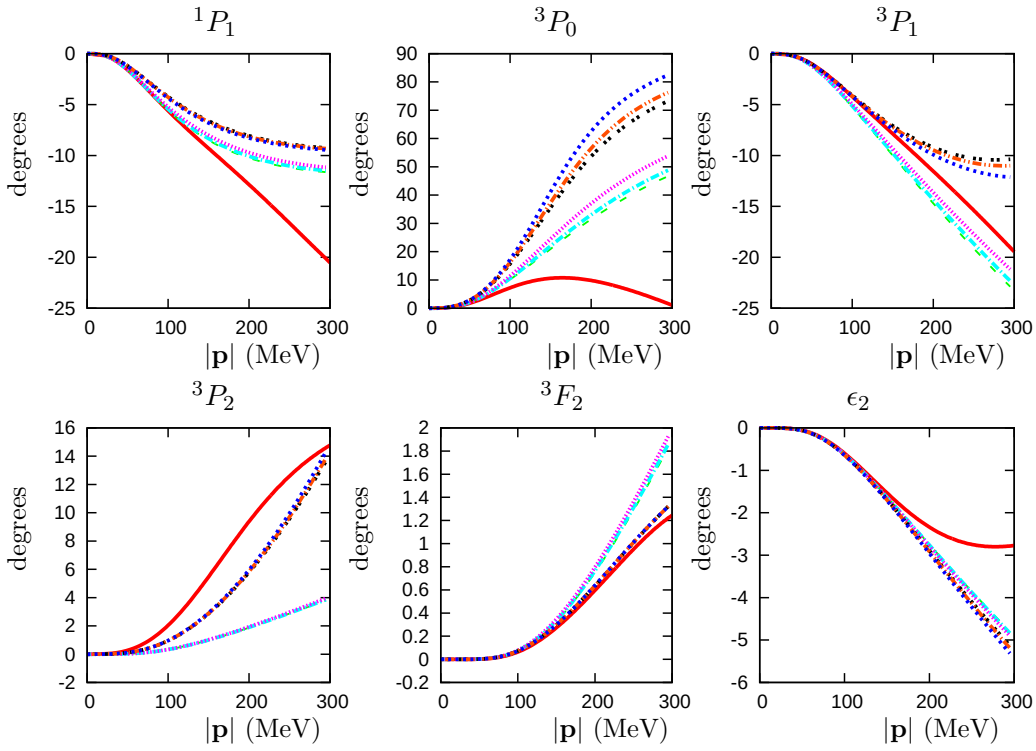

Figure 4.9: $^1P_1$, $^3P_0$, $^3P_1$, $^3P_2$, $^3F_2$ phase shifts and the mixing angle ϵ_2 as a function of $|\mathbf{p}|$. For notation, see fig. 4.8.

$1/g_0 \sim -1.8 m_\pi^{-2}$. On the other hand, let us recall that negative values for g_0, and not far from $-0.5 m_\pi^2$, are the required ones in order to optimize the perturbative solution of eq. (4.16). For the leading order results the lines are the dashed, dot-dashed and dotted lines, corresponding to $g_0 = -(1/4)m_\pi^2$, $-(1/3)m_\pi^2$ and $-(1/2)m_\pi^2$, respectively. While to next-to-leading order these are the double-dotted, double-dot-dashed and short-dashed lines, in the same order. For $|\mathbf{p}| \simeq 360$ MeV the pion production threshold opens and it does not make sense to compare with data above this point, particularly with the simple input employed for N_{JI}. At least an $\mathcal{O}(p^2)$ calculation, which includes important new physical mechanisms, as non-reducible two-pion exchanges between others, as indicated above before eq. (4.14), is presumably needed. E.g., it is well known that for the $^1S_0$ partial wave an $\mathcal{O}(p^2)$ chiral counterterm, in the standard chiral counting,[#4] is required in order to reproduce its relatively large effective range so that the agreement with data improves. This can be understood by considering the effective range expansion. For the $^1S_0$ partial wave $1/a_s$ is extremely small so that the contribution from the effective range $r_0\mathbf{p}^2/2$ rapidly overcomes $-1/a_s$ (the leading order contribution). Then, this problem is not so much related to the fact of having too large higher order corrections but more it arises because the leading order is anomalously small. The largest differences in absolute values between the leading and next-to-leading order results are observed in the $^3S_1$-$^3D_1$ and $^3P_0$ partial waves. These partial waves, as discussed in depth in [FMS00a, FMS00b], have large non-analytic corrections from two potential-pion-exchange. For the $^3P_1$, $^3P_2$ and $^3D_3$ waves the difference in absolute terms is small, a few degrees, although relatively it can be large typically for $|\mathbf{p}| \gtrsim 150$ MeV. For higher partial waves these differences are typically much smaller since the iteration of one-pion exchange becomes smaller [KBW97]. Our

[#4] At $\mathcal{O}(p^0)$ in the KSW counting [KSW98a, KSW98b].

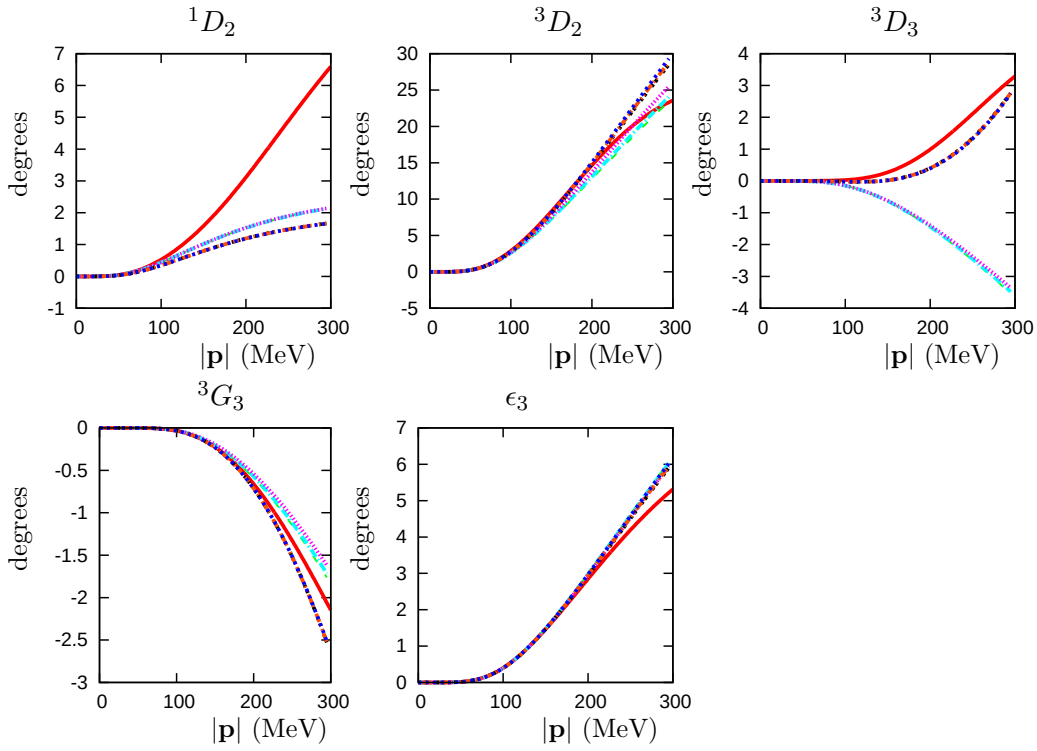

Figure 4.10: $^1D_2$, $^3D_2$, $^3D_3$, $^3G_3$ phase shifts and the mixing angle ϵ_3 as a function of $|\mathbf{p}|$. For notation, see fig. 4.8.

$\mathcal{O}(p)$ results are of comparable quality to those obtained at leading order within the Weinberg's counting approach [EGM00, EGM05]. The $^3P_0$ phase shifts are also not well reproduced at this order in [EGM00, EGM05]. Both approaches share the same input for $\mathrm{Im}T_{JI}$ along the left-hand cut, and at $\mathcal{O}(p)$ we have already considered the iteration of one g factor in determining N_{JI}, as discussed above. The main differences between our results and [EGM00, EGM05] at leading order concern ϵ_1 and the phase shifts for $^3P_1$ and $^3D_3$. For the latter our results are closer to experiment while for the two former observables the leading order calculation of [EGM00, EGM05] is closer to data. It is known that one-pion exchange has a too large tensor force which is reduced by higher order counterterms. In the meson exchange picture this cancellation at short distances of the one-pion exchange tensor force is produced by the exchange of ρ-mesons [BM94]. The mixing $^3S_1$-$^3D_1$ and the partial wave $^3P_0$ have large attractive matrix elements of the one-pion exchange tensor operator, as stressed in [NTK05, MLEA10]. These are the partial waves that depart more from data in absolute terms. The $^3P_0$ phase shifts were reproduced accurately in [NTK05] at leading order for low energies. In this reference, a counterterm was promoted to the leading order in all the partial waves with attractive tensor interactions. The results are cut-off independent for high enough values of the employed cut-off [NTK05, EM06].

As a result of the perturbative approach actually followed in this paper for determining N_{JI} by solving eq. (4.26) in an expansion in the number of two-nucleon reducible loops, a residual dependence on g_0 is left in the solution due to higher orders in this expansion (and not from the pure chiral one, eq. (3.23)). As more orders are included the exact solution of T_{JI}, obtained by solving eq. (4.16), is better approached and any dependence on g_0 should tend to vanish. From here one could also infer that contributions with one-pion exchange twice iterated in N_{JI} are expected to

be significant at least in those observables with a clear g_0 dependence in figs. 4.8-4.10. It is also worth noticing that the dependence on g_0 in figs. 4.8-4.10 at leading and next-to-leading order is much smaller for the P- and higher partial waves than for the S-waves. This should be expected because N_{JI} for $\ell \geq 1$ vanishes at threshold as $|\mathbf{p}|^{2\ell}$ so that both g and N_{JI} are small in the low energy part of the left-hand cut. In this way the perturbative solution of eq. (4.16) should typically converge faster for higher ℓ. Conversely, the convergence of the S-waves should be slower, something that it is clear for the ${}^3S_1 - {}^3D_1$ coupled channels from fig. 4.8. Particularly noticeable is the dependence on g_0 of ϵ_1, a fact that is in agreement with the results of Fleming, Mehen and Stewart [FMS00a, FMS00b]. The squared points in the panel for ϵ_1 in fig. 4.8 are obtained with $g_0 = -0.1\ m_\pi^2$. They agree closely with data [SKRS93, SKTS94], though such good agreement seems to be accidental.

4.3 In-medium nucleon-nucleon interactions

In order to perform calculations in the nuclear medium, one has to replace the free nucleon propagator with the full in-medium nucleon propagator of eqs. (3.9) or (3.11) in all instances of the calculation. When calculating a loop function in the nuclear medium we typically use the notation L_{ij}, where i indicates the number of two-nucleon states in the diagram (0 or 1) and j the number of pion exchanges (0, 1 or 2). In addition, we also use $L_{ij,f}$, $L_{ij,m}$ and $L_{ij,d}$, with the subscripts f, m and d indicating zero, one or two Fermi-sea insertions from the nucleon propagators in the nuclear medium, respectively. In this way, the function $g = L_{10,f}$ and its in-medium counterpart is

$$\begin{aligned} L_{10} &\doteq L_{10,f} + L_{10,m} + L_{10,d} \\ &\doteq L_{10,pp} + L_{10,hh} \ , \end{aligned} \tag{C.1}$$

depending whether we employ the free-space–density-dependent representation or the particle–hole representation of the nucleon propagators. Both are calculated in appendix C.2. Note that the full in-medium propagator also enters the calculation of N_{JI}.

The evaluation of the nucleon-nucleon scattering amplitudes in the nuclear medium at lowest order can be easily obtained from our previous result in the vacuum since the only modification without increasing the chiral order corresponds to use the full in-medium nucleon propagators. This is directly accomplished by replacing $g(A)$ by L_{10} in eq. (4.5). At any order for nucleon-nucleon scattering in the nuclear medium, we use eq. (4.5) but now with the function g substituted by L_{10} so that

$$T^{i_3}_{JI}(\ell, \bar{\ell}, S) = \left[I + N^{i_3}_{JI}(\ell, \bar{\ell}, S) \cdot L^{i_3}_{10} \right]^{-1} \cdot N^{i_3}_{JI}(\ell, \bar{\ell}, S) \ . \tag{4.31}$$

In eq. (4.31) we have included the superscript i_3, which corresponds to the third component of the total isospin of the two nucleons involved in the scattering process, both in the partial wave $T^{i_3}_{JI}(\ell, \bar{\ell}, S)$ and in $L^{i_3}_{10}$, as the Fermi momentum of the neutrons and protons are different for asymmetric nuclear matter. The function $L^{i_3}_{10}$ conserves total isospin I, because it is symmetric under the exchange of the two nucleons, though it depends on the charge (or third component of the total isospin) of the intermediate state. This is a general rule, all the $i_3 = 0$ operators are symmetric under the exchange $p \leftrightarrow n$, so that they do not mix isospin representations with different exchange symmetry properties.

The same mechanism as discussed in section 4.2 is followed to fix N_{JI} in the nuclear medium. Note that any other in-medium contribution requires $V_\rho = 1$, which increases the chiral order at least by

one more unit, cf. eq. (3.22). This new in-medium generalized vertex must be associated with the nucleon-nucleon scattering diagrams of leading order. The modification of the meson propagators (both heavy and pionic ones) by the inclusion of an in-medium generalized vertex increases the chiral order by two units. However, the modification of the enhanced nucleon propagators with one in-medium generalized vertex only increases the order by one unit and these contributions must be kept at next-to-leading order. It goes beyond the scope of this work to offer a complete study of all presented processes at next-to-next-to-leading order ($\mathrm{N^2LO}$) where the full next-to-leading order in-medium nucleon-nucleon interactions are needed. It will be pointed out in the corresponding chapters how far we calculate in the chiral expansion.

4.4 Derivatives and production processes

For practical calculations one will need derivatives of the scattering amplitudes and so-called generic "production" processes, where external sources are coupled inside a two-nucleon reducible loop. In the following, we will derive expressions for both. These are valid for calculations both in the nuclear medium and the vacuum, employing the corresponding master equation eq. (4.31) alternatively eq. (4.5).

4.4.1 Derivatives of the scattering amplitude

For calculations in the nuclear medium we will require several derivatives of the scattering amplitude. For that, let us obtain the generell expressions for the derivative of $\partial T_{JI}/\partial X$ with arbitrary X. We rewrite eqs. (4.5) or (4.31) as

$$T_{JI} = N_{JI} - N_{JI} \cdot L_{10} \cdot T_{JI} \ . \tag{4.32}$$

Taking the derivative on both sides of the previous equation and isolating $\partial T_{JI}/\partial X$,

$$\frac{\partial T_{JI}}{\partial X} = D_{JI}^{-1} \cdot \left[\frac{\partial N_{JI}}{\partial X} - \left(\frac{\partial N_{JI}}{\partial X} \cdot L_{10} + N_{JI} \cdot \frac{\partial L_{10}}{\partial X} \right) \cdot D_{JI}^{-1} \cdot N_{JI} \right] \ , \tag{4.33}$$

with

$$D_{JI}^{i_3}(\ell, \bar{\ell}, S) = I + N_{JI}^{i_3}(\ell, \bar{\ell}, S) \cdot L_{10}^{i_3} \ , \tag{4.34}$$

the same matrix whose inverse is multiplying $N_{JI}(\ell, \bar{\ell}, S)$ in eqs. (4.5) or (4.31). Eq. (4.33) can be simplified by dragging taking N_{JI} through D_{JI} so that

$$\frac{\partial T_{JI}}{\partial X} = [D_{JI}]^{-1} \cdot \left[\frac{\partial N_{JI}}{\partial X} - N_{JI} \cdot \frac{\partial L_{10}}{\partial X} \cdot N_{JI} \right] \cdot [D_{JI}^{r}]^{-1} \ , \tag{4.35}$$

where the superscript r denotes the reversed order of N_{JI} and L_{10} just in case they do not commute. If L_{10} is proportional to the unit matrix, i.e. there is no breaking of flavor symmetry involved, L_{10} and N_{JI} commute and we have

$$\frac{\partial T_{JI}}{\partial X} = [D_{JI}]^{-1} \cdot \left[\frac{\partial N_{JI}}{\partial X} - N_{JI}^2 \frac{\partial L_{10}}{\partial X} \right] \cdot [D_{JI}]^{-1} \ . \tag{4.36}$$

As a last step, one has to consider the chiral expansion of eq. (4.36) up to the desired order.

4.4.2 Production processes inside nucleon-nucleon scattering

We now consider the calculation of those contributions that originate from external sources coupling into a two-nucleon reducible loop. Such a loop has to be corrected by *initial state interactions* (ISI) and *final state interactions* (FSI), as will be denoted in figures by an ellipsis which represents iterated nucleon-nucleon interactions. This iteration is the same as occurs for the nucleon-nucleon scattering in the nuclear medium, see fig. 4.2. The "elementary" nucleon-nucleon interaction N_{JI} is dressed by the iterative process which gives rise to eq. (4.31), with N_{JI} multiplied by the inverse of the matrix D_{JI}. In this way, if we denote by $\xi_{JI}(\ell,\bar{\ell},S)$ the elementary partial wave for a production process, $F_{JI}(\ell,\bar{\ell},S)$, then it is dressed by FSI in a way that

$$F_{JI}(\ell,\bar{\ell},S)=\sum_{\ell'}\left[D_{JI}(\ell,\ell',S)\right]^{-1}\cdot\xi_{JI}(\ell',\bar{\ell},S)\ . \tag{4.37}$$

The matrix D_{JI}, eq. (4.34), is already known from the study of the nucleon-nucleon interactions up to some order. On the other hand, ξ_{JI} can be fixed following an analogous procedure to that used before for determining N_{JI} in section 4.2. In this way, $\xi_{JI}^{(n)}$ is determined by expanding eq. (4.37) in powers of L_{10} up to $(L_{10})^n$ and then comparing with a full χPT calculation up to $\mathcal{O}(p^{m+n})$, with at most $n+1$ two-nucleon reducible diagrams, and $\mathcal{O}(p^m)$ the order of the addional structures of the production process. In addition the ISI has also to be taken into account. So, instead of eq. (4.37), we have

$$H_{JI}(\ell,\bar{\ell},S)=\sum_{\ell',\ell''}\left[D_{JI}(\ell,\ell',S)\right]^{-1}\cdot\xi_{JI}(\ell',\ell'',S)\cdot\left[D^{r}_{JI}(\ell'',\bar{\ell},S)\right]^{-1}\ , \tag{4.38}$$

where the superscript r denotes the reversed order of N_{JI} and L_{10} just in case they do not commute. The leading order result requires to employ $D_{JI}^{(0)}$ and to calculate the two-nucleon reducible loop to which the external sources are attached by factorizing on-shell the nucleon-nucleon scattering amplitudes. We use the notation $D_{JI}^{(n);i_3}=I+N_{JI}^{(n);i_3}\cdot L_{10}^{i_3}$, with n the chiral order,

$$\begin{aligned}\xi_{JI}^{(0)}&=-\left(N_{JI}^{(0)}\right)^2\cdot DL_{10}\ ,\\ H_{JI}|_{LO}&=\left[D_{JI}^{(0)}\right]^{-1}\cdot\xi_{JI}^{(0)}\cdot\left[D_{JI}^{(0)}\right]^{-1}\ .\end{aligned} \tag{4.39}$$

DL_{10} abbreviates the expression for the unitarity loop with the external sources coupled to.

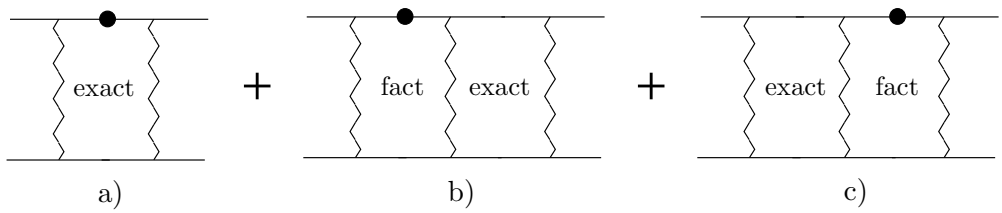

Figure 4.11: Example of diagrams that contribute to the calculation of $\xi_{JI}^{(1)}$. The blob denotes the coupling of arbitrary sources in the corresponding nucleon propagator. Those two-nucleon reducible loops that contain the label "exact" must be calculated exactly in the EFT, while those with the label "fact" must be calculated with the on-shell factorization of the pertinent vertices.

At next-to-leading order one has an extra two-nucleon reducible loop. Expanding the D_{JI}^{-1} matrices in eq. (4.38) up to one L_{10} and ξ_{JI} up to $\mathcal{O}(p)$ we obtain

$$\xi_{JI}^{(0)}+\xi_{JI}^{(1)}-2N_{JI}^{(0)}\cdot L_{10}\cdot\xi_{JI}^{(0)}\ . \tag{4.40}$$

We now match the previous equation with the result of fig. 4.11. In this figure we have included inside each loop the labels "exact" or "fact" according to whether the loop is calculated exactly or by factorizing on-shell the nucleon-nucleon vertices. The filled circle refers to the scattering process of the nucleon with external sources. We denote by $L_{JI}^{(1)}$ the two-nucleon reducible loop without sources calculated exactly in χPT and that occurs in figs. 4.11b and 4.11c. There is also the new contribution of fig. 4.11a whose exact calculation is denoted by $DL_{JI}^{(1)}$. The result is

$$DL_{JI}^{(1)} - N_{JI}^{(0)} \cdot DL_{10} \cdot L_{JI}^{(1)} - L_{JI}^{(1)} \cdot DL_{10} \cdot N_{JI}^{(0)} \ . \tag{4.41}$$

The equality of eqs. (4.40) and (4.41), taking into account eq. (4.39) for $\xi_{JI}^{(0)}$, implies that

$$\xi_{JI}^{(0)} + \xi_{JI}^{(1)} = DL_{JI}^{(1)} - \left\{ L_{JI}^{(1)} + \left(N_{JI}^{(0)}\right)^2 \cdot L_{10},\, N_{JI}^{(0)} \right\} \cdot DL_{10} \ . \tag{4.42}$$

In the last term we have the combination $L_{JI}^{(1)} + (N_{JI}^{(0)})^2 \cdot L_{10}$ which is $\mathcal{O}(p)$ in our counting because it corresponds to the difference between an exact calculation of a two-nucleon reducible loop and that obtained by factorizing the vertices on-shell. The other contribution to $\xi_{JI}^{(1)}$ is given by $DL_{JI}^{(1)} - \xi_{JI}^{(0)}$, as follows from eq. (4.42), that is also $\mathcal{O}(p)$ by the same token.

4.5 Summary and conclusions

In the present chapter, we have developed the required non-perturbative techniques that allow us to perform necessary resummations both in scattering as well as in production processes. These non-perturbative methods are based on Unitary χPT, which are adapted now to the nuclear medium by implementing the power counting of eq. (3.23). Following the novel power counting, we have determined the vacuum nucleon-nucleon scattering at leading order and next-to-leading order. For nuclear matter the leading order nucleon-nucleon scattering amplitudes have also been obtained. The infrared enhancement of the two-nucleon reducible loops have it made necessary to resum the right-hand cut. This is accomplished by a once-subtracted dispersion relation of the inverse of a partial wave giving rise to the master equation of UχPT, eq. (4.5). It results as an approximate solution to the dispersive treatment of nucleon-nucleon scattering in a chiral expansion of the imaginary part of the scattering amplitudes along the left-hand cut, taking advantage of the suppression of the two-nucleon unitarity loops along this cut. The important function $g(A)$, eq. (4.7), which is defined in terms of a subtraction constant, $g(D)$ or g_0, is introduced. It has been argued that the subtraction constant is $\mathcal{O}(p^0)$, because by changing the subtraction point B the subtraction constant is modified reshuffling the form of the function $g(A)$, which is invariant. The process for determining the interaction kernel N_{JI}, eq. (4.5), has been also discussed in detail. It was obtained that the subtraction point D acts as a "renormalization scale" where an experimental point is reproduced. The subtraction constant $g(D)$ just fixes the "renormalization scheme" and the exact results should not depend on it. A natural value for $g_0 \sim -mm_\pi/4\pi$ was argued to be adequate for obtaining N_{JI} as a perturbative solution of eq. (4.16) in order to suppress the effects of the iterative factor $|1 + gN_{JI}|^2$ in the equation. The couplings C_S and C_T from the local nucleon-nucleon Lagrangian, eq. (4.1), have been fixed in terms of g_0 up-to-and-including next-to-leading order reproducing the S-wave nucleon-nucleon scattering lengths. These couplings keep their estimated size of $\mathcal{O}(p^0)$ after the iteration, despite the well known fact that the nucleon-nucleon scattering lengths are much larger than $1/m_\pi$. The resulting phase shifts and mixing angles at leading and next-to-leading order are depicted in figs. 4.8, 4.9 and 4.10. It is argued that higher orders should

be included in order to improve the reproduction of data. Particularly, a next-to-next-to leading order (N^2LO) analysis should be pursued since it would include the important two-pion irreducible exchange and new counterterms, in particular the one necessary to reproduce the effective range for the $^1S_0$ partial wave [EHM09]. This is left as a future task since our present main aim is to work the results up-to-and-including next-to-leading order and settle the formalism in detail.

In addition we have extended the formalism to be applicable to calculations in the nuclear medium. Some technical issues for practical calculations were also given. Both will be made use of in subsequent chapters.

Chapter 5

In-medium nucleon self-energy[#5]

As a first application, our theory developed in the chapters 3 and 4 is applied to some basic calculations of the in-medium nucleon self-energy in this chapter. We will not give a full analysis of the topic. The present chapter should be treated rather as an anticipation of the following chapters, as we will need the results in later calculations.

5.1 Introduction

To study the nucleon self-energy in nuclear matter is an interesting topic in itself. Properties that can be considered for instance are the nucleon masses, single particle energies, nucleon-nucleus optical potentials and spectral functions. The self-energy of the nucleon in the nuclear medium is actually a function of the energy k^0 and the three-momentum $\mathbf{k}$, separately. In addition it depends on the density ρ_F respectively the Fermi momentum ξ_F. Some studies of the nucleon self-energy in nuclear matter are given in [ACS81, JMi91, CFG91, FGC92, AFCO96, TPRM98, MNRS04, PFF06, DM10] using various, mostly relativistic, approaches. In this chapter we will not investigate those quantities in our given framework but will merely provide the necessary input from the leading nucleon self-energy diagrams, which we will need for the calculations of later chapters.

After this introduction we will define the in-medium nucleon self-energy in section 5.2. Subsubsection 5.2.1 deals with the leading correction term due to the quark masses. In section 5.3 there will be given the contributions from pion-nucleon chiral dynamics, as well for the vacuum as for the medium part. Section 5.4 provides contributions due to nucleon-nucleon interactions.

5.2 The nucleon self-energy

In a quantum field theory the quantum field's strength itself, namely the wave-function, has to be renormalized. In the language of Feynman diagrams this happens by loop corrections to the field's two-point function, the propagator. These corrections are called the *self-energy* $\Sigma(\cdot)$.

In the vacuum the dressed non-relativistic nucleon propagator in its Heavy Baryon formulation

[#5] Some contents of this chapter have been published in [LOMb].

takes the form

$$S(k^0) = \frac{1}{p\cdot v - \mathring{m} + \Sigma(k^0) + i\epsilon} = \frac{1}{k^0 + \Sigma(k^0) + i\epsilon} \ , \tag{5.1}$$

see section 2.3 for definitions. Note our sign convention for the self-energy. The propagator develops a pole at $p = m_N v$, with m_N the renormalized nucleon mass

$$m_N = \mathring{m} - \Sigma(0) \ . \tag{5.2}$$

The nucleon's wave-function renormalization constant Z_N,

$$S(k^0) = \frac{Z_N}{p\cdot v - m_N} \ , \tag{5.3}$$

is determined by the residue of the propagator at the physical mass pole given by

$$Z_N^{-1} = 1 + \left.\frac{d\Sigma(k^0)}{dk^0}\right|_{k^0=0} \ . \tag{5.4}$$

In the nuclear medium things become a bit more involved. First, following our improved in-medium power counting, the nucleon propagators becomes enhanced. Counting our propagators as $\mathcal{O}(p^{-2})$, we have to resum the kinetic terms $E(\mathbf{k}) = \mathbf{k}^2/(2m_N)$. Second, in the nuclear medium the nucleon self-energy obtains new contributions, which are dependent on the three-momentum $|\mathbf{k}|$, due to the choice of a certain frame of reference, and on the Fermi limits (symbolized by ξ_F), due to Fermi blocking. In-medium contributions will lead to a shift in relation between energy and momentum and will have impact on the wave-function renormalization. The non-relativistic in-medium nucleon propagator, dressed by the in-medium self-energy, reads

$$G_0(k,\xi_F)_{i_3} = \frac{\theta(|\mathbf{k}| - \xi_{i_3})}{k^0 - E(\mathbf{k}) + \Sigma(k^0,|\mathbf{k}|,\xi_F) + i\epsilon} + \frac{\theta(\xi_{i_3} - |\mathbf{k}|)}{k^0 - E(\mathbf{k}) + \Sigma(k^0,|\mathbf{k}|,\xi_F) - i\epsilon} \ , \tag{5.5}$$

in the particle-hole representation, eq. (3.9), or

$$G_0(k,\xi_F)_{i_3} = \frac{1}{k^0 - E(\mathbf{k}) + \Sigma(k^0,\mathbf{k},\xi_F) + i\epsilon} + 2\pi i\,\delta\big(k^0 - E(\mathbf{k}) + \Sigma(k^0,\mathbf{k},\xi_F)\big)\,\theta(\xi_{i_3} - |\mathbf{k}|) \ , \tag{5.6}$$

in the free-space and density-dependent representation, eq. (3.11).

5.2.1 Quark mass corrections

Figure 5.1: Contributions to the nucleon self-energy of leading order, $\mathcal{O}(p^2)$, due to quark mass insertion.

The most basic contributions to the nucleon self-energy is due to quark mass insertions from the Langrangian term with a χ_+ field. The quark mass dependence can be parameterized in terms of meson masses. The contributions reads

$$\Sigma^\chi = 4c_1 m_\pi^2 \ . \tag{5.7}$$

Since the term is of $\mathcal{O}(p^2)$, which is the same order as the energy of our nucleon propagator, the contribution is resummed inducing the dressing of the nucleon propagator as suggested in eqs. (5.5) and (5.6). The term is absorbed into the nucleon mass, leading to a mass shift that vanishes in the chiral limit [BKM95].

5.3 Pion-nucleon contributions

Let us consider the contributions to the nucleon self-energy in the nuclear medium due to pion-nucleon dynamics.

5.3.1 Free-space contribution

As a preliminary result let us evaluate the nucleon self-energy in the nuclear medium corresponding to fig. 5.2. First, we consider the case of a neutral pion. The results for the charged pion contributions follow immediately from the π^0 case.

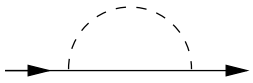

Figure 5.2: Contributions to the nucleon self-energy up to next-to-leading order, $\mathcal{O}(p^3)$, due to pion-nucleon dynamics. The pions are indicated by the dashed lines.

In HBχPT the proton self-energy due to the one-π^0 loop is given by,

$$\begin{aligned}\Sigma_p^{\pi^0} &= -i\frac{g_A^2}{f_\pi^2} S_\mu S_\nu \int \frac{d^D\ell}{(2\pi)^D} \frac{\ell^\mu \ell^\nu}{\ell^2 - m_\pi^2 + i\epsilon} \frac{1}{v(k-\ell) + i\epsilon} \\ &\quad + 2\pi \frac{g_A^2}{f_\pi^2} S_\mu S_\nu \int \frac{d^D\ell}{(2\pi)^D} \frac{\ell^\mu \ell^\nu}{\ell^2 - m_\pi^2 + i\epsilon} \delta(v(k-\ell))\theta(\xi_p - |\mathbf{k}-\mathbf{l}|) \ . \end{aligned} \tag{5.8}$$

Here, $\mathbf{l}$ is the vector made up from the spatial components of ℓ and v is the four-velocity normalized to unity ($v^2 = 1$), such that the four-momentum of a nucleon is given by $p = mv + k$, with k a small residual momentum ($v \cdot k \ll m$). In practical calculations we take $v = (1, \mathbf{0})$ and $D \to 4$. Notice that the last integral in the previous equation is convergent because of the presence of the Dirac delta and Heaviside step functions. Instead of the full non-relativistic nucleon propagator eq. (3.9), HBχPT typically implies the so-called extreme non-relativistic limit in which $E(\mathbf{k}) \to 0$, see e.g. [BKM95]. Given the properties of the covariant spin operator S_μ [BKM95] it follows that

$$S_\mu S_\nu \ell^\mu \ell^\nu = \frac{1}{2}\{S_\mu, S_\nu\}\ell^\mu \ell^\nu = \frac{1}{4}\left((v\cdot\ell)^2 - \ell^2\right) \ . \tag{5.9}$$

For the vacuum part we then have the integral

$$\Sigma_{p,f}^{\pi^0} = -i\frac{g_A^2}{4f_\pi^2} \int \frac{d^D\ell}{(2\pi)^D} \frac{(v\ell)^2 - \ell^2}{(\ell^2 - m_\pi^2 + i\epsilon)(v(k-\ell) + i\epsilon)} \ . \tag{5.10}$$

This can be evaluated straightforwardly in dimensional regularization. Adding the contributions from the charged pions one has the free nucleon self-energy due to a one-pion loop [BKM95], denoted in the following by Σ_f^π,

$$\begin{aligned}\Sigma_f^\pi &\doteq \Sigma_{p,f}^\pi = \Sigma_{n,f}^\pi \\ &= \frac{3g_A^2 b}{32\pi^2 f_\pi^2}\left\{-\omega + \sqrt{b}\left[\pi + i\ln\left(\frac{\omega + i\sqrt{b}}{-\omega + i\sqrt{b}}\right)\right]\right\} - \frac{3g_A^2 m_\pi^3}{32\pi f_\pi^2} \ , \end{aligned} \tag{5.11}$$

where $\omega = v\cdot k = k^0$ and $b = m_\pi^2 - \omega^2 - i\epsilon$ with $\epsilon \to 0^+$. In all the calculations that follow the square roots and logarithms have the cut along the negative real axis. In eq. (5.11) we have subtracted the value of the one-pion loop nucleon self-energy at $\omega = 0$ since we are using the physical nucleon mass. Later, we will also need its derivative given by

$$\frac{\partial \Sigma_f^\pi}{\partial w} = \frac{3g_A^2}{32\pi^2 f_\pi^2}\left\{ m_\pi^2 + \omega^2 - 3\omega\sqrt{b}\left[\pi + i\ln\left(\frac{\omega + i\sqrt{b}}{-\omega + i\sqrt{b}}\right)\right]\right\} \ . \tag{5.12}$$

5.3.2 Density-dependent contribution

The in-medium contribution to the proton self-energy due to the one-π^0 loop corresponds to the last line in eq. (5.8). Taking also into account the charged pions in the loop we have for the in-medium part of the one-pion loop contribution to the proton and neutron self-energies, $\Sigma_{p,m}$ and $\Sigma_{n,m}$, respectively,

$$\begin{aligned}
\Sigma_{p,m}^\pi &= 2\pi\frac{g_A^2}{f_\pi^2} S_\mu S_\nu \int \frac{d^4\ell}{(2\pi)^4}\frac{\ell^\mu \ell^\nu}{\ell^2 - m_\pi^2 + i\epsilon}\delta(v(k-\ell))\Big[\theta(\xi_p - |\mathbf{k}-\mathbf{l}|) + 2\theta(\xi_n - |\mathbf{k}-\mathbf{l}|)\Big] \ , \\
\Sigma_{n,m}^\pi &= 2\pi\frac{g_A^2}{f_\pi^2} S_\mu S_\nu \int \frac{d^4\ell}{(2\pi)^4}\frac{\ell^\mu \ell^\nu}{\ell^2 - m_\pi^2 + i\epsilon}\delta(v(k-\ell))\Big[\theta(\xi_n - |\mathbf{k}-\mathbf{l}|) + 2\theta(\xi_p - |\mathbf{k}-\mathbf{l}|)\Big] \ .
\end{aligned} \tag{5.13}$$

$S_\mu S_\nu l^\mu l^\nu = \mathbf{l}^2/4$ for our choice of v and the second integral on the right hand side of eq. (5.8) reads

$$I_m^{(1)} = 2\pi \int \frac{d^4\ell}{(2\pi)^4}\frac{\mathbf{l}^2\delta(k^0 - \ell^0)\theta(\xi_p - |\mathbf{k}-\mathbf{l}|)}{\ell^2 - m_\pi^2 + i\epsilon} = \int \frac{d^3\ell}{(2\pi)^3}\frac{\mathbf{l}^2\theta(\xi_p - |\mathbf{k}-\mathbf{l}|)}{k_0^2 - \mathbf{l}^2 - m_\pi^2 + i\epsilon} \ . \tag{5.14}$$

The step function in the previous integral implies the requirement $\xi_p^2 \geq (\mathbf{k}-\mathbf{l})^2 = \mathbf{k}^2 + \mathbf{l}^2 - 2|\mathbf{k}||\mathbf{l}|\cos\theta$. Then,

$$\cos\theta \geq \frac{\mathbf{k}^2 + \mathbf{l}^2 - \xi_p^2}{2|\mathbf{k}||\mathbf{l}|} = y_0 \ . \tag{5.15}$$

It is necessary that $y_0 \leq 1$, otherwise $\cos\theta$ would be larger than 1. This implies that

$$|\mathbf{k}| - \xi_p \leq |\mathbf{l}| \leq |\mathbf{k}| + \xi_p \ . \tag{5.16}$$

On the other hand, if $|\mathbf{l}| \geq \xi_p - |\mathbf{k}|$ then $y_0 \geq -1$. Taking into account these constraints, one has

$$\begin{aligned}
&a)\ |\mathbf{k}| \geq \xi_p: \quad |\mathbf{l}| \in \big[|\mathbf{k}| - \xi_p, |\mathbf{k}| + \xi_p\big] \ \wedge \ \cos\theta \in \big[y_0, 1\big] \ , \\
&b)\ \xi_p \geq |\mathbf{k}|: \quad |\mathbf{l}| \in \big[0, \xi_p - |\mathbf{k}|\big] \ \wedge \ \cos\theta \in \big[-1, 1\big] \ ; \\
&\qquad\qquad\quad |\mathbf{l}| \in \big[\xi_p - |\mathbf{k}|, \xi_p + |\mathbf{k}|\big] \ \wedge \ \cos\theta \in \big[y_0, 1\big] \ .
\end{aligned} \tag{5.17}$$

The same expression of $I_m^{(1)}$ results for the cases a) and b),

$$\begin{aligned}
I_m^{(1)}(\xi_p) = -\frac{\rho_p}{2} + \frac{b}{4\pi^2}\Bigg\{ &\xi_p - \sqrt{b}\,\arctan\left(\frac{\xi_p - |\mathbf{k}|}{\sqrt{b}}\right) - \sqrt{b}\,\arctan\left(\frac{\xi_p + |\mathbf{k}|}{\sqrt{b}}\right) \\
&- \frac{\mathbf{k}^2 - \xi_p^2 - b}{4|\mathbf{k}|}\ln\left(\frac{(\xi_p + |\mathbf{k}|)^2 + b}{(\xi_p - |\mathbf{k}|)^2 + b}\right)\Bigg\} \ .
\end{aligned} \tag{5.18}$$

In terms of $I_m^{(1)}$ the in-medium part of the one-pion loop contribution to the nucleon self-energy, eq. (5.13), reads

$$\begin{aligned}\Sigma_{p,m}^{\pi} &= \Sigma_{p,m}^{\pi^0} + \Sigma_{p,m}^{\pi^+} = \frac{g_A^2}{4f_\pi^2}\left(I_m^{(1)}(\xi_p) + 2I_m^{(1)}(\xi_n)\right) \ , \\ \Sigma_{n,m}^{\pi} &= \Sigma_{n,m}^{\pi^0} + \Sigma_{n,m}^{\pi^-} = \frac{g_A^2}{4f_\pi^2}\left(I_m^{(1)}(\xi_n) + 2I_m^{(1)}(\xi_p)\right) \ ,\end{aligned} \tag{5.19}$$

where the superscript refers to the pion species in the loop. From eq. (5.18) one has for the derivative,

$$\begin{aligned}\frac{\partial I_m^{(1)}(\xi_p)}{\partial\omega} = -\frac{\omega}{2\pi^2}\Bigg\{&\xi_p - \frac{3\sqrt{b}}{2}\arctan\left(\frac{\xi_p - |\mathbf{k}|}{\sqrt{b}}\right) - \frac{3\sqrt{b}}{2}\arctan\left(\frac{\xi_p + |\mathbf{k}|}{\sqrt{b}}\right) \\ &+ \frac{2b - \mathbf{k}^2 + \xi_p^2}{4|\mathbf{k}|}\ln\left(\frac{(\xi_p + |\mathbf{k}|)^2 + b}{(\xi_p - |\mathbf{k}|)^2 + b}\right)\Bigg\} \ ,\end{aligned} \tag{5.20}$$

in terms of which it is straightforward to calculate $\partial\Sigma_{p(n),m}^{\pi}/\partial\omega$.

5.3.3 Sum of pion-nucleon contributions

The full in-medium nucleon self-energy is given by the sum of eqs. (5.11) and (5.19). In this way, the proton and neutron self-energies due to the one-pion loop are, in that order,

$$\begin{aligned}\Sigma_p^{\pi} &= \Sigma_f^{\pi} + \Sigma_{p,m}^{\pi} \ , \\ \Sigma_n^{\pi} &= \Sigma_f^{\pi} + \Sigma_{n,m}^{\pi} \ .\end{aligned} \tag{5.21}$$

The self-energies for both the proton and neutron can joined to one expression given by

$$\Sigma^{\pi} = \frac{1+\tau_3}{2}\Sigma_p^{\pi} + \frac{1-\tau_3}{2}\Sigma_n^{\pi} \ . \tag{5.22}$$

This can be as a building block for upcoming calculations, where the isospin structure will project on the correct state.

Let us now briefly discuss the implications of the previous calculations on the two-point correlation function of the nucleon up to the order at which we are working.

The nucleon mass renormalization contribution from the free-space part of the self-energy reads

$$\delta m_N = -\Sigma_f(0) = -4c_1 m_\pi^2 - \frac{3g_A^2 m_\pi^3}{32\pi f_\pi^2} \ . \tag{5.23}$$

Since we are working at the physical nucleon mass, these contributions are absorbed into the mass and will not occur in any calculations. For the same reason, this contribution has been subtracted in eq. (5.11).

The shift between energy and momentum is isospin dependent. We obtain for the proton and the neutron, respectively,

$$\begin{aligned}\delta(k^0)_p(|\mathbf{k}|,\xi_p,\xi_n) &= -\,\Sigma^{\pi}_{p,m}\big|_{k^0=0}\ ,\\ \delta(k^0)_n(|\mathbf{k}|,\xi_p,\xi_n) &= -\,\Sigma^{\pi}_{n,m}\big|_{k^0=0}\ ,\end{aligned} \tag{5.24}$$

where $\Sigma_{i_3,m}$ are given in eq. (5.19).

The vacuum contributions to the nucleon wave-function renormalization of the nucleon field from the free-space part of the self-energy reads

$$\delta Z_N = -\left.\frac{d\Sigma_f(k^0)}{dk^0}\right|_{k^0=0} = -\frac{3g_A^2 m_\pi^2}{32\pi^2 f_\pi^2}\ . \tag{5.25}$$

The in-medium contributions to the nucleon wave-function renormalization is isospin-dependent and read for proton and neutron, respectively,

$$\begin{aligned}\delta Z_p(|\mathbf{k}|,\xi_p,\xi_n) &= -\left.\frac{d\Sigma_{p,m}(k^0)}{dk^0}\right|_{k^0=0}\ ,\\ \delta Z_n(|\mathbf{k}|,\xi_p,\xi_n) &= -\left.\frac{d\Sigma_{n,m}(k^0)}{dk^0}\right|_{k^0=0}\ .\end{aligned} \tag{5.26}$$

The contributions can be obtained from eqs. (5.20) and (5.11).

5.4 Nucleon-nucleon contributions

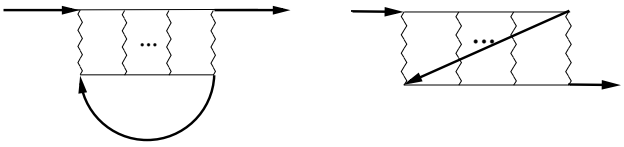

Figure 5.3: Contributions to the in-medium nucleon self-energy up to next-to-leading order, $\mathcal{O}(p^3)$, steming from nucleon-nucleon interaction. A wiggly line corresponds to the nucleon-nucleon interaction kernel, fig. 4.1, whose iteration is denoted by the ellipsis.

The nucleon self-energy due to the nucleon-nucleon interactions, represented in fig. 5.3, is given by the expression

$$\Sigma^{NN}_{\alpha_1} = -i\sum_{\alpha_2,\sigma_2}\int\frac{d^4k_2}{(2\pi)^4}e^{ik_2^0\eta}G_0(k_2)_{\alpha_2}T_{NN}(k_1\sigma_1\alpha_1,k_2\sigma_2\alpha_2|k_1\sigma_1\alpha_1,k_2\sigma_2\alpha_2) \tag{5.27}$$

where T_{NN} is the two-nucleon scattering operator between the nucleon states characterized by the four-momentum k_i, spin σ_i and third component of isospin α_i. Note that in the equation there is a sum over all the quantum numbers of the second nucleon.

The self-energies for both the proton and neutron can be joined to one expression given by

$$\Sigma^{NN} = \frac{1+\tau_3}{2}\Sigma^{NN}_p + \frac{1-\tau_3}{2}\Sigma^{NN}_n\ , \tag{5.28}$$

with Σ_p^{NN} and Σ_n^{NN} the proton and neutron self-energies generated by eq. (5.27).

We also employ the relative coordinates

$$P = \frac{1}{2}(k_1 + k_2) \ , \ p = \frac{1}{2}(k_1 - k_2) \ , \tag{5.29}$$

and the off-shell parameter

$$A = 2mP^0 - \mathbf{P}^2 \ . \tag{5.30}$$

If the nucleon-nucleon interaction is put on-shell one has $A = \mathbf{p}^2$. In terms of these variables we can introduce the somewhat shorter notation

$$T^{\sigma_1\sigma_2}_{\alpha_1\alpha_2}(\mathbf{p}, \mathbf{P}; A) = T_{NN}(k_1\sigma_1\alpha_1, k_2\sigma_2\alpha_2 | k_1\sigma_1\alpha_1, k_2\sigma_2\alpha_2) \ , \tag{5.31}$$

that is more convenient for forward scattering than the notation followed in appendix A.

It is convenient to give the nucleon-nucleon scattering amplitude as an expansion in partial waves, eq. (A.9). The partial wave decomposition of the nucleon-nucleon amplitudes is derived in detail in appendix A. A nucleon-nucleon partial wave is denoted by $T^{i_3}_{JI}(\ell', \ell, S)$, where $\vec{J} = \vec{\ell} + \vec{S}$ is the total angular momentum, I is the total isospin, $i_3 = \alpha_1 + \alpha_2$, ℓ' and ℓ are the final and initial orbital angular momenta, respectively, and S is the total spin. The partial wave is a function of $\mathbf{P}^2$, $\mathbf{p}^2$ and A for our previously calculated nucleon-nucleon amplitudes. Since typically $A \neq \mathbf{p}^2$ an analytical extrapolation in A of $T^{i_3}_{JI}(\ell', \ell, S)$ is necessary. While eq. (A.9) is given in the center-of-mass frame of the two nucleons involved in the scattering process, eq. (5.27) is given in the nuclear matter rest-frame. This implies that one must take into account the boost from the former frame to the latter in order to use eq. (A.9). However, as is shown in appendix B, the angle of the associated Wigner rotation is suppressed and it is of $\mathcal{O}((p/m)^2)$. Then, the leading and next-to-leading order nucleon-nucleon scattering amplitudes can be used as Lorentz invariants, similarly as for the meson-meson ones, and eq. (A.9) can be directly used in eq. (5.27). Relativistic corrections would occur at the next-to-next-to-leading order ($\mathrm{N^2LO}$) of the nucleon-nucleon interaction.

Obtaining the renormalized nucleon mass and wave-function from eq. (5.27) is straightforward and will not be performed explicitely here.

Chapter 6

Nuclear matter ground state energy per particle[#6]

In this chapter our theory developed in the chapters 3 and 4 is applied to the problem of calculating the energy density in symmetric nuclear matter and pure neutron matter up-to-and-including next-to-leading order. We find that the main trends for the energy density for both are already reproduced at that order. In addition, an accurate description of the neutron matter equation of state, compared to sophisticated many-body calculations, is obtained by varying only slightly a subtraction constant around its expected value. The case of symmetric nuclear matter requires the introduction of an additional fine-tuned subtraction constant, parameterizing the effects from higher order contributions. With that, the empirical saturation point and the nuclear matter incompressibility are well reproduced while the binding energy per nucleon as a function of density closely agrees with sophisticated calculations in the literature.

6.1 Introduction

Nuclear matter is an infinite system of nucleons, with a fixed ratio of neutron and proton numbers and no electromagnetic interaction. It can be thought of as an idealization of matter inside a large nucleus. When studying such a system the first question arises how to obtain empirical information about its properties. This is not an easy task, since nuclear matter does not exist in the laboratory. Astronomical measurements of neutron stars are rather indirect and therefore subject to large uncertainties. There are only two properties one can obtain directly from heavy nuclei: the binding energy per nucleon E/A, which can be obtained by extrapolating the fits of nuclear masses, and the saturation density ξ_0, which is the density of nucleons inside the nuclear medium and heavy nuclei. That symmetric nuclear matter does saturate we know from the semi-empirical Bethe-Weizsäcker mass formula in section 1.3. It is desirable to have a theory, which is able to describe this behavior by fundamental principles. For a long time non-relativistic nuclear many-body theory was unsatisfactory, since the saturation properties are not well described when only two-body forces were considered. A saturation mechanism was needed, which provides an attraction at low density and a repulsion at high density. It was found that it is possible to obtain roughly the correct saturation properties, when three-body forces were introduced. It had also

[#6] The contents of this chapter have been published in [LOMb].

to be recognized, that not only particle-particle interactions have to be considered, but hole-hole scattering contributes as well. To complicate things even more, in order to reach the densities of nuclear matter saturation, also explicit pion degrees of freedom have to be included. Finally it is demanded from the theory that it is able to obtain bulk properties such as the exact binding energy, equilibrium (saturation) density, symmetry energy, incompressibility etc. simultaneously.

The calculation of the energy density of nuclear matter starting from nuclear forces is a venerable problem in nuclear physics [PW79, Da81, SW86, RDP89, RPD89, BM90, APR98, LFA00, KFW02, KFW05]. Our calculation of the energy density $\mathcal{E}$ up-to-and-including next-to-leading order already leads to saturation for symmetric nuclear matter and repulsion for neutron matter. Indeed, an accurate reproduction of the equation of state for neutron matter can be achieved by varying slightly one subtraction constant around its expected value. For the case of symmetric nuclear matter an additional fine-tuning of a subtraction constant is necessary to obtain a remarkable good agreement between our results and previously existing sophisticated many-body calculations [PW79, En97, APR98]. The saturation point and nuclear matter incompressibility are reproduced in good agreement with experiments.

After this introduction we will present the calculations of the contributions up-to-and-including next-to-leading order in section 6.2. In section 6.3 results and a discussion thereof will be given, while a phenomenological ansatz to improve our results will be made in subsection 6.3.1. A summary with conclusions and outlook will be given in section 6.4.

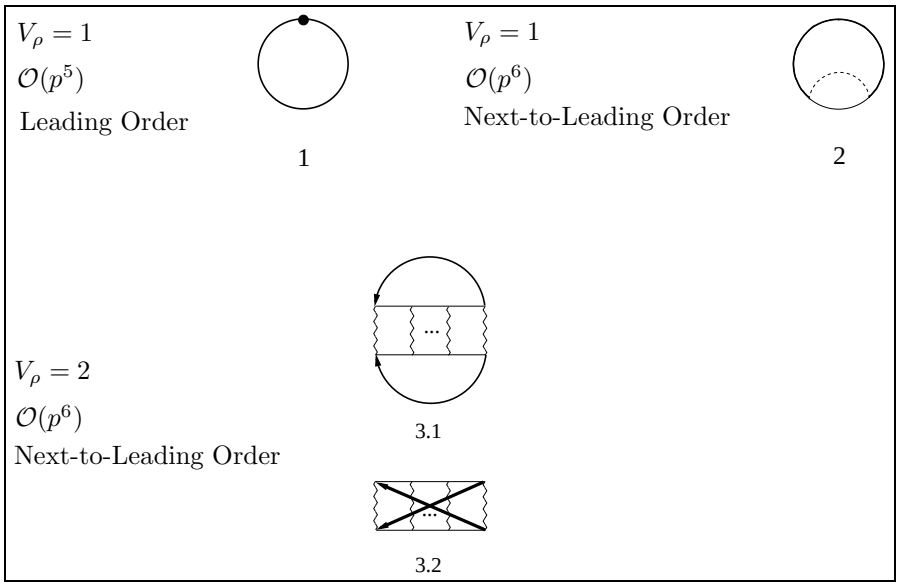

Figure 6.1: Contributions $\mathcal{E}_i$ to the energy density of nuclear matter up-to-and-including next-to-leading order, $\mathcal{O}(p^6)$. The pions are indicated by the dashed lines and a wiggly line corresponds to the nucleon-nucleon interaction kernel, fig. 4.1, whose iteration is denoted by the ellipsis. The diagrams 2 and 3 have a symmetry factor of 1/2.

6.2 Nuclear matter ground state energy density

The binding energy per particle in nuclear matter is connected to the energy density

$$\mathcal{E} = \langle \Omega | \mathcal{H}_{eff} | \Omega \rangle \ , \tag{6.1}$$

of the ground state via $\mathcal{E}/\rho = E/A$. The diagrams required to study the problem of the nuclear matter equation of state, by applying eq. (3.23) up-to-and-including next-to-leading order, are shown in fig. 6.1. The kinetic energy closed by a Fermi sea insertion is depicted by diagram 1 and corresponds to the energy of a free Fermi gas. All other diagrams are obtained by considering nucleon self-energy contributions which are closed with the full in-medium propagator G_0, eq. (3.12). In the following we indicate by $\mathcal{E}_i$ the contribution to the ground state energy density of nuclear matter due to the diagram i in fig. 8.1.

The contribution of diagram 1, $\mathcal{E}_1$, is given by

$$\mathcal{E}_1 = \frac{3}{10m}(\rho_p\, \xi_p^2 + \rho_n\, \xi_n^2) \ , \tag{6.2}$$

and is the only $\mathcal{O}(p^5)$ contribution. Nonetheless, since this is a recoil correction originating from the first term of $\mathcal{L}^{(2)}_{\pi N}$, eq. (2.55), one expects it to be suppressed numerically, because it involves the inverse power of the hard scale m instead of $\sim \sqrt{m m_\pi}$, the one in $1/g_0$. In addition, as shown below, there is further a dimensional suppression. Hence, the next-to-leading order contributions involving the nucleon-nucleon interactions, suppressed by just one extra chiral order, could be of comparable size. This is of course an important remark for the possible saturation of nuclear matter.

The next-to-leading order or $\mathcal{O}(p^6)$ contributions comprise the second and third diagrams. The former is the energy due to the one-pion loop nucleon self-energy whose expression, including a symmetry factor of 1/2 and a factor 2 from the sum over the nucleon spins, is

$$\begin{aligned}\mathcal{E}_2 &= -i \int \frac{d^4k}{(2\pi)^4} e^{ik^0\eta} \sum_{i_3} G_0(k)_{i_3} \Sigma^\pi_{i_3} \\ &= \int \frac{d^3k}{(2\pi)^3} \Big[\theta(\xi_p - |\mathbf{k}|)\Sigma^\pi_p + \theta(\xi_n - |\mathbf{k}|)\Sigma^\pi_n\Big] - i \int \frac{d^4k}{(2\pi)^4} \frac{e^{ik^0\eta}}{k^0 - E(\mathbf{k}) + i\epsilon} \left(\Sigma^\pi_p + \Sigma^\pi_n\right) \ ,\end{aligned} \tag{6.3}$$

with the convergence factor $e^{ik^0\eta}$, $\eta \to 0^+$, associated with any closed loop made up by a single nucleon line [FW03]. The cut in k^0 from the free one-pion loop nucleon self-energy is restricted to the lower half-plane of the k^0-complex plane, see eq. (5.10). In this way, by closing the first integral on the right hand side of the previous equation along an infinite semicircle centered at the origin and on the upper k^0-complex plane, the contribution from the free part of $\Sigma^\pi_{i_3}$ cancels. Concerning the last term, an analogous reasoning to that given section 7.2 in connection with fig. 7.2 can be also applied here for the in-medium contribution $\Sigma^\pi_{i_3,m}$ of $\Sigma^\pi_{i_3}$. This part is accounted for by the diagram 3.2 of fig. 6.1. Thus, the contribution that we keep now for the nuclear matter energy density from the second diagram of fig. 6.1, $\mathcal{E}_2$, is

$$\mathcal{E}_2 = \int \frac{d^3k}{(2\pi)^3} \Big[\theta(\xi_p - |\mathbf{k}|) + \theta(\xi_n - |\mathbf{k}|)\Big] \Sigma^\pi_f - i \int \frac{d^4k}{(2\pi)^4} \frac{e^{ik^0\eta}}{k^0 - E(\mathbf{k}) + i\epsilon} \left(\Sigma^\pi_{p,m} + \Sigma^\pi_{n,m}\right) \ . \tag{6.4}$$

Let us show that up to $\mathcal{O}(p^6)$ these two integrals give the same result. Taking into account the expression for the in-medium part of the one-pion loop nucleon self-energy, eq. (5.13), the first term on the right hand side of eq. (6.4) yields the integrals

$$\int \frac{d^4q}{(2\pi)^4}\frac{\mathbf{q}^2}{q^2-m_\pi^2+i\epsilon}\int\frac{d^4k}{(2\pi)^4}\frac{1}{k^0-E(\mathbf{k})+i\epsilon}(2\pi)\delta(k^0-q^0-E(\mathbf{k}-\mathbf{q}))\theta(\xi_{i_3}-|\mathbf{k}-\mathbf{q}|)\ , \quad (6.5)$$

where the order of the integrations have been changed. We perform the shift $k\to k+q$ in the last integral, that is finite. In this way, eq. (6.5) can be rewritten as

$$i\int\frac{d^3k}{(2\pi)^3}\theta(\xi_{i_3}-|\mathbf{k}|)(-i)\int\frac{d^4q}{(2\pi)^4}\frac{\mathbf{q}^2}{q^2-m_\pi^2+i\epsilon}\frac{1}{-q^0+E(\mathbf{k})-E(\mathbf{k}-\mathbf{q})+i\epsilon}\ . \quad (6.6)$$

If the higher order corrections from the difference $E(\mathbf{k})-E(\mathbf{k}-\mathbf{q})$ are neglected in the previous equation, the last integral is the one defining Σ_f^π, compare with eq. (5.10). Then, after summing over i_3, we have the same contribution as the last one in eq. (6.4) up-to-and-including next-to-leading order. So finally we can write

$$\mathcal{E}_2=2\int\frac{d^3k}{(2\pi)^3}\Big(\theta(\xi_p-|\mathbf{k}|)+\theta(\xi_n-|\mathbf{k}|)\Big)\Sigma_f^\pi\ . \quad (6.7)$$

Let us evaluate now the diagrams 3.1 and 3.2 of fig. 6.1, that collectively are denoted as diagrams 3 in the following. These diagrams fully involve the nucleon-nucleon scattering. Their contribution to the energy density $\mathcal{E}_3$ is

$$\mathcal{E}_3=-\frac{1}{2}\sum_{\sigma_1,\sigma_2}\sum_{\alpha_1,\alpha_2}\int\frac{d^4k_1}{(2\pi)^4}\frac{d^4k_2}{(2\pi)^4}e^{ik_1^0\eta}e^{ik_2^0\eta}G_0(k_1)_{\alpha_1}G_0(k_2)_{\alpha_2}T_{NN}(k_1\sigma_1\alpha_1,k_2\sigma_2\alpha_2|k_1\sigma_1\alpha_1,k_2\sigma_2\alpha_2)\ . \quad (6.8)$$

In this expression we have explicitly shown the symmetry factor 1/2 and the sum over the spin (σ_i) and isospin (α_i) labels, with $\eta\to 0^+$. Performing an expansion in partial waves according to eq. (7.37) we can write eq. (6.8) as

$$\mathcal{E}_3=-\frac{1}{2}\int\frac{d^4k_1}{(2\pi)^4}\frac{d^4k_2}{(2\pi)^4}e^{ik_1^0\eta}e^{ik_2^0\eta}\sum_{I,J,\ell,S,i_3}(2J+1)\chi(S\ell I)^2G_0(k_1)_{\alpha_1}G_0(k_2)_{\alpha_2}T_{JI}^{i_3}(\ell,\ell,S)\ , \quad (6.9)$$

with $i_3=\alpha_1+\alpha_2$.

The leading order in-medium nucleon-nucleon scattering amplitude calculated in section 4.3 does not depend on p^0. The interaction kernel N_{JI} only depends on $\mathbf{p}^2$ at this order, while the resummation over the two-nucleon intermediate states, that gives rise to L_{10}, appendix C.2, depends on A and $|\mathbf{P}|$ as well. In the following we use as integration variables P and p introduced in eq. (5.29). The p^0-integration from eq. (6.8) can be readily performed, with the result

$$\int\frac{dp^0}{2\pi}G_0(P+p)G_0(P-p)=-i\Bigg[\frac{\theta(|\mathbf{P}+\mathbf{p}|-\xi_{\alpha_1})\theta(|\mathbf{P}-\mathbf{p}|-\xi_{\alpha_2})}{2P^0-E(\mathbf{P}+\mathbf{p})-E(\mathbf{P}-\mathbf{p})+i\epsilon}$$
$$-\frac{\theta(\xi_{\alpha_1}-|\mathbf{P}+\mathbf{p}|)\theta(\xi_{\alpha_2}-|\mathbf{P}-\mathbf{p}|)}{2P^0-E(\mathbf{P}+\mathbf{p})-E(\mathbf{P}-\mathbf{p})-i\epsilon}\Bigg]\ . \quad (6.10)$$

Here, we have made use of the fact that only those terms with poles located in opposite halves of the p^0-complex plane survive after the p^0 integration. Those terms with the two poles located at the same half of the p^0-complex plane vanish, as it is clear by closing the integration contour with a semicircle at infinite along the other half. We insert eq. (6.10) into eq. (6.8), and use the variable A, eq. (5.30), instead of P^0. Thus,

$$\mathcal{E}_3 = 4i \sum_{\sigma_1,\sigma_2} \sum_{\alpha_1,\alpha_2} \int \frac{d^3P}{(2\pi)^3} \frac{d^3p}{(2\pi)^3} \frac{dA}{2\pi} e^{iA\eta}\, T^{\sigma_1\sigma_2}_{\alpha_1\alpha_2}(\mathbf{p},\mathbf{P};A) \left[\frac{\theta(|\mathbf{P}+\mathbf{p}|-\xi_{\alpha_1})\theta(|\mathbf{P}-\mathbf{p}|-\xi_{\alpha_2})}{A-\mathbf{p}^2+i\epsilon} \right.$$
$$\left. - \frac{\theta(\xi_{\alpha_1}-|\mathbf{P}+\mathbf{p}|)\theta(\xi_{\alpha_2}-|\mathbf{P}-\mathbf{p}|)}{A-\mathbf{p}^2-i\epsilon} \right] , \quad (6.11)$$

where we made used that $k_1^0+k_2^0=(A+\mathbf{P}^2)/2m$. The resulting redefinition of η is not indicated as it is not relevant for the following manipulations, as well as the factor $\exp(i\eta\mathbf{P}^2)$ that is not shown. The first term between the square brackets on the right hand side of eq. (6.11) corresponds to the particle-particle part while the last one corresponds to the hole-hole part. Both of them originate by closing the nucleon lines in the diagrams 3 of fig. 6.1. Making use of

$$\theta(|\mathbf{P}+\mathbf{p}|-\xi_{\alpha_1})\theta(|\mathbf{P}-\mathbf{p}|-\xi_{\alpha_2}) = \Big(1-\theta(\xi_{\alpha_1}-|\mathbf{P}+\mathbf{p}|)\Big)\Big(1-\theta(\xi_{\alpha_2}-|\mathbf{P}-\mathbf{p}|)\Big)$$
$$= 1-\theta(\xi_{\alpha_1}-|\mathbf{P}+\mathbf{p}|)-\theta(\xi_{\alpha_2}-|\mathbf{P}-\mathbf{p}|)+\theta(\xi_{\alpha_1}-|\mathbf{P}+\mathbf{p}|)\theta(\xi_{\alpha_2}-|\mathbf{P}-\mathbf{p}|) , \quad (6.12)$$

eq. (6.11) becomes

$$\mathcal{E}_3 = 4i \sum_{\sigma_1,\sigma_2} \sum_{\alpha_1,\alpha_2} \int \frac{d^3P}{(2\pi)^3} \frac{d^3p}{(2\pi)^3} \frac{dA}{2\pi} e^{iA\eta}\, T^{\sigma_1\sigma_2}_{\alpha_1\alpha_2}(\mathbf{p},\mathbf{P};A) \left[\frac{1}{A-\mathbf{p}^2+i\epsilon} \right.$$
$$\left. - \frac{\theta(\xi_{\alpha_1}-|\mathbf{P}+\mathbf{p}|)+\theta(\xi_{\alpha_2}-|\mathbf{P}-\mathbf{p}|)}{A-\mathbf{p}^2+i\epsilon} - 2\pi i\delta(A-\mathbf{p}^2)\theta(\xi_{\alpha_1}-|\mathbf{P}+\mathbf{p}|)\theta(\xi_{\alpha_2}-|\mathbf{P}-\mathbf{p}|) \right] . \quad (6.13)$$

Let us discuss the calculation of the integral

$$\int_{-\infty}^{+\infty} \frac{dA}{2\pi} \frac{e^{iA\eta}}{A-\mathbf{p}^2+i\epsilon} T^{\sigma_1\sigma_2}_{\alpha_1\alpha_2}(\mathbf{p},\mathbf{P};A) . \quad (6.14)$$

This integral is involved in the first two terms of eq. (6.13). As a preliminary result let us discuss the particle-particle and hole-hole parts in L_{10}, since they represent the inclusion of two-nucleon intermediate states in the nuclear medium. It is then convenient to express the function L_{10} employing the first form of the nucleon propagator in eq. (3.9). In this way

$$L_{10}^{i_3} = i \int \frac{d^4k}{(2\pi)^4} \left[\frac{\theta(\xi_1-|\mathbf{P}-\mathbf{k}|)}{P^0-k^0-E(\mathbf{P}-\mathbf{k})-i\epsilon} + \frac{\theta(|\mathbf{P}-\mathbf{k}|-\xi_1)}{P^0-k^0-E(\mathbf{P}-\mathbf{k})+i\epsilon} \right]$$
$$\times \left[\frac{\theta(\xi_2-|\mathbf{P}+\mathbf{k}|)}{P^0+k^0-E(\mathbf{P}+\mathbf{k})-i\epsilon} + \frac{\theta(|\mathbf{P}+\mathbf{k}|-\xi_2)}{P^0+k^0-E(\mathbf{P}+\mathbf{k})+i\epsilon} \right] . \quad (6.15)$$

Similarly as in eq. (6.10), only those contributions in eq. (6.15) with the two poles in k^0 lying on opposite halves of the k^0-complex plane contribute. Then,

$$L_{10}^{i_3} = m \int \frac{d^3k}{(2\pi)^3} \left[\frac{\theta(|\mathbf{P}-\mathbf{k}|-\xi_1)\theta(|\mathbf{P}+\mathbf{k}|-\xi_2)}{A-\mathbf{k}^2+i\epsilon} - \frac{\theta(\xi_1-|\mathbf{P}-\mathbf{k}|)\theta(|\xi_2-|\mathbf{P}+\mathbf{k}|)}{A-\mathbf{k}^2-i\epsilon} \right] . \quad (6.16)$$

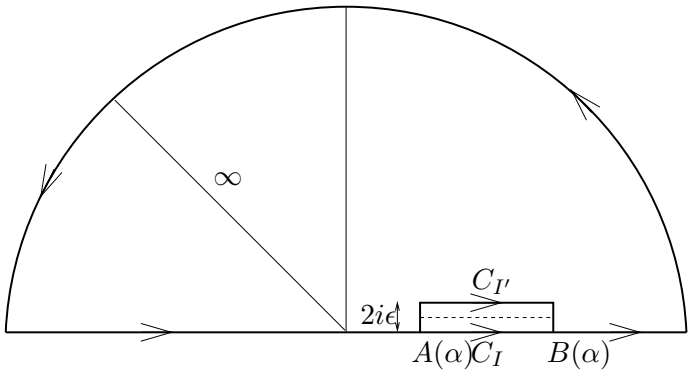

Figure 6.2: Contours of integration C_I and $C_{I'}$ on the A-complex plane used to perform the integral in eq. (6.14). The former contour runs below the cut (dashed line) and the latter above it. The limits of the cut in A due to the hole-hole part of L_{10}, eq. (6.16), are indicated by $A(\alpha)$ and $B(\alpha)$.

The first term is the particle-particle part and the last is the hole-hole one. Notice the different position of the cuts in A. While for the particle-particle case A has a negative imaginary part, $-i\epsilon$, for the hole-hole part the cut takes values with positive imaginary part, $+i\epsilon$. It is also worth mentioning that the extent of the cut in A for the hole-hole part is finite. This cut in the last term of eq. (6.16) requires $\mathbf{k}^2 = A$, but $|\mathbf{k}|$ is bounded so that the two θ-functions in the numerator are simultaneously satisfied. The extension of this cut is given in eq. (C.18). We denote its lower limit by $A(\alpha)$ and its upper one by $B(\alpha)$, corresponding to logarithmic branch points, where $\alpha = |\mathbf{P}|$. This observation is very useful for performing the integral of eq. (6.14). For its evaluation we consider the contours C_I and $C_{I'}$ of fig. 6.2. The dashed line in the figure represents the cut in $T^{\sigma_1\sigma_2}_{\alpha_1\alpha_2}(\mathbf{p},\mathbf{P};A)$ due to that in the hole-hole part of L_{10} for $A(\alpha) < \mathrm{Re}(A) < B(\alpha)$ and positive imaginary part $+i\epsilon$. Physically it represents a real reshuffling of the occupied states by an in-medium pair of baryons respecting energy and three-momentum conservation. All the contours of integration include a semicircle at infinity centered at the origin along the upper part of the A-complex plane. While the contour C_I runs along the real axis, and then below the cut, the contour $C_{I'}$ runs above it, with the imaginary part $+2i\epsilon$. In both cases the pole in the denominator of eq. (6.14) at $\mathbf{p}^2 - i\epsilon$ is outside the contours of integration. Because of the convergence factor the integration along the semicircle at infinity is zero so that we can write

$$\int_{-\infty}^{+\infty} \frac{dA}{2\pi} \frac{e^{iA\eta}}{A - \mathbf{p}^2 + i\epsilon} T^{\sigma_1\sigma_2}_{\alpha_1\alpha_2}(\mathbf{p},\mathbf{P};A) = \oint_{C_I} \frac{dA}{2\pi} \frac{e^{iA\eta}}{A - \mathbf{p}^2 + i\epsilon} T^{\sigma_1\sigma_2}_{\alpha_1\alpha_2}(\mathbf{p},\mathbf{P};A) \ . \tag{6.17}$$

Since the cut is outside the contour $C_{I'}$, see fig. 6.2, the integration along this contour is zero

$$\oint_{C_{I'}} \frac{dA}{2\pi} \frac{e^{iA\eta}}{A - \mathbf{p}^2 + i\epsilon} T^{\sigma_1\sigma_2}_{\alpha_1\alpha_2}(\mathbf{p},\mathbf{P};A) = 0 \ . \tag{6.18}$$

Subtracting eq. (6.18) to eq. (6.17) we are left with

$$\begin{aligned} &\oint_{C_I} \frac{dA}{2\pi} \frac{e^{iA\eta}}{A - \mathbf{p}^2 + i\epsilon} T^{\sigma_1\sigma_2}_{\alpha_1\alpha_2}(\mathbf{p},\mathbf{P};A) - \oint_{C_{I'}} \frac{dA}{2\pi} \frac{e^{iA\eta}}{A - \mathbf{p}^2 + i\epsilon} T^{\sigma_1\sigma_2}_{\alpha_1\alpha_2}(\mathbf{p},\mathbf{P};A) \\ &= \int_{A(\alpha)}^{B(\alpha)} \frac{dA}{2\pi} \frac{T^{\sigma_1\sigma_2}_{\alpha_1\alpha_2}(\mathbf{p},\mathbf{P};A) - T^{\sigma_1\sigma_2}_{\alpha_1\alpha_2}(\mathbf{p},\mathbf{P};A + 2i\epsilon)}{A - \mathbf{p}^2 + i\epsilon} \ . \end{aligned} \tag{6.19}$$

Since the branch points are just of logarithmic type the integration along the vertical segments at $A(\alpha)$ and $B(\alpha)$ in fig. 6.2 do not contribute in the limit $\epsilon \to 0^+$. Notice as well that the limit

$\eta \to 0^+$ is already taken in the last line of eq. (6.19). The amplitude $T^{\sigma_1\sigma_2}_{\alpha_1\alpha_2}(\mathbf{p},\mathbf{P},A)$ can be obtained from the analytical extrapolation in A of the partial waves amplitudes

$$T^{i_3}_{JI}(\ell',\ell,S;\mathbf{p}^2,\mathbf{P}^2,A) = \Big[N^{i_3}_{JI}(\ell',\ell,S)^{-1} + L^{i_3}_{10}(\mathbf{P}^2,A)\Big]^{-1} \ . \tag{6.20}$$

At leading order N_{JI} depends only on $\mathbf{p}^2$, although for higher orders it could depend also on i_3, A and $\mathbf{P}^2$ in addition to $\mathbf{p}^2$. We can also apply here eq. (7.37), keeping explicitly the separation between the $\mathbf{p}^2$ and A variables,

$$\sum_{\sigma_1,\sigma_2} T^{\sigma_1\sigma_2}_{\alpha_1\alpha_2}(\mathbf{p}^2,\mathbf{P}^2,A) = \sum_{I,J,\ell,S} (2J+1)\chi(S\ell I)^2(\alpha_1\alpha_2 i_3|I_1I_2I)^2 T^{i_3}_{JI}(\ell,\ell,S;\mathbf{p}^2,\mathbf{P}^2,A) \ . \tag{6.21}$$

The analytical extrapolation in A does not affect the expansion of the nucleon-nucleon scattering in spherical harmonics associated to the angular variables. From eq. (6.20) it follows that

$$\begin{aligned} T^{i_3}_{JI}(\mathbf{p}^2,\mathbf{P}^2,A) - T^{i_3}_{JI}(\mathbf{p}^2,\mathbf{P}^2,A+2i\epsilon) &= \Big[{N^{i_3}_{JI}}^{-1} + L^{i_3}_{10}(\mathbf{P}^2,A)\Big]^{-1} - \Big[{N^{i_3}_{JI}}^{-1} + L^{i_3}_{10}(\mathbf{P}^2,A+2i\epsilon)\Big]^{-1} \\ &= \Big[{N^{i_3}_{JI}}^{-1} + L^{i_3}_{10}(\mathbf{P}^2,A)\Big]^{-1} \Big[L^{i_3}_{10}(\mathbf{P}^2,A+2i\epsilon) - L^{i_3}_{10}(\mathbf{P}^2,A)\Big] \Big[{N^{i_3}_{JI}}^{-1} + L^{i_3}_{10}(\mathbf{P}^2,A+2i\epsilon)\Big]^{-1} \ . \end{aligned} \tag{6.22}$$

In this equation we have taken into account that although N_{JI} could depend on A for higher orders, in the difference $N^{i_3}_{JI}(\mathbf{p}^2,\mathbf{P}^2,A) - N^{i_3}_{JI}(\mathbf{p}^2,\mathbf{P}^2,A+2i\epsilon)$ this dependence cancels. The point is that the discontinuity in $T^{i_3}_{JI}$ due to the right-hand cut is fully taken into account by multiplying the loop function L_{10} by the kernel N_{JI} on-shell, as in eqs. (4.5) and (4.31). The right-hand cut associated to the variable A is then removed in the process of calculating N_{JI} order by order, as discussed in sections 4.2 and 4.3.

As commented above, the difference $L^{i_3}_{10}(\mathbf{P}^2,A+2i\epsilon) - L^{i_3}_{10}(\mathbf{P}^2,A)$ is due entirely to the hole-hole part of $L^{i_3}_{10}$, the last term on the right hand side of eq. (6.16). From eq. (6.16) we have

$$\begin{aligned} L^{i_3}_{10}(\mathbf{P}^2,A+2i\epsilon) - L^{i_3}_{10}(\mathbf{P}^2,A) &= -m\int \frac{d^3q}{(2\pi)^3}\theta(\xi_{\alpha_1}-|\mathbf{P}+\mathbf{q}|)\theta(\xi_{\alpha_2}-|\mathbf{P}-\mathbf{q}|)\bigg(\frac{1}{A-\mathbf{q}^2+i\epsilon} \\ &\quad - \frac{1}{A-\mathbf{q}^2-i\epsilon}\bigg) = i2\pi m\int \frac{d^3q}{(2\pi)^3}\theta(\xi_{\alpha_1}-|\mathbf{P}+\mathbf{q}|)\theta(\xi_{\alpha_2}-|\mathbf{P}-\mathbf{q}|)\delta(A-\mathbf{q}^2) \ . \end{aligned} \tag{6.23}$$

Thanks to $\delta(A-\mathbf{q}^2)$ the A-integration in eq. (6.19) is now trivial. The values of $\mathbf{q}^2$ that satisfy the two in-medium θ-functions in eq. (6.23) for a given $|\mathbf{P}|$ are comprised in the interval $[A(\alpha),B(\alpha)]$, which is the domain of the A-integration in eq. (6.19). As a result eq. (6.13) turns into

$$\begin{aligned} \mathcal{E}_3 = 4\sum_{I,J,\ell,S}\sum_{i_3=-1}^{1}(2J+1)\chi(S\ell I)^2 \int \frac{d^3P}{(2\pi)^3}\frac{d^3q}{(2\pi)^3}\theta(\xi_{\alpha_1}-|\mathbf{P}+\mathbf{q}|)\theta(\xi_{\alpha_2}-|\mathbf{P}-\mathbf{q}|) \\ \times\Bigg[T^{i_3}_{JI}(\mathbf{q}^2,\mathbf{P}^2,\mathbf{q}^2) + m\int\frac{d^3p}{(2\pi)^3}\frac{1-\theta(\xi_{\alpha_1}-|\mathbf{P}+\mathbf{p}|)-\theta(\xi_{\alpha_2}-|\mathbf{P}-\mathbf{p}|)}{\mathbf{p}^2-\mathbf{q}^2-i\epsilon} \\ \times\Big[N^{i_3}_{JI}(\mathbf{p}^2)^{-1} + L^{i_3}_{10}(\mathbf{P}^2,\mathbf{q}^2)\Big]^{-1}\cdot\Big[N^{i_3}_{JI}(\mathbf{p}^2)^{-1} + L^{i_3}_{10}(\mathbf{P}^2,\mathbf{q}^2+2i\epsilon)\Big]^{-1}\Bigg]_{(\ell,\ell,S)} \ , \end{aligned} \tag{6.24}$$

where we have indicated explicitly the integration variables in the different functions. The isospin index $i_3 = \alpha_1 + \alpha_2$ and for $i_3 = 0$ one should take just one the two possible cases with $\alpha_1 = -\alpha_2$, $|\alpha_1| = 1/2$. It is straightforward to show that $\mathcal{E}_3$ given in eq. (6.24) is purely real, as it should be. First, the two θ-functions in the first line of eq. (6.24) imply that only the hole-hole part of L_{10} can have an imaginary part. It follows that $L_{10}^{i_3}(\mathbf{q}^2 + 2i\epsilon) = L_{10}^{i_3}(\mathbf{q}^2)^*$ and since, furthermore, $N_{JI}^{-1}(\mathbf{p}^2) + L_{10}^{i_3}(\mathbf{q}^2)$ is a symmetric matrix (for the $S = 1$ and $J = \ell \pm 1$ partial waves) or just a number (for the rest of partial waves), the diagonal elements of the product

$$\Big[N_{JI}^{i_3}(\mathbf{p}^2)^{-1} + L_{10}^{i_3}(\mathbf{q}^2)\Big]^{-1} \cdot \Big[N_{JI}^{i_3}(\mathbf{p}^2)^{-1} + L_{10}^{i_3}(\mathbf{q}^2 + 2i\epsilon)\Big]^{-1} \ , \tag{6.25}$$

are positive real numbers. In this way we have for the imaginary part of $\mathcal{E}_3$,

$$\begin{aligned}\mathrm{Im}(\mathcal{E}_3) = 4 \sum_{I,J,\ell,S} \sum_{i_3=-1}^{1} (2J+1)\chi(S\ell I)^2 \int \frac{d^3P}{(2\pi)^3}\frac{d^3q}{(2\pi)^3}\theta(\xi_{\alpha_1} - |\mathbf{P}+\mathbf{q}|)\theta(\xi_{\alpha_2} - |\mathbf{P}-\mathbf{q}|) \\ \times \Bigg[\mathrm{Im}T_{JI}^{i_3}(\mathbf{q}^2, \mathbf{P}^2, \mathbf{q}^2) + m\int \frac{d^3p}{(2\pi)^3}\Big\{1 - \theta(\xi_{\alpha_1} - |\mathbf{P}+\mathbf{p}|) - \theta(\xi_{\alpha_2} - |\mathbf{P}-\mathbf{p}|)\Big\} \\ \times \pi\delta(\mathbf{p}^2 - \mathbf{q}^2) T_{JI}^{i_3}(\mathbf{p}^2, \mathbf{P}^2, \mathbf{q}^2) \cdot T_{JI}^{i_3}(\mathbf{p}^2, \mathbf{P}^2, \mathbf{q}^2)^*\Bigg]_{(\ell,\ell,S)} .\end{aligned} \tag{6.26}$$

Taking into account eq. (4.31) and the expression for L_{10}, eq. (6.16), the imaginary part of $T_{JI}^{i_3}$ can also be calculated in terms of that of the hole-hole part of L_{10}. Substituting the result in eq. (6.26), it follows that

$$\begin{aligned}\mathrm{Im}(\mathcal{E}_3) = 4 \sum_{I,J,\ell,S} \sum_{i_3=-1}^{1} (2J+1)\chi(S\ell I)^2 \int \frac{d^3P}{(2\pi)^3}\frac{d^3q}{(2\pi)^3}\theta(\xi_{\alpha_1} - |\mathbf{P}+\mathbf{q}|)\theta(\xi_{\alpha_2} - |\mathbf{P}-\mathbf{q}|) \\ \times m\int \frac{d^3p}{(2\pi)^3}\pi\delta(\mathbf{p}^2 - \mathbf{q}^2)\Big\{1 - \theta(\xi_{\alpha_1} - |\mathbf{P}+\mathbf{p}|) - \theta(\xi_{\alpha_2} - |\mathbf{P}-\mathbf{p}|) \\ + \theta(\xi_{\alpha_1} - |\mathbf{P}+\mathbf{p}|)\theta(\xi_{\alpha_2} - |\mathbf{P}-\mathbf{p}|)\Big\} T_{JI}^{i_3} \cdot T_{JI}^{i_3\,*}\Big|_{(\ell,\ell,S)} .\end{aligned} \tag{6.27}$$

The quantity between curly brackets in the previous equation is

$$\big[1 - \theta(\xi_{\alpha_1} - |\mathbf{P}+\mathbf{p}|)\big]\big[1 - \theta(\xi_{\alpha_2} - |\mathbf{P}-\mathbf{p}|)\big] = \theta(|\mathbf{P}+\mathbf{p}| - \xi_{\alpha_1})\theta(|\mathbf{P}-\mathbf{p}| - \xi_{\alpha_2}) \ . \tag{6.28}$$

But given $|\mathbf{P}|$ and $|\mathbf{q}|$ satisfying simultaneously the θ-functions in the first line, corresponding to two Fermi-sea insertions, it is not possible that they also satisfy simultaneously the two θ-functions in eq. (6.28), corresponding to the particle-particle part. Note that due to the Dirac δ-function in eq. (6.27) $|\mathbf{q}| = |\mathbf{p}|$. As as result, it is clear that $\mathrm{Im}(\mathcal{E}_3) = 0$ once eq. (6.28) is inserted in eq. (6.27).

Writing explicitly

$$T_{JI}^{i_3}(\mathbf{p}^2, \mathbf{P}^2, \mathbf{q}^2) \cdot T_{JI}^{i_3}(\mathbf{p}^2, \mathbf{P}^2, \mathbf{q}^2)^*\Big|_{(\ell,\ell,S)} = \sum_{\ell'} T_{JI}^{i_3}(\ell, \ell', S; \mathbf{p}^2, \mathbf{P}^2, \mathbf{q}^2) T_{JI}^{i_3}(\ell', \ell, S; \mathbf{p}^2, \mathbf{P}^2, \mathbf{q}^2)^*, \tag{6.29}$$

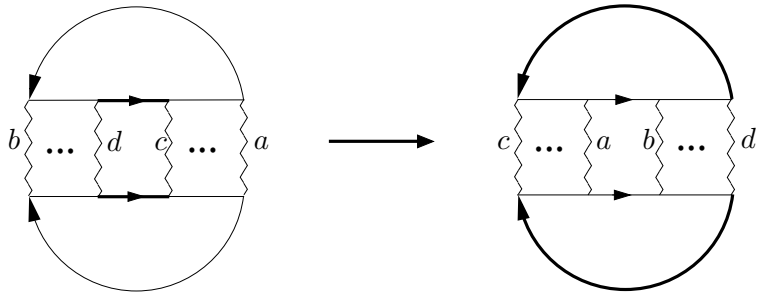

Figure 6.3: Cyclic permutation of the free nucleon propagators with Fermi-sea insertions. The labels on the potential lines are included to appreciate the permutation of lines in the graph. As usual the thick lines in fig. 6.3 refer to the insertion of a Fermi-sea.

we have for eq. (6.24)

$$\begin{aligned}\mathcal{E}_3 = 4 \sum_{I,J,\ell,S} \sum_{i_3=-1}^{1} (2J+1)\chi(S\ell I)^2 \int \frac{d^3P}{(2\pi)^3}\frac{d^3q}{(2\pi)^3}\theta(\xi_{\alpha_1}-|\mathbf{P}+\mathbf{q}|)\theta(\xi_{\alpha_2}-|\mathbf{P}-\mathbf{q}|) \\ \times \left[T^{i_3}_{JI}(\ell,\ell,S;\mathbf{q}^2,\mathbf{P}^2,\mathbf{q}^2) + m\int \frac{d^3p}{(2\pi)^3}\frac{1-\theta(\xi_{\alpha_1}-|\mathbf{P}+\mathbf{p}|)-\theta(\xi_{\alpha_2}-|\mathbf{P}-\mathbf{p}|)}{\mathbf{p}^2-\mathbf{q}^2-i\epsilon} \right. \\ \left. \times \sum_{\ell'} T^{i_3}_{JI}(\ell,\ell',S;\mathbf{p}^2,\mathbf{P}^2,\mathbf{q}^2) T^{i_3}_{JI}(\ell',\ell,S;\mathbf{p}^2,\mathbf{P}^2,\mathbf{q}^2)^* \right] . \end{aligned} \tag{6.30}$$

The process followed from eq. (6.13) up to here can be schematically drawn as in fig. 6.3. The particle-particle part that results by closing the external lines in the diagrams 3 of fig. 6.1 is transferred to a reducible two-nucleon loop entering the in-medium nucleon-nucleon partial waves. This corresponds to the integration in $\mathbf{p}$ in eq. (6.30), which is sandwiched between two partial waves amplitudes, one of them complex conjugated. The integration on $\mathbf{p}^2$ in eq. (6.30) is linearly divergent because of the first integral on the second line. The product

$$\sum_{\ell'} T^{i_3}_{JI}(\ell,\ell',S;\mathbf{p}^2,\mathbf{P}^2,\mathbf{q}^2) T^{i_3}_{JI}(\ell',\ell,S;\mathbf{p}^2,\mathbf{P}^2,\mathbf{q}^2)^* \tag{6.31}$$

tends to a constant for $\mathbf{p}^2 \to \infty$. Let us discuss how to regularize this integral, in the same way as already done for the calculation of the L_{ij} functions:

$$\begin{aligned} & - m\int \frac{d^3p}{(2\pi)^3}\frac{\sum_{\ell'} T^{i_3}_{JI}(\ell,\ell',S;\mathbf{p}^2,\mathbf{P}^2,\mathbf{q}^2) T^{i_3}_{JI}(\ell',\ell,S;\mathbf{p}^2,\mathbf{P}^2,\mathbf{q}^2)^*}{\mathbf{p}^2-\mathbf{q}^2-i\epsilon} \\ & = -\frac{m}{2\pi^2}\int_0^\infty dp \frac{\mathbf{p}^2}{\mathbf{p}^2-\mathbf{q}^2-i\epsilon} \sum_{\ell'} T^{i_3}_{JI}(\ell,\ell',S;\mathbf{p}^2,\mathbf{P}^2,\mathbf{q}^2) T^{i_3}_{JI}(\ell',\ell,S;\mathbf{p}^2,\mathbf{P}^2,\mathbf{q}^2)^* . \end{aligned} \tag{6.32}$$

Let us denote by $N^{i_3}_{JI;\infty}(\mathbf{P}^2,\mathbf{q}^2)^{-1}$ the limit for $\mathbf{p}^2 \to \infty$ of $N^{i_3}_{JI}(\mathbf{p}^2,\mathbf{P}^2,\mathbf{q}^2)^{-1}$. At leading order

this limit is a constant for each partial wave. Then, we rewrite the previous integral as

$$
\begin{aligned}
&-\frac{m}{2\pi^2}\int_0^\infty dp \frac{\mathbf{p}^2}{\mathbf{p}^2-\mathbf{q}^2-i\epsilon} \\
&\times\Bigg\{\left[N^{i_3}_{JI}(\mathbf{p}^2,\mathbf{P}^2,\mathbf{q}^2)^{-1}+L^{i_3}_{10}(\mathbf{P}^2,\mathbf{q}^2)\right]^{-1}\left[N^{i_3}_{JI}(\mathbf{p}^2,\mathbf{P}^2,\mathbf{q}^2)^{-1}+L^{i_3}_{10}(\mathbf{P}^2,\mathbf{q}^2+2i\epsilon)\right]^{-1} \\
&+\left[N^{i_3}_{JI,\infty}(\mathbf{P}^2,\mathbf{q}^2)^{-1}+L^{i_3}_{10}(\mathbf{P}^2,\mathbf{q}^2)\right]^{-1}\left[N^{i_3}_{JI,\infty}(\mathbf{P}^2,\mathbf{q}^2)^{-1}+L^{i_3}_{10}(\mathbf{P}^2,\mathbf{q}^2+2i\epsilon)\right]^{-1} \\
&-\left[N^{i_3}_{JI,\infty}(\mathbf{P}^2,\mathbf{q}^2)^{-1}+L^{i_3}_{10}(\mathbf{P}^2,\mathbf{q}^2)\right]^{-1}\left[N^{i_3}_{JI,\infty}(\mathbf{P}^2,\mathbf{q}^2)^{-1}+L^{i_3}_{10}(\mathbf{P}^2,\mathbf{q}^2+2i\epsilon)\right]^{-1}\Bigg\}\,. \qquad (6.33)
\end{aligned}
$$

Now, since ${N^{i_3}_{JI}}^{-1} \to {N^{i_3}_{JI,\infty}}^{-1} + \mathcal{O}(|\mathbf{p}|^{-2})$ the integral

$$
\begin{aligned}
&-\frac{m}{2\pi^2}\int_0^\infty dp \frac{\mathbf{p}^2}{\mathbf{p}^2-\mathbf{q}^2-i\epsilon} \\
&\times\Bigg\{\left[N^{i_3}_{JI}(\mathbf{p}^2,\mathbf{P}^2,\mathbf{q}^2)^{-1}+L^{i_3}_{10}(\mathbf{P}^2,\mathbf{q}^2)\right]^{-1}\left[N^{i_3}_{JI}(\mathbf{p}^2,\mathbf{P}^2,\mathbf{q}^2)^{-1}+L^{i_3}_{10}(\mathbf{P}^2,\mathbf{q}^2+2i\epsilon)\right]^{-1} \\
&-\left[N^{i_3}_{JI,\infty}(\mathbf{P}^2,\mathbf{q}^2)^{-1}+L^{i_3}_{10}(\mathbf{P}^2,\mathbf{q}^2)\right]^{-1}\left[N^{i_3}_{JI,\infty}(\mathbf{P}^2,\mathbf{q}^2)^{-1}+L^{i_3}_{10}(\mathbf{P}^2,\mathbf{q}^2+2i\epsilon)\right]^{-1}\Bigg\} \qquad (6.34)
\end{aligned}
$$

is convergent. The remaining integral in eq. (6.33) is expressed in terms of the function $g(\mathbf{q}^2)$, eq. (4.7),

$$
\begin{aligned}
&-\frac{m}{2\pi^2}\int_0^\infty dp \frac{\mathbf{p}^2}{\mathbf{p}^2-\mathbf{q}^2-i\epsilon}\left[N^{i_3}_{JI,\infty}(\mathbf{P}^2,\mathbf{q}^2)^{-1}+L^{i_3}_{10}(\mathbf{P}^2,\mathbf{q}^2)\right]^{-1}\left[N^{i_3}_{JI,\infty}(\mathbf{P}^2,\mathbf{q}^2)^{-1}\right. \\
&\left.+L^{i_3}_{10}(\mathbf{P}^2,\mathbf{q}^2+2i\epsilon)\right]^{-1} = g(\mathbf{q}^2)\sum_{\ell'} T^{i_3}_{JI,\infty}(\ell,\ell',S;\mathbf{P}^2,\mathbf{q}^2)T^{i_3}_{JI,\infty}(\ell',\ell,S;\mathbf{P}^2,\mathbf{q}^2)^*\,, \qquad (6.35)
\end{aligned}
$$

with

$$
T^{i_3}_{JI,\infty}(\ell',\ell,S;\mathbf{P}^2,\mathbf{q}^2) = \left[N^{i_3}_{JI,\infty}(\mathbf{P}^2,\mathbf{q}^2)^{-1}+L^{i_3}_{10}(\mathbf{P}^2,\mathbf{q}^2)\right]^{-1} = \lim_{\mathbf{p}^2\to\infty} T^{i_3}_{JI}(\ell',\ell,S;\mathbf{p}^2,\mathbf{P}^2,\mathbf{q}^2)\,. \qquad (6.36)
$$

To simplify the notation let us define the symbols

$$
\begin{aligned}
\Sigma_{p\ell} &= \sum_{\ell'} T^{i_3}_{JI}(\ell,\ell',S;\mathbf{p}^2,\mathbf{P}^2,\mathbf{q}^2)T^{i_3}_{JI}(\ell',\ell,S;\mathbf{p}^2,\mathbf{P}^2,\mathbf{q}^2)^*\,, \\
\Sigma_{\infty\ell} &= \sum_{\ell'} T^{i_3}_{JI,\infty}(\ell,\ell',S;\mathbf{P}^2,\mathbf{q}^2)T^{i_3}_{JI,\infty}(\ell',\ell,S;\mathbf{P}^2,\mathbf{q}^2)^*\,. \qquad (6.37)
\end{aligned}
$$

The function $g(\mathbf{q}^2)$ depends on the same subtraction constant g_0 already employed in the study of

the vacuum nucleon-nucleon interactions. The final expression for $\mathcal{E}_3$ in eq. (6.30) is then

$$\begin{aligned}\mathcal{E}_3 &= 4\sum_{I,J,\ell,S}\sum_{\alpha_1,\alpha_2}(2J+1)\chi(S\ell I)^2\int\frac{d^3P}{(2\pi)^3}\frac{d^3q}{(2\pi)^3}\theta(\xi_{\alpha_1}-|\mathbf{P}+\mathbf{q}|)\theta(\xi_{\alpha_2}-|\mathbf{P}-\mathbf{q}|)\Big[T^{i_3}_{JI}(\mathbf{q}^2,\mathbf{P}^2,\mathbf{q}^2)\\ &- g(\mathbf{q}^2)\Sigma_{\infty\ell} - m\int\frac{d^3p}{(2\pi)^3}\Big\{\frac{\theta(\xi_{\alpha_1}-|\mathbf{P}+\mathbf{p}|)+\theta(\xi_{\alpha_2}-|\mathbf{P}-\mathbf{p}|)}{\mathbf{p}^2-\mathbf{q}^2-i\epsilon}\Sigma_{p\ell}-\frac{\Sigma_{p\ell}-\Sigma_{\infty\ell}}{\mathbf{p}^2-\mathbf{q}^2-i\epsilon}\Big\}\Big]_{(\ell,\ell,S)}\\ &= 4\sum_{I,J,\ell,S}\sum_{\alpha_1,\alpha_2}(2J+1)\chi(S\ell I)^2\int\frac{d^3P}{(2\pi)^3}\frac{d^3q}{(2\pi)^3}\theta(\xi_{\alpha_1}-|\mathbf{P}+\mathbf{q}|)\theta(\xi_{\alpha_2}-|\mathbf{P}-\mathbf{q}|)\Big[T^{i_3}_{JI}(\mathbf{q}^2,\mathbf{P}^2,\mathbf{q}^2)\\ &- g_0\Sigma_{\infty\ell} + m\int\frac{d^3p}{(2\pi)^3}\Big\{\frac{1-\theta(\xi_{\alpha_1}-|\mathbf{P}+\mathbf{p}|)-\theta(\xi_{\alpha_2}-|\mathbf{P}-\mathbf{p}|)}{\mathbf{p}^2-\mathbf{q}^2-i\epsilon}\Sigma_{p\ell}-\frac{1}{\mathbf{p}^2}\Sigma_{\infty\ell}\Big\}\Big]_{(\ell,\ell,S)}\,. \qquad (6.38)\end{aligned}$$

6.3 Discussion and Results

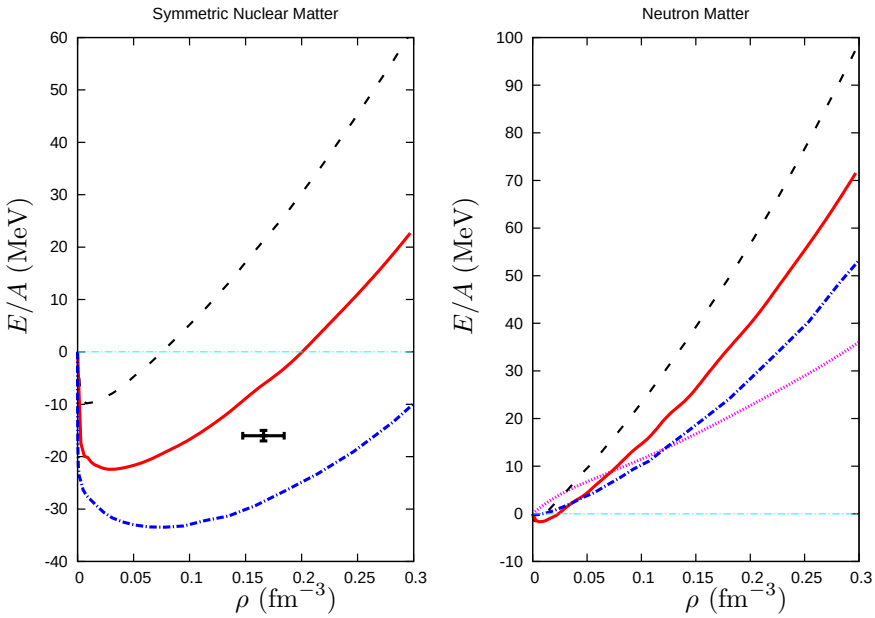

Figure 6.4: Binding energy per nucleon, $\mathcal{E}/\rho$, for symmetric nuclear matter, left panel, and for neutron matter, right panel. The (magenta) dotted line in the right panel is the result from the many-body calculation of [APR98] using realistic nucleon-nucleon potentials. The rest of the lines from top to bottom correspond to different values of the subtraction constant $g_0 = -0.25$, -0.37 and $-0.5\ m_\pi^2$, respectively. The cross in the left panel is the empirical saturation one for nuclear matter [BM90].

The sum of eqs. (6.2), (6.7) and (6.38) gives our result for the energy density $\mathcal{E}$ in nuclear matter at next-to-leading order,

$$\mathcal{E} = \mathcal{E}_1 - \mathcal{E}_2 - \mathcal{E}_3\ . \qquad (6.39)$$

We evaluate eq. (6.38) using the in-medium nucleon-nucleon partial waves determined at leading order in section 4.3. The sum over partial waves shows good convergence already for maximum $J = 4$ and we sum up to $J = 5$. The results for the binding energy per nucleon, $E/A = \mathcal{E}/\rho$, are shown in fig. 6.4 for symmetric nuclear matter, left panel, and for neutron matter, right panel. The

inserted point with errors on the left panel of fig. 6.4 corresponds to the experimental values for the saturation of nuclear matter $E/A = (-16 \pm 1)$ MeV and $\rho = (0.166 \pm 0.018)$ fm^{-3} quoted in [BM90]. The dotted line in the right panel is the result for neutron matter from the many-body calculation of the Urbana group [APR98]. It employs realistic nucleon-nucleon potentials and a fitted density dependent three-nucleon force in order to reproduce the experimental saturation point for nuclear matter. The rest of the curves, from top to bottom in both panels, correspond to the values of $g_0 = -0.25$, -0.37 and $-0.5\ m_\pi^2$, in order. We observe that our curves for symmetric nuclear

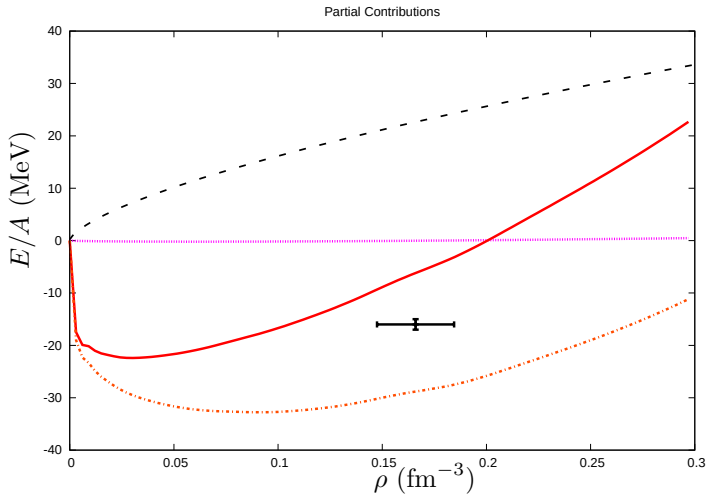

Figure 6.5: The partial contributions to $\mathcal{E}/\rho$, for symmetric nuclear matter and $g_0 = -0.37\ m_\pi^2$ are shown. The (black) dashed, (magenta) dotted, (orange) dot-dashed and solid lines are for $\mathcal{E}_1/\rho$, $-\mathcal{E}_2/\rho$, $-\mathcal{E}_3/\rho$ and their sum, respectively. The cross denotes the saturation point one for nuclear matter [BM90].

matter does have a minimum with a value in agreement with the experimental one, -16 ± 1 MeV, for $g_0 \simeq -0.30$. However, the position is displaced towards too low values of $\xi = \xi_n = \xi_p \sim 150$ MeV, too small by a factor 1.7 compared with the value $\xi \simeq 266 \pm 10$ MeV [BM90]. For the case of neutron matter, the curves are repulsive and are larger than the calculation of the Urbana group [APR98] above some density. It is clear from fig. 4.8 and 4.9 that we are employing for the calculation of eq. (6.38) nucleon-nucleon partial waves that do not reproduce closely the Nijmegen data in several partial waves, see figs. 4.8-4.10. As commented above, we are just employing the iteration of the one-pion exchange and two four-nucleon local vertices. One needs more elaborated nucleon-nucleon partial waves. Indeed, there are many mutual cancellations involved in the case of symmetric nuclear matter, between the purely kinetic energy term, $\mathcal{E}_1$, and between the S- and P-waves in $\mathcal{E}_3$, with $\mathcal{E}_2$ negligible small. Nevertheless, we find rather encouraging that our curves in fig. 6.4 can reproduce the main trends of $\mathcal{E}/\rho$ both for symmetric nuclear and neutron matter despite they are obtained employing in-medium nucleon-nucleon amplitudes calculated only at leading order. We already pointed out in section 4.2 that the one-pion exchange has a too large tensor force which is reduced by higher order counterterms (in the meson exchange approach this reduction is achieved by the exchange of ρ-mesons [BM94].) In [MLEA10] this point is emphasized in its study of nuclear binding because a large tensor force leads to less binding energy. Indeed, the partial waves $^3S_1$-$^3D_1$ and $^3P_0$ have large matrix elements of the one-pion exchange tensor operator [MLEA10] and these partial waves are not well reproduced in our study at leading order. We show in fig. 6.5 the different contributions to $\mathcal{E}/\rho$ for symmetric nuclear matter and $g_0 = -0.37\ m_\pi^2$, that corresponds to the solid lines in fig. 6.4. Namely, $\mathcal{E}_1/\rho$, $-\mathcal{E}_2/\rho$ and $-\mathcal{E}_3/\rho$ are given by the dashed, dotted and dot-dashed lines, with the sum corresponding to the full curve. As expected,

the contribution from $\mathcal{E}_2$, eq. (6.7), is very small since the derivative of Σ_f with respect to k^0 is $\mathcal{O}(p^2)$, as discussed in section 7.2. Notice that $\Sigma_f(k^0)=0$ for $k^0=0$ and $E(\mathbf{k})$ is very small. The other terms, $\mathcal{E}_1$ and $\mathcal{E}_3$ have similar size, though the former is $\mathcal{O}(p^5)$ and the latter $\mathcal{O}(p^6)$. This is due to the fact that the kinetic energy term is a recoil correction stemming from $\mathcal{L}^{(2)}_{\pi N}$, eq. (2.55), being suppressed numerically by the inverse of the large nucleon mass m. Notice that $\mathcal{E}_3/\rho$ scales like ρC, which introduces, compared with $\mathcal{E}_1/\rho$, the additional power of ξ times $1/2\pi^2$ from the density and $4\pi/p$ from $mC\sim m/g_0$. Both contributions have the same order of magnitude as the resulting factor $2\xi/\pi p\sim 1$. Additionally, there is also an extra suppression of the kinetic term contribution because of the dimensionality of space. The point is that $\mathcal{E}_1$ contains the integral of $\int_0^\xi d|\mathbf{k}||\mathbf{k}|^4=\xi^5/5$, while the extra factor of density in $\mathcal{E}_3$ goes like $\xi^3/3$, so that a numerical factor $3/5=0.6$ is suppressing $\mathcal{E}_1$. Then, the cancellation between the kinetic energy term and the one due to the nucleon-nucleon interactions is a consequence of keeping the natural size for the chiral counterterms, of similar size to the one-pion exchange as seen in section 4.2. Of course, the precise value resulting from such cancellations depends on g_0 as shown in fig. 6.4. Additionally, the presence of such cancellation enhance this dependence. E.g. for the neutron matter case the kinetic energy dominates the binding energy per nucleon and the dependence on g_0 is smaller indeed. $\mathcal{E}_3$ depends implicitly on g_0 through the nucleon-nucleon partial waves. Additionally, there is an explicit dependence from the first term on the last line of eq. (6.38), $g_0\Sigma_{\infty\ell}$. The implicit dependence is due to the truncated solution of eq. (4.16), as discussed in detail in section 4.2. The explicit one should be also related to this truncation given the close similarity between them. To make this clear let us notice that the partial wave $-T^{i_3}_{JI}(\ell,\ell,S;\mathbf{q}^2,\mathbf{P}^2,\mathbf{q}^2)$ appearing in eq. (6.38) can also be written from eq. (4.31) as:

$$
\begin{aligned}
&-T^{i_3}_{JI}(\ell,\ell,S;\mathbf{q}^2,\mathbf{P}^2,\mathbf{q}^2)=-\left[{N^{i_3}_{JI}}^{-1}(\mathbf{q}^2)+L^{i_3}_{10}(\mathbf{P}^2,\mathbf{q}^2)\right]^{-1}\\
&=-\sum_{\ell',\ell''}T^{i_3}_{JI}(\ell,\ell',S;\mathbf{q}^2,\mathbf{P}^2,\mathbf{q}^2)T^{i_3}_{JI}(\ell',\ell'',S;\mathbf{q}^2,\mathbf{P}^2,\mathbf{q}^2)^*\left({N^{i_3}_{JI}}^{-1}(\ell'',\ell,S;\mathbf{q}^2)+L^{i_3}_{10}(\mathbf{P}^2,\mathbf{q}^2)^*\delta_{\ell''\ell}\right)\,.
\end{aligned}
\tag{6.40}
$$

From the previous equation the term proportional to L_{10} is

$$
-L^{i_3}_{10}(\mathbf{P}^2,\mathbf{q}^2)^*\sum_{\ell'}T^{i_3}_{JI}(\ell,\ell',S;\mathbf{q}^2,\mathbf{P}^2,\mathbf{q}^2)T^{i_3}_{JI}(\ell',\ell,S;\mathbf{q}^2,\mathbf{P}^2,\mathbf{q}^2)^*=\left(-\mathrm{Re}L^{i_3}_{10}+i\,\mathrm{Im}L^{i_3}_{10}\right)\Sigma_{q\ell}\,.
\tag{6.41}
$$

Then, a similar dependence on g_0 as that of $g_0\Sigma_{\infty\ell}$ results from eq. (6.41) as $-g_0\Sigma_{q\ell}$. The sum of both is $-g_0(\Sigma_{q\ell}-\Sigma_{\infty\ell})$. Thus, as a higher order calculation should dismiss the dependence on $-g_0\Sigma_{q\ell}$, by analogy, we expect this to be the case also for $g_0\Sigma_{\infty\ell}$.

Another way of considering our power counting in eq. (3.23) is to use it for correcting order by order nucleon-nucleon amplitudes determined in vacuum. In this way, one can use better nucleon-nucleon partial waves, e.g. calculated at higher orders in momentum, and use in-medium corrections (whose calculation is always more cumbersome than diagrams in the vacuum) at lower orders. Another interesting issue left for further work is to explore the three-nucleon force influence on $\mathcal{E}$. This requires to consider the calculation of the energy density in the nucleon medium one order higher or $\mathcal{O}(p^7)$, since $V_\rho=3$.

6.3.1 Some phenomenology

In this section, we will give up the strict power counting scheme employed so far and try to analyse the possible effects of higher orders by some phenomenologically guided parameter fine-tuning. This will allow us to better understand the results obtained for nuclear and neutron matter in comparison to other recent studies, as e.g. in [LFA00, KFW02, KFW05].

As a first exercise, let us vary the parameter g_0 in order to improve the description of $\mathcal{E}/\rho$ for the case of neutron matter, so that our results agree better with the dotted line in fig. 6.4 corresponding to the sophisticated many-body calculation of [APR98]. The dashed line in fig. 6.6 is obtained employing $g_0 = -0.62\ m_\pi^2$. The so obtained fine-tuned curve is very close to the results of [APR98], even up to rather high densities (the deviation is then less than 10%.) Note as well that this result is obtained with a value of g_0 still of natural size, in the expected range around $-0.55\ m_\pi^2$. However, if we employ the same g_0 for evaluating $\mathcal{E}$ for symmetric nuclear matter the resulting curve has the minimum at its right position, $\rho \simeq 0.16$ fm^{-3}, but the value of the binding energy per nucleon is around -42 MeV, which is an over-binding by a factor 2.5.

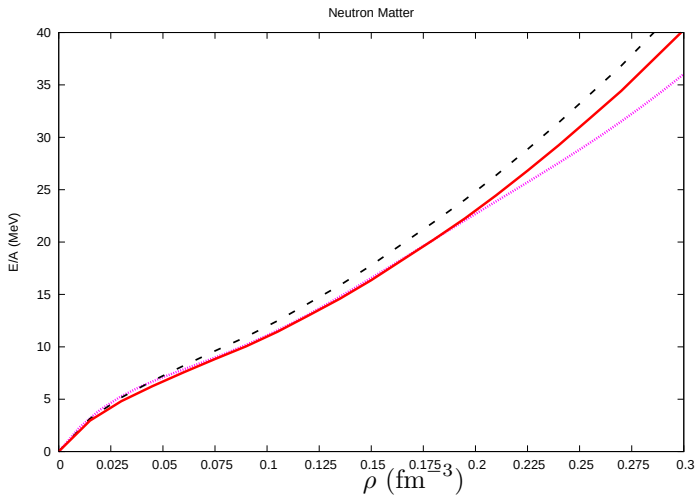

Figure 6.6: $\mathcal{E}/\rho$ for neutron matter. The (magenta) dotted line corresponds to the result of [APR98]. The (black) dashed line is obtained from eq. (6.38) with $g_0 = -0.62\ m_\pi^2$. The (red) solid line represents eq. (6.42) with $g_0 = -0.62\ m_\pi^2$ and $\widetilde{g}_0 = -0.65\ m_\pi^2$. See the text for further details.

To further analyse the density dependence of nuclear matter, we rewrite the contribution from the nucleon-nucleon interactions introducing by hand a new parameter, so that

$$\mathcal{E}_3 = 4 \sum_{I,J,\ell,S} \sum_{\alpha_1,\alpha_2} (2J+1)\chi(S\ell I)^2 \int \frac{d^3P}{(2\pi)^3}\frac{d^3q}{(2\pi)^3}\theta(\xi_{\alpha_1} - |\mathbf{P}+\mathbf{q}|)\theta(\xi_{\alpha_2} - |\mathbf{P}-\mathbf{q}|)\Big[T^{i_3}_{JI}(\mathbf{q}^2,\mathbf{P}^2,\mathbf{q}^2)$$
$$- \widetilde{g}_0\Sigma_\infty + m\int \frac{d^3p}{(2\pi)^3}\Big\{\frac{1-\theta(\xi_{\alpha_1}-|\mathbf{P}+\mathbf{p}|)-\theta(\xi_{\alpha_2}-|\mathbf{P}-\mathbf{p}|)}{\mathbf{p}^2-\mathbf{q}^2-i\epsilon}\Sigma_p - \frac{1}{\mathbf{p}^2}\Sigma_\infty\Big\}\Big]_{(\ell,\ell,S)} . \qquad (6.42)$$

Here we have distinguished between $\widetilde{g}_0$, that corresponds to the parameter g_0 that appears explicitly in $\mathcal{E}_3$ because of the diverging integral in eq. (6.32), and g_0, on which $\mathcal{E}_3$ depends implicitly through the dependence on the nucleon-nucleon partial waves. The idea is to mock up higher order effects by varying independently g_0 and $\widetilde{g}_0$ and exploit the phenomenological implications of such a procedure. While g_0 affects nucleon-nucleon scattering in vacuum, as discussed at length in section 4.2, $\widetilde{g}_0$

affects only the nuclear matter equation of state. E.g. employing $\widetilde{g}_0 = -0.67\ m_\pi^2$, which implies a change of 7% with respect to $g_0 = -0.62\ m_\pi^2$ used above, and that we also keep here, the solid curve in fig. 6.6 is obtained. The agreement for $\rho \lesssim 0.2$ fm^{-3} between our results and [APR98] is almost perfect.

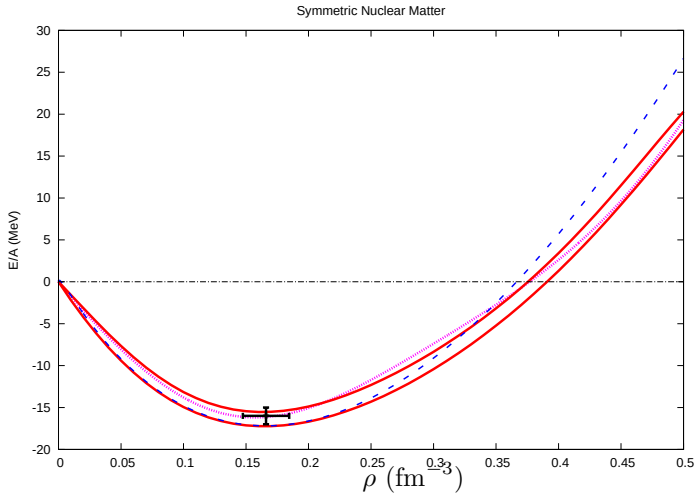

Figure 6.7: $\mathcal{E}/\rho$ for symmetric nuclear matter. The two (red) solid lines correspond from top to bottom to $(g_0, \widetilde{g}_0) = (-0.977, -0.512)\ m_\pi^2$ and $(-0.967, -0.525)\ m_\pi^2$, in order. The (blue) dashed line is obtained from eq. (6.43) adjusting to the minimum position and value of the lowest of our curves. The (magenta) dotted line is the result of [APR98].

For the case of symmetric nuclear matter the best results are obtained with $\widetilde{g}_0 = -0.52\ m_\pi^2$, and $g_0 = -0.97\ m_\pi^2$. Again the magnitude of both numbers is of natural size. This is shown in fig. 6.7 by the two solid lines which have $(g_0, \widetilde{g}_0) = (-0.977, -0.512)\ m_\pi^2$ and $(-0.967, -0.525)\ m_\pi^2$, in order from top to bottom in the figure. The corresponding value for E/A at the saturation point is -15.4 and -17.1 MeV, respectively. The experimental value given by the cross corresponds to -16 ± 1 MeV. The position of the minima for the same lines is $\rho = 0.169$ and $\rho = 0.168$ fm^{-3}, compared to the empirical value $\rho = 0.166 \pm 0.019$ fm^{-3}. In addition, the dotted line is the result from the many-body calculation of [APR98] employing realistic nucleon-nucleon interactions, that includes a free parameter to fix the three-nucleon interaction in the nuclear medium to reproduce the saturation point. We observe that our results reproduce very well the saturation point and agree closely with the calculation of [APR98].

As done in [KFW02] it is illustrative to compare our curves in fig. 6.7 with the following simple parameterization for the binding energy per nucleon in symmetric nuclear matter

$$\frac{\mathcal{E}}{\rho} = \frac{3\xi^2}{10m} - \alpha\frac{\xi^3}{m^2} + \beta\frac{\xi^4}{m^3}\ . \tag{6.43}$$

Interestingly, the nuclear matter incompressibility [Bl80, Vr97]

$$K = \xi^2 \frac{\partial^2 \mathcal{E}/\rho}{\partial \xi^2}\bigg|_{\xi_0} \tag{6.44}$$

is correctly given once α and β are known by adjusting the empirical nuclear matter saturation point. In this equation ξ_0 is the Fermi momentum at the saturation point. For the central values

of the point in fig. 6.7, $\rho = 0.166$ fm^{-3} and $E/A = -16$ MeV, the resulting nuclear matter incompressibility is $K = 259$ MeV, which is compatible with the experimental value $K = 250 \pm 25$ MeV [Bl80]. Our curves can be also described rather accurately by eq. (6.43), as shown by the dashed curve in fig. 6.7 obtained by adjusting the minimum position and value of the lowest of solid curves. Both curves run very close to each other and start to deviate for densities above $\rho \simeq 0.25$ fm^{-3}. The resulting nuclear matter incompressibility calculated from our results is $K = 254$ and 233 MeV, for the upper and lower solid curves, respectively. These values are compatible with the experimental value. The close agreement between our results and eq. (6.44) shows that, to a good approximation, the former admits an expansion in powers of the Fermi momentum as in eq. (6.43) for low ξ.

$^1S_0$	-8.80	-31.03	$^1D_2$	-1.56	-1.54	$^3S_1$	-42.85	-38.39	$^3G_3$	0.47	0.62
$^3P_0$	9.37	-1.42	$^3F_3$	1.71	1.76	$^3D_1$	-9.31	2.94	$^1F_3$	0.60	0.61
$^3P_1$	10.20	12.30	$^3F_4$	-0.04	-0.05	$^1P_1$	2.48	2.78	$^3G_4$	0.29	0.15
$^3P_2$	-1.13	-1.13	$^3H_4$	0.03	0.028	$^3D_2$	0.07	-1.65	$^3G_5$	0.32	0.35
$^3F_2$	-0.28	-0.28	$^1G_4$	-0.38	-0.38	$^3D_3$	0.91	1.11	$^3I_5$	0.23	0.26

Table 6.1: Contributions to E/A (MeV) in nuclear matter for the different partial waves considered at $\rho = 0.16$ fm^{-3}. The first column to the right of every partial wave corresponds to $g_0 = -0.977\ m_\pi^2$ and the second one to $g_0 = -0.521\ m_\pi^2$, with $\widetilde{g}_0$ fixed to $-0.512\ m_\pi^2$. The former is the top solid line in fig. 6.7 and the latter is nearly the dot-dashed line in the right panel of fig. 6.4.

In Table 6.1 we show the contributions to $\mathcal{E}_3$ (MeV) in nuclear matter for the different partial waves considered at the saturation point $\rho = 0.16$ fm^{-3}. The first column to the right of every partial wave corresponds to $g_0 = -0.977\ m_\pi^2$ and the second one to $g_0 = -0.521\ m_\pi^2$, and $\widetilde{g}_0$ is fixed to $-0.512\ m_\pi^2$ in the two cases. The former case is the top solid line in fig. 6.7 and the latter is nearly the dot-dashed line in the left panel of fig. 6.4. The kinetic energy contributes with 22.11 MeV per nucleon. One observes clearly the dominant role of the S-, P- and $^3D_1$ waves. It is remarkable the large influence of the medium on the $^3P_0$ partial wave that despite being attractive in vacuum gives a repulsive contribution in the medium for $(g_0, \widetilde{g}_0) = (-0.977, -0.512)\ m_\pi^2$, and only slightly attractive for $g_0 = \widetilde{g}_0 = -0.512\ m_\pi^2$. The change of the $^1S_0$ contribution with g_0 is due to the fact that for $g_0 = -0.977\ m_\pi^2$ the phase shifts decrease with energy (they are 30 and 20 degrees at $|\mathbf{p}| \simeq 100$ and 300 MeV, respectively), instead of stabilizing at around 60 degrees like happens for $g_0 = -0.512\ m_\pi^2$, see fig. 4.8. In this way, its contribution is less attractive. We also remark that the non-elastic partial waves, e.g. the $^3S_1 \to {}^3D_1$, also contribute to $\mathcal{E}_3$ from $\Sigma_{p\ell}$ and $\Sigma_{\infty\ell}$ and are included in the elastic ones. For a given partial wave they correspond to one term in the sum of two terms on ℓ' in eq. (6.37).

Thus, we are able to reproduce the equation of state of symmetric and neutron matter in terms of one fine-tuned free parameter, the value of $g_0 \simeq -0.97\ m_\pi^2$ for the symmetric nuclear matter case. The parameter $\widetilde{g}_0$ comes out always with a value close to the expected one, $-mm_\pi/4\pi = -0.54\ m_\pi^2$. For neutron matter one has $\widetilde{g}_0 \simeq -0.62\ m_\pi^2$ and for symmetric nuclear matter $\widetilde{g}_0 \simeq -0.52\ m_\pi^2$. In addition, it is worth stressing that the resulting values for g_0 are all negative with the appropriate size, so it is justified to solve approximately eq. (4.16) making use of UχPT. We think that this achievement is not a trivial fact and clearly indicates that our power counting, eq. (3.23), is able to map out properly the important dynamics in the nuclear medium and establish a useful hierarchy to allow for systematic calculations. We thus expect that when including higher orders in future calculations, it would not be necessary to adjust any parameter from the equation of state but all

appearing constants would be determined by considering the data in vacuum.

6.4 Conclusions and outlook

We have addressed the calculation of the energy density of nuclear matter $\mathcal{E}$. The non-perturbative technique developed gives rise to different contributions to $\mathcal{E}$ whose imaginary parts cancel between each other and a real value results, as it should. We obtain saturation in symmetric nuclear matter and repulsion for neutron matter. The contributions from the nucleon-nucleon interactions are of similar size to those from the kinetic energy term, the latter being suppressed by the inverse of the large nucleon mass and a dimensional factor. It is remarkable that we obtain for $g_0 \simeq -0.62 m_\pi^2$ a very good reproduction of sophisticated many-body calculations that employ realistic nucleon-nucleon potentials for the equation of state of neutron matter up to rather high nuclear densities. We can also achieve such a good agreement for the case of nuclear matter by allowing to distinguish between $\widetilde{g}_0$ and g_0, where the former parameter appears explicitly in the calculation of the binding energy per nucleon while the latter appears implicitly through the nucleon-nucleon scattering amplitudes involved. By this splitting, we can mock up the effects of higher orders. The parameter $\widetilde{g}_0$ can be fixed from the neutron matter equation of state. We then obtain a very accurate reproduction to $\mathcal{E}$ as function of density in symmetric nuclear matter for $g_0 = -0.97\ m_\pi^2$, with saturation at $\rho = 0.17$ fm^{-3} and $E/A = -16$ MeV, cf. the experimental values $\rho = 0.166 \pm 0.019$ fm^{-3} and $E/A = -16 \pm 1$ MeV. Furthermore, the nuclear matter incompressibility comes out with a value between 240-250 MeV, in perfect agreement with the experimental one of 250 ± 25 MeV. We interpret the success of our reproduction of the nuclear matter equation of state for both symmetric and neutron matter in terms of one free parameter for each of them as an indication that our power counting is a realistic one and that it is able to establish a useful hierarchy within the many contributions and complications inherent to nuclear dynamics. This opens the way to proceed systematically improving the calculations in a controlled way.

Certainly, higher orders should be worked out to obtain more precise results concerning the interesting problems considered here, and in particular predict the results in nuclear matter without any need of further fitting apart from that performed in vacuum to the scattering data. In particular, higher order calculations will address the interesting question about the importance of three-nucleon forces for nuclear matter saturation.

Chapter 7

In-medium pion self-energy[#7]

In this chapter our theory developed in the chapters 3 and 4 is applied to the problem of calculating the pion self-energy in asymmetric nuclear matter up-to-and-including next-to-leading order. We find that different next-to-leading order contributions to the isovector pion self-energy from in-medium nucleon-nucleon interactions cancel each other. The cancellation is shown once employing the developed non-perturbative techniques of Unitary χPT and another time by just considering general arguments. Some next-to-next-to-leading order contributions to the pion self-energy in the nuclear medium are also evaluated for further illustration of the non-perturbative methods. As a result, there are no corrections up to this order to the linear density approximation for the in-medium pion self-energy.

7.1 Introduction

The in-medium pion self-energy is applicable to a variety of physical problems. For instance a phase transition of nuclear or rather neutron matter due to the condensation of charged pions in dense nuclear matter has been extensively discussed since it was first suggested in the early seventies [Mi71, Sa72, Sc72, Mi78, OTW82]. Such a condensate is thought to occur at about twice the nuclear density, where attractive P-wave $n\pi^-$ interactions make the appearance of π^- energetically favorable. Another more recently debated example is the existence of narrow pionic $1s$ and $2p$ states in Pb and Sn that have been observed at GSI [Gi00, It00, Ge02, Su04]. Those deeply bound pionic states owe their existence to the subtle balance between the attractive Coulomb potential and the repulsive S-wave optical potential. The low-density theorem [DHL71] states, that to linear order in the density the optical potential is given by the T-matrix of πN-scattering at threshold times the density. It is known that threshold pion-nucleus interactions in the nuclear medium are more repulsive than in the vacuum, which is why corrections beyond linear density are demanded to have significant impact. Corrections beyond the linear density approximation have been derived in [EE66] employing analogies with optics. Those corrections can be interpreted as double-scattering in the nuclear medium, with the relevant πN-interactions parameterized through their scattering length. But it was found, that those still miss the required repulsiveness, therefore contributions from many-body interactions are expected to be substantial. For recent calculations see [KW01, PJM02, MOW02, CEO03, KKW03, GRW05, DO08].

[#7] The contents of this chapter have been published in [LOMb].

Our novel power counting and the developed non-perturbative methods are applied to the problem of calculating the pion self-energy in asymmetric nuclear matter at next-to-leading order. This problem is related to that of pionic atoms since the pion self-energy and the pion-nucleus optical potential are tightly connected [EE66, BGF97, FG07]. Despite being an old subject, a conclusive calculation of the pion self-energy in a systematic and controlled expansion is still lacking. In particular, the problem of the missing S-wave repulsion, the renormalization of the isovector scattering length a^- in the nuclear medium [CEO03, DO08] and the energy-dependence of the isovector amplitude [FG07] is not settled yet, despite the recent progress [MOW02, KKW03, FG07].

After this introduction we present the basic formalism and the resulting topological contributions to the in-medium pion self-energy up to next-to-leading order in subsection 8.1.1. We give the calculation of the $V_\rho = 1$ contributions in section 7.2 and the $V_\rho = 2$ contributions in section 7.3. A mutual cancellation of the isovector parts of the pion self-energy due to nucleon-nucleon interactions will be discussed in detail in section 7.4. Results and their discussion will be given in section 7.5 and a summary with conclusions and outlook in section 7.6.

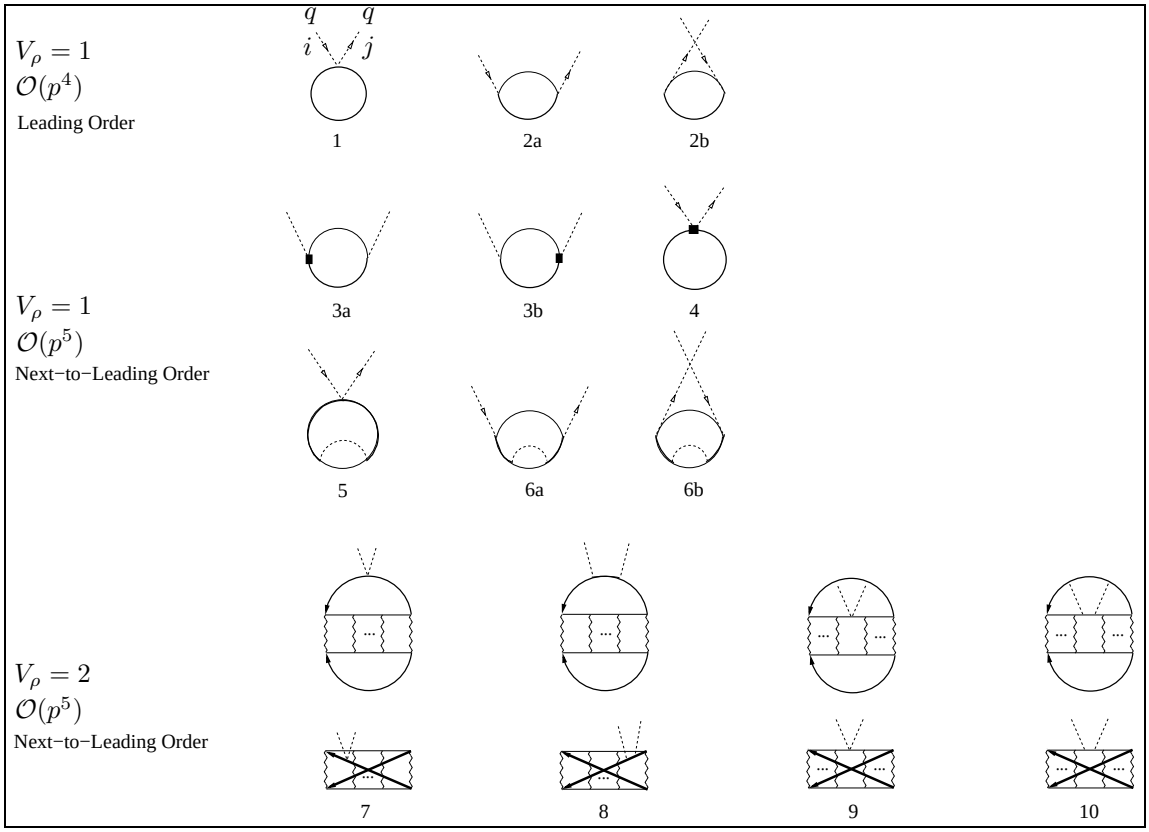

Figure 7.1: Contributions Π_i to the in-medium pion self-energy up-to-and-including next-to-leading order, $\mathcal{O}(p^5)$. The pions are indicated by the dashed lines and the squares correspond to next-to-leading order pion-nucleon vertices. A wiggly line corresponds to the nucleon-nucleon interaction kernel, fig. 4.1, whose iteration is denoted by the ellipsis. Note that for diagrams 3a, 3b, 8 and 10 the momentum flow of the external pion lines may enter or leave the diagram. The diagrams 9 and 10 have a symmetry factor of 1/2.

7.1.1 Topological contributions

In terms of the pion self-energy Π the dressed pion propagator reads

$$i\Delta(q) = \frac{i}{q^2 - m_\pi^2 + \Pi + i\epsilon} \ . \tag{7.1}$$

Note our sign convention. The different contributions to the in-medium pion self-energy are denoted by Π_i and shown in fig. 7.1. To determine the set of diagrams needed for their calculation up to next-to-leading order we proceed by increasing V_ρ step by step in eq. (3.22). For each V_ρ we then determine the possible configurations of vertices and lines according to eq. (3.22). The diagrams can easily be identified by considering the vacuum diagrams of pion-nucleon scattering, but then closing the external nucleon lines with the full in-medium propagator G_0, eq. (3.12).

7.2 $V_\rho = 1$ contributions

First we consider those contributions to the pion self-energy in the nuclear medium due to pion-nucleon dynamics. They are depicted in the diagrams 1–6 of fig. 7.1.

7.2.1 Leading order

The first diagram in fig. 7.1 corresponds to

$$\Pi_1 = i\varepsilon_{ij3}\,\frac{-q_0}{2f_\pi^2}(\rho_p - \rho_n) \ , \tag{7.2}$$

and arises by closing the Weinberg-Tomozawa (WT) term in pion-nucleon scattering. In the previous equation $\rho_{p(n)} = \xi^3_{p(n)}/3\pi^2$ is the proton(neutron) density. Π_1 is an S-wave isovector self-energy.

The diagram 2a in fig. 7.1 is represented by Π_{2a} and is obtained by closing the nucleon pole terms in pion-nucleon scattering, with the one-pion vertex from the lowest order meson-baryon chiral Lagrangian $\mathcal{L}^{(1)}_{\pi N}$ [BKM95],

$$\Pi_{2a} = -\frac{g_A^2}{4f_\pi^2}\int \frac{d^3k}{(2\pi)^3}\ \mathrm{Tr}\left[\left(\frac{1+\tau_3}{2}\theta(\xi_p - |\mathbf{k}|) + \frac{1-\tau_3}{2}\theta(\xi_n - |\mathbf{k}|)\right)\frac{\tau^i\tau^j\,\vec{\sigma}\cdot\mathbf{q}\vec{\sigma}\cdot\mathbf{q}}{E(\mathbf{k}) - q_0 - E(\mathbf{k}-\mathbf{q}) + i\epsilon}\right] \ , \tag{7.3}$$

In eq. (7.3) we have not included the in-medium part of the intermediate nucleon propagator because $q_0 \simeq m_\pi \gg E(\mathbf{k}) - E(\mathbf{k}-\mathbf{q})$, so that the argument of the in-medium Dirac delta-function of eq. (3.11) cannot be fulfilled. By the same token

$$\frac{1}{E(\mathbf{k}) - E(\mathbf{k}-\mathbf{q}) - q_0} = -\frac{1}{q_0} - \frac{E(\mathbf{k}) - E(\mathbf{k}-\mathbf{q})}{q_0^2} + \mathcal{O}(q) \ , \tag{7.4}$$

and the $\mathcal{O}(q)$ terms contribute one order higher than next-to-leading order. On the other hand,

$$E(\mathbf{k}) - E(\mathbf{k}-\mathbf{q}) = -\frac{\mathbf{q}^2 - 2\mathbf{k}\cdot\mathbf{q}}{2m} \ , \tag{7.5}$$

and the $\mathbf{k}\cdot\mathbf{q}$ term, when included in eq. (7.3), does not contribute because of the angular integration. Then,

$$\Pi_{2a} = \frac{g_A^2}{4f_\pi^2 q_0}\left(1-\frac{\mathbf{q}^2}{2mq_0}\right)\int\frac{d^3k}{(2\pi)^3}\ \mathrm{Tr}\left[\left(\frac{1+\tau_3}{2}\theta(\xi_p-|\mathbf{k}|)+\frac{1-\tau_3}{2}\theta(\xi_n-|\mathbf{k}|)\right)\tau^i\tau^j\,\vec{\sigma}\cdot\mathbf{q}\vec{\sigma}\cdot\mathbf{q}\right]\ . \tag{7.6}$$

The same procedure can be applied to the diagram 2b of fig. 7.1 (which corresponds to the same expression as Π_{2a} but with the exchanges $q_0\to -q_0$ and $i\leftrightarrow j$). Summing both, one has

$$\Pi_2^{iv} = i\varepsilon_{ij3}\,\frac{g_A^2\,\mathbf{q}^2}{2f_\pi^2 q_0}(\rho_p-\rho_n)\ , \tag{7.7}$$

$$\Pi_2^{is} = \delta_{ij}\,\frac{-g_A^2\mathbf{q}^2}{2f_\pi^2 q_0^2}\frac{\mathbf{q}^2}{2m}(\rho_p+\rho_n)\ . \tag{7.8}$$

The superscripts iv and is refer to the isovector and isoscalar nature of the corresponding contribution to Π_2, respectively. Both are P-wave self-energies but Π_2^{is} is a recoil correction of Π_2^{iv} and it is suppressed by the inverse of the nucleon mass.

7.2.2 Next-to-leading order

We now consider the sum of the diagrams 3a and 3b of fig. 7.1, where the squares indicate a next-to-leading order one-pion vertex from $\mathcal{L}_{\pi N}^{(2)}$, eq. (2.55). It should be understood that the pion lines can leave or enter these diagrams. We also employ the expansion of eq. (7.4) for the nucleon propagator, although for this case it is only necessary to keep the term $\pm 1/q_0$ because the diagram is already a next-to-leading order contribution. The calculation yields

$$\Pi_3 = \delta_{ij}\,\frac{g_A^2\mathbf{q}^2}{2mf_\pi^2}(\rho_p+\rho_n)\ . \tag{7.9}$$

This is an isoscalar P-wave contribution. In this case the next-to-leading order pion-nucleon vertex is a recoil correction of the leading order one and this is why Π_3 is suppressed by the inverse of the nucleon mass.

The diagram 4 in fig. 7.1 is given by

$$\Pi_4 = \delta_{ij}\,\frac{2}{f_\pi^2}\left(-2c_1m_\pi^2+q_0^2\Big(c_2+c_3-\frac{g_A^2}{8m}\Big)-c_3\mathbf{q}^2\right)(\rho_p+\rho_n)\ . \tag{7.10}$$

Π_4 is an isoscalar contribution in which the term $-2\delta_{ij}c_3\mathbf{q}^2(\rho_p+\rho_n)/f_\pi^2$ is P-wave and the rest is S-wave. Indeed, the low-energy constant c_3 is known to be dominated by the contribution of the $\Delta(1232)$ [BKM97]. For a Fermi momentum $\xi\simeq 2m_\pi$, corresponding to symmetric nuclear matter saturation, the Fermi energy of a two-nucleon system is around 80 MeV, which is still significantly smaller than the Δ-nucleon mass difference. One then expects that integrating out the Δ-resonance and parameterizing its effects in terms of the chiral counterterms is meaningful in the range of energies we are considering. This is indeed an important conclusion of [KEM07, KEM08] where chiral EFTs with/without Δs are employed to evaluate different orders of the two-nucleon and three-nucleon potentials. We leave as a future improvement of our results to include explicitly the Δ resonances.

The diagram 5 of fig. 7.1 originates by dressing the in-medium nucleon propagator eq. (3.9), with the in-medium one-pion loop nucleon self-energy eq. (5.21). Its contribution Π_5 can be written as

$$\Pi_5 = \varepsilon_{ijk}\,\frac{q_0}{2f_\pi^2}\int\frac{d^4k}{(2\pi)^4}e^{ik^0\eta}\;\mathrm{Tr}\left\{\tau^k\,G_0(k)\,\Sigma^\pi(k)\,G_0(k)\right\}\;, \tag{7.11}$$

with the convergence factor $e^{ik^0\eta}$, $\eta\to 0^+$, associated with any closed loop made up by a single nucleon line [FW03]. The trace acts in the spin and isospin spaces, performing it gives the result

$$\Pi_5 = \varepsilon_{ijk}\,\frac{q_0}{f_\pi^2}\int\frac{d^4k}{(2\pi)^4}e^{ik^0\eta}\left(G_0(k)_p^2\Sigma_p^\pi - G_0(k)_n^2\Sigma_n^\pi\right)\;. \tag{7.12}$$

Next, we employ the identity

$$G_0(k)_{i_3}^2 = -\frac{\partial}{\partial k^0}G_0(k)_{i_3}\;, \tag{7.13}$$

that follows from the right hand side of the first line of eq. (3.9). A similar identity also holds at the matrix level

$$G_0(k)^2 = -\frac{\partial}{\partial k^0}G_0(k)\;, \tag{7.14}$$

because of the orthogonality of the isospin projectors $(1+\tau_3)/2$ and $(1-\tau_3)/2$. Integrating by parts, as the convergence factor allows, we then have

$$\Pi_5 = \varepsilon_{ij3}\frac{q_0}{f_\pi^2}\int\frac{d^4k}{(2\pi)^4}e^{ik^0\eta}\left(G_0(k)_p\frac{\partial\Sigma_p^\pi}{\partial k^0} - G_0(k)_n\frac{\partial\Sigma_n^\pi}{\partial k^0}\right)\;. \tag{7.15}$$

We perform the integration over k^0 making use of the Cauchy-integration theorem. For that we close the integration contour along the upper k^0-complex plane with an infinite semicircle. Because of the convergence factor the integration over the infinite semicircle is zero as $\mathrm{Im}k^0\to+\infty$ along it. One should then study the positions of the poles and cuts in k^0 for $G_0(k)_{i_3}$ and $\Sigma_{i_3}^\pi$ in eq. (7.15). First let us note that Σ_f has only singularities for $\mathrm{Im}k^0 < 0$, as follows from eq. (5.10). This is also evident for the free part of $G_0(k)_{i_3}$, see eq. (3.9). As a result, there is no contribution when the integrand in eq. (7.15) involves only free nucleon propagators.

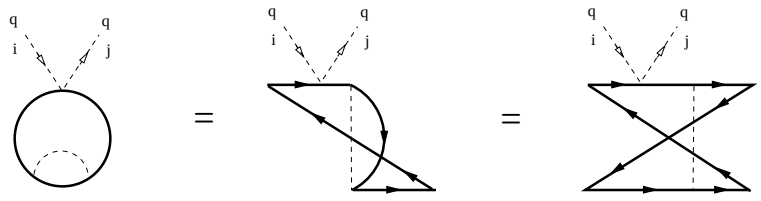

Figure 7.2: The equivalence between the diagram 5 of fig. 7.1, when only density-dependent parts in the nucleon propagators are considered, and the one-pion exchange reduction of the diagram 7 is shown. The second diagram from the left is an intermediate step in the continuous transformation of the diagram from the far left to that on the far right.

The contribution with only the density-dependent part both in $G_0(k)_{i_3}$ as well as in the nucleon propagator involved in the loop for $\Sigma_{i_3}^\pi$ is part of the diagram 7 in fig. 7.1, corresponding to a $V_\rho = 2$ contribution. In fig. 7.2 we depict such an equivalence for the diagrams 5 and 7 of fig. 7.1.

An analogous result would hold for the diagrams 6 and 8. The different $V_\rho = 2$ contributions are evaluated in section 7.3.1, so we skip them right now.

Consequently we consider in this section only the contributions of eq. (7.15) where we have simultaneously one free-space and one density-dependent part involved in the nucleon propagator G_0 and the nucleon self-energy Σ^π. Two contributions arise: the first one results by employing the density-part of the in-medium propagator $G_0(k)_{i_3}$, given in eq. (3.11).[#8] The integration over k^0 is trivial due to the Dirac-delta function, with the result

$$\Pi_5^I = i\varepsilon_{ij3}\frac{q_0}{f_\pi^2}\int\frac{d^3k}{(2\pi)^3}\big[\theta(\xi_p-|\mathbf{k}|)-\theta(\xi_n-|\mathbf{k}|)\big]\left.\frac{\partial\Sigma_f^\pi}{\partial k^0}\right|_{k^0=E(\mathbf{k})} . \tag{7.16}$$

The other contribution involves the free part of $G_0(k)_{i_3}$ and can be written as

$$\Pi_5^{II} = -\varepsilon_{ij3}\frac{q_0}{f_\pi^2}\int\frac{d^4k}{(2\pi)^4}e^{ik^0\eta}\left[\frac{\partial}{\partial k^0}\frac{1}{k^0-E(\mathbf{k})+i\epsilon}\right]\big[\Sigma_{p,m}^\pi-\Sigma_{n,m}^\pi\big] . \tag{7.17}$$

Following an analogous calculation as for the diagram $\mathcal{E}_2$ in section 6.2, but taking into account the isovector nature of the problem at hand, we can further evaluate eq. (7.17)

$$\Pi_5^{II} = i\varepsilon_{ij3}\frac{1}{3}\frac{q_0}{f_\pi^2}\int\frac{d^3k}{(2\pi)^3}\big[\theta(\xi_p-|\mathbf{k}|)-\theta(\xi_n-|\mathbf{k}|)\big]\left.\frac{\partial\Sigma_f^\pi}{\partial k^0}\right|_{k^0=E(\mathbf{k})} . \tag{7.18}$$

where the factor of $1/3$ arises due to the isovector structure in combination with the flavor content of the self-energies $\Sigma_{i_3,m}^\pi$, eqs. (5.19). The sum of both contributions is then given by

$$\Pi_5 = i\varepsilon_{ij3}\frac{4}{3}\frac{q_0}{f_\pi^2}\int\frac{d^3k}{(2\pi)^3}\big[\theta(\xi_p-|\mathbf{k}|)-\theta(\xi_n-|\mathbf{k}|)\big]\left.\frac{\partial\Sigma_f^\pi}{\partial k^0}\right|_{k^0=E(\mathbf{k})} . \tag{7.19}$$

Π_5 is an isovector S-wave contribution to the pion self-energy. We find that this contribution is of order $\mathcal{O}(p^6)$ and therefore N^{2}LO. This due to the fact that $\partial\Sigma_f^\pi/\partial k^0 = \mathcal{O}(p^2)$, as follows directly from eq. (5.12). We originally counted Π_5^a as $\mathcal{O}(p^5)$ because $\partial\Sigma_f^\pi/\partial k^0$ was taken as $\mathcal{O}(p)$, since $\Sigma_f^\pi = \mathcal{O}(p^3)$ and $k^0 = \mathcal{O}(p^2)$. However, this evaluation of the order of a derivative, based on dimensional analysis, represents indeed a lower bound and its actual order might be higher, as it is the case here. This mismatch is due to the presence of the variable b, defined after eq. (5.11), in addition to k^0. The chiral order of the former is fixed by m_π^2 and not by k_0^2. In [LOMb] it was argued, that the part Π_5^{II} is one order higher than assumed and therefore neglected. The part Π_5^I was kept, but at the end is was found that it is also suppressed by one order. On the contrary, as we have seen, both parts are of the same order and can be brought to the same form with comparable prefactors. In the sake of evaluating the contributions numerically in section 7.5 we keep both parts here. Comparing our result with the one of [KW01] we find that there is in fact behavior beyond linear density from the particular contribution Π_5, eq. (7.19). However, this is a resummation of higher order effects steming from the fixing $k^0 = E(\mathbf{k})$ for $\partial\Sigma_f^\pi/\partial k^0$, while the authors of [KW01] imposed the extreme non-relativistic limit by taking $k^0 = 0$.

Now we consider the diagrams 6 of fig. 7.1. The diagram 6a gives

$$\Pi_{6a} = i\frac{g_A^2}{4f_\pi^2}\int\frac{d^4k}{(2\pi)^4}e^{ik^0\eta}\ \mathrm{Tr}\left\{\frac{\tau^i\vec\sigma\cdot\mathbf{q}\ \tau^j\vec\sigma\cdot(-\mathbf{q})}{k^0-q^0-E(\mathbf{k}-\mathbf{q})+i\epsilon}\,G_0(k)\,\Sigma^\pi(k)\,G_0(k)\right\} \tag{7.20}$$

[#8] For the remainder of this section we deviate from depicting the content of [LOMb] regarding the evaluation of the contributions of diagrams 5 and 6, see text.

where we have omitted the Fermi sea insertion in the intermediate propagator, following the discussion after eq. (7.3). We now take into account that $(\vec{\sigma}\cdot\mathbf{q})^2 = \mathbf{q}^2$ and perform the traces. Integrating by parts in k^0, eq. (7.20) becomes

$$\Pi_{6a} = -i\frac{g_A^2\mathbf{q}^2}{2f_\pi^2}\int\frac{d^4k}{(2\pi)^4}e^{ik^0\eta}\sum_{i_3}(\tau^i\tau^j)_{i_3i_3}\,G_0(k)_{i_3}\,\frac{\partial\Sigma^\pi(k)_{i_3}}{\partial k^0}\frac{1}{k^0-q^0-E(\mathbf{k}-\mathbf{q})+i\epsilon}$$
$$-\,i\frac{g_A^2\mathbf{q}^2}{2f_\pi^2}\int\frac{d^4k}{(2\pi)^4}e^{ik^0\eta}\sum_{i_3}(\tau^i\tau^j)_{i_3i_3}\,G_0(k)_{i_3}\,\Sigma^\pi(k)_{i_3}\frac{\partial}{\partial k^0}\frac{1}{k^0-q^0-E(\mathbf{k}-\mathbf{q})+i\epsilon}\,, \qquad (7.21)$$

where i_3 denote the isospin indices. Π_{6b} is obtained from Π_{6a} by replacing $q^\mu \to -q^\mu$ and $i \leftrightarrow j$. The free propagator on the far right hand side of eq. (7.21) can be expanded around q^0, since it is counted as $\mathcal{O}(p)$ while the other quantities are $\mathcal{O}(p^2)$. (Alternatively one could keep the propagator during the evaluation and employ eq. (7.4) in the end, since there will always occur the fixing term $k^0 = E(\mathbf{k})$ due to a delta function.) Adding the diagrams Π_{6a} and Π_{6b} we obtain

$$\Pi_6 = i\frac{g_A^2\mathbf{q}^2}{2f_\pi^2q_0}\int\frac{d^4k}{(2\pi)^4}e^{ik^0\eta}\sum_{i_3}[\tau^i,\tau^j]_{i_3i_3}\,G_0(k)_{i_3}\,\frac{\partial\Sigma^\pi(k)_{i_3}}{\partial k^0}$$
$$+\,i\frac{g_A^2\mathbf{q}^2}{2f_\pi^2q_0^2}\int\frac{d^4k}{(2\pi)^4}e^{ik^0\eta}\sum_{i_3}\{\tau^i,\tau^j\}_{i_3i_3}\,G_0(k)_{i_3}\,\Sigma^\pi(k)_{i_3}\,, \qquad (7.22)$$

Following an analogous procedure to the one given for Π_5 below eq. (7.15), the integration over k^0 is performed first. As a result, for the previous equation we only take the contributions that simultaneously involve one free-space and one density-dependent part of the nucleon propagators in $G_0(k)$ and in the loop giving rise to $\Sigma^\pi(k)$. The contribution with only free-space parts vanishes because the integration over k^0 along the upper half-plane. While that with only density-dependent parts is included in the evaluation of the diagram 8 of fig. 7.1 in section 7.3.1. According to the discussion of Π_5, we have two remaining contributions with each time one free-space and one density-dependent part in the propagator $G_0(k)$ and the nucleon self-energy $\Sigma^\pi(k)$. In this way, the contribution denoted by Π_6^I, that involves $\Sigma_f^\pi(k)$ and the density-dependent parts in $G_0(k)$, is given by

$$\Pi_6^I = -i\varepsilon_{ij3}\frac{g_A^2\mathbf{q}^2}{f_\pi^2q_0}\int\frac{d^3k}{(2\pi)^3}\big[\theta(\xi_p-|\mathbf{k}|)-\theta(\xi_n-|\mathbf{k}|)\big]\,\frac{\partial\Sigma_f^\pi(k)}{\partial k^0}\bigg|_{k0=E(\mathbf{k})}$$
$$-\,\delta_{ij}\frac{g_A^2\mathbf{q}^2}{f_\pi^2q_0^2}\int\frac{d^3k}{(2\pi)^3}\big[\theta(\xi_p-|\mathbf{k}|)+\theta(\xi_n-|\mathbf{k}|)\big]\,\Sigma_f^\pi(k)\big|_{k0=E(\mathbf{k})}\,. \qquad (7.23)$$

We denote by Π_6^{II} the contribution with $\Sigma_{i_3,m}^\pi(k)$ and the free part of $G_0(k)$ that is given by

$$\Pi_6^{II} = \varepsilon_{ij3}\frac{g_A^2\mathbf{q}^2}{f_\pi^2q_0}\int\frac{d^4k}{(2\pi)^4}e^{ik^0\eta}\left[\frac{\partial}{\partial k^0}\frac{1}{k^0-E(\mathbf{k})+i\epsilon}\right]\big[\Sigma_{p,m}^\pi-\Sigma_{n,m}^\pi\big]$$
$$+\,i\delta_{ij}\frac{g_A^2\mathbf{q}^2}{f_\pi^2q_0^2}\int\frac{d^4k}{(2\pi)^4}e^{ik^0\eta}\frac{1}{k^0-E(\mathbf{k})+i\epsilon}\big[\Sigma_{p,m}^\pi+\Sigma_{n,m}^\pi\big]\,. \qquad (7.24)$$

Proceeding as we did in the calculations for $\mathcal{E}_2$ and Π_5 we obtain

$$\Pi_6^{II} = -i\varepsilon_{ij3}\frac{1}{3}\frac{g_A^2\mathbf{q}^2}{f_\pi^2q_0}\int\frac{d^3k}{(2\pi)^3}\big[\theta(\xi_p-|\mathbf{k}|)-\theta(\xi_n-|\mathbf{k}|)\big]\,\frac{\partial\Sigma_f^\pi(k)}{\partial k^0}\bigg|_{k0=E(\mathbf{k})}$$
$$-\,\delta_{ij}\frac{g_A^2\mathbf{q}^2}{f_\pi^2q_0^2}\int\frac{d^3k}{(2\pi)^3}\big[\theta(\xi_p-|\mathbf{k}|)+\theta(\xi_n-|\mathbf{k}|)\big]\,\Sigma_f^\pi(k)\big|_{k0=E(\mathbf{k})}\,. \qquad (7.25)$$

Finally, adding Π_6^I and Π_6^{II} we obtain for the isovector part the factor 4/3 as for Π_5 and for the isoscalar part the factor 2 as for $\mathcal{E}_2$,

$$\Pi_6^{iv} = -i\varepsilon_{ij3}\frac{4}{3}\frac{g_A^2}{f_\pi^2}\frac{\mathbf{q}^2}{q_0}\int\frac{d^3k}{(2\pi)^3}\big[\theta(\xi_p-|\mathbf{k}|)-\theta(\xi_n-|\mathbf{k}|)\big]\;\frac{\partial\Sigma_f}{\partial k^0}\Big|_{k^0=E(\mathbf{k})}\;, \tag{7.26}$$

$$\Pi_6^{is} = -\delta_{ij}2\frac{g_A^2}{f_\pi^2}\frac{\mathbf{q}^2}{q_0^2}\int\frac{d^3k}{(2\pi)^3}\big[\theta(\xi_p-|\mathbf{k}|)+\theta(\xi_n-|\mathbf{k}|)\big]\;\Sigma_f|_{k^0=E(\mathbf{k})}\;. \tag{7.27}$$

Π_6 is a P-wave self-energy contribution. Actually Π_6^{iv} is one order higher than expected, similarly to Σ_5. For Π_6^{is} this follows obviously from its explicit expression in eq. (7.23) as $\Sigma_f^\pi = \mathcal{O}(p^3)$. Note, that we would have obtained the same result if we had kept the free propagator of the Born term and had made the separation in the two part I and II for diagrams 6a and 6b, distinctively. After the integration in k^0 we would have employed eq. (7.4). Adding the diagrams and their two parts afterwards, yields the same result.

In this section we have undertaken the calculation of the diagrams in fig. 7.1 that can be fully accounted for by pion-nucleon dynamics. All the contributions calculated in this sections, Π_1 to Π_4, as well as the leading contributions of Π_5 and Π_6, are linear in density. We have shown that up to next-to-leading order only the leading contributions, Π_1 and Π_2, and the next-to-leading order ones Π_3 and Π_4 have to be kept. Π_5 and Π_6 are finally one order higher.

7.3 $V_\rho = 2$ contributions

We now consider those next-to-leading order contributions to the pion self-energy in the nuclear medium that involve the nucleon-nucleon interactions. They are depicted in the diagrams of the last two rows of fig. 7.1, where the ellipsis indicate the iteration of the two-nucleon reducible loops.

7.3.1 Contributions from the nucleon self-energy due to nuclear interactions

In this section we consider those diagrams in fig. 7.1 that include the nucleon-nucleon contributions to the nucleon self-energy in the nuclear medium, diagrams 7 and 8. In turn, for each of these figures the one on the top corresponds to the direct nucleon-nucleon interactions, while the exchange part gives rise to the diagram on the bottom (that includes the part of the diagrams 5 and 6 with all nucleon propagators corresponding to Fermi sea insertions).

First, let us consider the evaluation of the diagrams 7 in fig. 7.1, denoted by Π_7. It is given by

$$\Pi_7 = \varepsilon_{ijk}\frac{q_0}{2f_\pi^2}\int\frac{d^4k_1}{(2\pi)^4}e^{ik_1^0\eta}\;\mathrm{Tr}\left\{\tau^k G_0(k_1)\Sigma^{NN}G_0(k_1)\right\}\;, \tag{7.28}$$

where Σ^{NN} defined in eq. (5.28). Note, that the crossed term of diagram 7 is included in Σ^{NN}. Performing the trace in isospin,

$$\Pi_7 = \varepsilon_{ij3}\frac{q_0}{2f_\pi^2}\sum_{\sigma_1}\int\frac{d^4k_1}{(2\pi)^4}e^{ik_1^0\eta}\left(G_0(k_1)_p^2\Sigma_p^{NN}-G_0(k_1)_n^2\Sigma_n^{NN}\right)\;. \tag{7.29}$$

Here σ_1 corresponds to the spin of the incident nucleon. Taking into account the identity eq. (7.13) we can integrate by parts eq. (7.29) with the result

$$\Pi_7 = \varepsilon_{ij3}\frac{q_0}{2f_\pi^2}\sum_{\sigma_1}\int\frac{d^4k_1}{(2\pi)^4}e^{ik_1^0\eta}\left(G_0(k_1)_p\frac{\partial\Sigma_p^{NN}}{\partial k_1^0}-G_0(k_1)_n\frac{\partial\Sigma_n^{NN}}{\partial k_1^0}\right)\ . \tag{7.30}$$

This, after using eq. (5.27), becomes

$$\Pi_7 = i\varepsilon_{ij3}\frac{-q_0}{2f_\pi^2}\sum_{\sigma_1,\sigma_2}\int\frac{d^4k_1}{(2\pi)^4}\frac{d^4k_2}{(2\pi)^4}e^{ik_1^0\eta}e^{ik_2^0\eta}\Bigg(G_0(k_1)_pG_0(k_2)_p\frac{\partial}{\partial k_1^0}T_{pp}^{\sigma_1\sigma_2}(\mathbf{p},\mathbf{P};A)$$
$$-G_0(k_1)_nG_0(k_2)_n\frac{\partial}{\partial k_1^0}T_{nn}^{\sigma_1\sigma_2}(\mathbf{p},\mathbf{P};A)\Bigg)\ . \tag{7.31}$$

In order to obtain this result we have used that

$$\sum_{\sigma_1,\sigma_2}\int\frac{d^4k_1}{(2\pi)^4}\frac{d^4k_2}{(2\pi)^4}e^{ik_1^0\eta}e^{ik_2^0\eta}\Bigg(G_0(k_1)_pG_0(k_2)_n\frac{\partial}{\partial k_1^0}T_{NN}(k_1\sigma_1p,k_2\sigma_2n|k_1\sigma_1p,k_2\sigma_2n)$$
$$-G_0(k_1)_nG_0(k_2)_p\frac{\partial}{\partial k_1^0}T_{NN}(k_1\sigma_1n,k_2\sigma_2p|k_1\sigma_1n,k_2\sigma_2p)\Bigg)=0\ , \tag{7.32}$$

which follows for two reasons. First, let us notice that because of Fermi-Dirac statistics

$$T_{NN}(k_1\sigma_1p,k_2\sigma_2n|k_1\sigma_1p,k_2\sigma_2n)=T_{NN}(k_2\sigma_2n,k_1\sigma_1p|k_2\sigma_2n,k_1\sigma_1p)\ . \tag{7.33}$$

Second, at leading order the amplitude T_{NN} is given by the iteration of the wiggly line in fig. 4.2. The latter does neither depend on k_1^0 nor on k_2^0, see eqs. (4.2) and (4.3). Since the two-nucleon reducible loop $L_{10}^{i_3}$ depends on k_1^0 and k_2^0 only through their sum $k_1^0+k_2^0$, the scattering amplitude T_{NN} at leading order also only depends on them in the same way. Thus $\partial T_{NN}/\partial k_1^0=\partial T_{NN}/\partial k_2^0$ holds. Taking these two facts into account, as k_i and σ_i are dummy variables, eq. (7.32) is obtained.

From eqs. (7.29) and (5.27) one has to sum over the spins σ_1 and σ_2. The fact that both the initial and final nucleon-nucleon states are the same implies a great simplification in the equations. First, if we set $\sigma_1=\sigma_1'$ and $\sigma_2=\sigma_2'$ in eq. (A.9) and sum,

$$\sum_{\sigma_1,\sigma_2}(\sigma_1\sigma_2s_3'|s_1s_2S')(\sigma_1\sigma_2s_3|s_1s_2S)=\delta_{s_3's_3}\delta_{S'S}\ . \tag{7.34}$$

The sum over the third components of orbital angular momentum and s_3 in the partial wave decomposition of eq. (5.27) becomes

$$\sum_{m',m,s_3}(m's_3\mu|\ell'SJ)(ms_3\mu|\ell SJ)Y_{\ell'}^{m'}(\hat{\mathbf{p}})Y_\ell^m(\hat{\mathbf{p}})^*=\delta_{\ell'\ell}\frac{2J+1}{4\pi}\ . \tag{7.35}$$

Here we have made use of the symmetry properties of the Clebsch-Gordan coefficients and of the addition theorem for the spherical harmonics [Ro95],

$$(m's_3\mu|\ell'SJ)=(-1)^{s_3+S}\left(\frac{2J+1}{2\ell'+1}\right)^{1/2}(-s_3\mu m'|SJ\ell')\ ,$$
$$\frac{1}{2\ell+1}\sum_m|Y_\ell^m(\hat{\mathbf{p}})|^2=\frac{1}{4\pi}\ . \tag{7.36}$$

Whence, the sum of partial waves that matters for eq. (7.28) can be expressed as

$$\sum_{\sigma_1,\sigma_2} T^{\sigma_1\sigma_2}_{\alpha_1\alpha_2}(\mathbf{p},\mathbf{P};A) = \sum_{I,J,\ell,S} (2J+1)\chi(S\ell I)^2 T^{i_3}_{JI}(\ell,\ell,S)(\alpha_1\alpha_2 i_3|I_1 I_2 I)^2 \ , \tag{7.37}$$

with $\chi(S\ell 1)$ defined in eq. (A.8). Inserting eq. (7.37) in eq. (7.31) the following expression for Π_7 results

$$\Pi_7 = i\varepsilon_{ij3}\frac{-q_0}{2f_\pi^2}\int \frac{d^4k_1}{(2\pi)^4}\frac{d^4k_2}{(2\pi)^4} e^{ik_1^0\eta}e^{ik_2^0\eta} \sum_{J,\ell,S,i_3} i_3\,(2J+1)\chi(S\ell 1)^2 \\ \times G_0(k_1)_{\alpha_1} G_0(k_2)_{\alpha_2} \frac{\partial}{\partial k_1^0} T^{i_3}_{J1}(\ell,\ell,S) \ , \tag{7.38}$$

where $i_3 = \alpha_1 + \alpha_2$. Π_7 is an S-wave isovector self-energy contribution. This should be expected due to the presence of the WT vertex for the coupling of the in- and out-going pions with a nucleon, see diagram 7 of fig. 7.1 and eq. (7.30).

We now consider the diagrams 8 in fig. 7.1, that involve the Born terms of pion-nucleon scattering. They are similar to the diagrams 6, though the nucleon self-energy is now due to the in-medium nucleon-nucleon interactions. Making use of eq. (7.13) and then integrating by parts, we have

$$\Pi_8 = i\varepsilon_{ij3}\frac{ig_A^2}{2f_\pi^2}\frac{\mathbf{q}^2}{q_0}\sum_{\sigma_1}\int \frac{d^4k_1}{(2\pi)^4} e^{ik_1^0\eta}\left(\frac{\partial\Sigma_p^{NN}}{\partial k_1^0}G_0(k_1)_p - \frac{\partial\Sigma_n^{NN}}{\partial k_1^0}G_0(k_1)_n\right) \\ + \delta_{ij}\frac{ig_A^2}{2f_\pi^2}\frac{\mathbf{q}^2}{q_0^2}\sum_{\sigma_1}\int \frac{d^4k_1}{(2\pi)^4} e^{ik_1^0\eta}\Big(\Sigma_p^{NN}G_0(k_1)_p + \Sigma_n^{NN}G_0(k_1)_n\Big) \ , \tag{7.39}$$

where the first term on the right hand side of the previous expression is isovector and the last one is isoscalar. The former is referred to as Π_8^{iv} and the latter as Π_8^{is}. Taking into account eq. (7.37) one is left with

$$\Pi_8^{iv} = i\varepsilon_{ij3}\frac{g_A^2}{2f_\pi^2}\frac{\mathbf{q}^2}{q_0}\int \frac{d^4k_1}{(2\pi)^4}\frac{d^4k_2}{(2\pi)^4} e^{ik_1^0\eta}e^{ik_2^0\eta} \sum_{J,\ell,S,i_3} i_3\,(2J+1)\chi(S\ell 1)^2 G_0(k_1)_{\alpha_1} G_0(k_2)_{\alpha_2} \frac{\partial}{\partial k_1^0} T^{i_3}_{J1}(\ell,\ell,S) \tag{7.40}$$

$$\Pi_8^{is} = \delta_{ij}\frac{g_A^2}{2f_\pi^2}\frac{\mathbf{q}^2}{q_0^2}\int \frac{d^4k_1}{(2\pi)^4}\frac{d^4k_2}{(2\pi)^4} e^{ik_1^0\eta}e^{ik_2^0\eta} \sum_{J,\ell,S,I,i_3} (2J+1)\chi(S\ell I)^2 G_0(k_1)_{\alpha_1} G_0(k_2)_{\alpha_2} T^{i_3}_{JI}(\ell,\ell,S) \ . \tag{7.41}$$

Eqs. (7.38) and (7.40) involve the knowledge of the derivative of the nucleon-nucleon partial wave amplitude with respect to the energy k_1^0. Instead of the variable k_1^0 we use the variable A, eq. (5.30), which is also the argument of L_{10} and use the relation

$$\frac{\partial f(P^0)}{\partial k_1^0} = \frac{\partial f(P^0)}{\partial k_2^0} = \frac{m\partial}{\partial A} f(P^0) \ , \tag{7.42}$$

with $f(P^0)$ an arbitrary function that depends on k_1^0 and k_2^0 only through their sum. Let us now obtain expressions for the derivative of $\partial T_{JI}/\partial A$. At leader order (LO) and next-to-leading order (NLO) the expression of eq. (4.36) reduces to

$$\left.\frac{\partial T_{JI}}{\partial A}\right|_{LO} = D_{JI}^{(0)\,-1}\cdot\left[-\big(N_{JI}^{(0)}\big)^2\cdot\frac{\partial L_{10}}{\partial A}\right]\cdot D_{JI}^{(0)\,-1} \ , \\ \left.\frac{\partial T_{JI}}{\partial A}\right|_{NLO} = D_{JI}^{(1)\,-1}\cdot\left[\frac{\partial L_{JI}^{(1)}}{\partial A} - \Big\{N_{JI}^{(1)},N_{JI}^{(0)}\Big\}\cdot\frac{\partial L_{10}}{\partial A}\right]\cdot D_{JI}^{(1)\,-1} \ . \tag{7.43}$$

with the anti-commutator $\{B, C\} = B \cdot C + C \cdot B$ and

$$D_{JI}^{(0)} = I + N_{JI}^{(0)} \cdot L_{10} \ ,$$
$$D_{JI}^{(1)} = I + \left(N_{JI}^{(0)} + N_{JI}^{(1)}\right) \cdot L_{10} = D_{JI}^{(0)} + N_{JI}^{(1)} \cdot L_{10} \ . \tag{7.44}$$

Eqs. (7.38), (7.40) and (7.41) represent the contributions from diagrams 7 and 8 of fig. 7.1 to the pion self-energy in the nucleon medium. Their contributions are denoted by Π_7 and Π_8, respectively. The former is purely isovector while the latter contains both an isovector and an isoscalar part, proportional to ε_{ij3} and δ_{ij}, in that order. Π_7 and Π_8^{iv} are given by the same expression except by the global factor, proportional to q_0 for the former and to $-g_A^2\mathbf{q}^2/q_0$ for the latter. This is just a consequence of the chiral expansion eq. (7.4) in the Born terms. On the other hand, Π_8^{is} is a N^{2}LO contribution because it originates from the derivative with respect to k_1^0 of the nucleon-propagator between the two pion lines. This propagator is not enhanced so that one order higher results in comparison with the isovector part.

7.3.2 Nucleon-nucleon contributions with pion production terms

We now consider the calculation of those contributions that originate from the diagrams 9 and 10 of fig. 7.1, where a pion scatters inside a two-nucleon reducible loop. They are denoted by Π_9 and Π_{10}, in order. As usual the diagram on the top corresponds to the direct part of the nucleon-nucleon scattering while that on the bottom represents the exchange part. We refer to the discussion of subsection 4.4.2 where we obtained the final expressions

$$\xi_{JI}^{(0)} = -\left(N_{JI}^{(0)}\right)^2 \cdot DL_{10} \ , \tag{4.39}$$

and

$$\xi_{JI}^{(0)} + \xi_{JI}^{(1)} = DL_{JI}^{(1)} - \left\{L_{JI}^{(1)} + \left(N_{JI}^{(0)}\right)^2 \cdot L_{10},\, N_{JI}^{(0)}\right\} \cdot DL_{10} \ . \tag{4.42}$$

Note that in the previous expressions the two pions are attached to the loops DL_{10} and $DL_{JI}^{(1)}$, while the remaining terms originate because of nucleon-nucleon scattering. The nucleon propagator

Figure 7.3: Born terms in pion-nucleon scattering. The vertices correspond to the lowest order pion-nucleon vertex.

before and after the filled circles in fig. 4.11 is the same so that it appears squared. This is required as the initial and final pion is also the same. We rewrite the nucleon propagator squared as

$$\left[\frac{\theta(\xi_\alpha - |\mathbf{p}_1 - \mathbf{k}|)}{p_1^0 - k_1^0 - E(\mathbf{p}_1 - \mathbf{k}) - i\epsilon} + \frac{\theta(|\mathbf{p}_1 - \mathbf{k}| - \xi_\alpha)}{p_1^0 - k_1^0 - E(\mathbf{p}_1 - \mathbf{k}) + i\epsilon}\right]^2$$
$$= -\frac{\partial}{\partial z}\left[\frac{1}{p_1^0 + z - k_1^0 - E(\mathbf{p}_1 - \mathbf{k}) + i\epsilon} + i(2\pi)\delta(p_1^0 + z - k_1^0 - E(\mathbf{p}_1 - \mathbf{k}))\theta(\xi_\alpha - |\mathbf{p}_1 - \mathbf{k}|)\right]_{z=0} . \tag{7.45}$$

The filled circles in fig. 4.11 consists of a WT pion-nucleon vertex and of the pion-nucleon scattering Born terms shown in fig. 7.3. Its sum is

$$-\frac{iq_0}{2f_\pi^2}\varepsilon_{ijk}\tau^k-\left(\frac{g_A}{2f}\right)^2\mathbf{q}^2\Big\{\frac{\tau^j\tau^i}{q^0+p_1^0-k_1^0-E(\mathbf{p}_1-\mathbf{k}+\mathbf{q})+i\epsilon} + \frac{\tau^i\tau^j}{-q^0+p_1^0-k_1^0-E(\mathbf{p}_1-\mathbf{k}-\mathbf{q})+i\epsilon}\Big\}\ . \quad (7.46)$$

We do not include the in-medium part of the nucleon propagator in the previous equation because for $q_0=\mathcal{O}(m_\pi)$ the argument of the Dirac delta-function in eq. (3.9) is never satisfied as $m_\pi\gg\mathcal{O}$(nucleon kinetic energy). For the same reason, when performing the k_1^0-integration in the loop, the poles at $k_1^0=p_1^0\pm q_0-E(\mathbf{p}_1-\mathbf{k}\pm\mathbf{q})$, resulting from eq. (7.46), are not considered because the nucleon propagators will not be any longer of $\mathcal{O}(p^{-2})$ but just of $\mathcal{O}(p^{-1})$ (standard counting). A contribution two orders higher would then result. Once the k_1^0-integration is done the latter acquires from eq. (7.45) the value $z+p_1^0-E(\mathbf{p}_1-\mathbf{k})$. The integration on k_1^0 for the evaluation of the two-nucleon reducible loop is analogous to the one performed in appendix C.2 for calculating the L_{10} function. The point is that L_{10} only depends on the energy of the external legs through the variable $A=m(p_1^0+p_2^0)-\mathbf{P}^2$, eq. (5.30), that in turn only depends on the total energy. As a result, when the derivative with respect to z acts on a baryon propagator not entering in eq. (7.46), one has

$$\frac{\partial L^{ab\ldots}_{k\ell,r}}{\partial z}=\frac{\partial L^{ab\ldots}_{k\ell,r}}{\partial p_1^0}=m\frac{\partial L^{ab\ldots}_{k\ell,r}}{\partial A}=\frac{\partial L^{ab\ldots}_{k\ell,r}}{\partial p_2^0}\ . \quad (7.47)$$

Taking into account the chiral expansion of the nucleon propagators involved in eq. (7.46) for the pole terms and summing with the WT term, we have the leading contribution

$$i\varepsilon_{ijk}\tau^k\frac{q_0}{2f_\pi^2}\left(g_A^2\frac{\mathbf{q}^2}{q_0^2}-1\right)\doteq i\varepsilon_{ijk}\tau^k\,\kappa_{iv}\ . \quad (7.48)$$

The antisymmetric tensor in eq. (7.48) gives rise to the isospin factor $2i_3$ in the evaluation of the loops in fig. 4.11. Notice that in the loop the pions are attached to the propagators of the two nucleons, the upper and the lower ones, and these two contributions sum symmetrically. We can then plug into eqs. (4.39) and (4.42) for this case

$$DL_{10;iv}=i\varepsilon_{ij3}\,2i_3\,\kappa_{iv}\frac{m\partial}{\partial A}L_{10}^{i_3}\ . \quad (7.49)$$

In this equations we have included the subscript iv given its isovector character. In the same way for $DL_{JI}^{(1)}$ one has

$$DL^{(1)}_{JI;iv}=i\varepsilon_{ij3}\,2i_3\,\kappa_{iv}\frac{m\partial}{\partial A}L_{JI}^{(1);i_3}\ , \quad (7.50)$$

which corresponds to eq. (7.49) but substituting the term between brackets, where the nucleon-nucleon vertices are on-shell, by its exact calculation. By applying eq. (4.42) we can fix $\xi^{(1)}_{JI;iv}$ in terms of eqs. (7.49) and (7.50).

We now consider the case where the derivative with respect to z from eq. (7.45) acts on the baryon propagators involved in the Born terms of eq. (7.46) with $k_1^0=p_1^0+z-E(\mathbf{p}_1-\mathbf{k})$. The term

$E(\mathbf{p}_1 - \mathbf{k}) - E(\mathbf{p}_1 - \mathbf{k} \pm \mathbf{q})$ can be neglected when summed with q_0 for our calculation to next-to-leading order, so that the derivative with respect to z of eq. (7.46) yields the isoscalar contribution

$$-\delta_{ij} \frac{g_A^2}{2f_\pi^2} \frac{\mathbf{q}^2}{q_0^2} \doteq \delta_{ij}\, \kappa_{is} \ . \tag{7.51}$$

For any i_3 the isospin identity operator gives rise to $+2$, instead of the factor $2i_3$ of the isovector case. In this way, we can employ eqs. (7.49) and (7.50) substituting the vertex eq. (7.48) by eq. (7.51) and removing the action of the derivative $m\partial/\partial A$. Thus,

$$\begin{aligned} DL_{10;is} &= \delta_{ij}\, 2\, \kappa_{is}\, L_{10}^{i_3} \ , \\ DL_{JI;is}^{(1)} &= \delta_{ij}\, 2\, \kappa_{is}\, L_{JI}^{(1);i_3} \ . \end{aligned} \tag{7.52}$$

Here the subscript is is introduced given their isoscalar character. They give rise to Π_{10}^{is}. Notice that both $DL_{10;is}$ and $DL_{JI;is}^{(1)}$ are one order higher than the analogous isovector terms in eqs. (7.49) and (7.50), respectively. This makes that Π_{10}^{is} starts to contribute at N^{2}LO.

Next, we proceed to obtain the expressions for the pion self-energy corresponding to the diagrams 9 and 10 of fig. 7.1 as a sum over partial waves. The leading contribution is obtained by using $\xi_{JI;iv}^{(0)}$, eq. (7.49), with the result

$$\begin{aligned} \left(\Pi_9 + \Pi_{10}^{iv}\right)\big|_{NLO} = i\varepsilon_{ij3}\kappa_{iv} \frac{m}{2} \int \frac{d^4k_1}{(2\pi)^4} \frac{d^4k_2}{(2\pi)^4} e^{ik_1^0\eta} e^{ik_2^0\eta} \sum_{J,\ell,S,i_3} 2i_3\,(2J+1)\chi(S\ell 1)^2 \\ \times G_0(k_1)_{\alpha_1} G_0(k_2)_{\alpha_2} [D_{J1}^{(0);i_3}]^{-1} \cdot N_{J1}^{(0)} \cdot \frac{\partial L_{10}^{i_3}}{\partial A} \cdot N_{J1}^{(0)} \cdot [D_{J1}^{(0);i_3}]^{-1} \ , \end{aligned} \tag{7.53}$$

where the part corresponding to Π_{10}^{iv} is the one proportional to g_A^2 in the previous equation. A symmetry factor $1/2$ is included given the symmetry under the exchange of the two nucleonic external lines when they are finally closed.

In section 7.4 it will be established that at $\mathcal{O}(p^5)$ all the contributions to the pion self-energy involving nucleon-nucleon interactions vanish ($V_\rho = 2$). This implies that the contributions Π_7, Π_8^{iv}, Π_9 and Π_{10}^{iv} must cancel mutually at this order. Recall that the isoscalar ones, Π_8^{is} and Π_{10}^{is}, are $\mathcal{O}(p^6)$. The argument given is a general one, without assuming any specific procedure for resumming the nucleon-nucleon interactions. We now show that UχPT fulfills this requirement. When substituting into eqs. (7.38) and (7.40) the derivative $\partial T_{JI}/\partial A$ eq. (7.43) at the lowest order, the following result is obtained

$$\begin{aligned} \left(\Pi_7 + \Pi_8^{iv}\right)\big|_{NLO} = -i\varepsilon_{ij3}\kappa_{iv} m \int \frac{d^4k_1}{(2\pi)^4} \frac{d^4k_2}{(2\pi)^4} e^{ik_1^0\eta} e^{ik_2^0\eta} \sum_{J,\ell,S,i_3} i_3\,(2J+1)\chi(S\ell 1)^2 \\ \times G_0(k_1)_{\alpha_1} G_0(k_2)_{\alpha_2} [D_{J1}^{(0);i_3}]^{-1} \cdot N_{J1}^{(0)} \cdot \frac{\partial L_{10}^{i_3}}{\partial A} \cdot N_{J1}^{(0)} \cdot [D_{J1}^{(0);i_3}]^{-1} \ , \end{aligned} \tag{7.54}$$

This equation is the same as eq. (7.53) but with opposite sign so that the cancellation with $\Pi_9 + \Pi_{10}^{iv}$ takes place.

7.3.3 Partial higher order contributions

In the following of this section we work out several N^{2}LO contributions that comprise the isoscalar term Π_{10}^{is} as well those that are obtained by employing $\partial T/\partial A$ to next-to-leading order and $DL_{JI;iv}^{(1)}$

in $\Pi_7 + \Pi_8^{iv}$ and $\Pi_9 + \Pi_{10}^{iv}$, respectively. For the leading isoscalar contribution from diagram 10, Π_{10}^{is}, which is already $\mathcal{O}(p^6)$ due to the same reason as for Π_8^{is}, we obtain

$$\Pi_{10}^{is}\big|_{N^2LO} = \delta_{ij}\kappa_{is}\int \frac{d^4k_1}{(2\pi)^4}\frac{d^4k_2}{(2\pi)^4}e^{ik_1^0\eta}e^{ik_2^0\eta}\sum_{J,\ell,S,I,i_3}(2J+1)\chi(S\ell I)^2 \\ \times G_0(k_1)_{\alpha_1}G_0(k_2)_{\alpha_2}[D_{JI}^{(0);i_3}]^{-1}\cdot N_{JI}^{(0)}\cdot L_{10}^{i_3}\cdot N_{JI}^{(0)}\cdot[D_{JI}^{(0);i_3}]^{-1}\ . \quad (7.55)$$

For comparison we also give the isoscalar expression of diagram 8 that enter at N^{2}LO

$$\Pi_8^{is}\big|_{N^2LO} = -\delta_{ij}\kappa_{is}\int \frac{d^4k_1}{(2\pi)^4}\frac{d^4k_2}{(2\pi)^4}e^{ik_1^0\eta}e^{ik_2^0\eta}\sum_{J,\ell,S,I,i_3}(2J+1)\chi(S\ell I)^2 \\ \times G_0(k_1)_{\alpha_1}G_0(k_2)_{\alpha_2}[D_{JI}^{(0);i_3}]^{-1}\cdot N_{JI}^{(0)}\ , \quad (7.56)$$

which obviously does not cancel with eq. (7.55).

Including one more order in the calculation of Π_9 and Π_{10}^{iv} requires the use of $DL_{JI}^{(1)}$, eq. (4.42). The input functions $DL_{JI}^{(1)}$ are given in eqs. (7.50) and (7.52) for the isovector and isoscalar cases, respectively. In this way,

$$\big(\Pi_9+\Pi_{10}^{iv}\big)\big|_{N^2LO} = -i\varepsilon_{ij3}\kappa_{iv}\frac{m}{2}\int \frac{d^4k_1}{(2\pi)^4}\frac{d^4k_2}{(2\pi)^4}e^{ik_1^0\eta}e^{ik_2^0\eta}\sum_{J,\ell,S,i_3}2i_3\,(2J+1)\chi(S\ell 1)^2G_0(k_1)_{\alpha_1} \\ \times G_0(k_2)_{\alpha_2}[D_{J1}^{(1);i_3}]^{-1}\cdot\left(\frac{\partial L_{J1}^{(1);i_3}}{\partial A}-\left\{L_{J1}^{(1);i_3}+[N_{J1}^{(0)}]^2\cdot L_{10}^{i_3},N_{J1}^{(0)}\right\}\cdot\frac{\partial L_{10}^{i_3}}{\partial A}\right)\cdot[D_{J1}^{(1);i_3}]^{-1}\ . \quad (7.57)$$

It is straightforward to show that $\Pi_7 + \Pi_8^{iv}$ calculated with $\partial T_{JI}/\partial A$ evaluated at next-to-leading order with eq. (7.43) cancels with eq. (7.57):

$$\big(\Pi_7+\Pi_8^{iv}\big)\big|_{N^2LO} = i\varepsilon_{ij3}\kappa_{iv}m\int \frac{d^4k_1}{(2\pi)^4}\frac{d^4k_2}{(2\pi)^4}e^{ik_1^0\eta}e^{ik_2^0\eta}\sum_{J,\ell,S,i_3}i_3\,(2J+1)\chi(S\ell 1)^2G_0(k_1)_{\alpha_1}G_0(k_2)_{\alpha_2} \\ \times[D_{J1}^{(1);i_3}]^{-1}\cdot\left(\frac{\partial L_{J1}^{(1);i_3}}{\partial A}-\left\{L_{J1}^{(1);i_3}+[N_{J1}^{(0)}]^2\cdot L_{10}^{i_3},N_{J1}^{(0)}\right\}\cdot\frac{\partial L_{10}^{i_3}}{\partial A}\right)\cdot[D_{J1}^{(1);i_3}]^{-1}\ . \quad (7.58)$$

In the previous expression we have replaced $N_{JI}^{(1)}$ by its explicit expression in terms of $L_{JI}^{(1)}$, $N_{JI}^{(1)} = L_{JI}^{(1)} + N_{JI}^{(0)}\cdot L_{10}\cdot N_{JI}^{(0)}$.

In appendix E.6 we evaluate explicitly $DL_{JI}^{(1)}$ and $L_{JI}^{(1)}$ needed for determining $N_{JI}^{(1)}$ and $\xi_{JI}^{(1)}$, eqs. (4.13) and (4.42), in order. Some steps introduced in the derivations of this and the previous section are also calculated explicitly.

In summary, we have considered the calculation of the diagrams 7, 8, 9 and 10 of fig. 7.1. We have shown explicitly that up-to-and-including next-to-leading order the contributions Π_9 and Π_{10}^{iv} vanish with those evaluated previously, Π_7 and Π_8^{iv}. In fact, the obtained cancellation between these contributions is valid to all orders in the expansion of the scattering amplitude, which will be proven in general in the following section. Some other contributions at N^{2}LO have also been calculated, though they do not exhaust a full calculation to this order of the in-medium pion self-energy. It is then shown that at N^{2}LO the cancellation between the isovector contributions takes

place as required. Note that at this order the full calculation of the two-nucleon reducible loops takes place. This clearly shows that the cancellation is beyond the factorization approximation valid at next-to-leading order.

7.4 Cancellation of the isovector $V_\rho = 2$ contributions[#9]

As we have seen in the last section, remarkably, the next-to-leading and next-to-next-to-leading order isovector contributions from nucleon-nucleon interaction cancel mutually. We now wish to show on general grounds, that the isovector contributions of that particular structure vanishes to all orders in the chiral expansion of the nucleon-nucleon scattering amplitude.

Diagrams 7 and 9 of fig. 7.1 involve the WT vertex while 8 and 10 contain the pole terms of pion-nucleon scattering. We can discuss simultaneously all the diagrams in the last two rows of fig. 7.1 employing the vertex eq. (7.48). The sum of diagram 7 and the isovector part of diagram 8 of fig. 7.1 can be written in terms of the nucleon self-energy in the nuclear medium due to the nucleon-nucleon scattering. It reads

$$\Pi_7 + \Pi_8^{iv} = \varepsilon_{ijk}\frac{q_0}{2f_\pi^2}\left(1 - g_A^2\frac{\mathbf{q}^2}{q_0^2}\right)\int\frac{d^4k_1}{(2\pi)^4}e^{ik_1^0\eta}\ \mathrm{Tr}\Big\{\tau^k\left(\frac{1+\tau_3}{2}G_0(k_1)_p + \frac{1-\tau_3}{2}G_0(k_1)_n\right)\Sigma^{NN} \times\left(\frac{1+\tau_3}{2}G_0(k_2)_p + \frac{1-\tau_3}{2}G_0(k_2)_n\right)\Big\}\ . \tag{7.59}$$

Σ^{NN} is given in eq. (5.28). Proceeding similarly as in section 7.4, including the integration by parts, we can write

$$\Pi_7 + \Pi_8^{iv} = \varepsilon_{ij3}\frac{q_0}{2f_\pi^2}\left(1 - g_A^2\frac{\mathbf{q}^2}{q_0^2}\right)\sum_{\sigma_1}\int\frac{d^4k_1}{(2\pi)^4}e^{ik_1^0\eta}\left(G_0(k_1)_p\frac{\partial\Sigma_p^{NN}}{dk_1^0} - G_0(k_1)_n\frac{\partial\Sigma_n^{NN}}{dk_1^0}\right)\ . \tag{7.60}$$

Inserting in the previous equation the explicit expression for $\Sigma_{i_3}^{NN}$ of eq. (5.27) one has

$$\begin{aligned}\Pi_7 + \Pi_8^{iv} = -i\varepsilon_{ij3}\frac{q_0}{2f_\pi^2}\left(1 - g_A^2\frac{\mathbf{q}^2}{q_0^2}\right)\sum_{\sigma_1,\sigma_2}\int\frac{d^4k_1}{(2\pi)^4}\frac{d^4k_2}{(2\pi)^4}e^{ik_1^0\eta}e^{ik_2^0\eta} \\ \times\Bigg(G_0(k_1)_pG_0(k_2)_p\frac{\partial}{\partial k_1^0}T_{NN}(k_1\sigma_1 p, k_2\sigma_2 p|k_1\sigma_1 p, k_2\sigma_2 p) \\ - G_0(k_1)_nG_0(k_2)_n\frac{\partial}{\partial k_1^0}T(k_1\sigma_1 n, k_2\sigma_2 n|k_1\sigma_1 n, k_2\sigma_2 n)\Bigg)\ .\end{aligned} \tag{7.61}$$

This result is obtained from eq. (7.60) by using eq. (7.32).

Let us now consider the diagrams 9 and 10 of fig. 7.1 whose contribution is denoted by $\Pi_9 + \Pi_{10}^{iv}$. These diagrams consist of the pion-nucleon scattering in a two-nucleon reducible loop which is corrected by initial and final state interactions. The iterations are indicated by the ellipsis on both

[#9] The contents of this section have been published in [LOMa].

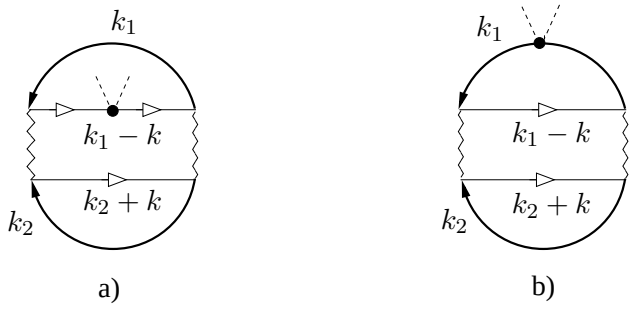

Figure 7.4: Contribution to the pion self-energy with a two-nucleon reducible loop. The pion scatters inside/outside the loop for the diagram a)/b).

sides of the diagrams. In order to see that these diagrams cancel with eq. (7.29) let us take first the diagram a) of fig. 7.4 with a twice iterated wiggly line vertex. It is given by

$$\left(\Pi_9 + \Pi_{10}^{iv}\right)^L = i\varepsilon_{ij3}\frac{q_0}{2f_\pi^2}\left(1 - g_A^2\frac{\mathbf{q}^2}{q_0^2}\right)\sum_{\alpha,\beta}\sum_{\sigma_1,\sigma_2}\int\frac{d^4k_1}{(2\pi)^4}\frac{d^4k_2}{(2\pi)^4}e^{ik_1^0\eta}e^{ik_2^0\eta}G_0(k_1)_\alpha G_0(k_2)_\beta$$
$$\times\left(\frac{-i}{2}\int\frac{d^4q}{(2\pi)^4}\sum_{\alpha',\beta'}\sum_{\sigma_1',\sigma_2'}V_{\alpha\beta;\alpha'\beta'}(q)\frac{\partial G_0(k_1-q)_{\alpha'}}{\partial k_1^0}\,\tau_3|_{\alpha'\alpha'}\,V_{\alpha'\beta';\alpha\beta}(-q)G_0(k_2+q)_{\beta'}\right), \tag{7.62}$$

where the superscript L indicates that this scattering amplitude is calculated at the one-loop level. $V_{\alpha\beta;\gamma\delta}$ corresponds to the wiggly line with the indices α and γ belonging to the out-/in-going first particle, in that order, and similarly β and γ for the second one. To shorten the notation, we have only indicated the isospin indices in V in the previous equation, although V depends also on spin. A symmetry factor $1/2$ is also included because $V_{\alpha\beta;\gamma\delta}$ contains both the direct and exchange terms, as explicitly shown in eqs. (4.2) and (4.3). The derivative with respect to k_1^0 arises in eq. (7.62) because the nucleon propagator to which the two pions are attached appears squared and we have made used of eq. (7.13). This is so because for the $\pi^\pm$, i and j can be either 1 or 2, so that the only surviving contribution is $k = 3$. For the π^0, $i = j = 3$ and then there is no contribution. Thus, because one has either 0 or τ^3, which is a diagonal matrix, the nucleon propagator before and after the two-pion vertex is the same. The q-loop integral in eq. (7.62) is typically divergent. Nevertheless, the parametric derivative with respect to k_1^0 can be extracted out of the integral as soon as it is regularized. Of course, the same regularization method as that used to calculate T_{NN} should be employed. Once the derivative is taken out of the integral, the quantity between the squared brackets in eq. (7.62) corresponds to the twice iterated wiggly line contribution to $T_{NN}(k_1\sigma_1\alpha, k_2\sigma_2\beta|k_1\sigma_1\alpha, k_2\sigma_2\beta)$. In addition, the isovector nature of the modified WT vertex of eq. (7.48) implies that only the difference between the proton-proton and neutron-neutron contributions arises. This can be worked out straightforwardly from the isospin structure of the local four-nucleon vertex and that of the one-pion exchange as it was done in the last section. As a result we can write

$$\left(\Pi_9 + \Pi_{10}^{iv}\right)^L = i\varepsilon_{ij3}\frac{q_0}{2f_\pi^2}\left(1 - g_A^2\frac{\mathbf{q}^2}{q_0^2}\right)\sum_{\sigma_1,\sigma_2}\int\frac{d^4k_1}{(2\pi)^4}\frac{d^4k_2}{(2\pi)^4}e^{ik_1^0\eta}e^{ik_2^0\eta}$$
$$\times\Bigg(G_0(k_1)_p G_0(k_2)_p\frac{\partial}{\partial k_1^0}T_{NN}^L(k_1\sigma_1 p, k_2\sigma_2 p|k_1\sigma_1 p, k_2\sigma_2 p)$$

$$- G_0(k_1)_n G_0(k_2)_n \frac{\partial}{\partial k_1^0} T^L_{NN}(k_1\sigma_1 n, k_2\sigma_2 n | k_1\sigma_1 n, k_2\sigma_2 n) \Bigg) \ , \tag{7.63}$$

This result then cancels exactly with that of diagram b) of fig. 7.4, corresponding to the twice iterated wiggly line exchange contribution to T_{NN} in eq. (7.29). This cancellation is explicit by reducing eq. (7.29) to the one-loop case for calculating T_{NN}. Notice as well that the contribution to T_{NN} given by the exchange of only one wiggly line vanishes when inserted in eq. (7.29) because it is independent of k_1^0.

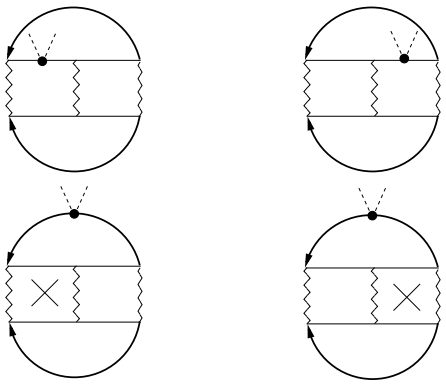

Figure 7.5: In this figure the cross indicates the action of the derivative with respect to k_1^0 in eq. (7.29). When the derivative is performed over a baryon propagator the latter becomes squared, according to eq. (7.13). In this way, the first diagram on the second row of the figure is the same as the one to the left of the first row but with opposite sign and they cancel each other. The same applies to the second diagrams on the first and second rows.

This process of mutual cancellation between $\Pi_7 + \Pi_8^{iv}$ and $\Pi_9 + \Pi_{10}^{iv}$ can be generalized to any number of two-nucleon reducible loops of the diagrams 7, 8, 9 and 10 of fig. 7.1. An $n+1$ iterated wiggly line exchange in these figures implies n two-nucleon reducible loops. The two pions can be attached for $\Pi_9 + \Pi_{10}^{iv}$ to any of them, while for $\Pi_7 + \Pi_8^{iv}$ the derivative with respect to k_1^0 can also act on any of the loops. The iterative loops are the same for both cases but a relative minus sign results from the loop on which the two pions are attached with respect to the one on which the derivative is acting, as just discussed. This is exemplified in fig. 7.5 for the case with two two-nucleon reducible loops. Hence,

$$\Pi_7 + \Pi_9 = 0 \ , \quad \text{and} \quad \Pi_8^{iv} + \Pi_{10}^{iv} = 0 \ . \tag{7.64}$$

The basic simple reason for such cancellation is that while for $\Pi_7 + \Pi_8^{iv}$ the presence of a nucleon propagator squared gives rise to $(-1)^2 \partial/\partial k_1^0$, for $\Pi_9 + \Pi_{10}^{iv}$ it yields $-\partial/\partial k_1^0$, cf. eqs. (7.29) and (7.62), respectively. The extra (-1) for $\Pi_7 + \Pi_8^{iv}$ results because it involves an integration by parts, as discussed above.

The same cancellation does not happen for the isoscalar contributions Π_8^{is} and Π_{10}^{is}: for those diagrams, the derivative vanishes because the next-to-leading order term of the expansion of the pole-term propagator cancels the square of the propagator which closes the diagram. In diagram 8 the "elementary" nucleon-nucleon interaction N_{JI} is dressed by an iterative process according to eq. (4.31), whereas for diagram 10 the nucleon-nucleon amplitude is given by the pion scattering term corrected by initial and final state interactions eq. (4.42).

7.5 Discussion and results[#10]

We now discuss here the numerical results that we obtain for the π^- self-energy in the nuclear medium according to our approach. In the plots we draw $\Pi = \sum_i \Pi_i$ in compliance with the standard convention in nuclear physics. We distinguish between the different contributions. For the case of the π^+ the isovector contributions will have opposite sign to those for the π^- self-energy. For the π^0 they are absent. The isoscalar contributions are the same for all the three charge species of pions. In the following we fix

$$\xi_n = 1.157\,\xi_p \ , \tag{7.65}$$

with the proportionality factor corresponding to neutron rich nuclei like $^{208}_{82}$Pb, that has $\xi_p = 241$ MeV and $\xi_n = 279$ MeV.

7.5.1 Isoscalar S-wave contribution

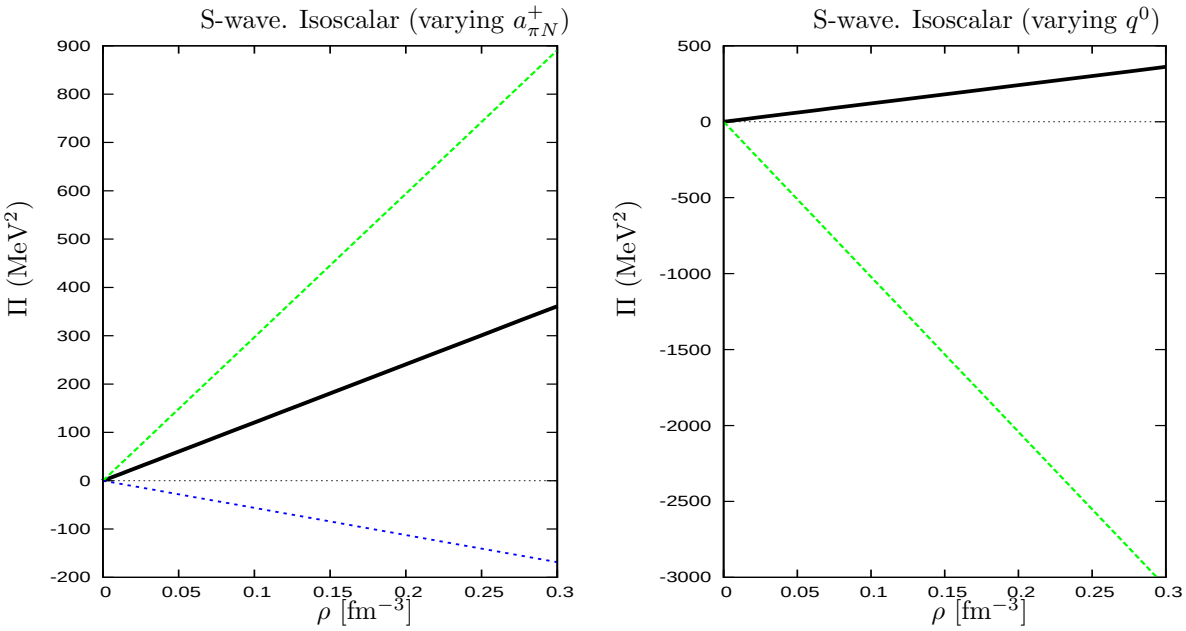

Figure 7.6: The isoscalar S-wave pion self-energy in asymmetric nuclear matter. The left panel is the contribution Π_4 for $q^0 = m_\pi$. The solid (black), dashed (green) and dotted (blue) lines correspond to the central value of $T^+_{\pi N}$, plus and minus one σ, in that order, according to eq. (7.68). The right panel is the comparison between Π_4 calculated with the central value of $a^+_{\pi N}$ and $q^0 = m_\pi$, solid (black) line, and $q^0 = 1.1 m_\pi$, dashed (green) line.

The only isoscalar S-wave contribution that we have stems from Π_4, eq. (7.10), without the term proportional to $c_3\mathbf{q}^2$ which is P-wave. Recall that Π_4 is already a next-to-leading order contribution. It depends on the $\mathcal{O}(p^2)$ χPT low-energy constants c_1, c_2 and c_3. It is more accurate to rewrite them in terms of measured quantities. For that, taking into account [BKM97], one has for the πN-scattering T-matrix at threshold

$$T^+_{\pi N}(m_\pi) = 4\pi\Big(1 + \frac{m_\pi}{m}\Big)a^+_{\pi N} = \frac{2m_\pi^2}{f_\pi^2}\left(-2c_1 + c_2 + c_3 - \frac{g_A^2}{8m}\right) + \mathcal{O}(m_\pi^3) \ . \tag{7.66}$$

[#10]The contents of this section have not been published.

Then the isoscalar contribution of eq. (7.10) can be expressed as

$$\Pi_4 = \delta_{ij}\left[T^+_{\pi N} + (q_0^2 - m_\pi^2)\left(\frac{T^+_{\pi N}}{m_\pi^2} + \frac{4c_1}{f_\pi^2}\right)\right](\rho_p + \rho_n)\ . \tag{7.67}$$

For the isoscalar S-wave πN scattering length $a^+_{\pi N}$ we use the value of the determination in [MRR06] steming from an analysis of pionic hydrogen and pionic deuterium data

$$a^+_{\pi N} = (+0.0015 \pm 0.0022) m_\pi^{-1}\ . \tag{7.68}$$

Note, there are also older evaluations for a^+ and a^- [Ar04], yielding $a^+_{\pi N} = (-0.0010 \pm 0.0012) m_\pi^{-1}$. For the low-energy constant c_1 we take the value [BM00]

$$c_1 = (-0.81 \pm 0.12)\ \text{GeV}^{-1}\ . \tag{7.69}$$

This value is based on a chiral expansion of the πN scattering amplitude inside the Mandelstam triangle where the chiral expansion converges faster. Note that there are also alternative determinations of the low-energy constants, for instance from vacuum nucleon-nucleon scattering (see [EHM09] and references therein). The values of low-energy constants are still under debate, while all have in common that they are quite inaccurate. It is desirable to obtain those from lattice QCD simulations.

In fig. 7.6 we show the S-wave part of Π_4 as a function of the total density ρ with $q^0 = m_\pi$, at the pion threshold. The solid, dashed and dotted lines in the left panel of fig. 7.6 correspond to the central value of $T^+_{\pi N}$, plus and minus one σ, in order, as given in eq. (7.68). One sees that this contribution is very small and compatible with zero, as it is $T^+_{\pi N}$, because for $q^0 = m_\pi$ the two quantities, Π_4 and $T^+_{\pi N}$, are proportional. On the right panel of fig. 7.6 one can testify the huge impact of the second term in eq. (7.67), when the pion mass goes off-shell.

At the order of our calculation we cannot address the interesting problem of the missing repulsion, having to do with a repulsive contribution in the isoscalar S-wave piece of the pion optical potential [NOG93, KKW03, DO08], that is needed to fit data from pionic atoms. New contributions to the isoscalar S-wave pion self-energy will emerge in a calculation just one order higher to the one performed here. E.g. the well known Ericson-Ericson Pauli corrected S-wave rescattering term [EE66] would appear at $\mathcal{O}(p^6)$ because it involves an extra nucleon propagator that is not enhanced. Of course, since $T^0_{\pi N}$ is so tiny higher order corrections will have impact. Once a N^{2}LO calculation is done one could elaborate more on the interesting issue of the missing repulsion for the S-wave low-energy interactions of pions with nuclei. See also section 7.5.5 below.

7.5.2 Isovector S-wave contribution

The evaluated isovector S-wave contribution are Π_1, Π_5, Π_7 and Π_9, eqs. (7.2), (7.19), (7.54) and (7.53), respectively. Of them, the leading contribution is Π_1. The next-to-leading order cancels, $\Pi_7 + \Pi_9 = 0$, as derived in subsection 7.3.2 and section 7.4. Finally Π_5 is suppressed by one order and therefore N^{2}LO.

In fig. 7.7 we show the contributions Π_1 and Π_5 to the isovector S-wave π^- self-energy for $q^0 = m_\pi$. In the figure Π_1 is the solid (red) line and Π_5 is the dashed (green) line. The thicker solid (black) line corresponds to the sum of both contributions and it runs quite close to the leading order line because Π_5 is much smaller than Π_1.

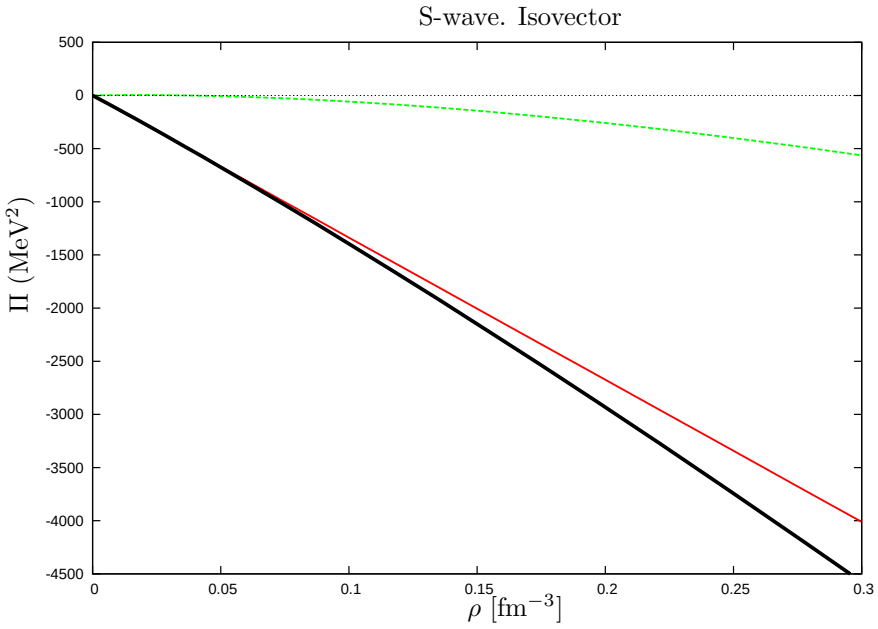

Figure 7.7: The non-vanishing contributions of the isovector S-wave pion self-energy in asymmetric nuclear matter for $q^0 = m_\pi$. The thinner solid (red) line is Π_1 and the dashed (green) one is Π_5. The sum of both is given by the thicker solid (black) line.

7.5.3 Isoscalar P-wave contribution

The different contributions for the isoscalar P-wave pion self-energy Π_2^{is}, Π_3, the P-wave contribution of Π_4, Π_6^{is} and Π_8^{is}, eqs. (7.8), (7.9), (7.10), (7.27) and (7.56), respectively, are shown in fig. 7.8 left panel. (Π_{10}^{is} is not shown, read below.) The sum of all listed contributions is indicated by the thick solid black line and it is set $q^0 = |\mathbf{q}| = m_\pi$ in all the curves. For the subtraction constant in Π_8^{is}, Π_{10}^{is} and the sum we used the parameter set $(g_0, \tilde{g}_0) = -(0.972, 0.517) m_\pi^2$ determined in subsection 6.3.1. Note that the contributions Π_6^{is}, Π_8^{is} and Π_{10}^{is} are already N^{2}LO, where the Π_8^{is} and Π_{10}^{is} are calculated at leading order in the nucleon-nucleon scattering as described in subsection 7.3.3. We want to draw some special attention to Π_6^{is}, whose contribution is tiny in particular in comparison with Π_5 or Π_6^{iv}. Recall that eq. (7.27) involves the integration inside a Fermi sphere of the free nucleon self-energy, with the nucleon entering the subdiagram put on-shell. Since we use the physical nucleon mass in all our calculations, we had to subtract the term with $k^0 = 0$ in the nucleon self-energy in eq. (5.11). Therefore there is no contribution linear in density from this particular diagram, and the remaining tiny structure displays residual higher order dependence non-linear in density. The isoscalar P-wave pion self-energy is overwhelmingly dominated by the P-wave part of Π_4, that is proportional to c_3, eq. (7.10). In turn, this low-energy constant is dominated by the Δ resonance [BKM97], which stresses the important role played by this resonance in the P-wave pion self-energy [OTW82]. The results presented in this figure have been calculated with the central values [FMS98, BM00, FM00]

$$\begin{aligned} c_2 &= (\ \ 3.22 \pm 0.25)\ \text{GeV}^{-1}\ , \\ c_3 &= (-4.70 \pm 1.16)\ \text{GeV}^{-1}\ . \end{aligned} \tag{7.70}$$

The dependence on the subtraction constant g_0 of contribution Π_8^{iv} is shown in fig. 7.8 right panel. We find that it is quite large at leading order in the nucleon-nucleon interaction as was already

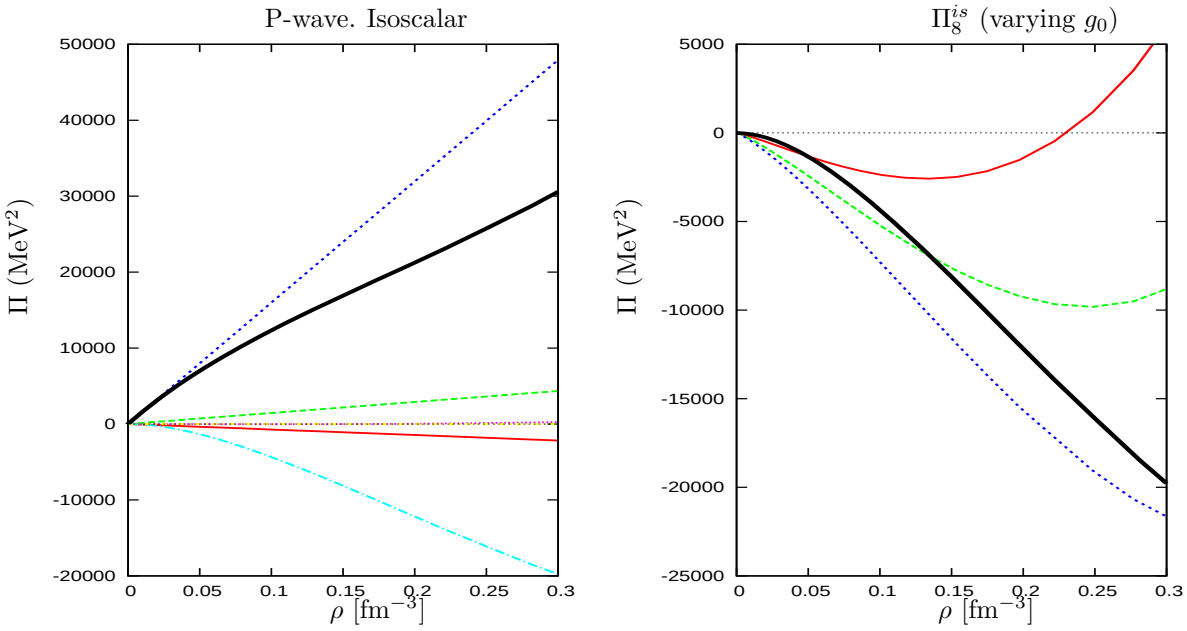

Figure 7.8: The non-vanishing contributions of the isoscalar P-wave pion self-energy in asymmetric nuclear matter for $q^0 = |\mathbf{q}| = m_\pi$. Left panel: contributions from the different diagrams. Π_2^{is} is the thinner solid (red) line, Π_3 is the dashed (green) line, the P-wave contribution of Π_4 is the wide-dotted (blue) line, Π_6^{is} is the narrow-dotted (magenta) line and Π_8^{is} is the dot–long-dashed (cyan) line. The thicker solid (black) corresponds to the sum of all these contributions. For the subtraction constant is used the parameter set to $(g_0, \tilde{g}_0) = -(0.972, 0.517) m_\pi^2$. Right panel: shown is Π_8^{is} with different values of the subtraction constant g_0. The solid (red), dashed (green) and dotted (blue) line represents values of $g_0 = \tilde{g}_0 = -0.25$, -0.37 and -0.50 in units of m_π^2, respectively. The thicker solid (black) line corresponds to the parameter set $(g_0, \tilde{g}_0) = -(0.972, 0.517) m_\pi^2$ (see text).

found for the nuclear matter energy density in section 6.2. The thicker solid (black) line corresponds to how the curve behaves if the fine-tuned parameter-set $(g_0, \tilde{g}_0)$ of the (symmetric) nuclear matter energy density obtained in subsection 6.3.1 is employed. We choose the average values of the band given in fig. 6.7 as $(g_0, \tilde{g}_0) = -(0.972, 0.517) m_\pi^2$.

Note, that we have skipped the contribution Π_{10}^{is} which should be shown in coherence with Π_8^{is}. However, there is still the task of its regularization to perform, which we have postponed for the moment. A regularization of Π_{10}^{is}, eq. (7.55), would be in analogy to the one of diagram $\mathcal{E}_3$ in section 6.2, which had straightforwardly been adopted for Π_8^{is}.

7.5.4 Isovector P-wave contribution

The isovector P-wave contributions stem from Π_2^{iv}, Π_6^{iv}, Π_8^{iv} and Π_{10}^{iv}, eqs. (7.7), (7.26), (7.54) and (7.53), respectively. Π_2^{iv} is the leading order. Let us recall that the sum of Π_8^{iv} and Π_{10}^{iv} cancels as derived in subsection 7.3.2 and section 7.4. Π_6^{iv} is already N^{2}LO.

We show in fig. 7.9 the contributions Π_2^{iv}, Π_6^{iv} and their sum, calculated for $q^0 = |\mathbf{q}| = m_\pi$. We see that, similar to the case for the isovector S-wave Π_6^{iv} is much smaller in modulus than Π_2^{iv}.

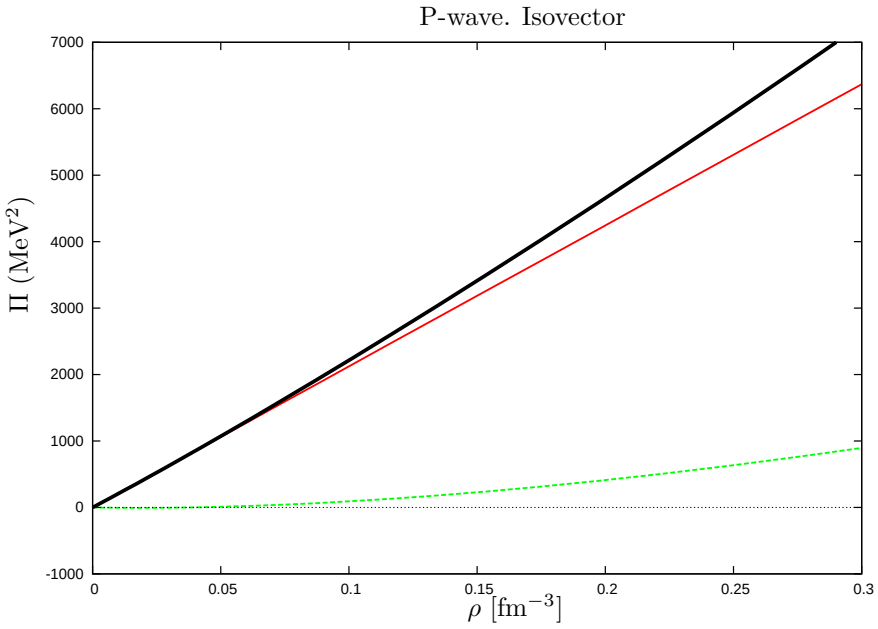

Figure 7.9: The non-vanishing isovector P-wave pion self-energy in asymmetric nuclear matter contributions for $q^0 = |\mathbf{q}| = m_\pi$. The thinner solid (red) line is Π_2^{iv} and the dashed (green) one is Π_6^{iv}. The sum of both is given by the thicker solid (black) line.

7.5.5 The π^- mass in nuclear matter

We now discuss the pion mass in the nuclear medium. The latter, denoted by $\tilde{m}_\pi$, is defined by

$$\tilde{m}_\pi^2 = m_\pi^2 - \mathrm{Re}\,\Pi(q^0 = \tilde{m}_\pi, \mathbf{q} = 0) \ . \tag{7.71}$$

It corresponds to the energy at rest of the nuclear pionic modes. When applying this equation in an asymmetric nuclear medium one has to distinguish between the $\pi^\pm$ and π^0 masses. We first discuss the π^- mass, since this is the one involved in pionic atoms. On the other hand, given the relation between the S-wave pion self-energy and the pion optical potential

$$2\mu\, U_{opt} = \Pi(q^0 = \tilde{m}_\pi, \mathbf{q} = 0) \ , \tag{7.72}$$

with the reduced mass μ, eq. (7.71) can be used to compare our values for the effective pion masses with those stemming from potentials fitted to pionic atom data.

The authors of [Gi00, It00] fitted some terms in the pion-nucleus optical potential to accommodate the values of the energy and width of the deeply bound pionic atoms they discovered. The other terms were taken from fits to the bulk of pionic atom data. In [Gi00, It00] eq. (7.71) was not solved self-consistently but perturbatively so that the equation actually employed is

$$\tilde{m}_\pi = m_\pi - \frac{1}{2m_\pi}\mathrm{Re}\Pi(q^0 = m_\pi, \mathbf{q} = 0) \ , \tag{7.73}$$

with the threshold energy of the pion fixed to its vacuum mass. This is the so-called energy-independent approximation for the pion optical potential. [Gi00, It00] report

$$\Delta m_{\pi^-} = \tilde{m}_{\pi^-} - m_{\pi^-} = 23 - 27 \text{ MeV} \ . \tag{7.74}$$

We now give a similar discussion on the in-medium pion mass as in [MOW02]. However, we now include in addition Π_5 and present slightly different results.

i) First we consider eq. (7.73). We have

$$\Delta m_\pi = -\frac{1}{2m_\pi}\mathrm{Re}\left(\Pi_1 + \Pi_4 + \Pi_5\right) \ , \tag{7.75}$$

with the argument q^0 in the different Π_i fixed to m_π. We obtain the result

$$\Delta m_{\pi^-} = (8.20 \pm 0.04) \text{ MeV} \ , \tag{7.76}$$

where the small error is given by the error of $T^+_{\pi N}$, eq. (7.68). This number is very similar to that of [MOW02] because Π_5 is much smaller than Π_1, as shown on the right panel of fig. 7.7. Furthermore, the contribution from Π_4 is negligible given the smallness of $T^+_{\pi N}$.

ii) The energy dependence of the pion optical potential cannot be neglected when studying pionic atoms since this is an important source of repulsion as shown in [ET82, KKW03]. When solving the Klein-Gordon equation a proper treatment of the Coulomb potential, $V_c(r)$, requires the argument of the pion self-energy to be $\Pi(q^0 - V_c(r))$ [KKW03], instead of $\Pi(q^0 = m_\pi)$. As a result one should expect a mismatch between that calculation of the pionic potential and its parameterization from purely phenomenological studies [Gi00], where the energy is fixed to m_π. In order to take care of this we use eq. (7.73) but evaluated at $q^0 = m_\pi + 10$ MeV and $q^0 = m_\pi + 20$ MeV, similarly as in [DO08]. Note that $-V_c(r)$ is ~ 16 MeV at around the nuclear surface and ~ 25 MeV at the center, see e.g. fig. 10 of [Gi00, It00]. The resulting values obtained for Δm_π are

$$\begin{aligned} q^0 &= m_\pi + 10 \text{ MeV} \ , \ \Delta m_{\pi^-} = (13.5 \pm 0.7) \text{ MeV} \ , \\ q^0 &= m_\pi + 20 \text{ MeV} \ , \ \Delta m_{\pi^-} = (19.2 \pm 1.5) \text{ MeV} \ . \end{aligned} \tag{7.77}$$

The errors quoted in eq. (7.77) are given by the error in c_1, eq. (7.69), since the contribution from the uncertainty in $T^+_{\pi N}$ is negligible. As announced, the increase of $q^0 > m_\pi$ gives rise to an extra repulsion and then an enhanced π^- mass compared to eq. (7.76). The leading Weinberg-Tomozawa linear density term experiences a small increase. The main source of the q^0-dependence in Δm_π as q^0 slightly increases in eq. (7.77) is the quadratic term in q^0 present in Π_4, eq. (7.67). This term is zero for $q^0 = m_\pi$ but 10 MeV for $q^0 = m_\pi + 20$ MeV, see also the right panel of fig. 7.6.

iii) The self-consistent solution of eq. (7.71) gives rise to results very similar to those with $\tilde{m}_\pi = m_\pi + 20$ MeV in eq. (7.77).

$$(\tilde{m}_\pi^2 - m_\pi^2)\left[1 + \left(\frac{T^+_{\pi N}}{m_\pi^2} + \frac{4c_1}{f_\pi^2}\right)(\rho_p + \rho_n)\right] + \tilde{m}_\pi\left[\frac{\rho_p - \rho_n}{2f_\pi^2} + \frac{\Pi_5}{\tilde{m}_\pi}\right] + T^+_{\pi N}(\rho_p + \rho_n) = 0 \ . \tag{7.78}$$

Note that Π_5 is linear in $q^0 = \tilde{m}_\pi$. Solving it exactly for $q^0 = \tilde{m}_\pi$ one has

$$\Delta m_{\pi^-} = (16 \pm 2) \text{ MeV} \ , \tag{7.79}$$

with the error bar due to that of c_1.

iv) Eq. (7.78) can be solved to a good approximation in terms of $\delta q_0^2 = \tilde{m}_\pi^2 - m_\pi^2$. In this way it is clear why the previous result is around a factor two larger than the perturbative solution in eq. (7.76). Neglecting terms of order $\delta q_0^2/m_\pi^2 \ll 1$, the solution is approximately given by

$$\begin{aligned} \delta q_0^2 &= \frac{-T^+_{\pi N}(\rho_p + \rho_n) + m_\pi\left[(\rho_n - \rho_p)/2f_\pi^2 - \Pi_5/q^0\right]}{1 + \left(4c_1/f_\pi^2 + T^+_{\pi N}/m_\pi^2\right)(\rho_p + \rho_n) + (\rho_p - \rho_n)/4f_\pi^2 m_\pi + \Pi_5/q^0 2m_\pi} \ , \\ \Delta\tilde{m}_{\pi^-} &= \frac{\delta q_0^2}{2m_\pi} = (17 \pm 2) \text{ MeV} \ . \end{aligned} \tag{7.80}$$

The denominator in eq. (7.80) is around 0.5 instead of 1, where the correction is dominated by the term proportional to c_1 with $4c_1(\rho_p + \rho_n)/f_\pi^2 = -0.46$. This denominator corresponds to the square of the wave function renormalization of pions in the nuclear medium and is also the major source for dressing the pion decay constant in a nuclear environment. Its importance for the study of the pion mass in the nuclear medium was first shown in [MOW02]. For the π^+ we have the shift

$$\Delta m_{\pi^+} = (-14.4 \pm 1.7) \text{ MeV} . \tag{7.81}$$

The shift in the π^0 mass is negligible at this order.

7.6 Conclusions and outlook

The pion self-energy in nuclear matter up-to-and-including next-to-leading order, $\mathcal{O}(p^5)$, was determined together with some higher order contributions at next-to-next-to-leading order (N^2LO), $\mathcal{O}(p^6)$. The latter are calculated to further illustrate the application of the non-perturbative techniques to non-trivial calculations and for studies on the issue of the size of higher orders corrections.

The cancellation between all leading corrections beyond the linear density approximation for the pion self-energy is explicitly shown. In particular, it is derived that the leading corrections from nucleon-nucleon scattering mutually cancel. This was as well shown utilizing the non-perturbative methods as comfirmed by considering just general arguments of the scattering amplitudes. The cancellation also affects some other N^2LO contributions which is a good check for the consistency of the approach of UχPT. The suppression on the whole is interesting since it allows to understand from first principles the phenomenological success of fitting data on pionic atoms with only meson-baryon interactions [KKW03, FG07] and is actually a novelty in the literature.

We found that the resulting N^2LO contributions to the isoscalar P-wave in-medium pion self-energy from nucleon-nucleon scattering with the scattering amplitude calculated at leading order is of similar size to other next-to-leading order contributions obtained by closing pion-nucleon diagrams.

A complete N^2LO calculation of the pion self-energy, employing the present techniques, is a very interesting task and should be pursued. It will merge important pion-nucleon mechanisms like e.g. the Ericson-Ericson-Pauli rescattering effect [EE66], with novel multi-nucleon contributions that can be worked out systematically within our effective field theory. In [KW01] the Ericson-Ericson rescattering term was estimated to contribute an extra +6 MeV to Δm_π. If this N^2LO piece is added to the lower result in eq. (7.77) from our next-to-leading order calculation, then one would obtain $\Delta m_\pi \sim 25$ MeV, in agreement with the result of [Gi00, It00]. However, the full rescattering model of [DO08], where the in-medium isovector amplitude is used in the rescattering, obtains a significant reduction of the Ericson-Ericson repulsion or even an attraction. From our side a full N^2LO calculation is mandatory.

In the pion-nucleon sector the contribution proportional to the constant c_3 from Π_4 exceeds by far the contributions of other diagrams. Supposedly, this is due to large contributions from the Δ-resonance in that particular kinematic region. Therefore an investigation with the Δ as an explicit degree of freedom should be pursued.

Another interesting topic to investigate is the occurence of pion absorption in nuclear matter, which was recently argued to be phenomenologically [OFT86, Wey90] subject to an expansion in hole lines [DO08].

Chapter 8

In-medium chiral quark condensate[#11]

Making use of the theory for physics of nuclear matter developed in the chapters 3 and 4, we evaluate the in-medium chiral quark condensate up to next-to-leading order for both symmetric nuclear matter and neutron matter. Our calculation includes the full in-medium iteration of the leading order local and one-pion exchange nucleon-nucleon interactions. Interestingly, the contributions stemming from the quark mass dependence of the nucleon mass cancel each other. Only those originating from the explicit dependence of the pion mass on the quark mass survives. We obtain that the linear density contribution to the in-medium chiral quark condensate is slightly modified for pure neutron matter by the nucleon-nucleon interactions. For symmetric nuclear matter the in-medium corrections are significantly larger, although damped as compared to other approaches due to the full iteration of the lowest order nucleon-nucleon tree-level amplitudes. Our calculation satisfies the Hellmann-Feynman theorem to the order worked out.

8.1 Introduction

The QCD ground state, or vacuum, is characterized by the presence of a strong condensate $\langle 0|\bar{q}q|0\rangle$ of scalar quark-antiquark pairs – the *chiral quark condensate* – which represents an order parameter for spontaneous chiral symmetry breaking in QCD [CGL01]. It is accepted on phenomenological grounds that the lightest pseudoscalar mesons, the pions, are identified with the Goldstone bosons of the spontaneously broken chiral symmetry [Na60a, Na60b]. Spontaneous chiral symmetry breaking results because the axial charge, $Q_A^i = \int d^3x A_0^i(x)$, does not annihilate the ground state. The coupling of the Goldstone bosons to the axial-vector charge is given in terms of the pion decay constant f_π, which determines the chiral scale $4\pi f_\pi \sim 1$ GeV that governs the size of the quantum corrections in Chiral Perturbation Theory (χPT) [Ge09]. Chiral symmetry is also explicitly broken due to the small masses of the lightest quarks, u and d. An interesting issue for the discussion of the QCD phase diagram is the dependence of the chiral quark condensate on temperature and density. It is expected that with growing temperature, the quark condensate melts [GL88, Ao06, BMZ87]. There is an indication that this is also the case at zero temperature and increasing density as follows from the direct application of the Hellmann-Feynman theorem [CFG91] to the energy density of a Fermi sea. A restoration of chiral symmetry is believed to be linked to a phase transition in QCD. A nonvanishing chiral quark condensate represents a sufficient condition for the

[#11] The contents of this chapter have been published in [LOMd].

spontaneous breakdown of chiral symmetry. Note, that it is not a necessary one, such one would be the Goldstone boson (pion) decay constant, therefore chiral symmetry might as well be broken with a vanishing quark condensate. Many recent calculations in nuclear matter share the assumption that spontaneous chiral symmetry breaking still holds for finite density nuclear systems. The form of the chiral Lagrangians changes depending on whether the chiral quark condensate $\langle\Omega|\bar{u}u+\bar{d}d|\Omega\rangle$ is large or small. In the former case we have the standard χPT [We79, GL84, GL85] and in the latter generalized χPT [FSS91, FSS93] should be employed. It has been shown that the first case holds [CGL01] in vacuum for SU(2) χPT. For modern applications of chiral symmetry to nuclear systems we refer to [EHM09]. The in-medium chiral quark condensate for symmetric nuclear matter in the linear approximation [CFG92, TW95, WT95, KW96, KW97, MOW02] decreases with density as $1-(0.35\pm0.09)\rho/\rho_0$, with the error governed by that of the knowledge of the pion-nucleon sigma term, $\sigma=\hat{m}\partial m/\partial\hat{m}=45\pm8$ MeV [GLS91, Ko82], with $\hat{m}=(m_u+m_d)/2$ the mean of the u and d quark masses, m the nucleon mass and $\rho_0\simeq0.16$ fm^{-3} the nuclear matter saturation density. Thus, if the low energy linear decrease in the quark condensate is extrapolated to higher densities the quark condensate would vanish for $\rho=(2.9\pm0.7)\rho_0$ and standard χPT would not be appropriate. Of course, higher order corrections could spoil this tendency. Hence, the calculation of the in-medium quark condensate is of great interest beyond the linear approximation. The quark condensate in the nuclear medium and the quest for restoration of chiral symmetry at finite baryon density (and temperature) has a long and outstanding history, see e.g. [HK85, RD87, CFG92, TW95, WT95, BW96, KW96, KW97, LFA00, HZC02, MOW02, TSTV07, KHW08, KW09, PF07].

In this work we concentrate on the application of in-medium baryon χPT to the calculation of the quark condensate and go beyond the linear density approximation. The authors of [LFA00, KHW08] also calculated corrections to this approximation however our approach offers two novel features: i) It follows a strict chiral power counting that includes both long- and short-range (multi-)nucleon interactions. It is applied both in the vacuum and in the medium so that a clear connection between the two cases is established and used. ii) We do not take as starting point the Hellmann-Feynman theorem but directly apply the power counting mentioned to the problem of the calculation of the quark condensate. The fulfiling of the Hellmann-Feynman theorem is a consequence of the consistency of the approach order by order. In this way, the dependence on the quark mass of the input parameters in the theory, like f_π, g_A, nucleon and pion masses etc., is built in.

After this introduction, we present the basic formalism and the resulting topological contributions to the in-medium chiral quark condensate up to next-to-leading order in subsection 8.1.1. The contributions stemming from pion-nucleon chiral dynamics are given in section 8.2. The terms due to the in-medium nucleon-nucleon interactions are calculated in section 8.3. Results and discussions thereof are given in section 8.4. The last section, 8.5, is dedicated to offer our conclusions.

8.1.1 Basic formalism

The explicit chiral symmetry breaking due to the quark masses is incorporated by $s(x)=\mathcal{M}+\delta s(x)$ with $\mathcal{M}=diag(m_u,m_d)$ the quark mass matrix. From the generating functional $\mathcal{Z}(v,a,s,p)$ the quark condensate is obtained by partial functional differentiation

$$\langle\Omega|\bar{q}_iq_j|\Omega\rangle=-\frac{\delta}{\delta s_{ij}(x)}\mathcal{Z}(v,a,s,p)|_{v,a,s,p=0}\ , \tag{8.1}$$

with $q_1=u$ and $q_2=d$ quarks. Notice that the quark condensate has a global minus sign compared to diagrams calculated by using ordinary Feynman rules. See [Ol02] for a derivation of

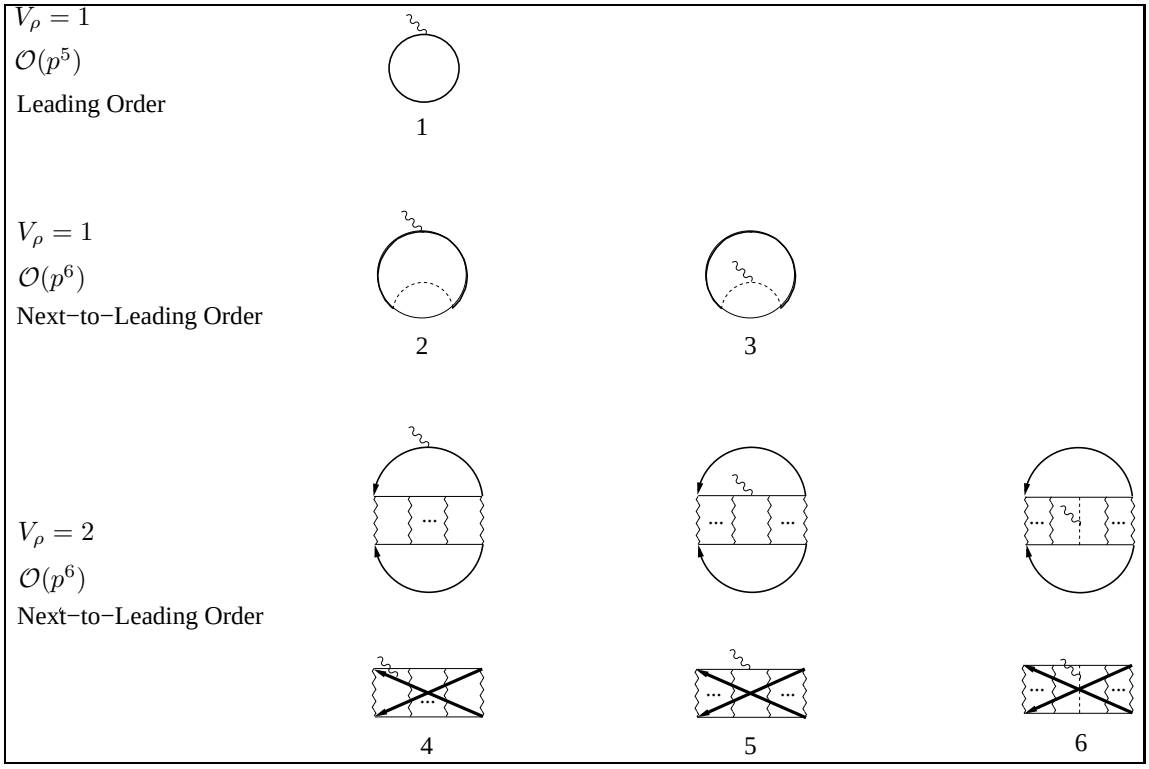

Figure 8.1: Contributions Ξ_i to the in-medium quark condensate up-to-and-including next-to-leading order, $\mathcal{O}(p^6)$. The scalar source with zero momentum-transfer is indicated by the wavy line and the pions by the dashed lines. A wiggly line corresponds to the nucleon-nucleon interaction kernel, fig. 4.1, whose iteration is denoted by the ellipsis. The diagrams 3, 5 and 6 have a symmetry factor of 1/2.

the generating functional $\mathcal{Z}(v, a, s, p)$ in the nuclear medium making use of functional methods, although keeping only pion-nucleon interactions. We also refer to [MOW02] for more details on the use of external sources in relation with in-medium χPT calculations.

The quantity we will calculate in the following is the in-medium correction Ξ to the chiral quark condensate given by

$$m_q \langle \Omega | \bar{q}_i q_j | \Omega \rangle = m_q \langle 0 | \bar{q}_i q_j | 0 \rangle - m_q \, \Xi \; , \tag{8.2}$$

where m_q is the mass of a certain quark flavor. The resulting contributions are denoted by Ξ_i and are shown in fig. 8.1. To determine the set of diagrams needed for the calculation of the in-medium chiral quark condensate up to next-to-leading order we proceed by increasing V_ρ step by step in eq. (3.22). For each V_ρ we then determine the possible configurations of vertices and lines according to eq. (3.22). The resulting diagrams are shown in fig. 8.1. They can easily be identified by considering the corresponding vacuum diagrams. For $V_\rho = 1$ the first diagram is the lowest-order contribution to the nucleon sigma-term. The rest of diagrams in fig. 8.1 are NLO. The diagrams 2 and 3 stem from the one-pion loop self-energy with the scalar source attached to a nucleon or pion propagator, respectively. For $V_\rho = 2$ one can conveniently think of the nucleon-nucleon scattering in the presence of a scalar source in vacuum. Then proceed by closing the diagrams, which corresponds to sum over the states in the Fermi seas of the nucleons. The upper row of diagrams 4, 5 and 6 in fig. 8.1 involves the direct nucleon-nucleon interactions while the lower row originates from the exchange part. In the following we indicate by Ξ_i the contribution to the in-medium quark condensate due to the diagram i in fig. 8.1. One could think of similar Feynman

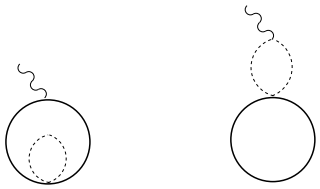

Figure 8.2: These diagrams are zero because of the manner in which the Weinberg-Tomozawa vertex, coupling two nucleons with two pions, is contracted.

graphs to diagrams 2 and 3 of fig. 8.1 but involving two-pions in one vertex from the Weinberg-Tomozawa term of $\mathcal{L}^{(1)}_{\pi N}$ eq. (2.55). These are depicted in fig. 8.2. However, these diagrams are zero because of the antisymmetric isospin structure of the Weinberg-Tomozawa vertex, proportional to $\epsilon_{lmc}\tau^c$. The same type of pion is involved in the tadpole loop. This is clear for both diagrams due to the diagonal structure of the vertex coupling the scalar source with two pions. As a result, both diagrams are zero when the pion indices are contracted with the antisymmetric tensor.

8.2 $V_\rho = 1$ contributions

First we consider the contributions to the in-medium chiral quark condensate from pion-nucleon chiral dynamics. They are depicted in diagrams 1–3 of fig. 8.1.

8.2.1 Leading order

For the evaluation of the different diagrams we need the vertex with the scalar source s_{ij}, with quark indices i,j, coupling to a pair of nucleons with isospin indices l, m. It can be readily worked out from $\mathcal{L}^{(2)}_{\pi N}$ eq. (2.55), with the result

$$2iB\big[2c_1\delta_{ij} + c_5\vec{\tau}_{ji}\cdot\vec{\tau}_{lm}\big] \ , \tag{8.3}$$

where we have taken into account that $2\delta_{il}\delta_{jm} - \delta_{ij}\delta_{lm} = \vec{\tau}_{ji}\cdot\vec{\tau}_{lm}$. The diagram 1 of fig. 8.1 then yields

$$\Xi_1 = 2B\left[2c_1\delta_{ij}(\rho_p+\rho_n) + c_5(\tau^3)_{ij}(\rho_p-\rho_n)\right] \doteq \Xi_1^{is} + \Xi_1^{iv} \ , \tag{8.4}$$

where the ρ_p and ρ_n are the proton and neutron densities given by $\rho_{p(n)} = \xi^3_{p(n)}/3\pi^2$. Notice that the isospin breaking contribution proportional to c_5 only involves the Pauli matrix τ^3, so that for $i \neq j$ the contribution vanishes, as required. The contribution in eq. (8.4) proportional to c_1 corresponds to Ξ_1^{is} and that proportional to c_5 to Ξ_1^{iv}. The superscripts is and iv refer to the isoscalar and isovector character of these contributions, respectively.

8.2.2 Next-to-leading order

Let us proceed to the evaluation of the contributions to the chiral quark condensate at next-to-leading order with only one Fermi sea insertion, the term proportional to the Dirac delta function in eq. (3.9). Diagram 2 of fig. 8.1 originates by dressing the in-medium nucleon propagator of

diagram 1 with the one-pion loop nucleon self-energy.

$$\Xi_2 = 2iB \int \frac{d^4k}{(2\pi)^4} e^{ik^0\eta} \, \mathrm{Tr}\left\{ \left[2c_1\delta_{ij} + c_5 \vec{\tau}_{ji} \cdot \vec{\tau} \right] G_0(k) \, \Sigma^\pi \, G_0(k) \right\} \doteq \Xi_2^{is} + \Xi_2^{iv} \ , \tag{8.5}$$

with the convergence factor $e^{ik^0\eta}$, $\eta \to 0^+$, associated with any closed loop made up by a single nucleon line [FW03]. The trace, indicated by Tr, acts both in spin and isospin spaces. Similarly as in eq. (8.4) the term proportional to c_1 is denoted by Ξ_2^{is} and that proportional to c_5 by Ξ_2^{iv}. The contribution from diagram 2 with only free parts in all the nucleon propagators involved, including that in Σ^π, vanishes. This is discussed in detail in section 7.2.2 for similar diagrams that appear in the calculation of the in-medium pion self-energy and nuclear matter energy. Briefly, it follows just by closing the integration contour on the complex k^0 half-plane opposite to that where the poles lie. Another important point to keep in mind is that the contributions with only Fermi sea insertions in all nucleon propagators is part of the $V_\rho = 2$ contribution of diagram 4 in fig. 8.1. This is shown diagrammatically in fig. 7.2, where the two external pion sources should be replaced by the scalar source for the case at hand. The different $V_\rho = 2$ contributions are evaluated in section 8.3. Consequently we consider in this section only the parts where we have free-space as well as density-dependent parts of the nucleon propagators. For the evaluation of these contributions the calculation of diagram Π_5 in eq. (7.19) can be adopted, with just replacing the vertex. For the isoscalar part, due to the sum of proton and neutron contribution we do not encounter an isospin asymmetry arising from Σ^π_{m,i_3} (see the discussion of Π_5 section 7.2). Thus, performing the integration by parts leads to a cancellation of the two terms which means a vanishing of the isoscalar contribution

$$\Xi_2^{is} = 0 \ . \tag{8.6}$$

This leaves us with the isovector contribution

$$\Xi_2^{iv} = -\frac{16}{3} B c_5 (\tau^3)_{ij} \int \frac{d^3k}{(2\pi)^3} \Big(\theta(\xi_p - |\mathbf{k}|) - \theta(\xi_n - |\mathbf{k}|) \Big) \frac{\partial \Sigma_f^\pi(k)}{\partial k^0} \bigg|_{k^0 = E(\mathbf{k})} \ . \tag{8.7}$$

For the same reason as in section 7.2 Ξ_2^{iv} turns to be of $\mathcal{O}(p^6)$ or next-to-next-to-leading order. This is due to the appearance of the derivative of the free part of the nucleon one-pion loop, Σ_f^π, with respect to energy. This derivative is finally suppressed by one chiral order.

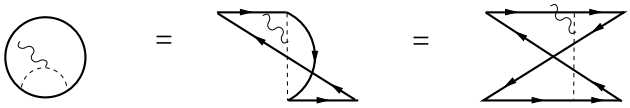

Figure 8.3: The equivalence between diagram 3 and the crossed part of the one-pion exchange reduction of diagram 6 of fig. 8.1 is shown. The diagram in the middle is an intermediate step in the continuous transformation of the diagram on the left hand side to the one on the right hand side.

We now consider diagram 3 of fig. 8.1 where the scalar source is attached to the pion originally in the pion-loop nucleon self-energy. The part of diagram 3, where the nucleon propagator involved in the pion loop is an in-medium insertion, is contained in the exchanged part of diagram 6 of fig. 8.1. This is the same mechanism already found for diagram 2 and the deformation is shown in fig. 8.3. Thus, we consider here that the nucleon propagator in the pion loop contains exclusively the vacuum part, while the remnant is evaluated in the next section dedicated to the next-to-leading order $V_\rho = 2$ contributions. The vertex coupling of the scalar source to two pions can be evaluated

straightforwardly with the result

$$-iB\delta_{\ell m}\delta^{ab} \ , \tag{8.8}$$

where the superscripts a and b refer to the pions coupled (π^a, $a = 1, 2, 3$). There is a close relationship between diagram 3 of fig. 8.1 and diagram 2 fig. 6.1. Of course, this is a requirement from the Hellmann-Feynman theorem. It is straightforward to check that

$$\Xi_3 = -iB\delta_{ij}\frac{1}{2}\int \frac{d^4k}{(2\pi)^4} e^{ik^0\eta}\mathrm{Tr}\left\{G_0(k)\frac{\partial\Sigma^\pi(k)}{\partial m_\pi^2}\right\} = B\delta_{ij}\frac{\partial\mathcal{E}_2}{\partial m_\pi^2} \ , \tag{8.9}$$

with the derivative affecting only the explicit dependence of Σ_f^π on the pion propagator, and not including the implicit one from the the nucleon mass dependence on it. One has to subtract the value of the one-pion loop nucleon self-energy at $k^0 = 0$ since we are using the physical nucleon mass. After performing the k^0 integration, one has the expression

$$\Xi_3 = 2B\delta_{ij}\int \frac{d^3k}{(2\pi)^3}\Big(\theta(\xi_p - |\mathbf{k}|) + \theta(\xi_n - |\mathbf{k}|)\Big)\frac{\partial\Sigma_f^\pi(\omega)}{\partial m_\pi^2} \ , \tag{8.10}$$

with $\omega = E(\mathbf{k})$. Performing explicitly the derivative it results,

$$\frac{\partial\Sigma_f^\pi(\omega)}{\partial m_\pi^2} = \frac{3g_A^2}{64\pi^2 f_\pi^2 m_\pi^2}\left[2\omega^3 - 4\omega m_\pi^2 - 3\pi m_\pi^3 + 3m_\pi^2\sqrt{b}\left(\pi + i\ln\frac{\omega + i\sqrt{b}}{-\omega + i\sqrt{b}}\right)\right] \ , \tag{8.11}$$

with $b = m_\pi^2 - \omega^2 - i\epsilon$ and $\epsilon \to 0^+$. Notice that Ξ_3 is an $\mathcal{O}(p^7)$ or next-to-next-o-leading order contribution because $\partial\Sigma_f^\pi/\partial m_\pi^2 = \mathcal{O}(p^2)$. The $\mathcal{O}(p)$ contribution from the term $-3\pi m_\pi$ is cancelled by that coming from $3\sqrt{b}\pi$. The former term arises because we are working at the physical nucleon mass. We then conclude that the only contribution with $V_\rho = 1$ up-to-and-including next-to-leading order is given by Ξ_1, eq. (8.4).

8.3 $V_\rho = 2$ contributions

We now consider those next-to-leading order contributions to the in-medium chiral quark condensate that involve the nucleon-nucleon interactions. They are depicted in diagrams 4–6 of the last two rows of fig. 8.1.

8.3.1 Cancellation of Ξ_4 and Ξ_5

Diagrams 4 and 5 of fig. 8.1 are analogous to diagrams 7 and 9 of fig. 7.1. There it has been shown that those diagrams cancel each other. This argument was developed in subsection 7.3.2 within a specific method for resumming the iteration of the wiggly lines for the non-perturbative nucleon-nucleon interactions. We expect that this cancellation also takes place for the case of the in-medium chiral quark condensate. However, the vertex coupling two nucleons with the scalar source, eq. (8.3), has both an isoscalar and an isovector term while for the aforementioned cancellation in the case of the pion self-energy only an isovector vertex was involved. Here we want to show on general grounds that the cancellation also takes place for the in-medium chiral quark condensate, following similar arguments as those in subsection 7.3.2.

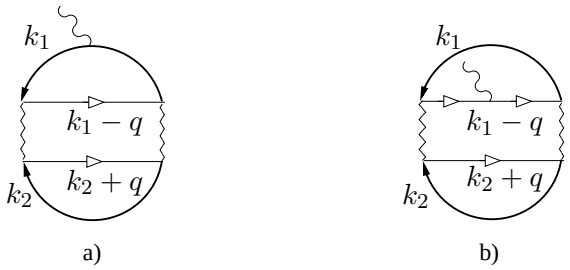

Figure 8.4: Contribution to the chiral quark condensate with a two-nucleon reducible loop. The scalar source couples outside the loop for diagram 4 and inside it for diagram 5.

Diagram 4 of fig. 8.1 can be written in terms of the nucleon self-energy due to the in-medium nucleon-nucleon scattering, denoted by Σ^{NN}. It reads

$$\Xi_4 = 2iB \int \frac{d^4k_1}{(2\pi)^4} e^{ik_1^0\eta}\ \mathrm{Tr}\Big\{ \big[2c_1\delta_{ij} + c_5\vec{\tau}_{ji}\cdot\vec{\tau}\big] G_0(k_1)\Sigma^{NN}G_0(k_1)\Big\}\ . \tag{8.12}$$

The expression for $\Sigma_{\alpha_1,NN}$, corresponding to the self-energy of a nucleon with isospin α_1, is

$$\Sigma_{i_3,NN} = -i\sum_{\alpha_2,\sigma_2}\int \frac{d^4k_2}{(2\pi)^4} e^{ik_2^0\eta} G_0(k_2)_{\alpha_2} T^{\sigma_1\sigma_2}_{\alpha_1\alpha_2}(k_1,k_2)\ . \tag{5.27}$$

Here α_2, σ_2 correspond to the running third components of isospin and spin, respectively, while σ_1 is the third component of the spin of the external nucleon. In addition, $T^{\sigma_1\sigma_2}_{\alpha_1\alpha_2}(k_1,k_2)$ refers to the elastic in-medium nucleon-nucleon scattering amplitude for $N_{\alpha_1,\sigma_1}(k_1)N_{\alpha_2,\sigma_2}(k_2) \to N_{\alpha_1,\sigma_1}(k_1)N_{\alpha_2,\sigma_2}(k_2)$. We also make use of the identity $\partial G_0(k)/\partial k^0 = -G_0(k)^2$. As a result, eq. (8.12) can be expressed as

$$\begin{aligned}\Xi_4 = 2B \sum_{\alpha_1,\alpha_2}\sum_{\sigma_1,\sigma_2}\int \frac{d^4k_1}{(2\pi)^4}\frac{d^4k_2}{(2\pi)^4} e^{ik_1^0\eta}e^{ik_2^0\eta} G_0(k_1)_{\alpha_1}\big[2c_1\delta_{ij} + c_5(\tau^3)_{ij}(\tau^3)_{\alpha_1\alpha_1}\big] \\ \times G_0(k_2)_{\alpha_2}\frac{\partial T^{\sigma_1\sigma_2}_{\alpha_1\alpha_2}(k_1,k_2)}{\partial k_1^0}\ ,\end{aligned} \tag{8.13}$$

where in the last equation an integration by parts in k_1^0 has been performed. In order to see the cancellation between diagrams 4 and 5 of fig. 8.1 let us proceed similarly as in subsection 7.3.2, for the case of the in-medium pion self-energy, and consider first the case with only one reducible two-nucleon diagram, fig. 8.4. The contribution of diagram a), Ξ_4^L, can be readily worked from eq. (8.13) by reducing $T^{\sigma_1\sigma_2}_{\alpha_1\alpha_2}(k_1,k_2)$ to its one-loop calculation. It results

$$\begin{aligned}\Xi_4^L = -i\,2B \sum_{\alpha_1,\alpha_2}\sum_{\sigma_1,\sigma_2}\int \frac{d^4k_1}{(2\pi)^4}\frac{d^4k_2}{(2\pi)^4} e^{ik_1^0\eta}e^{ik_2^0\eta} G_0(k_1)_{\alpha_1}\big[2c_1\delta_{ij} + c_5(\tau^3)_{ij}(\tau^3)_{\alpha_1\alpha_1}\big]G_0(k_2)_{\alpha_2} \\ \times \frac{\partial}{\partial k_1^0}\Big[\frac{1}{2}\sum_{\alpha_1',\alpha_2'}\int\frac{d^4q}{(2\pi)^4} V_{\alpha_1\alpha_2;\alpha_1'\alpha_2'}(q)G_0(k_1-q)_{\alpha_1'}G_0(k_2+q)_{\alpha_2'}V_{\alpha_1'\alpha_2';\alpha_1\alpha_2}(-q)\Big]\ .\end{aligned} \tag{8.14}$$

where $V_{\alpha\beta;\gamma\delta}$ corresponds to the wiggly line with the first pair of labels belonging to the outgoing nucleons and the second pair to the in-going ones. Note that a symmetry factor 1/2 is included because V contains both the direct and exchange terms. In addition, V also will depend generally

on spin. Both isospin and spin indices are globally indicated in the labels of V with Greek letters. The quantity in squared brackets in the previous equation is $T^{\sigma_1\sigma_2}_{\alpha_1\alpha_2}(k_1,k_2)$ at the one-loop level. It is not necessary to consider $T^{\sigma_1\sigma_2}_{\alpha_1\alpha_2}$ at the tree-level, consisting of the exchange of one wiggly line, fig. 4.1, because it is then independent on k_1^0 so that the derivative with respect to k_1^0 is zero.

One can similarly write down the contribution from the diagram b) of fig. 8.4, denoted by Ξ_5^L. It reads

$$\Xi_5^L = \frac{i}{2}\sum_{\alpha_1,\alpha_2}\sum_{\sigma_1,\sigma_2}\int\frac{d^4k_1}{(2\pi)^4}\frac{d^4k_2}{(2\pi)^4}e^{ik_1^0\eta}e^{ik_2^0\eta}G_0(k_1)_{\alpha_1}G_0(k_2)_{\alpha_2}\frac{\partial}{\partial k_1^0}\Big[2B\sum_{\alpha_1',\alpha_2'}\int\frac{d^4q}{(2\pi)^4}V_{\alpha_1\alpha_2;\alpha_1'\alpha_2'}(k)$$
$$\times\left[2c_1\delta_{ij}+c_5(\tau^3)_{ij}(\tau^3)_{\alpha_1'\alpha_1'}\right]G_0(k_1-q)_{\alpha_1'}G_0(k_2+q)_{\alpha_2'}V_{\alpha_1'\alpha_2';\alpha_1\alpha_2}(-q)\Big]\ . \tag{8.15}$$

with the global symmetry factor 1/2 from closing the lines. The appearance of the derivatives with respect to k_1^0 is again due to the fact that the propagator attached to the scalar source appears squared. The loop integrals between the squared brackets in eqs. (8.14) and (8.15) are typically divergent. Nevertheless, the parametric derivative with respect to k_1^0 can be extracted out of the integral of eq. (8.15) as soon as it is regularized. Summing over all isospin states makes clear that the position of the vertex associated with the coupling of the scalar source to two nucleons, either inside or outside the squared brackets, does not yield a difference. For that one has to keep in mind that $T^{\sigma_1\sigma_2}_{\alpha_1\alpha_2}(k_1,k_2)=T^{\sigma_2\sigma_1}_{\alpha_2\alpha_1}(k_2,k_1)$, due to the Fermi-Dirac statistics for a pair of two-nucleon states. Furthermore, notice that all the indices and four-momenta associated with the nucleons 1 and 2 are summed and integrated, respectively. In this way eqs. (8.14) and (8.15) mutually cancel.

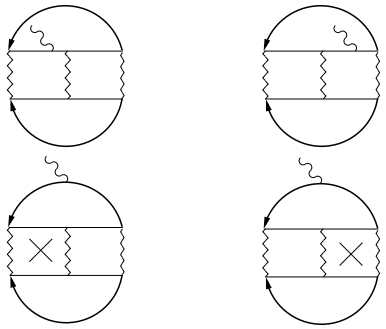

Figure 8.5: After performing the integration by parts in eq. (8.13) the derivative with respect to k_1^0 acts onto the scattering amplitude. This gives a sum of derivatives acting on two-nucleon reducible loops, indicated by the crosses. When the derivative acts on a baryon propagator the latter becomes squared. In this way, the first diagram in the second row of the figure equals the one of the first row but with opposite sign and they cancel each other. The same applies to the second diagrams in both rows.

This process of mutual cancellation can be generalized to any number of two-nucleon reducible loops, using the same argument as given in subsection 7.3.2 for the case of the in-medium pion self-energy. An $n+1$ iterated wiggly line exchange implies n two-nucleon reducible loops. The scalar source can be attached to any of them for Ξ_5, while for Ξ_4 the derivative with respect to k_1^0 can also act on any of the loops. This is exemplified in fig. 8.5 for the case with two two-nucleon reducible loops. Hence,

$$\Xi_4+\Xi_5=0\ . \tag{8.16}$$

The basic simple reason for such cancellation is that while for Ξ_5 there is a derivative acting onto the scattering amplitude, Ξ_4 involves an integration by parts in order to do so, which then introduces an extra minus sign.

The previous cancellation is also explicitly obtained making use of Unitary χPT applied to nuclear matter. The intermediate result can be used straightforwardly by considering that instead of the Weinberg-Tomozawa vertex and Born terms, used in the problem of the in-medium pion self-energy, one has the nucleon vertex of eq. (8.3) with the scalar source. The partial wave decomposition of Ξ_4 reads

$$\Xi_4 = 2B \sum_{J,\ell,S,I} \sum_{\alpha_1,\alpha_2} (2J+1)\chi(S\ell I)^2 \int \frac{d^4k_1}{(2\pi)^4}\frac{d^4k_2}{(2\pi)^4} e^{ik_1^0\eta} e^{ik_2^0\eta} \big[2c_1\delta_{ij} + I_3 c_5 (\tau^3)_{ij}\big] \times G_0(k_1)_{\alpha_1} G_0(k_2)_{\alpha_2} \frac{m\partial}{\partial A} T^{I_3}_{JI}(\ell,\ell,S) \ , \tag{8.17}$$

with $\alpha_1 + \alpha_2 = I_3$, the third component of the total isospin I of the two-nucleon state. Other symbols used are J the total angular momentum, ℓ the orbital angular momentum and S the total spin of the nucleon-nucleon pair. We also employ the kinematical variable $A = 2mP^0 - \mathbf{P}^2$, where $P = (k_1 + k_2)/2$ and $\mathbf{P}$ is the three-vector made by the spatial components of P. For on-shell scattering $A = \mathbf{p}^2$, with $\mathbf{p}$ the three-momentum in the two-nucleon rest frame. Due to the isovector character of the vertex involving c_5 only the difference between the proton-proton and neutron-neutron contributions survives. For the expressions at $\mathcal{O}(p^6)$ and $\mathcal{O}(p^7)$ we plug into eq. (8.17) the derivative $\partial T_{JI}/\partial A$ at leading and next-to-leading order according to eqs. (7.43) and (7.44), respectively. For the contribution Ξ_5 the general partial wave decomposition yields

$$\Xi_5 = \frac{1}{2} \sum_{J,\ell,S,I} \sum_{\alpha_1,\alpha_2} (2J+1)\chi(S\ell I)^2 \int \frac{d^4k_1}{(2\pi)^4}\frac{d^4k_2}{(2\pi)^4} e^{ik_1^0\eta} e^{ik_2^0\eta} \times G_0(k_1)_{\alpha_1} G_0(k_2)_{\alpha_2} \left[D^{I_3}_{JI}\right]^{-1} \cdot \xi^{I_3}_{JI} \cdot \left[D^{I_3}_{JI}\right]^{-1} \ . \tag{8.18}$$

The expressions for $D^{I_3}_{JI}$ at leading and next-to-leading order are given in eq. (7.44) and $\xi^{I_3}_{JI}$ is calculated order by order. For that one has to work out the partial wave decomposition of the two-nucleon reducible diagram with the scalar source attached to one of the nucleon propagators inside the loop. Following those calculations one obtains for the leading order (LO) and next-to-leading order (NLO)

$$\xi_{JI}\big|_{LO} = -\big[N^{(0)}_{JI}\big]^2 \cdot DL_{10} \ , \tag{4.39}$$

$$\xi_{JI}\big|_{NLO} = DL^{(1)}_{JI} - \Big\{L^{(1)}_{JI} + \big[N^{(0)}_{JI}\big]^2 L_{10}, N^{(0)}_{JI}\Big\} DL_{10} \ , \tag{4.42}$$

$$DL_{10} = 4B\big[2c_1\delta_{ij} + I_3 c_5(\tau^3)_{ij}\big]\frac{m\partial}{\partial A} L_{10} \ , \tag{8.19}$$

$$DL^{(1)}_{JI} = 4B\big[2c_1\delta_{ij} + I_3 c_5(\tau^3)_{ij}\big]\frac{m\partial}{\partial A} L^{(1)}_{JI} \ . \tag{8.20}$$

The contribution Ξ_5 at $\mathcal{O}(p^6)$ and $\mathcal{O}(p^7)$ results when the just given expressions for ξ_{JI}, in order, are inserted in eq. (8.18). It is straightforward to check that they exactly cancel with Ξ_4 accordingly.

8.3.2 Contribution Ξ_6

Let us now consider the calculation of diagram 6 of fig. 8.1, where the scalar source is attached to an exchanged wiggly line. Since the scalar source coupling to a local term is of higher order, it only couples to the pion exchange lines here. The appearance of the pion propagator squared with a

zero momentum scalar source leads to its derivative with respect to the pion mass. The local term is independent of the pion mass, so we may act the derivative onto the explicit dependence on the pion-mass of the full nucleon-nucleon scattering amplitude. The implicit dependence of the latter on m_π^2 due to that of the nucleon mass is the content of the diagrams 4 and 5 of fig. 8.1, which have been shown above to cancel mutually. We can write

$$\begin{aligned}\Xi_6 &= -\frac{1}{2}\sum_{\alpha_1,\alpha_2}\sum_{\sigma_1,\sigma_2}\int\frac{d^4k_1}{(2\pi)^4}\frac{d^4k_2}{(2\pi)^4}e^{ik_1^0\eta}e^{ik_2^0\eta}G_0(k_1)_{\alpha_1}G_0(k_2)_{\alpha_2}\left[T^{\sigma_1\sigma_2}_{\alpha_1\alpha_2}(k_1,k_2)\right]_{ij}\\ &= -B\delta_{ij}\frac{1}{2}\sum_{\alpha_1,\alpha_2}\sum_{\sigma_1,\sigma_2}\int\frac{d^4k_1}{(2\pi)^4}\frac{d^4k_2}{(2\pi)^4}e^{ik_1^0\eta}e^{ik_2^0\eta}G_0(k_1)_{\alpha_1}G_0(k_2)_{\alpha_2}\frac{\partial T^{\sigma_1\sigma_2}_{\alpha_1\alpha_2}(k_1,k_2)}{\partial m_\pi^2}\\ &= B\delta_{ij}\frac{\partial\mathcal{E}_3}{\partial m_\pi^2}\ .\end{aligned} \tag{8.21}$$

Where $\mathcal{E}_3$ is the contribution to the nuclear matter energy due to the in-medium nucleon-nucleon at leading order, evaluated in section 6.2. In order to proceed we have to evaluate the derivative of the nucleon-nucleon scattering amplitude with respect to m_π^2. We decompose the amplitude in a sum over nucleon-nucleon partial waves $T_{JI}(\ell',\ell,S)$, with J the total angular momentum of the two-nucleon system, S/I its spin/isospin and ℓ'/ℓ the final/inital orbital angular momentum. In terms of the nucleon-nucleon interaction kernel $N_{JI}(\ell',\ell,S)$, the nucleon-nucleon partial wave T_{JI} in UχPT is given by

$$T_{JI}(\ell',\ell,S) = \left[1 + N_{JI}(\ell',\ell,S)\cdot L_{10}\right]^{-1}\cdot N_{JI}(\ell',\ell,S) \doteq [D_{JI}]^{-1}\cdot N_{JI}\ , \tag{4.31}$$

with L_{10} the nucleon-nucleon unitarity scalar function, eq. (C.1). The previous equation can also be rewritten as

$$T_{JI} = N_{JI} - N_{JI}\cdot L_{10}\cdot T_{JI}\ . \tag{4.32}$$

Taking the derivative with respect to the explicit dependence on m_π^2 on both sides of the previous equation results in

$$\frac{\partial T_{JI}}{\partial m_\pi^2} = [D_{JI}]^{-1}\cdot\frac{\partial N_{JI}}{\partial m_\pi^2}\cdot[D_{JI}]^{-1}\ , \tag{8.22}$$

where the dependence of the nucleon mass on the pion mass is not taken into account, therefore the derivative acting on L_{10} vanishes. At the order we are calculating the in-medium chiral quark condensate we need the nucleon-nucleon partial waves calculated at leading order

$$\left.\frac{\partial T_{JI}}{\partial m_\pi^2}\right|_{LO} = \left[D_{JI}^{(0)}\right]^{-1}\cdot\frac{\partial N_{JI}^{(0)}}{\partial m_\pi^2}\cdot\left[D_{JI}^{(0)}\right]^{-1}\ , \tag{8.23}$$

where $N_{JI}^{(0)}$, corresponding to the one-wiggle exchange in fig. 4.1. In terms of this equation the partial wave decomposition of Ξ_6 at its leading order is

$$\Xi_6 = -B\delta_{ij}\frac{1}{2}\sum_{J,\ell,S,I,I_3}(2J+1)\chi(S\ell I)^2\int\frac{d^4k_1}{(2\pi)^4}\frac{d^4k_2}{(2\pi)^4}e^{ik_1^0\eta}e^{ik_2^0\eta}G_0(k_1)_{\alpha_1}G_0(k_2)_{\alpha_2}\left.\frac{\partial T_{JI}^{I_3}}{\partial m_\pi^2}\right|_{LO}\ , \tag{8.24}$$

where in the superscript the third component of the total isospin $I_3 = \alpha_1+\alpha_2$ is shown. Concerning the problem of regularizing this amplitude, we refer to the detailed discussion in section 6.2.

8.4 Discussion and results

It follows from our calculation for the in-medium corrections shown in fig. 8.1 that up-to-and-including next-to-leading order the chiral quark condensate is given by

$$m_q\langle\Omega|\bar{q}_i q_j|\Omega\rangle = m_q\langle 0|\bar{q}_i q_j|0\rangle - m_q\big(\Xi_1^{is} + \Xi_1^{iv} + \Xi_2^{iv} + \Xi_3 + \Xi_6\big) \ . \tag{8.25}$$

Here we have taken into account that Ξ_2^{is} vanishes, while $\Xi_4 + \Xi_5 = 0$. Also, note that Ξ_2^{iv} and Ξ_3 are suppressed by one order, so we will neglect them. Ξ_1, Ξ_3 and Ξ_6 are clearly connected with the corresponding contribution to the nuclear matter energy, as required by the Hellmann-Feynman theorem [CFG91, DL91, LFA00].

$$\begin{aligned} m_q\langle\Omega|\bar{q}_i q_j|\Omega\rangle - m_q\langle 0|\bar{q}_i q_j|0\rangle &= \frac{m_q}{2}\left(\delta_{ij}\frac{d}{d\hat{m}} + (\tau^3)_{ij}\frac{d}{d\bar{m}}\right)\left(\frac{E_{tot}}{V}\right) \\ &= \frac{m_q}{2}\left(\delta_{ij}\frac{d}{d\hat{m}} + (\tau^3)_{ij}\frac{d}{d\bar{m}}\right)(\rho\, m_N + \mathcal{E}) \ , \end{aligned} \tag{8.26}$$

with $\bar{m} = (m_u - m_d)/2$ and $\mathcal{E}$ the energy density of the nuclear matter system. This result is fulfilled in our case, where Ξ_1, eq. (8.25), is the leading derivative with respect to m_π^2 of the nucleon mass. In turn, Ξ_3 and Ξ_6 correspond to the explicit derivative of the nuclear matter energy due to the nucleon-nucleon interactions with respect to m_π^2, eq. (8.21). Notice, that the implicit dependence on m_π^2 of the in-medium nucleon-nucleon interactions does not give contribution to Ξ because of mutual cancellation between Ξ_4 and Ξ_5.

The energy density and energy per particle $\mathcal{E}/\rho$ have been calculated in section 6.2. In this reference, it is obtained from first principles the saturation of symmetric nuclear matter. In addition, a remarkable good agreement with sophisticated many-body calculations [PW79] was obtained for the equation of state of both neutron and symmetric nuclear matter in terms of just one free parameter for each. Only one of the two free parameters was fined tuned for symmetric nuclear matter. The other one turns out to be around its expected natural size. Values in perfect agreement with experiment were obtained for the saturation density, energy per particle and compression modulus, subsection 6.3.1. We use the results of this reference in order to evaluate Ξ_6, eq. (8.21), by taking the derivative with respect to the explicit dependence on m_π^2 of $\mathcal{E}_3$.

The term Ξ_1^{is} can be written directly in terms of the pion-nucleon sigma-term, $\sigma = \hat{m}\partial m_N/\partial\hat{m}$. This term is reproduced in χPT by $\sigma = -4c_1 m_\pi^2 + \mathcal{O}(m_\pi^3)$ [GSS88, BKM97] and we obtain the result

$$\Xi_1^{is} = \langle 0|\bar{q}_i q_j|0\rangle\frac{\sigma}{f_\pi^2 m_\pi^2}(\rho_p + \rho_n) \ , \tag{8.27}$$

where it has been use of the Gell-Mann–Oakes–Renner relation (GMOR) [GOR68], $\delta_{ij} m_\pi^2 f_\pi^2 = -2\hat{m}\langle 0|\bar{q}_i q_j|0\rangle$, valid at lowest order in the chiral expansion [Me93]. Regarding the numerical value of σ one has the earlier extraction of [Ko82, GLS91] ($\sigma = 45 \pm 8$ MeV) or the one from the more recent partial wave analysis of pion-nucleon scattering [PSWA02] ($\sigma = 64 \pm 7$ MeV). In both cases the dispersion analysis of the nucleon scalar form factor of [GLS91] to estimate the departure between the sigma-term and the πN scattering amplitude evaluated at the (unphysical) Cheng-Dashen point is used. The term sensitive to nuclear dynamics is Ξ_6. Making also use of GMOR it can be written as

$$\Xi_6 = -\langle 0|\bar{q}_i q_j|0\rangle\frac{1}{f_\pi^2}\frac{\partial\mathcal{E}_3}{\partial m_\pi^2}(1 + \mathcal{O}(m_\pi^2)) \ . \tag{8.28}$$

In asymmetric matter there are additional symmetry breaking terms proportional to c_5 stemming from diagrams 1 and 2, giving rise to the next-to-leading order contribution Ξ_1^{iv}, eq. (8.4). This contribution, which distinguishes between the $\bar{u}u$ and $\bar{d}d$ quark condensates, are suppressed because they are proportional to the numerically small low-energy constant $c_5 = -0.09 \pm 0.01$ GeV^{-1} [BKM97]. For symmetric nuclear matter this contribution is zero since it is proportional to the difference of proton and neutron densities.

Putting together eqs. (8.27) and (8.28), together with Ξ_1^{iv}, we then have to next-to-leading order

$$\frac{\langle\Omega|\bar{q}_i q_j|\Omega\rangle}{\langle 0|\bar{q}_i q_j|0\rangle} = 1 - \frac{\sigma}{f_\pi^2 m_\pi^2}(\rho_p + \rho_n) + (\tau^3)_{ij}\frac{2c_5}{f_\pi^2}(\rho_p - \rho_n) + \frac{1}{f_\pi^2}\frac{\partial \mathcal{E}_3}{\partial m_\pi^2} \ . \tag{8.29}$$

The input parameters taken are $g_A = 1.26$, $f_\pi = 92.4$ MeV, $m_\pi = 138$ MeV, $m_N = 939$ MeV and $\sigma = 45$ MeV. In addition the subtraction constants needed for the evaluation of $\mathcal{E}_3$ are taken with their values that reproduce better the equation of state of symmetric nuclear matter and neutron matter (the latter in comparison with sophisticated many-body calculation [PW79, APR98]). These values are $g_0 = \widetilde{g}_0 = -0.62\ m_\pi^{-2}$ for the case of neutron matter and $g_0 = -0.97$, $\widetilde{g}_0 = -0.52\ m_\pi^{-2}$ for symmetric nuclear matter. Notice that $\widetilde{g}_0$ is very close in both cases. It has the natural size expected from the arguments given in subsection 6.3.1. Only g_0 for the case of symmetric nuclear matter was fine tuned in order to reproduce the experimental results. The equations of state for both cases are shown in section 6.3.1, where the figures 6.6 and 6.7 correspond to neutron and symmetric nuclear matter, respectively. The magenta lines are from the many-body calculations of [APR98, PW79] employing to so-called realistic nucleon-nucleon potentials. In all the cases the Fermi momentum at most is 3 fm^{-1}

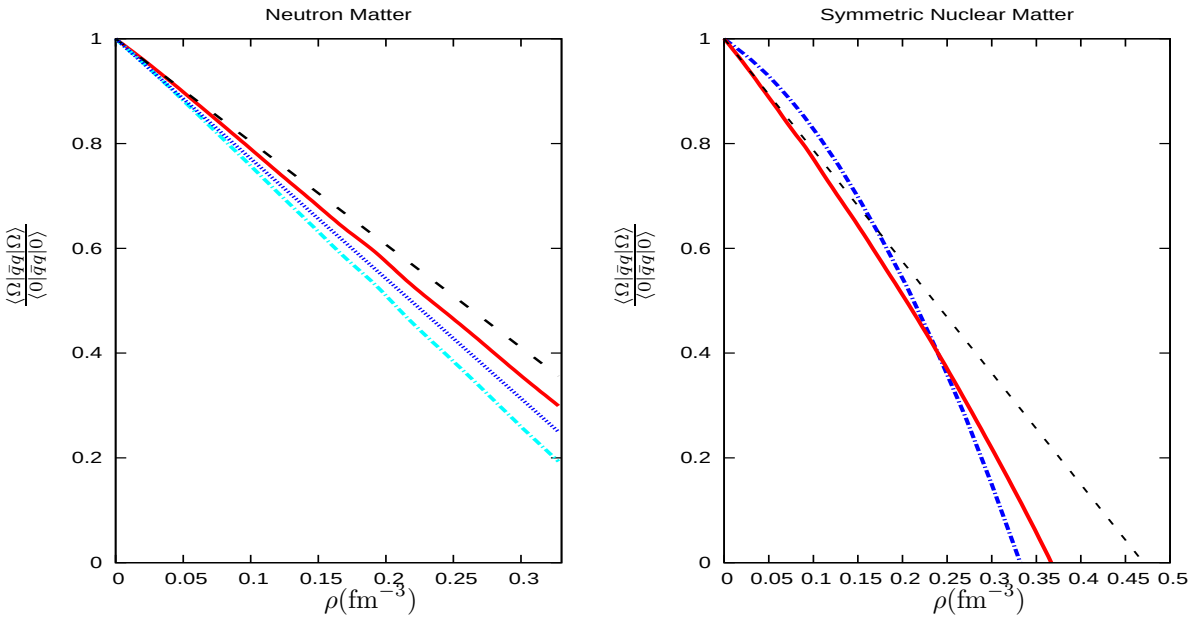

Figure 8.6: The ratio between the in-medium– and vacuum chiral quark condensate, $\langle\Omega|\bar{q}q|\Omega\rangle/\langle 0|\bar{q}q|0\rangle$, eq. (8.29), for neutron matter, left panel, and symmetric nuclear matter, right panel. Left panel: The (red) solid and (cyan) dot-dashed lines are our results, eq. (8.29), for $\bar{q}q = \bar{u}u$ and $\bar{q}q = \bar{d}d$, respectively. The (black) dashed and (blue) dotted lines correspond to the linear density approximation (Ξ_1). Right Panel: The (red) solid and (black) dashed lines are the full results and the linear approximation, in this order, with $\sigma = 45$ MeV [GLS91]. The (blue) dot-dashed line is the full calculation with $\sigma = 64$ MeV [PSWA02].

In fig. 8.6 we show the quotient of $\langle\Omega|\bar{q}q|\Omega\rangle$ and $\langle 0|\bar{q}q|0\rangle$, eq. (8.29), for pure neutron (left panel) and symmetric nuclear matter (right panel) employing $\sigma = 45$ MeV. From the figure we observe that the leading order correction Ξ_1, eq. (8.4), is the dominant one. The next-to-leading order corrections rising from Ξ_6, eq. (8.28), are small for neutron matter but larger for the symmetric nuclear matter. They also increase with density, as expected since with a larger Fermi momentum the three-momenta of the nuclear are larger. For neutron matter they are a 9% of the leading order corrections at $\rho = 0.3$ fm^{-3}. For symmetric nuclear matter they are 20% at $\rho = 0.3$ fm^{-3} and 40% for $\rho = 0.5$ fm^{-3} of the leading correction, respectively. The next-to-leading order corrections, Ξ_6, tend to speed the tendency towards a vanishing quark condensate in the nuclear medium (a signal of a possible restoration of chiral symmetry in nuclear matter). On the other hand, the dependence on the subtraction constants g_0 and $\widetilde{g}_0$ of the in-medium quark condensate to next-to-leading order is just at the level of a few per cent in the range of densities shown. In this way, the quark condensate is significantly less dependent on g_0 than E/A. Had we used $\sigma = 64$ MeV, according with the more recent determination [PSWA02], the dominant linear density contribution will drop faster the in-medium quark condensate. E.g. at this level of approximation, the dashed line in the right panel of fig. 8.6, crosses the zero at $\rho \approx 2\rho_0$. To this result one should add the difference between the solid and dashed lines corresponding to the contributions from the in-medium nucleon-nucleon contributions. This is shown in the figure by the dot-dashed line.

To this order one-pion exchange, together with the contact nucleon-nucleon interaction terms from $\mathcal{L}^{(0)}_{NN}$ eq. (4.1), are fully iterated, as represented by the ellipsis in the diagrams 4–6 of fig. 8.1. In [KHW08] only one iteration of the one-pion exchange is considered, and not nucleon-nucleon contact interactions at the same chiral order are included. These authors find a further suppression of the quark condensate in symmetric nuclear matter compared with the linear density approximation, as we also do, while [LFA00, PF07] find a positive corrections. However, the contribution from once-iterated one-pion exchange in [KHW08] is notoriously larger than our solid line in the right panel of fig. 8.6. Keeping only this extra contribution, together with the linear density one, [KHW08] finds that the quark condensate vanishes at $\rho \simeq 0.24$ fm^{-3}, while in our case this happens for the larger $\rho = 0.37$ fm^{-3}. Compare our fig. 8.6 with fig. 6 of [KHW08]. This indicates that the further iteration of one-pion exchange, together with the inclusion of the associated nucleon-nucleon local terms of $\mathcal{L}^{(0)}_{NN}$, have an important impact. We agree on the observation performed in [KHW08, PF07] that the short-range nucleon-nucleon interactions effects are suppressed for the evaluation of the in-medium quark condensate. This a consequence of eq. (8.22). At the order we are working, if only the local nucleon-nucleon interactions from $\mathcal{L}^{(0)}_{NN}$ were kept the derivative of T_{JI} with respect to m_π^2 would be zero and $\Xi_6 \to 0$. Thus, only the linear density contribution would survive. Other mechanisms were included in [KHW08]. They indicate a tendency towards a stabilization of the in-medium quark condensate in nuclear matter for densities above ρ_0. Since no power counting is followed by the authors in [KHW08] we consider as an interesting future task to include the higher orders needed and confirm, if possible, their far reaching results. On the other hand, we agree with [KW09] that for pure neutron matter the linear tendency of the quark condensate is only weakly modified by the higher order corrections. It is also worth noting that the approach of the Munich group [KFW02, KFW05, KW09] has some difficulties in providing a good reproduction of the equation of state for neutron matter while in our approach [LOMb] it emerges in a quite straightforward way at next-to-leading order.

8.5 Conclusions and outlook

Employing the in-medium power counting and the methods of Unitary χPT for taking into account the resummation of non-perturbative effects we have calculated the chiral quark condensate up-to-and-including next-to-leading order, $\mathcal{O}(p^6)$ in nuclear matter. We have found an interesting cancellation between the diagrams involving the nucleon-nucleon interactions. In this way, those contributions that arise due to the leading quark mass dependence of the nucleon mass mutually cancel. This corresponds to the diagrams 4 and 5 in fig. 8.1. As a result, only the diagrams 6 in the figure, that stem from the quark mass dependence of the pion mass, survive. This is the reason why previous calculations have found that short range nucleon-nucleon interactions are suppressed for the calculation of the in-medium quark condensates. Note that we did not exploit the Hellmann-Feynman theorem, but obtained our results explicitly from the generating functional, eq. (8.1). We conclude that the corrections are small for the quark condensate in the case of pure neutron matter. However, these corrections are more significant for the the case of symmetric nuclear matter. It is also worth pointing out that the full iteration of the nucleon-nucleon interactions reduces the force of such extra damping of the quark condensate as compared with other references. The dependence of our results on the subtraction constant g_0 is at the level of a few percent, much smaller than for the case of the bounding energy (chapter 6). On top of these nuclear effects one has to take into account the present large uncertainty of the still actively debated sigma-term of pion-nucleon scattering.

Higher order calculations are a very interesting task as they provide the important two-pion exchange and multi-nucleon forces. Such an effect furthermore merges meson-baryon mechanisms with novel multi-nucleon contributions that can be worked out systematically within our EFT. The large impact of the Δ-isobar excitation to symmetric nuclear matter in [KHW08], which is then partially compensated by the three-body interactions terms proportional to the low-energy constant c_1, leads to freezing in the dropping of the in-medium chiral quark condensate at $\sim 2\rho_0$. This interesting fact requires confirmation within our power counting so as to keep all the terms contributing at the same chiral order, while keeping the full iteration of lowest order local and one-pion exchange diagrams. As commented above, the latter has a significant impact in the contribution at next-to-leading order. In addition, one should keep in mind that the proper way to address the issue of chiral symmetry restoration in the nuclear medium is the calculation of the temporal pion decay constant in the nuclear medium [MOW02].

Chapter 9

In-medium pion decay[#12]

In this chapter our theory developed in the chapters 3 and 4 is applied to the problem of calculating the in-medium contributions to the pion decay. We find that the next-to-leading order contributions to the pion decay constant from in-medium nucleon-nucleon interactions cancel each other, in the same way as it had been in the case of the isovector pion self-energy. In particular we find no violation of the Gell-Mann–Oakes–Renner relation due to in-medium corrections up to next-to-leading order in the chiral counting.

9.1 Introduction

Many recent calculations in nuclear matter share the assumption that spontaneous chiral symmetry breaking still holds for finite density nuclear systems. This assumption can be cross-checked by calculating the temporal pion decay constant in the nuclear medium. Let us consider the axial-vector current $A^i_\mu(x) = \bar{q}(x)\gamma_\mu\gamma_5(\tau^i/2)q(x)$, with $q(x)$ a two-dimensional vector corresponding to the light quarks fields and τ^i the Pauli matrices. Spontaneous chiral symmetry breaking results because the axial charge, $Q^i_A = \int d^3x A^i_0(x)$, does not annihilate the ground state, denoted by $|\Omega\rangle$. As long as the matrix element $\langle\Omega|Q^i_A|\pi^a(\mathbf{p})\rangle = i(2\pi)^3 f_t p_0 \delta(\mathbf{p})$ is not zero, the ground state is not left invariant by the action of the axial charge and spontaneous chiral symmetry breaking happens. In the previous equation $|\pi^a(\mathbf{p})\rangle$ denotes a pion state with Cartesian coordinate a, three-momentum $\mathbf{p}$, energy p_0 and f_t is the temporal weak pion decay coupling. (Mathematically one can obtain meaningful results from $i\delta(\mathbf{p})p_0$ in the chiral limit by considering wave packets, $\int d\mathbf{p}|\mathbf{p}|^{-1} f(\mathbf{p}^2)|\pi^a(\mathbf{p})\rangle$ with $f(0)$=constant [GSW62].)

Due to the presence of the nuclear medium one should distinguish between the spatial and temporal couplings of the pion to the axial-vector current. The fact that $f_t \neq f_s$ in nuclear matter and some consequences thereof have already been discussed in [KR93, Le94, TW95, WT95, KW96, PT96, KW97, Pi97, Ki02, MOW02]. The calculations in [MOW02] indicate a linear decreasing of f_t with density, $f_t = f_\pi(1 - (0.26 \pm 0.04)\rho/\rho_0)$, where $f_\pi = 92.4$ MeV is the weak pion decay constant in the vacuum and ρ_0 is the nuclear matter saturation density. This result indicates that it makes sense to use chiral Lagrangians in the nuclear medium up to central nuclear densities. However, the result so far has been obtained by considering pion-nucleon dynamics only, but nucleon-nucleon interactions have not been taken into account. Therefore the calculation up to next-to-leading

[#12]The contents of this chapter have been published in [LOMd].

order has to be reconsidered in our approach.

After this introduction we will briefly discuss the calculations of the contributions up-to-and-including next-to-leading order in section 9.2. A summary with conclusions and outlook will be given in section 9.3.

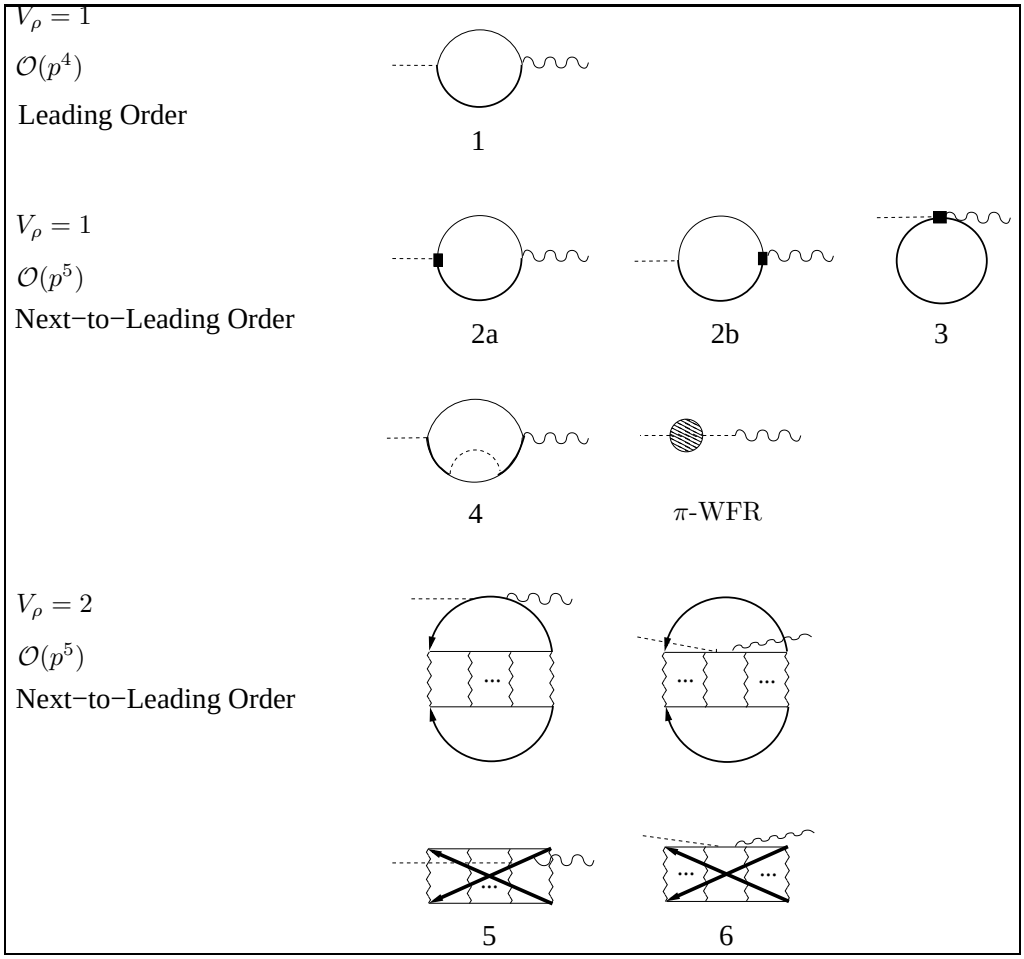

Figure 9.1: Contributions to the in-medium pion decay constant up-to-and-including next-to-leading order, $\mathcal{O}(p^5)$. The axial-vector source is indicated by the wavy line and the pions by the dashed lines. A wiggly line corresponds to the nucleon-nucleon interaction kernel, fig. 4.1, whose iteration is denoted by the ellipsis. The blob of the diagram labelled with π-WFR indicates the contribution from the wave function renormalization of the pion. The diagram 6 has a symmetry factor of 1/2.

9.2 In-medium pion decay

We depict the contributions to the process of the in-medium pion decay $\langle\Omega|A_\mu^j|\pi^i\rangle$ in fig. 9.1. Diagrams 1–3 were already considered in ref. [MOW02]. Regarding diagram 4 one has to take into account the same comments as previously given in section 8.2 concerning diagrams 2 and 3. The contribution with only the free part of the nucleon propagators vanishes and that with only the density dependent part is taken into account by the diagrams 5 and 6. The remaining

contributions, with one density dependent part for one nucleon propagator and a free one for the other, is suppressed by one order. The reason is because it implies the derivative of Σ_f^π with respect to energy. This already occurred for the diagram 2 of fig. 8.1 in section 8.2. For the diagrams 5 and 6 we find a mutual cancellation. In the same way as we already found that for the case of the isovector contributions to the pion self-energy of diagrams (b) and (d) in fig. 7.1 of section 7.4. Because of this there are no new contributions from the pion wave function renormalization (diagram indicated by π-WFR in fig. 9.1) beyond those already considered in ref. [MOW02]. The driving mechanism for such cancellation has been explained in subsection 8.3.1 for the case of the chiral quark condensate involving the mutual cancellation of Ξ_4 and Ξ_5. Due to suppression and cancellation of new contributions, we find that there are no additional contributions to those already given in [MOW02] eq. (4.24) for the in-medium pion decay.

9.2.1 In-medium pion decay constant

Because of the breaking of covariance due to the presence of the nuclear medium, it is convenient to separate between temporal and spatial couplings of the pions to the axial-vector currents. Our results are

$$\begin{aligned}
\langle\Omega|A_0^3|\pi^0\rangle &= if_\pi q_0\left[1+\frac{\rho_p+\rho_n}{f_\pi^2}\left(c_2+c_3-\frac{g_A^2}{8m_N}\frac{m_\pi^2}{q_0^2}\right)\right]\,,\\
\langle\Omega|A_i^3|\pi^0\rangle &= if_\pi q_i\left[1-\frac{\rho_p+\rho_n}{f_\pi^2}\left(c_2-c_3+\frac{g_A^2}{8m_N}\frac{m_\pi^2}{q_0^2}\right)\right]\,,\\
\langle\Omega|A_0^1-iA_0^2|\pi^+\rangle &= i\sqrt{2}f_\pi q_0\left[1+\frac{\rho_p+\rho_n}{f_\pi^2}\left(c_2+c_3-\frac{g_A^2}{8m_N}\frac{m_\pi^2}{q_0^2}\right)-\frac{\rho_p-\rho_n}{8f_\pi^2 q_0}\left(3+\frac{g_A^2\mathbf{q}^2}{q_0^2}\right)\right]\,,\\
\langle\Omega|A_i^1-iA_i^2|\pi^+\rangle &= i\sqrt{2}f_\pi q_i\left[1-\frac{\rho_p+\rho_n}{f_\pi^2}\left(c_2-c_3+\frac{g_A^2}{8m_N}\frac{m_\pi^2}{q_0^2}\right)+\frac{\rho_p-\rho_n}{8f_\pi^2 q_0}\left(1-4g_A^2-\frac{g_A^2\mathbf{q}^2}{q_0^3}\right)\right]\,,\\
\langle\Omega|A_0^1+iA_0^2|\pi^-\rangle &= i\sqrt{2}f_\pi q_0\left[1+\frac{\rho_p+\rho_n}{f_\pi^2}\left(c_2+c_3-\frac{g_A^2}{8m_N}\frac{m_\pi^2}{q_0^2}\right)+\frac{\rho_p-\rho_n}{8f_\pi^2 q_0}\left(3+\frac{g_A^2\mathbf{q}^2}{q_0^2}\right)\right]\,,\\
\langle\Omega|A_i^1+iA_i^2|\pi^-\rangle &= i\sqrt{2}f_\pi q_i\left[1-\frac{\rho_p+\rho_n}{f_\pi^2}\left(c_2-c_3+\frac{g_A^2}{8m_N}\frac{m_\pi^2}{q_0^2}\right)-\frac{\rho_p-\rho_n}{8f_\pi^2 q_0}\left(1-4g_A^2-\frac{g_A^2\mathbf{q}^2}{q_0^3}\right)\right]\,,
\end{aligned}\tag{9.1}$$

where f_π is the *vacuum* weak pion decay constant. From eq. (9.1) we can read off the temporal, f_t, and spatial, f_s, in-medium decay constants. In the isospin limit ($\bar{m}=0$, $\rho_p=\rho_n$) the weak pion decay coupling for all the pions are equal and given by

$$\begin{aligned}
f_t &= f_\pi\left[1+\frac{\rho_p+\rho_n}{f_\pi^2}\left(c_2+c_3-\frac{g_A^2}{8m_N}\right)\right]\,,\\
f_s &= f_\pi\left[1-\frac{\rho_p+\rho_n}{f_\pi^2}\left(c_2-c_3+\frac{g_A^2}{8m_N}\right)\right]\,.
\end{aligned}\tag{9.2}$$

We also need the in-medium pion mass, which is given by the pole of the pion propagator eq. (7.1). We just take into account all contributions up-to-and-including next-to-leading order, strictly, which

in fact implies the results of the diagrams 1–4 of fig. (7.1). From eq. (7.71) we obtain the relations

$$\begin{aligned}
\tilde{m}^2_{\pi^0} &= m^2_{\pi^0}\left(1+4c_1\frac{\rho_p+\rho_n}{f_\pi^2}\right) - 2\tilde{m}^2_{\pi^0}\frac{\rho_p+\rho_n}{f_\pi^2}\left(c_2+c_3-\frac{g_A^2}{8m_N}\right) + 2c_5\hat{m}^2_\pi\frac{\bar{m}}{\hat{m}}\frac{\rho_p-\rho_n}{f_\pi^2}\ ,\\
\tilde{m}^2_{\pi^+} &= m^2_{\pi^+}\left(1+4c_1\frac{\rho_p+\rho_n}{f_\pi^2}\right) - 2\tilde{m}^2_{\pi^+}\frac{\rho_p+\rho_n}{f_\pi^2}\left(c_2+c_3-\frac{g_A^2}{8m_N}\right) - \tilde{m}_{\pi^+}\frac{\rho_p-\rho_n}{f_\pi^2}\ ,\\
\tilde{m}^2_{\pi^-} &= m^2_{\pi^-}\left(1+4c_1\frac{\rho_p+\rho_n}{f_\pi^2}\right) - 2\tilde{m}^2_{\pi^-}\frac{\rho_p+\rho_n}{f_\pi^2}\left(c_2+c_3-\frac{g_A^2}{8m_N}\right) - \tilde{m}_{\pi^-}\frac{\rho_p-\rho_n}{f_\pi^2}\ .
\end{aligned} \tag{9.3}$$

Several ways of solving these equations are given in subsection 7.5.5. Solving eqs. (9.3) in the isospin limit perturbatively by setting $\tilde{m}_\pi = m_\pi$ in all terms with density dependence we obtain the common expression for all pion masses

$$\tilde{m}^2_\pi = m^2_\pi\left[1+2\frac{\rho_p+\rho_n}{f_\pi^2}\left(2c_1-c_2-c_3+\frac{g_A^2}{8m_N}\right)\right]\ . \tag{9.4}$$

9.2.2 The Gell-Mann–Oakes–Renner relation

Together with the relation for the chiral quark condensate, eq. (8.29), we can write down the Gell-Mann–Oakes–Renner (GMOR) relation for *symmetric* nuclear matter [MOW02]

$$\tilde{m}^2_\pi f_t^2 = -\hat{m}\langle\Omega|\bar{u}u+\bar{d}d|\Omega\rangle + \delta_0\ , \tag{9.5}$$

where $\tilde{m}_\pi$ is the in-medium pion mass and δ_0 corresponds to corrections that start at $\mathcal{O}(p^4)$ in vacuum χPT, which implies that the GMOR relation is only exact at lowest order. The stability of the GMOR relation under the in-medium corrections as well as the fact that it is the temporal coupling f_t, and not the spatial one f_s, the one involved in the GMOR relation has previously been reported in [TW95, WT95, KW96, KW97] within the mean field approximation, and in [Ki02] in the framework of QCD sum rules. Expanding the in-medium contributions to the pion mass, the pion decay constant and the chiral quark condensate explicitly we find

$$m^2_\pi f^2_\pi\left(1+\delta^{(2)}_{m^2_\pi}+\delta^{(3)}_{m^2_\pi}+\ldots\right)\left(1+2\delta^{(2)}_{f_\pi}+2\delta^{(3)}_{f_\pi}+\ldots\right) = -\hat{m}\langle 0|\bar{u}u+\bar{d}d|0\rangle\left(1+\delta^{(3)}_\Xi+\delta^{(4)}_\Xi+\ldots\right)+\delta_0\ , \tag{9.6}$$

where $\delta^{(i)}_{m^2_\pi}$, $\delta^{(i)}_{f_\pi}$ and $\delta^{(i)}_\Xi$ denote the in-medium corrections of the pion mass squared, pion decay constant and chiral quark condensate, respectively, and the superscript indicates the corresponding chiral order. The relative $\mathcal{O}(p^2)$ corrections on the left-hand-side of eq. (9.6), $\delta^{(2)}_{m^2_\pi}$ and $\delta^{(2)}_{f_\pi}$, only appear for the charged pions and correspond to isospin breaking due to different proton and neutron densities in asymmetric nuclear matter [MOW02]. These in-medium corrections to the pion mass and the pion decay constant vanish for symmetric nuclear matter. They also cancel if we take the average of the pion masses or accordingly the pion decay constant. For these reasons, we can neglect the relative corrections at $\mathcal{O}(p^2)$ for the consideration of the GMOR relation.

As previously discussed, up to next-to-leading order the leading nucleon-nucleon contributions to the pion decay, and therefore to the decay constant, cancel in $\delta^{(3)}_{f_\pi}$. The same observation was already made for the pion self-energy in subsection 7.2.2 and, therefore, contributions due to nucleon-nucleon interactions are absent in $\delta^{(3)}_{m^2_\pi}$ as well. Regarding the right hand side of eq. (9.6), $\delta^{(3)}_\Xi$ has been calculated in section 8.2 and corresponds to Ξ_1, eq. (8.4). In contrast to $\tilde{m}^2_\pi$ and f_t there is a non-vanishing next-to-leading order in-medium correction to the quark condensate

due to the in-medium nucleon-nucleon interactions and given by Ξ_6, eq. (8.24). Thus, $\delta_\Xi^{(4)} \neq 0$. However, this is $\mathcal{O}(p^6)$, one order above the contributions discussed for the left hand side of eq. (9.6). Whence, it would be needed a full next-to-next-to-leading order calculation for f_t and $\tilde{m}_\pi^2$ in order to ascertain the stability of the in-medium corrections to the GMOR relation up to $\mathcal{O}(p^6)$, which is beyond the scope of the present work. On the other hand, as shown in [MOW02], the pion-nucleon dynamics that gives rise to $\delta_{m_\pi^2}^{(3)}$, $\delta_{f_\pi}^{(3)}$ and $\delta_\Xi^{(3)}$ for symmetric nuclear matter does not violate the in-medium Gell-Mann–Oakes–Renner relation, eq. (9.6). Then, we conclude that the in-medium corrections, including nucleon-nucleon interactions, do not spoil the validity of the Gell-Mann–Oakes–Renner relation up-to-and-including next-to-leading order or $\mathcal{O}(p^5)$ in our in-medium power counting scheme.

9.3 Conclusions and outlook

We have addressed the calculations of the pion decay constant and tested the validity of the Gell-Mann–Oakes–Renner relation up to next-to-leading order in our chiral counting. The nucleon-nucleon contributions for the in-medium corrections vanish at next-to-leading order, not only for the calculation of the pion mass but also for the in-medium pion decay constant. This implies that the findings of [MOW02], that the in-medium contributions at next-to-leading order do not spoil the Gell-Mann–Oakes–Renner relation, are still valid within our Effektive Field Theory.

In order to test eq. (9.6) up to next-to-leading order in the chiral quark condensate, $\delta_\Xi^{(4)}$, a task for the future is, to calculate the contributions to the pion self-energy and the pion decay at next-to-next-to-leading order, $\mathcal{O}(p^6)$. A complete next-to-next-to-leading order calculation of the pion self-energy and decay, employing the present techniques, is an interesting task. For the self-energy for instance, it will merge important pion-nucleon mechanisms like e.g. the Ericson-Ericson-Pauli rescattering effect [EE66], with novel multi-nucleon contributions.

Chapter 10

Strangeness contributions in the nuclear medium

In this chapter we discuss the inclusion of the strange quark into in-medium chiral effective theory. We will extend the framework to three-flavor chiral dynamics by introducing the $SU(3)_f$ chiral Lagrangian. Also we will present the results for the chiral quark condensate for three quark flavors and the self-energy of the ground state meson octet.

10.1 Introduction

In order to obtain predictions on the strangeness content of nuclear matter and on strange particles interacting with nuclear matter, one is able to make use of the straightforward extension of Chiral Perturbation Theory to three flavors [GL85]. In this approach the strange quark mass is also regarded as an $\mathcal{O}(p)$ quantity. Convergence is expected to be slow, since the strange quark mass over the scale parameterized in terms of the kaon mass as M_K/Λ_χ is not a very small expansion parameters. Nonetheless, an expansion in this parameter is still possible.

One interesting topic is the exploration of possible kaon condensation in nuclear matter. The basic idea behind meson condensation in matter is that due to attractive interactions, the dispersion curve $\omega(\mathbf{k})$ of a meson lies lower in matter than in the vacuum. If for some value of the momentum, $\mathbf{k}$, the energy ω dips down to the level of the meson's chemical potential μ, then the meson field develops a finite expectation value. If the interactions of a meson do not involve derivatives, the condensation already occurs at $\mathbf{k} = 0$. It was found that this happens in case of the kaons [KN86, KN88] for densities between two and three times the nuclear matter saturation density, depending on the model. Pion condensation, on the other hand, is for symmetric nuclear matter driven by derivative interactions (P-wave) and is thus supposed to occur at non-zero momentum. The fact that a kaon condensate is energetically favoured, implies that the usual barrier of requiring simultaneous multiple weak interactions to build up a critical value of strangeness is no longer valid in nuclear matter. This would provide a pathway to three-flavor ("strange") quark matter. Another interesting subject is, of course, the behavior towards chiral symmetry restauration in nuclear and strange matter in the three-flavour sector.

Data from hyperon-nucleon and hyperon-hyperon scattering are not yet as reliable as in the nucleon-

nucleon sector. Therefore it is currently not in reach to perform thorough calculations in the nuclear medium employing full baryon-baryon interactions, so we will restrict the calculations of strangeness contributions to meson-baryon chiral dynamics.

After this introduction we will constitute the three-flavor chiral Lagrangian, that we are going to employ, in section 10.2. In section 10.3 we will discuss the chiral quark condensate in three-flavor space and in section 10.4 the self-energy of the ground state meson octet. Conclusion and outlook will be given in section 10.5.

10.2 Flavor $SU(3)$ Chiral Perturbation Theory

The derivation of the chiral Lagrangian in chapter 2 still holds for the three-flavor case. Symmetries and their breaking follow the same mechanisms as in the $SU(2)_I$ case with a simple exchange of the underlying symmetry group. One major difference is, while the nucleon douplet field in $SU(2)_I$ is represented in the fundamental representation of the group, the baryon octet field is represented by the adjoint representation of $SU(3)_f$. An implication of this fact is a fast growing number of Lagrangian terms each one of them accompanied by an independent low-energy constant.

10.2.1 Flavor $SU(3)$ Lagrangian

The effective Goldstone pseudo-boson chiral Lagrangian in $SU(3)_f$ to leading order is given correspondingly to the two-flavor case by

$$\mathcal{L}^{(2)}_{\phi\phi} \doteq \frac{f_\phi^2}{4}\langle u_\mu u^\mu + \chi_+\rangle \ , \tag{10.1}$$

where the chiral vielbein u^μ, that comprises the pion fields, was defined in eq. (2.41) and χ_+, which contains scalar and pseudoscalar sources, in eq. (2.44). The common meson decay constant f_ϕ is taken in the flavor-symmetry limit and we choose to fix it to $f_\phi = f_\pi = 92.4$ MeV. We employ the $SU(3)_f$ meson field ϕ, that reads

$$\phi = \phi^a\lambda^a = \sqrt{2}\begin{pmatrix} \frac{1}{\sqrt{2}}\pi^0 + \frac{1}{\sqrt{6}}\eta & \pi^+ & K^+ \\ \pi^- & -\frac{1}{\sqrt{2}}\pi^0 + \frac{1}{\sqrt{6}}\eta & K^0 \\ K^- & \bar{K}^0 & -\frac{2}{\sqrt{6}}\eta \end{pmatrix} \ , \tag{10.2}$$

here we inserted the Gell–Mann matrices λ^a as generators T^a. During this chapter we will denote the meson masses by a capital M_ϕ so that it is easier to distinguish them from quark or baryon masses.

The effective baryon-meson chiral Lagrangian is a bit more involved. We will give the Lagrangian in its covariant form, while we stick to the notation and definitions of [FM06]. The amplitudes we will calculate are obtained using those covariant terms and performing a $1/m$ expansion afterwards. With the baryon octet field

$$\Psi = \begin{pmatrix} \frac{1}{\sqrt{2}}\Sigma^0 + \frac{1}{\sqrt{6}}\Lambda & \Sigma^+ & p \\ \Sigma^- & -\frac{1}{\sqrt{2}}\Sigma^0 + \frac{1}{\sqrt{6}}\Lambda & n \\ \Xi^- & \Xi^0 & -\frac{2}{\sqrt{6}}\Lambda \end{pmatrix} \ , \tag{10.3}$$

the meson-baryon Lagrangian at leading order reads

$$\mathcal{L}^{(1)}_{\phi\Psi} = \langle\bar{\Psi}(i\gamma^\mu[D_\mu,\Psi] - m\Psi)\rangle + \frac{D/F}{2}\langle\bar{\Psi}\gamma^\mu\gamma_5[u_\mu,\Psi]_\pm\rangle \ , \tag{10.4}$$

where D and F are the axial-vector coupling constants. Their numerical values can be extracted from hyperon decays, and obey the $SU(2)_I$ constraint for the axial vector coupling $g_A = D + F = 1.26$, taken from neutron β-decay. They are determined to be $D = 0.804$ and $F = 0.463$. The full baryon-meson Lagrangian at second order reads

$$\begin{aligned}
\mathcal{L}^{(2)}_{\phi\Psi} \ = \ & b_{D/F}\langle\bar{\Psi}[\chi_+,\Psi]_\pm\rangle + b_0\langle\bar{\Psi}\Psi\rangle\langle\chi_+\rangle \\
& + b_{1/2}\langle\bar{\Psi}[u_\mu,[u^\mu,\Psi]_\mp]\rangle + b_3\langle\bar{\Psi}\{u_\mu,\{u^\mu,\Psi\}\}\rangle + b_4\langle\bar{\Psi}\Psi\rangle\langle u_\mu u^\mu\rangle \\
& + i\,b_{5/6}\langle\bar{\Psi}\sigma^{\mu\nu}[[u_\mu,u_\nu],\Psi]_\mp\rangle + i\,b_7\langle\bar{\Psi}u_\mu\rangle\sigma^{\mu\nu}\langle u_\nu\Psi\rangle \\
& + \frac{ib_{8/9}}{2\bar{m}}\Big(\langle\bar{\Psi}\gamma^\mu[u_\mu,[u_\nu,[D^\nu,\Psi]]_\mp]\rangle + \langle\bar{\Psi}\gamma^\mu[D^\nu,[u_\nu,[u_\mu,\Psi]]_\mp]\rangle\Big) \\
& + \frac{ib_{10}}{2\bar{m}}\Big(\langle\bar{\Psi}\gamma^\mu\{u_\mu,\{u_\nu,[D^\nu,\Psi]\}\}\rangle + \langle\bar{\Psi}\gamma^\mu[D^\nu,\{u_\nu,\{u_\mu,\Psi\}\}]\rangle\Big) \\
& + \frac{ib_{11}}{2\bar{m}}\Big(2\langle\bar{\Psi}\gamma^\mu[D^\nu,\Psi]\rangle\langle u_\mu u_\nu\rangle + \langle\bar{\Psi}\gamma^\mu\Psi\rangle\langle[D^\nu,u_\mu]u_\nu\rangle + \langle\bar{\Psi}\gamma^\mu\Psi\rangle\langle u_\mu[D^\nu,u_\nu]\rangle\Big) \\
& + b_{12/13}\langle\bar{\Psi}\sigma^{\mu\nu}[F^+_{\mu\nu},\Psi]_\mp\rangle \ .
\end{aligned} \tag{10.5}$$

The constants $b_{0/D/F}$ correspond to the $SU(2)_I$ constants c_1 and c_5. b_D and b_F yield the leading $SU(3)_f$ breaking effects in the baryon masses. b_0, which gives a common quark mass shift of the octet mass, cannot be disentangled without further information, but it is generally sufficient to absorb this term into the octet mass. Now we show the mapping of the $SU(2)_I$ low-energy constants c_i to the $SU(3)_f$ low-energy constants b_i,

$$\begin{aligned}
g_A &\to D + F \\
c_1 &\to (2b_0 + b_D + b_F)/2 \\
c_2 &\to b_8 + b_9 + b_{10} + 2b_{11} \\
c_3 &\to b_1 + b_2 + b_3 + 2b_4 \\
c_4 &\to 4(b_5 + b_6) \\
c_5 &\to b_D + b_F \\
c_6 &\to 8\mathring{m}(b_{12} + b_{13}) \\
c_7 &\to -16/3\mathring{m}b_{13} \ .
\end{aligned} \tag{10.6}$$

This corresponds to a projection of the $SU(3)_f$ group onto its isospin subgroup. A more thorough matching where the loop effects incorporating the strange quantum number are buried into the $SU(2)_I$ low-energy couplings is performed in [MBKM09]. We will refer to groups of $SU(3)_f$ couplings as the *c_i-type couplings*, by which we mean the $SU(3)_f$ couplings which share the same physics as the corresponding $SU(2)_I$ coupling constants c_i. As numerical values we take $b_0 = -0.61$ GeV^{-1}, $b_D = 0.08$ GeV^{-1}, $b_F = -0.32$ GeV^{-1}, $b_1 = -0.004$ GeV^{-1}, $b_2 = 0.19$ GeV^{-1}, $b_3 = 0.02$ GeV^{-1}, $b_4 = -0.11$ GeV^{-1}, $b_5 = 0.23$ GeV^{-1}, $b_6 = 0.62$ GeV^{-1} and $b_7 = 0.68$ GeV^{-1} [BM96, KM01]. Those values have to be treated with great care, because they are quite badly known with large uncertainties. For the remaining low-energy constants we give just the $SU(2)_I$ constraint $b_8 + b_9 + b_{10} + 2b_{11} = 3.22$ GeV^{-1}.

10.2.2 Explicit symmetry breaking via quark masses and breaking of flavor symmetry

The scalar source s incorporates the explicit symmetry breaking terms due to non-vanishing quark masses of the lighest three flavors,

$$s = \mathcal{M} + \dots \ , \qquad \mathcal{M} = \begin{pmatrix} m_u & 0 & 0 \\ 0 & m_d & 0 \\ 0 & 0 & m_s \end{pmatrix} \ . \tag{10.7}$$

The transformation law for eq. (2.42) can be motivated by considering the QCD mass term

$$\mathcal{L}_{QCD}^{\mathcal{M}} = -(\bar{q}_R \, \mathcal{M} \, q_L + \bar{q}_L \, \mathcal{M} \, q_R) \ , \tag{10.8}$$

written in terms of left– and right–handed quark fields. The transformation is made such as to leave the Lagrangian (10.8) invariant. Hence, the lowest order mass term in the meson chiral Lagrangian reads

$$\mathcal{L}_{\mathcal{M}}^{(2)} = \frac{f_\phi^2}{4} \langle \chi_+ \rangle \ , \tag{10.9}$$

which, expanded in the meson fields, results in the lowest order hadronic mass formulae for the mesons, eq. (10.10).

The difference between the strange quark mass m_s and the masses of the two lightest quarks m_u and m_d is quite large. Therefore, whenever considering three-flavor χPT one should take flavor symmetry breaking into account. The isospin symmetry can still be regarded as a good symmetry with good conscience, in comparison with the breaking due to the significantly larger strange quark mass. We define the *average light quark mass* $\hat{m} = (m_u + m_d)/2$ and with that the isospin-degenerate meson masses are given by

$$\begin{aligned} M_\pi^2 &= 2B\hat{m} + \mathcal{O}(m_q^2) \ , \\ M_K^2 &= B(\hat{m} + m_s) + \mathcal{O}(m_q^2) \ , \\ M_\eta^2 &= \frac{2}{3} B(\hat{m} + 2m_s) + \mathcal{O}(m_q^2) \ . \end{aligned} \tag{10.10}$$

Obviously, flavor symmetry breaking suspends the degeneracy of the meson and yields an $\mathcal{O}(p^2)$ effect. From eq. (10.10) we can directly derive the Gell-Mann–Okubo relation for mesons

$$M_\pi^2 - 4M_K^2 + 3M_\eta^2 = 0 + \mathcal{O}(m_q^2) \ . \tag{10.11}$$

Taking the quark mass corrections according to eq. (5.7) into account for the baryon masses, we obtain the following shifts

$$\begin{aligned} m_N = \mathring{m} + \Delta m_N &= \mathring{m} - 4\Big[b_D M_K^2 + b_F \big(M_\pi^2 - M_K^2 \big) \Big] \ , \\ m_\Lambda = \mathring{m} + \Delta m_\Lambda &= \mathring{m} - 4 b_D \left[\frac{4}{3} M_K^2 - \frac{1}{3} M_\pi^2 \right] \ , \\ m_\Sigma = \mathring{m} + \Delta m_\Sigma &= \mathring{m} - 4 b_D M_\pi^2 \ , \\ m_\Xi = \mathring{m} + \Delta m_\Xi &= \mathring{m} - 4\Big[b_D M_K^2 + b_F \big(M_K^2 - M_\pi^2 \big) \Big] \ , \end{aligned} \tag{10.12}$$

where $\mathring{m}$ is the *baryon mass in the chiral limit* and the baryon mass shift is also an $\mathcal{O}(p^2)$ effect. We have absorbed the low-energy constant b_0 into the chiral octet mass, since it only leads to the

same shift for all octet baryons. With these expressions one finds the Gell-Mann–Okubo relation for baryons

$$3m_\Lambda + m_\Sigma - 2m_N - 2m_\Xi = 0 + \mathcal{O}(m_q^2) \ . \tag{10.13}$$

The three parameters $\mathring{m}$, $b_{D/F}$ can now be fitted to the physical masses. We take the physical values of the meson octet $M_\pi = 0.138$ GeV, $M_K = 0.496$ GeV and $M_\eta = 0.548$ GeV and the baryon octet $m_N = 0.939$ GeV, $m_\Lambda = 1.116$ GeV, $m_\Sigma = 1.193$ GeV, $m_\Xi = 1.318$ GeV, respectively given as the average of the isospin multiplets. Performing the fit results in $\mathring{m} = 1.197$ GeV, $b_D = 0.066$ GeV^{-1} and $b_F = -0.209$ GeV^{-1}. Plugging these parameters again into eqs. (10.12) we obtain $m_N = 0.942$ GeV, $m_\Lambda = 1.111$ GeV, $m_\Sigma = 1.191$ GeV, $m_\Xi = 1.321$ GeV. We consider this accurate enough to put all baryon masses to their experimental values in numerical evaluations where symmetry breaking occurs. Everywhere else we will put the baryon masses to their average value, the *common baryon octet mass* $m_B = 1.151$ GeV. Notice, that the three fitted parameters are reasonably dependent on the used meson masses. Flavor symmetry breaking starts at next-to-next-to-leading order, while our present investigations are restricted to the next-to-leading order.

10.3 Strangeness contributions to the in-medium chiral quark condensate

In this section we consider the in-medium contribution to the chiral quark condensate, defined in eq. (8.2), including effects due to the strange quark. We consider the diagrams of fig. 7.1. As discussed in detail in chapter 8, the diagram 2 is suppressed by one order, thus we will neglect it in the following discussion. Regarding the diagrams 4 and 5 we refer to the outlook, we will also not consider those contributions here. Since we do not to address hyperon-baryon interactions yet, we do not obtain any new contributions from diagram 6. Still, the contribution Ξ_6 of chapter 8, where the source couples to the exchanged pion, holds in case of the $\bar{u}u$ and $\bar{d}d$ condensates. The pion has no strangeness content at the order we are working so the strange scalar source could only couple to an exchanged strange meson. Diagram 3 needs some extra considerations: we do not work at the physical nucleon mass in the $SU(3)_f$ case, in order to retrace effects from explicit flavor symmetry breaking. Therefore the cancellation mentioned in eq. (8.11) due to the discussion of eq. (5.11) does not happen, and we obtain contributions at next-to-leading order.

In order to keep expressions short we invent the following abbreviations:

$$\begin{aligned}
\hat{c}_1^\pi &= 4(2b_0 + b_D + b_F) \ , \\
\bar{c}_5^\pi &= 4(b_D + b_F) \ , \\
\hat{\gamma}_\pi &= (D+F)^2 \ , \\
\hat{\gamma}_K &= \frac{1}{6}(5D^2 - 6DF + 9F^2) \ , \\
\hat{\gamma}_\eta &= \frac{1}{3}(D-3F)^2 \ , \\
\bar{\gamma}_K &= \frac{1}{6}(D^2 - 6DF - 3F^2) \ .
\end{aligned} \tag{10.14}$$

Additionally we use the *average symmetric nuclear density*, $\hat{\rho} \doteq (\rho_p + \rho_n)/2$ and the *average antisymmetric nuclear density* $\bar{\rho} \doteq (\rho_p - \rho_n)/2$. In the following discussion we set the densities of the hyperonic Fermi-seas to zero. Their contributions were obtained straighforwardly, we just omit

them here to shorten expressions. The in-medium corrections to the chiral quark condensate of $\bar{u}u$ and $\bar{d}d$ read

$$\frac{\langle\Omega|\bar{u}u|\Omega\rangle}{\langle 0|\bar{u}u|0\rangle} = 1+\frac{\hat{\rho}}{f_\phi^2}\left[\hat{c}_1^\pi+\frac{1}{32\pi f_\phi^2}\Big(9\hat{\gamma}_\pi M_\pi+6\hat{\gamma}_K M_K+\hat{\gamma}_\eta M_\eta\Big)\right]+\frac{\bar{\rho}}{f_\phi^2}\left[\bar{c}_5^\pi-\frac{3\bar{\gamma}_K M_K}{16\pi f_\phi^2}\right], \quad (10.15)$$

$$\frac{\langle\Omega|\bar{d}d|\Omega\rangle}{\langle 0|\bar{d}d|0\rangle} = 1+\frac{\hat{\rho}}{f_\phi^2}\left[\hat{c}_1^\pi+\frac{1}{32\pi f_\phi^2}\Big(9\hat{\gamma}_\pi M_\pi+6\hat{\gamma}_K M_K+\hat{\gamma}_\eta M_\eta\Big)\right]-\frac{\bar{\rho}}{f_\phi^2}\left[\bar{c}_5^\pi-\frac{3\bar{\gamma}_K M_K}{16\pi f_\phi^2}\right]. \quad (10.16)$$

For definitions regarding the chiral quark condensate see chapter 8. The isospin symmetric c_1- and antisymmetric c_5-type contributions stem from diagram 1 and were already considered in chapter 8. The next-to-leading order terms proportional to the meson masses arise from diagram 3. The contributions to the $\bar{s}s$ condensate read

$$\frac{\langle\Omega|\bar{s}s|\Omega\rangle}{\langle 0|\bar{s}s|0\rangle} = 1+\frac{\hat{\rho}}{f_\phi^2}\left[8(b_0+b_D-b_F)+\frac{1}{8\pi f_\phi^2}\Big(3\hat{\gamma}_K M_K+\hat{\gamma}_\eta M_\eta\Big)\right], \quad (10.17)$$

which are only symmetric in the density. The sum of all three contributions gives the singlet chiral quark condensate

$$\frac{\langle\Omega|\bar{u}u+\bar{d}d+\bar{s}s|\Omega\rangle}{\langle 0|\bar{u}u+\bar{d}d+\bar{s}s|0\rangle} = 1+\frac{\hat{\rho}}{f_\phi^2}\left[\frac{8}{3}(3b_0+2b_F)+\frac{1}{16\pi f_\phi^2}\Big(3\hat{\gamma}_\pi M_\pi+4\hat{\gamma}_K M_K+\hat{\gamma}_\eta M_\eta\Big)\right]. \quad (10.18)$$

We also state the flavor symmetry breaking terms due to nuclear matter

$$\frac{\langle\Omega|\bar{u}u-\bar{d}d|\Omega\rangle}{\langle 0|\bar{q}q|0\rangle} = \frac{\bar{\rho}}{f_\phi^2}\left[\bar{c}_5^\pi-\frac{3\bar{\gamma}_K M_K}{16\pi f_\phi^2}\right], \quad (10.19)$$

$$\frac{\langle\Omega|\bar{u}u+\bar{d}d-2\bar{s}s|\Omega\rangle}{\langle 0|\bar{q}q|0\rangle} = \frac{\hat{\rho}}{f_\phi^2}\left[\frac{4}{3}(3b_F-b_D)+\frac{1}{32\pi f_\phi^2}\Big(3\hat{\gamma}_\pi M_\pi-2\hat{\gamma}_K M_K-\hat{\gamma}_\eta M_\eta\Big)\right]. \quad (10.20)$$

Interestingly, while the 3$^{\text{rd}}$ component ($SU(2)_I$ projection) of the octet chiral quark condensate is purely antisymmetric in the densities, the 8$^{\text{th}}$ component is purely symmetric.

All contributions are linear in the density. Above we stated the leading contributions stemming from diagram 2, which are linear in the meson masses. However those contributions are cancelled in the case of $\bar{u}u$ and $\bar{d}d$ by the next-to-leading order contributions steming from the baryon sigma terms [FM04, FMS05]. This would leave us only with the contributions proportional to c_1- and c_5-type couplings.

10.4 Strangeness contributions to the in-medium meson self-energy

Now we consider the in-medium meson self-energy Π^ϕ, defined in eq. (7.1), of the ground state octet explicitly taking into account effects from the strange quark flavor. We consider the diagrams of fig. 7.1. As discussed in detail in chapter 7, the diagrams 5 and 6 and the recoil correction parts of the diagrams 8 and 10 are next-to-next-to-leading order, thus we will neglect them in the following discussion. Regarding the diagrams 7 and 9 and the leading contributions of the diagrams 8 and 10 we refer to the outlook, we will also not consider those contributions here. The remaining diagrams evaluated here are 1–4.

In addition to the abbreviations defined in eq. (10.14) we need the following abbreviations:

$$\begin{aligned}
\hat{c}_2^\pi &= 4(b_8 + b_9 + b_{10} + 2b_{11}) \ , \\
\hat{c}_3^\pi &= 4(b_1 + b_2 + b_3 + 2b_4) \ , \\
\hat{c}_1^K &= 4b_0 + 3b_D - b_F \ , \\
\hat{c}_2^K &= 2(3b_8 - b_9 - b_{10} + 4b_{11}) \ , \\
\hat{c}_3^K &= 2(3b_1 - b_2 + 3b_3 + 4b_4) \ , \\
\bar{c}_2^K &= 2(b_8 + b_9 + b_{10}) \ , \\
\bar{c}_3^K &= 2(b_1 + b_2 + b_3) \ , \\
\bar{c}_5^K &= b_D + b_F \ , \\
\hat{c}_2^\eta &= 4(3b_8 - b_9 - b_{10} + 2b_{11}) \ , \\
\hat{c}_3^\eta &= \frac{4}{3}(9b_1 - 3b_2 + b_3 + 6b_4) \ , \\
\bar{c}_5^\eta &= \frac{4}{3}(b_D + b_F) \ , \\
\bar{M}_\phi^2 &= M_\phi^2 \frac{\bar{m}}{\hat{m}} \ .
\end{aligned} \tag{10.21}$$

With those, we are able to write the in-medium self-energies of the ground state meson octet in compact form. In order to keep expressions short we give only the contributions with nucleonic Fermi seas. Contributions with hyperonic Fermi seas are obtained straighforwardly. The in-medium contributions to the self-energies of the pion triplet read

$$\Pi^{\pi^0} = \frac{\hat{\rho}}{f_\phi^2}\left[q_0^2\Big(\hat{c}_2^\pi + \hat{c}_3^\pi - \frac{\hat{\gamma}_\pi}{2m_B}\Big) - \mathbf{q}^2\Big(\hat{c}_3^\pi - \frac{\hat{\gamma}_\pi}{m_B}\Big) - \frac{\mathbf{q}^4}{q_0^2}\frac{\hat{\gamma}_\pi}{2m_B} - \hat{c}_1^\pi M_\pi^2\right] - \frac{\bar{\rho}}{f_\phi^2}\bar{c}_5^\pi \bar{M}_\pi^2 \ , \tag{10.22}$$

$$\Pi^{\pi^+} = \frac{\hat{\rho}}{f_\phi^2}\left[q_0^2\Big(\hat{c}_2^\pi + \hat{c}_3^\pi - \frac{\hat{\gamma}_\pi}{2m_B}\Big) - \mathbf{q}^2\Big(\hat{c}_3^\pi - \frac{\hat{\gamma}_\pi}{m_B}\Big) - \frac{\mathbf{q}^4}{q_0^2}\frac{\hat{\gamma}_\pi}{2m_B} - \hat{c}_1^\pi M_\pi^2\right] - \frac{\bar{\rho}}{f_\phi^2}\left[q_0 - \frac{\mathbf{q}^2}{q_0}\hat{\gamma}_\pi\right] \ , \tag{10.23}$$

$$\Pi^{\pi^-} = \frac{\hat{\rho}}{f_\phi^2}\left[q_0^2\Big(\hat{c}_2^\pi + \hat{c}_3^\pi - \frac{\hat{\gamma}_\pi}{2m_B}\Big) - \mathbf{q}^2\Big(\hat{c}_3^\pi - \frac{\hat{\gamma}_\pi}{m_B}\Big) - \frac{\mathbf{q}^4}{q_0^2}\frac{\hat{\gamma}_\pi}{2m_B} - \hat{c}_1^\pi M_\pi^2\right] + \frac{\bar{\rho}}{f_\phi^2}\left[q_0 - \frac{\mathbf{q}^2}{q_0}\hat{\gamma}_\pi\right] \ . \tag{10.24}$$

Compared with the $SU(2)_I$ calculations [MOW02], there are no new contributions to the pion self-energies for $\rho_{hyperon} = 0$. We find a sizeable isovector contribution linear in the energy q^0 for anti-symmetric nuclear matter. For the contribution to the in-medium self-energy of the eta singlet the expressions look quite similar

$$\begin{aligned}
\Pi^\eta = \frac{\hat{\rho}}{f_\phi^2}\Bigg[q_0^2\Big(\hat{c}_2^\eta + \hat{c}_3^\eta - \frac{\hat{\gamma}_\eta}{2m_B}\Big) - \mathbf{q}^2\Big(\hat{c}_3^\eta - \frac{\hat{\gamma}_\eta}{m_B}\Big) - \frac{\mathbf{q}^4}{q_0^2}\frac{\hat{\gamma}_\eta}{2m_B} + \frac{1}{3}\Big(4(2b_0 + 3b_D - 5b_F)M_\pi^2 \\
- 32(b_0 + b_D - b_F)M_K^2\Big)\Bigg] - \frac{\bar{\rho}}{f_\phi^2}\bar{c}_5^\eta \bar{M}_\pi^2 \ .
\end{aligned} \tag{10.25}$$

The in-medium contributions to the self-energies of the kaon and anti-kaon douplets read

$$\begin{aligned}
\Pi^{\bar{K}^0} = \frac{\hat{\rho}}{f_\phi^2}\left[+\frac{3q_0}{2} - \frac{\mathbf{q}^2}{q_0}\hat{\gamma}_K + q_0^2\Big(\hat{c}_2^K + \hat{c}_3^K - \frac{\hat{\gamma}_K}{2m_B}\Big) - \mathbf{q}^2\Big(\hat{c}_3^K - \frac{\hat{\gamma}_K}{m_B}\Big) - \frac{\mathbf{q}^4}{q_0^2}\frac{\hat{\gamma}_K}{2m_B} - \hat{c}_1^K(2M_K^2 - \bar{M}_\pi^2)\right] \\
+ \frac{\bar{\rho}}{f_\phi^2}\left[-\frac{q_0}{2} - \frac{\mathbf{q}^2}{q_0}\bar{\gamma}_K - q_0^2\Big(\bar{c}_2^K + \bar{c}_3^K + \frac{\bar{\gamma}_K}{2m_B}\Big) + \mathbf{q}^2\Big(\bar{c}_3^K + \frac{\bar{\gamma}_K}{m_B}\Big) - \frac{\mathbf{q}^4}{q_0^2}\frac{\bar{\gamma}_K}{2m_B} + \bar{c}_5^K(2M_K^2 - \bar{M}_\pi^2)\right] \ ,
\end{aligned} \tag{10.26}$$

$$\Pi^{K^-} = \frac{\hat{\rho}}{f_\phi^2}\left[+\frac{3q_0}{2} - \frac{\mathbf{q}^2}{q_0}\hat{\gamma}_K + q_0^2\Big(\hat{c}_2^K + \hat{c}_3^K - \frac{\hat{\gamma}_K}{2m_B}\Big) - \mathbf{q}^2\Big(\hat{c}_3^K - \frac{\hat{\gamma}_K}{m_B}\Big) - \frac{\mathbf{q}^4}{q_0^2}\frac{\hat{\gamma}_K}{2m_B} - \hat{c}_1^K(2M_K^2 + \bar{M}_\pi^2)\right] + \frac{\bar{\rho}}{f_\phi^2}\left[+\frac{q_0}{2} + \frac{\mathbf{q}^2}{q_0}\bar{\gamma}_K + q_0^2\Big(\bar{c}_2^K + \bar{c}_3^K + \frac{\bar{\gamma}_K}{2m_B}\Big) - \mathbf{q}^2\Big(\bar{c}_3^K + \frac{\bar{\gamma}_K}{m_B}\Big) + \frac{\mathbf{q}^4}{q_0^2}\frac{\bar{\gamma}_K}{2m_B} - \bar{c}_5^K(2M_K^2 + \bar{M}_\pi^2)\right], \tag{10.27}$$

$$\Pi^{K^+} = \frac{\hat{\rho}}{f_\phi^2}\left[-\frac{3q_0}{2} + \frac{\mathbf{q}^2}{q_0}\hat{\gamma}_K + q_0^2\Big(\hat{c}_2^K + \hat{c}_3^K - \frac{\hat{\gamma}_K}{2m_B}\Big) - \mathbf{q}^2\Big(\hat{c}_3^K - \frac{\hat{\gamma}_K}{m_B}\Big) - \frac{\mathbf{q}^4}{q_0^2}\frac{\hat{\gamma}_K}{2m_B} - \hat{c}_1^K(2M_K^2 + \bar{M}_\pi^2)\right] + \frac{\bar{\rho}}{f_\phi^2}\left[-\frac{q_0}{2} - \frac{\mathbf{q}^2}{q_0}\bar{\gamma}_K + q_0^2\Big(\bar{c}_2^K + \bar{c}_3^K + \frac{\bar{\gamma}_K}{2m_B}\Big) - \mathbf{q}^2\Big(\bar{c}_3^K + \frac{\bar{\gamma}_K}{m_B}\Big) + \frac{\mathbf{q}^4}{q_0^2}\frac{\bar{\gamma}_K}{2m_B} - \bar{c}_5^K(2M_K^2 + \bar{M}_\pi^2)\right], \tag{10.28}$$

$$\Pi^{K^0} = \frac{\hat{\rho}}{f_\phi^2}\left[-\frac{3q_0}{2} + \frac{\mathbf{q}^2}{q_0}\hat{\gamma}_K + q_0^2\Big(\hat{c}_2^K + \hat{c}_3^K - \frac{\hat{\gamma}_K}{2m_B}\Big) - \mathbf{q}^2\Big(\hat{c}_3^K - \frac{\hat{\gamma}_K}{m_B}\Big) - \frac{\mathbf{q}^4}{q_0^2}\frac{\hat{\gamma}_K}{2m_B} - \hat{c}_1^K(2M_K^2 - \bar{M}_\pi^2)\right] + \frac{\bar{\rho}}{f_\phi^2}\left[+\frac{q_0}{2} + \frac{\mathbf{q}^2}{q_0}\bar{\gamma}_K - q_0^2\Big(\bar{c}_2^K + \bar{c}_3^K + \frac{\bar{\gamma}_K}{2m_B}\Big) + \mathbf{q}^2\Big(\bar{c}_3^K + \frac{\bar{\gamma}_K}{m_B}\Big) - \frac{\mathbf{q}^4}{q_0^2}\frac{\bar{\gamma}_K}{2m_B} + \bar{c}_5^K(2M_K^2 - \bar{M}_\pi^2)\right]. \tag{10.29}$$

We find sizeable corrections linear in the energy q^0 for both symmetric and anti-symmetric nuclear matter. This agrees with [KN86, KN88] in the sense that there are considerable S-wave corrections to the kaon masses. Setting $\mathbf{q} = 0$ and ignoring correction of $\mathcal{O}(p^2)$ we can analyze qualitatively the kaons' mass shifts in nuclear matter, due to those leading corrections. For symmetric nuclear matter we find a decrease of the strange douplet ($\bar{K}^0$,K^-) mass and an increase of the anti-strange douplet (K^+,K^0) mass. For the anti-symmetric part of nuclear matter with $\rho_n > \rho_p$ we find a decrease of the $\bar{K}^0$ and K^+ masses and an increase of the K^- and K^0 masses. However, higher orders are expected to be sizeable and should be studied carefully, especially the role of the $\Lambda(1405)$ in this process should be investigated (see outlook).

10.5 Conclusions and outlook

We have accessed the realm of strangeness contributions for nuclear matter properties. We have given the contributions for the in-medium chiral quark condensate and the ground state meson octet according to the framework of [MOW02]. Yet, there still is a lot of work to accomplish:

- Flavor symmetry breaking effects occur at next-to-next-to-leading order and are quite sizeable (see e.g. [La07, LKM07]). A systematic calculation up to that order has to take those contributions into account.

- Hyperon-baryon interactions in the vacuum are still under development. Provided that there is feasible input from hyperon-baryon scattering available, the impact of in-medium corrections from those interactions should be investigated. As discussed in detail in chapters 7 and 8 for the case of $SU(2)_I$, the contributions to the in-medium pion self-energy Π_7 & Π_9, the isospin-vector parts Π_8^{iv} & Π_{10}^{iv} and the contributions to the in-medium chiral quark condensate Ξ_4 & Ξ_5 cancel in pairs. This is a particularity of the underlying group structure. A proof of the cancellation in three-flavor space is still owing. In particular it would be interesting to investigate the implication of the strange quark on the Hellmann-Feynman theorem.

- The calculation of the in-medium meson self-energy corresponds to meson-baryon scattering, where instead of one scattering baryon there exists a whole sea of baryons. Phase space suggests the inclusion of resonances such as the $\Lambda(1405)$ which is not far from the heaviest ground state hyperon $m_\Xi = 1321$ MeV. The $\Lambda(1405)$ is today regarded as an overlap of actually two nearby resonances [OR98, OM01, Ji03], which correspond to one dynamically generated octet and one dynamically generated singlet. Those can be described by meson-baryon rescattering, employing a chiral unitary approach similar to the one we have employed for nucleon-nucleon scattering. The contribution to the calculation of the meson self-energy from such dynamically generated resonances is left for future investigations.

Summary and outlook

Throughout this work we have demonstrated theoretical tools that allow for a model-independent analysis of and in nuclear matter. The theory provides a common ground for different applications to obtain the properties of nuclear matter and of particles in the nuclear medium. In the end of each chapter, we have summarized the various results, such that we will only sketch the main points of our findings here.

- We have developed a novel power counting scheme for an Effective Field Theory in the nuclear medium that combines short- and long-range multi-nucleon interactions. For determining the set of diagrams to be calculated for a process in the nuclear medium we obtained the final formula

$$\nu = 4 - E_\pi + \sum_{i=1}^{V_\pi}(\ell_i + n_i - 4) + \sum_{i=1}^{V_B}(d_i + v_i + w_i - 2) + V_\rho \ . \tag{3.23}$$

  Here, E_π is the total number of external pion lines and V_π, V_B and V_ρ are the meson-meson, meson-baryon and in-medium generalized vertices, in this order. In simple terms, an in-medium generalized vertex corresponds to a closed nucleon loop that could contain an arbitrary number of bilinear baryon vertices. In the first sum of the previous equation the symbols ℓ_i and n_i are the chiral order and number of pionic lines of the ith purely pionic vertex, respectively. In the sum over the bilinear baryon vertices, d_i is the chiral dimension of the i^{th} baryon vertex, v_i is the total number of mesons lines attached to it (including both pion and heavy meson lines) while w_i is the number of the heavy mesons only. The heavy meson lines correspond to auxiliary fields responsible for the local multi-nucleon interactions when taking their masses to infinity [Bo07]. Eq. (3.23) counts every nucleon propagator as $\mathcal{O}(p^{-2})$ instead of $\mathcal{O}(p^{-1})$, as suggested by the standard counting of Baryon χPT [GSS88]. In this way, the infrared enhancements associated with the large nucleon mass are taken into account from the onset. Despite baryon propagators are counted as $\mathcal{O}(p^{-2})$ it is important to stress that eq. (3.23) is bounded from below. According to eq. (3.23) the number of lines in a diagram can be augmented without increasing the chiral power by adding i) pionic lines attached to lowest order pionic vertices, $\ell_i = n_i = 2$, ii) pionic lines attached to lowest order baryon vertices, $d_i = v_i = 1$ and iii) heavy mesonic lines attached to lowest order baryon vertices, $d_i = 0$, $w_i = 1$. In this way, resummations of infinite strings of diagrams are required, leading to non-perturbative physics. As a major difference between this counting and the Weinberg one [We90, We91], the former applies directly to the physical amplitudes while the latter does only to the potential. It is also important to stress that ν in eq. (3.23) is actually just a lower bound for the chiral power of a diagram, μ, with $\mu \geq \nu$. The chiral order might be higher than ν because nucleon propagators, always counted as $\mathcal{O}(p^{-2})$ in eq. (3.23), could follow the standard counting $\mathcal{O}(p^{-1})$ in some cases.

- We have developed the required non-perturbative techniques that allow us to perform necessary resummations both in scattering as well as in production processes. These non-perturbative methods are based on Unitary χPT, which are adapted now to the nuclear medium by implementing the power counting of eq. (3.23). Following the novel power counting, we have determined the vacuum nucleon-nucleon scattering at leading order and next-to-leading order. For nuclear matter the leading order nucleon-nucleon scattering amplitudes have also been obtained. The infrared enhancement of the two-nucleon reducible loops have made necessary to resum the right-hand cut. This is accomplished by a once-subtracted dispersion relation of the inverse of a partial wave giving rise to the master equation of UχPT,

$$T^{i_3}_{JI}(\ell,\bar{\ell},S) = \left[I + N^{i_3}_{JI}(\ell,\bar{\ell},S)\cdot L^{i_3}_{10}\right]^{-1}\cdot N^{i_3}_{JI}(\ell,\bar{\ell},S)\ . \tag{4.31}$$

  It results as an approximate solution to the dispersive treatment of nucleon-nucleon scattering in a chiral expansion of the imaginary part of the scattering amplitudes along the left-hand cut, taking advantage of the suppression of the two-nucleon unitarity loops along this cut. The important function

$$\begin{aligned} g(A) &= g(D) - \frac{m(A-D)}{4\pi^2}\int_0^\infty dk^2 \frac{k}{(k^2-A-i\epsilon)(k^2-D-i\epsilon)} \\ &= g_0 - i\frac{m\sqrt{A}}{4\pi}\ , \quad D\leq 0\ , \end{aligned} \tag{4.7}$$

  corresponding to the free part of $L^{i_3}_{10}$, with the subtraction constant $g(D)$ or g_0 is introduced. It has been argued that the subtraction constant is $\mathcal{O}(p^0)$, because by changing the subtraction point B the subtraction constant g_0 changes while the function $g(A)$ is invariant. The process for determining the interaction kernel $N_{JI}(A)$, eq. (4.31), has been also discussed in detail. It was obtained that the subtraction point D acts as a "renormalization scale" where an experimental point is reproduced. The subtraction constant $g(D)$ just fixes the "renormalization scheme" and the exact results should not depend on it. A natural value for $g_0 \sim -mm_\pi/4\pi$ was argued to be adequate for obtaining $N_{JI}(A)$ as a perturbative solution of eq. (4.16) in order to suppress the effects of the iterative factor $|1+gN_{JI}|^2$ in the equation. The couplings C_S and C_T from the local nucleon-nucleon Lagrangian, eq. (4.1), have been fixed in terms of g_0 up-to-and-including next-to-leading order reproducing the S-wave nucleon-nucleon scattering lengths. These couplings keep their estimated size of $\mathcal{O}(p^0)$ after the iteration, despite the well-known fact that the nucleon-nucleon scattering lengths are much larger than $1/m_\pi$.

- We have addressed the calculation of the energy density of nuclear matter $\mathcal{E}$ up-to-and-including next-to-leading order. Our calculation already leads to saturation in symmetric nuclear matter and repulsion for neutron matter without the need for a relativistic treatment or three-nucleon forces. It is remarkable that we obtain a very good reproduction of sophisticated many-body calculations that employ realistic nucleon-nucleon potentials for the equation of state of neutron matter up to rather high nuclear densities. We can achieve such a good agreement by distinguishing between g_0 and $\tilde{g}_0$, where the former parameter appears explicitly in the calculation of the binding energy per nucleon while the latter appears implicitly through the nucleon-nucleon scattering amplitudes involved. The second parameter is kept to its natural value, while the first one is fine-tuned. Furthermore, the nuclear matter incompressibility comes out with a value between 240-250 MeV, in perfect agreement with the experimental value of 250 ± 25 MeV.

- We have addressed the calculation of the chiral quark condensate in nuclear matter $\langle\Omega|\bar{q}_i q_j|\Omega\rangle$ up-to-and-including next-to-leading order. We have found that the contributions that arise due to the leading quark mass dependence of the nucleon mass mutually cancel. As a result, only contributions that stem from the quark mass dependence of the pion mass survive. This is the reason why previous calculations have found that short range nucleon-nucleon interactions are suppressed for the calculation of the in-medium quark condensates. We conclude that the corrections are small for the chiral quark condensate but it is also worth pointing out that the full iteration of the nucleon-nucleon interactions reduces the force of extra damping of the quark condensate as compared with other references. On top of nuclear effects one has to take into account the uncertainty of the sigma-term of pion-nucleon scattering, which are larger than the corrections due to nucleon-nucleon interactions.

- We have addressed the calculation of the pion self-energy in nuclear matter Π up-to-and-including next-to-leading order, together with some partial higher order contributions. We found a cancellation between all leading corrections beyond the linear density approximation. In particular, it is derived that the leading corrections from nucleon-nucleon scattering mutually cancel. This was shown as well utilizing the non-perturbative methods as comfirmed by considering general arguments of the scattering amplitudes. The suppression on the whole is interesting since it allows to understand from first principles the phenomenological success of fitting data on pionic atoms with only meson-baryon interactions [KKW03, FG07] and is actually a novelty in the literature.

- We have accessed the realm of strangeness contributions for nuclear matter properties. Yet, this was done on the basis of [MOW02], since the extension of Effective Field Theory for baryon-baryon interactions is still under development and not within reach for in-medium calculations, presently.

We interpret the success of our reproduction of the nuclear matter equation of state in terms of just one free parameter up to the considered chiral order as an indication that our power counting is realistic. With this one is able to establish a useful hierarchy within the many contributions and complications inherent to nuclear dynamics. Our framework promisingly opens the way to proceed systematically improving the calculations in a controlled way. Therefore the next steps in applying the established nuclear matter Effective Field Theory would be the following.

- For nucleon-nucleon scattering in the vacuum the resulting phase shifts and mixing angles at leading and next-to-leading order are depicted in subsection 4.8. It is argued that higher orders should be included in order to improve the reproduction of data. Particularly, a next-to-next-to-leading order analysis should be pursued since it would include the important two-pion irreducible exchange and new counterterms, in particular the one necessary to reproduce the effective range for the ${}^1S_0$ partial wave [EHM09]. This is left as a future task since our present aim is to work out the results up-to-and-including next-to-leading order and settle the in-medium formalism in detail.

- According to eq. (4.31) the imaginary part along the left-hand cut of the interaction kernel $N_{JI}(A)$ can be related to the left-hand cut of the scattering amplitude T_{JI}. We can then write down the interaction kernel as a once-subtracted dispersion relation

$$N_{JI}(A) = N_{JI}(D) + \frac{A-D}{\pi}\int_{-\infty}^{-m_\pi^2/4} dk^2 \frac{\mathrm{Im}T_{JI}(k^2)\,|1+g(k^2)N_{JI}(k^2)|^2}{(k^2-A-i\epsilon)(k^2-D)}\ . \tag{4.16}$$

We have solved $N_{JI}(A)$ perturbatively by performing an expansion of the scattering amplitude in the unitarity loop $g(A)$ and matching with a loop expansion in χPT (which only satisfies unitarity perturbatively). This leads to a dependence on the subtraction constant g_0. An exact solution of eq. (4.16) or equivalently eq. (4.26) would revoke this dependence and should be pursued in the future, probably including N/D methods [Ba65].

- The calculation of the pion decay constant's temporal component f_t indicates a linear decreasing with density, $f_t = f_\pi(1 - (0.26 \pm 0.04)\rho/\rho_0)$, where $f_\pi = 92.4$ MeV is the weak pion decay constant in the vacuum and ρ_0 is the nuclear matter saturation density. This result clearly indicates that it makes sense to use chiral Lagrangians in the nuclear medium up to central nuclear densities. We addressed a calculation up to next-to-leading order, $\mathcal{O}(p^5)$, and found no additional correction due to nucleon-nucleon interactions. Nonetheless, a more thorough calculation to $\mathcal{O}(p^6)$ of f_t within our present approach, including nucleon-nucleon correlations, should be pursued in order to check whether the dependence in density of f_t remains stable or is subject to significant corrections. In particular it is interesting if there are in-medium corrections to the Gell-Mann–Oakes–Renner relation at that order.

- Accessing higher orders in the chiral expansion will reveal new effects. In particular, higher order calculations will address the interesting question about the importance of three-nucleon forces for nuclear matter saturation. Regarding the multi-nucleon interactions, one will encounter the following ordering scheme.

  - Contributions with three in-medium generalized vertices (IGVs) $V_\rho = 3$ will enter one order beyond our present investigations and therefore enter at next-to-next-to-leading order ($\mathrm{N^2LO}$).
  - Contributions from two-pion exchanges, according to the Weinberg counting [We90], will enter in-medium calculations at $\mathrm{N^3LO}$, since they are of order p^2 on top of the required NLO for two IGVs.
  - Proper three-nucleon forces, according to the Weinberg counting [We90], will contribute to in-medium calculations at $\mathrm{N^4LO}$, since three-nucleon forces start at order p^2 on top of the required $\mathrm{N^2LO}$ for three IGVs. (Note that in the vacuum three-nucleon interactions start at order p^3, while p^2 contributions vanish or are suppressed. That does not necessarily happen in the nuclear medium due to the certain frame of reference.) Here, a *proper* three-nucleon force is understood as a three-body interaction, that cannot be disconnected by cutting through a single nucleon line, or, equivalently, three in-medium generalized vertices join in one vertex.

- In the pion-nucleon sector the contribution proportional to the low-energy constant c_3 exceeds by far the contributions of other diagrams. Supposedly, this is due to large contributions from the Δ-resonance in that particular kinematic region. Also in calculations of the chiral quark condensate in symmetric nuclear matter in [KHW08] the Δ-isobar excitation leads to large effects. Therefore an investigation with the Δ as an explicit degree of freedom should be pursued.

- Finally, a straightforward extension to flavor-$SU(3)$ including multi-baryon forces would be interesting, since it allows to estimate the contribution of the strange quantum number in all considered processes, and allows for an investigation of kaonic atoms in a systematic controlled way.

Appendix A

Partial wave decompositions of the nucleon-nucleon amplitudes

In this appendix, we derive the partial wave decomposition of the nucleon-nucleon scattering amplitudes in the center-of-mass (CM) frame. Our states are normalized as

$$\begin{aligned} &1-\text{particle state: } \langle \mathbf{p}', j|\mathbf{p}, i\rangle = \delta_{ij}(2\pi)^3\delta(\mathbf{p}'-\mathbf{p}) \\ &2-\text{particle state: } \langle \mathbf{p}', j_1 j_2|\mathbf{p}, i_1 i_2\rangle = \delta_{j_1 i_1}\delta_{j_2 i_2}(2\pi)^4\delta(\mathcal{P}_f-\mathcal{P}_i)\frac{4\pi^2 W}{pE_1E_2}\delta(\Omega-\Omega') \ , \end{aligned} \tag{A.1}$$

Here, $\mathcal{P}_f$ corresponds to the total four-momentum of the final state and $\mathcal{P}_i$ to that of the initial one, with $W = \mathcal{P}_i^0 = \mathcal{P}_f^0$, the total CM energy. E_1 and E_2 are the energies of the particles 1 and 2, in order. The indices i and j refer to any discrete quantum number used to characterize the states. The solid angle in the CM frame is denoted by Ω. Finally, $p = |\mathbf{p}|$ is the modulus of the three-momentum in the CM frame. The two-particle states with well defined orbital angular momentum are defined as,

$$|\ell m, i_1 i_2\rangle = \frac{1}{\sqrt{4\pi}}\int d\hat{\mathbf{p}}\, Y_\ell^m(\hat{\mathbf{p}})^*|\mathbf{p}, i_1 i_2\rangle \ . \tag{A.2}$$

Taking into account eq. (A.1) it follows then

$$\langle \ell' m', j_1 j_2|\ell m, i_1 i_2\rangle = \frac{\pi W}{pE_1E_2}\delta_{\ell'\ell}\delta_{m'm}\delta_{j_1 i_1}\delta_{j_2 i_2} \ . \tag{A.3}$$

The decomposition in states with well defined orbital angular momentum ℓ, total spin S and total angular momentum J with third components m, s_3 and j_3, respectively, is given by

$$|\mathbf{p}, \sigma_1\sigma_2\rangle = \sqrt{4\pi}\sum_{J,S,\ell,m}(\sigma_1\sigma_2 s_3|s_1 s_2 S)(m s_3 j_3|\ell S J)Y_\ell^m(\hat{\mathbf{p}})^*|J\ell S, j_3 m s_3\rangle \ , \tag{A.4}$$

where s_1, s_2 are the spins of the nucleons with third components σ_1, σ_2. For the Clebsch-Gordan coefficients we employ the notation $(c_1c_2c|C_1C_2C)$, where C_i is the quantum number and c_i its third component. $Y_\ell^m(\hat{\mathbf{p}})$ are the standard spherical harmonics. Now, we introduce the isospin of the nucleons τ_1, τ_2 with third components α_1, α_2, and decompose the free state in terms of states

that have well defined total isospin I with third component i_3. In addition, the antisymmetric nature of a two-nucleon state is introduced

$$\frac{1}{\sqrt{2}}\left(|\mathbf{p},\sigma_1\alpha_1\sigma_2\alpha_2\rangle - |-\mathbf{p},\sigma_2\alpha_2\sigma_1\alpha_1\rangle\right) = \sqrt{2\pi}\sum\Big\{(\sigma_1\sigma_2 s_3|s_1s_2S)(ms_3j_3|\ell SJ)(\alpha_1\alpha_2 i_3|\tau_1\tau_2 I)$$
$$\times Y_\ell^m(\hat{\mathbf{p}})^*|J\ell SI, j_3 m s_3 i_3\rangle - (\sigma_2\sigma_1 s_3|s_2s_1S)(ms_3j_3|\ell SJ)(\alpha_2\alpha_1 i_3|\tau_2\tau_1 I)Y_\ell^m(\hat{\mathbf{p}})^*|J\ell SI, j_3 m s_3 i_3\rangle\Big\}\ , \tag{A.5}$$

In this expression the repeated indices must be summed. This convention is used along this section. To simplify the notation we denote the left-hand-side of the previous equation as $|\mathbf{p},\sigma_1\alpha_1\sigma_2\alpha_2\rangle_A$, with the subscript A indicating that the state is antisymmetrized. Applying the symmetry relations,

$$\begin{aligned} Y_\ell^m(-\hat{\mathbf{p}}) &= (-1)^l Y_\ell^m(\hat{\mathbf{p}})\ , \\ (\sigma_2\sigma_1 s_3|s_2s_1S) &= (-1)^{S-s_1-s_2}(\sigma_1\sigma_2 s_3|s_1s_2S)\ , \\ (\alpha_2\alpha_1 i_3|\tau_2\tau_1 I) &= (-1)^{I-\tau_1-\tau_2}(\alpha_1\alpha_2 i_3|\tau_1\tau_2 I)\ , \end{aligned} \tag{A.6}$$

eq. (A.5) for the nucleon-nucleon case ($s_1 = s_2 = \tau_1 = \tau_2 = 1/2$) simplifies to

$$|\mathbf{p},\sigma_1\alpha_1\sigma_2\alpha_2\rangle_A = \sqrt{4\pi}\sum_{J,S,\ell,m,I,i_3}(\sigma_1\sigma_2 s_3|s_1s_2S)(ms_3j_3|\ell SJ)Y_\ell^m(\hat{\mathbf{p}})^*\chi(S\ell I)|J\ell SI, j_3 m s_3 i_3\rangle\ , \tag{A.7}$$

with

$$\chi(S\ell I) = \frac{1-(-1)^{\ell+S+I}}{\sqrt{2}} = \begin{cases} \sqrt{2} & \ell+S+I = \text{ odd} \\ 0 & \ell+S+I = \text{ even} \end{cases} \tag{A.8}$$

In this way, $\chi(S\ell I)$ ensures the well known rule that a partial wave contributes to nucleon-nucleon scattering only if $S+\ell+I$ is odd. Using the decomposition eq. (A.7) we have for the scattering amplitude,

$${}_A\langle\mathbf{p}',\sigma_1'\alpha_1'\sigma_2'\alpha_2'|T(\mathbf{P})|\mathbf{p},\sigma_1\alpha_1\sigma_2\alpha_2\rangle_A = 4\pi\sum(\sigma_1'\sigma_2' s_3'|s_1s_2S')(\sigma_1\sigma_2 s_3|s_1s_2S)(m's_3'j_3'|\ell'S'J')$$
$$\times(ms_3j_3|\ell SJ)(\alpha_1'\alpha_2' i_3|\tau_1\tau_2 I)(\alpha_1\alpha_2 i_3|\tau_1\tau_2 I)Y_{\ell'}^{m'}(\hat{\mathbf{p}}')Y_\ell^m(\hat{\mathbf{p}})^*\chi(S'\ell'I)\chi(S\ell I)T_{J'JI}(\ell'S';\ell S)\ . \tag{A.9}$$

Here, $T_{J'JI}(\ell'S';\ell S)$ is the partial wave with final total angular momentum J', initial one J, final total spin S', initial one S, isospin I and final and initial orbital angular momenta ℓ' and ℓ, respectively. Notice that in the previous equation we have distinguished between the final and initial total angular momenta J' and J, and similarly for the total spins S' and S. For elastic two nucleon scattering we have of course $J' = J$ because of angular momentum conservation. This conservation law, the conservation of parity and the rule $S+\ell+I =$ odd imply that $S' = S$. However, the resulting matrix elements in the nuclear medium depend additionally on the total three-momentum of the two nucleons because the nuclear medium rest-frame does not coincide in general with their center-of-mass. This is why we have included the total three-momentum $\mathbf{P}$ as an argument in the scattering operator. Note that the sum without indices symbolizes a summation over all repeated quantum numbers. Employing the orthogonality properties of the Clebsch-Gordan coefficients and spherical harmonics, one can invert eq. (A.9) with the result,

$$4\pi\chi(S'\ell'I)\chi(S\ell I)T_{J'JI}(\ell'S';\ell S) = \sum\int d\hat{\mathbf{p}}'\int d\hat{\mathbf{p}}\ {}_A\langle\mathbf{p}',\sigma_1'\alpha_1'\sigma_2'\alpha_2'|T(\mathbf{P})|\mathbf{p},\sigma_1\alpha_1\sigma_2\alpha_2\rangle_A(\sigma_1'\sigma_2' s_3'|s_1s_2S')$$
$$\times(\sigma_1\sigma_2 s_3|s_1s_2S)(m's_3'j_3'|\ell'S'J')(ms_3j_3|\ell SJ)(\alpha_1'\alpha_2' i_3|\tau_1\tau_2 I)(\alpha_1\alpha_2 i_3|\tau_1\tau_2 I)Y_{\ell'}^{m'}(\hat{\mathbf{p}}')^*Y_\ell^m(\hat{\mathbf{p}})\ . \tag{A.10}$$

This expression can be further reduced by making use of properties under rotational invariance so that the initial relative three-momentum $\mathbf{p}$ can be taken parallel to the $\hat{\mathbf{z}}$-axis. In deriving this simplification we omit the isospin indices that do not play any role in the following considerations, and introduce the symbol

$$T^{\sigma_1\alpha_1\sigma_2\alpha_2}_{\sigma_1'\alpha_1'\sigma_2'\alpha_2'}(\mathbf{p}',\mathbf{p},\mathbf{P}) = {}_A\langle \mathbf{p}',\sigma_1'\alpha_1'\sigma_2'\alpha_2'|T(\mathbf{P})|\mathbf{p},\sigma_1\alpha_1\sigma_2\alpha_2\rangle_A \ . \tag{A.11}$$

Now consider the rotation $R(\hat{\mathbf{p}})$, such that $R(\hat{\mathbf{p}})\hat{\mathbf{z}} = \hat{\mathbf{p}}$, that consists first of a rotation around the y-axis about an angle θ and then a rotation around the z-axis with an angle ϕ, with θ and ϕ the polar and azimuthal angles of $\hat{\mathbf{p}}$, respectively. We could also have taken first an arbitrary rotation of angle γ around the z-axis. Then,

$$\begin{aligned} R(\hat{\mathbf{p}})^\dagger|\mathbf{p},\mathbf{P};\sigma_1\sigma_2\rangle &= \sum_{\bar{s}_1,\bar{s}_2} D^{(1/2)}_{\bar{s}_1\sigma_1}(R^\dagger) D^{(1/2)}_{\bar{s}_2\sigma_2}(R^\dagger)|p\hat{\mathbf{z}},\mathbf{P}'';\bar{s}_1\bar{s}_2\rangle \ , \\ R(\hat{\mathbf{p}})^\dagger|\mathbf{p}',\mathbf{P};\sigma_1'\sigma_2'\rangle &= \sum_{\bar{s}_1',\bar{s}_2'} D^{(1/2)}_{\bar{s}_1'\sigma_1'}(R^\dagger) D^{(1/2)}_{\bar{s}_2'\sigma_2'}(R^\dagger)|\mathbf{p}'',\mathbf{P}'';\bar{s}_1'\bar{s}_2'\rangle \ , \end{aligned} \tag{A.12}$$

with $\mathbf{p}'' = R(\hat{\mathbf{p}})^{-1}\mathbf{p}'$ and $\mathbf{P}'' = R(\hat{\mathbf{p}})^{-1}\mathbf{P}$. The dependence on the total three-momentum has been made explicit in the state vectors to emphasize that the total three-momentum also is rotated. Inserting eq. (A.12) into eq. (A.10) we have,

$$\begin{aligned} 4\pi\chi(S'\ell'I)\chi(S\ell I)T_{J'JI}(\ell'S';\ell S) = \sum \int d\hat{\mathbf{p}}' \int d\hat{\mathbf{p}}\, T^{\bar{s}_1\bar{s}_2}_{\bar{s}_1'\bar{s}_2'}(\mathbf{p}'',p\hat{\mathbf{z}},\mathbf{P}'') D^{(1/2)}_{\bar{s}_1'\sigma_1'}(R^\dagger)^* D^{(1/2)}_{\bar{s}_2'\sigma_2'}(R^\dagger)^* D^{(1/2)}_{\bar{s}_1\sigma_1}(R^\dagger) \\ \times D^{(1/2)}_{\bar{s}_2\sigma_2}(R^\dagger) Y^{m'}_{\ell'}(\hat{\mathbf{p}}')^* Y^m_\ell(\hat{\mathbf{p}})(\sigma_1'\sigma_2's_3'|s_1s_2S')(m's_3'j_3'|\ell'S'J')(\sigma_1\sigma_2s_3|s_1s_2S)(ms_3j_3|\ell SJ) \ . \end{aligned} \tag{A.13}$$

The spherical harmonics satisfy the following transformation properties under rotations,

$$\begin{aligned} Y^{m'}_{\ell'}(\hat{\mathbf{p}}') &= \sum_{\bar{m}'} D^{(\ell')}_{\bar{m}'m'}(R^\dagger) Y^{\bar{m}'}_{\ell'}(\hat{\mathbf{p}}'') \ , \\ Y^m_\ell(\hat{\mathbf{p}}) &= \sum_{\bar{m}} D^{(\ell)}_{\bar{m}m}(R^\dagger) Y^{\bar{m}}_\ell(\hat{\mathbf{z}}) \ . \end{aligned} \tag{A.14}$$

Inserting these equalities into eq. (A.13) we are then left with the following product of rotation matrices,

$$D^{(1/2)}_{\bar{s}_1'\sigma_1'}(R^\dagger)^* D^{(1/2)}_{\bar{s}_2'\sigma_2'}(R^\dagger)^* D^{(\ell')}_{\bar{m}'m'}(R^\dagger)^* D^{(1/2)}_{\bar{s}_1\sigma_1}(R^\dagger) D^{(1/2)}_{\bar{s}_2\sigma_2}(R^\dagger) D^{(\ell)}_{\bar{m}m}(R^\dagger) \ . \tag{A.15}$$

For all these matrices the subscript on the left is not free but summed with some other coefficient in eq. (A.13). We now take into account the Clebsch-Gordan decomposition of rotation matrices [Ro95],

$$\sum_{M'} D^{(L)}_{M'M}(R)(m_1'm_2'M'|\ell_1\ell_2L) = \sum_{m_1,m_2} D^{(\ell_1)}_{m_1'm_1}(R) D^{(\ell_2)}_{m_2'm_2}(R)(m_1m_2M|\ell_1\ell_2L) \ . \tag{A.16}$$

Since eq. (A.15) appears in eq. (A.13) times Clebsch-Gordan coefficients we can make use of the previous composition repeatedly. First,

$$\begin{aligned} \sum D^{(1/2)}_{\bar{s}_1'\sigma_1'}(R^\dagger) D^{(1/2)}_{\bar{s}_2'\sigma_2'}(R^\dagger)(\sigma_1'\sigma_2's_3'|s_1s_2S') &= \sum D^{(S')}_{\bar{\sigma}_3's_3'}(R^\dagger)(\bar{s}_1'\bar{s}_2'\bar{\sigma}_3'|s_1s_2S') \ , \\ \sum D^{(1/2)}_{\bar{s}_1\sigma_1}(R^\dagger) D^{(1/2)}_{\bar{s}_2\sigma_2}(R^\dagger)(\sigma_1\sigma_2s_3|s_1s_2S) &= \sum D^{(S)}_{\bar{\sigma}_3s_3}(R^\dagger)(\bar{s}_1\bar{s}_2\bar{\sigma}_3|s_1s_2S) \ . \end{aligned} \tag{A.17}$$

The rotation matrix $D^{(S')}_{\bar{\sigma}'_3 s'_3}$, that appears on the right-hand-side of the first of the previous equalities, can then be combined in eq. (A.13) such that

$$\sum D^{(S')}_{\bar{\sigma}'_3 s'_3}(R^\dagger) D^{(\ell')}_{\bar{m}' m'}(R^\dagger)(m' s'_3 j'_3|\ell' S' J') = \sum D^{(J')}_{\bar{j}_3' j'_3}(R^\dagger)(\bar{m}' \bar{\sigma}'_3 \bar{j}_3'|\ell' S' J') \ . \tag{A.18}$$

Similarly

$$\sum D^{(S)}_{\bar{\sigma}_3 s_3}(R^\dagger) D^{(\ell)}_{\bar{m} m}(R^\dagger)(m s_3 j_3|\ell S J) = \sum D^{(J)}_{\bar{j}_3 j_3}(R^\dagger)(\bar{m} \bar{\sigma}_3 \bar{j}_3|\ell S J) \ . \tag{A.19}$$

Incorporating eqs. (A.18) and (A.19) in eq. (A.13), the latter takes the form

$$\begin{aligned} 4\pi \chi(S'\ell' I)\chi(S\ell I) T_{J'JI}(\ell' S';\ell S) &= \sum \int d\hat{\mathbf{p}}' \int d\hat{\mathbf{p}}\, T^{\sigma_1\sigma_2}_{\sigma'_1\sigma'_2}(\mathbf{p}'', p\mathbf{z}, \mathbf{P}'') Y^{\bar{m}'}_{\ell'}(\hat{\mathbf{p}}'')^* Y^{\bar{m}}_{\ell}(\hat{\mathbf{z}}) \\ &\times D^{(J')}_{\bar{j}_3' j'_3}(R^\dagger) D^{(J)}_{\bar{j}_3 j_3}(R^\dagger)(\bar{m}' \bar{\sigma}'_3 \bar{j}_3'|\ell' S' J')(\bar{s}'_1 \bar{s}'_2 \bar{\sigma}'_3|s_1 s_2 S')(\bar{m} \bar{\sigma}_3 \bar{j}_3|\ell S J)(\bar{s}_1 \bar{s}_2 \bar{\sigma}_3|s_1 s_2 S) \ . \end{aligned} \tag{A.20}$$

Let us first consider the vacuum case where the scattering amplitude does not depend on $\mathbf{P}$. In this way the integration over $\hat{\mathbf{p}}$ in the previous equation can be done explicitly taking into account the orthogonality relation between two rotation matrices [Ro95]. For that let us recall our previous remark about the fact that an arbitrary initial rotation over the $\mathbf{z}$-axis and angle γ can also be included. In this way we take

$$\frac{1}{2\pi}\int_0^{2\pi} d\gamma \int d\hat{\mathbf{p}} D^{(J')}_{\bar{j}_3' j'_3}(R^\dagger)^* D^{(J)}_{\bar{j}_3 j_3}(R^\dagger) = \frac{4\pi}{2J+1} \delta_{\bar{j}_3' \bar{j}_3} \delta_{j'_3 j_3} \delta_{JJ'} \ . \tag{A.21}$$

Inserting this back to eq. (A.20) one arrives at

$$\begin{aligned} \chi(S\ell' I)\chi(S\ell I) T_{JI}(\ell', \ell, S) &= \frac{Y^0_\ell(\hat{\mathbf{z}}) \delta_{JJ'} \delta_{j'_3 j_3}}{2J+1} \sum \int d\hat{\mathbf{p}}'' T^{\bar{s}_1 \bar{s}_2}_{\bar{s}'_1 \bar{s}'_2}(\mathbf{p}'', p\mathbf{z}) Y^{\bar{m}'}_{\ell'}(\hat{\mathbf{p}}'')(\bar{m}' \bar{\sigma}'_3 \bar{\sigma}_3|\ell' S J) \\ &\times (0 \bar{\sigma}_3 \bar{\sigma}_3|\ell S J)(\bar{s}'_1 \bar{s}'_2 \bar{\sigma}'_3|s_1 s_2 S)(\bar{s}_1 \bar{s}_2 \bar{\sigma}_3|s_1 s_2 S) \ . \end{aligned} \tag{A.22}$$

In this expression we have made use that only $\bar{m} = 0$ gives a contribution to $Y^{\bar{m}}_\ell(\hat{\mathbf{z}})$ and, as explained after eq. (A.9), $S' = S$. In addition, we have also used that $d\hat{\mathbf{p}}' = d\hat{\mathbf{p}}''$, since both vectors are related by a rotation. The subscript J' in $T_{J'JI}$ is redundant because $J' = J$. Also, we have introduced the shorter notation $T_{JI}(\ell', \ell, S) \doteq T_{JJI}(\ell' S; \ell S)$, which is employed throughout this thesis.

We now come back to the in-medium case and keep the dependence on $\mathbf{P}$. Here also $\bar{m} = 0$ so that $\bar{j}_3 = \bar{\sigma}_3$. Let us show first that a Fermi sea with all the free three-momentum states filled up to ξ has total spin zero. This is required because for a given three-momentum $\mathbf{p}_1$ one has two spin states that must be combined antisymmetrically because of the Fermi statistics so that $S = 0$ for this pair. Then, since this happens for any pair, the total spin of the Fermi sea must be zero. Regarding total angular momentum we now give a non-relativistic argument to claim that the orbital angular momentum must also be zero. This is due to the fact that the nuclear medium in the CM system of the two scattering nucleons is seen with a velocity parallel to $-\mathbf{P}$. In this way, both the CM position vector and the total three-momentum of the nuclear medium are also parallel so that their cross product vanishes. As a result, since the intrinsic orbital angular momentum of the nuclear medium is also zero, one expects that the total angular momentum is zero for the system also in the CM frame of the two nucleons. Thus, $J' = J$ also in this case and then, because of the same reasons as in vacuum, $S' = S$. After summing over the third components of total spin and orbital

angular momentum the labels ℓ and S diagonalize. Hence, because of the rule $\ell + S + I = \text{odd}$, I must be the same in the initial and final states. In addition the third component of total angular momentum must be conserved, $j_3 = j_3'$, and summing over j_3 one has

$$\frac{1}{2J+1}\sum_{j_3} D^{(J)}_{\bar{j}_3' j_3}(R^\dagger)^* D^{(J)}_{\bar{j}_3 j_3}(R) = \frac{\delta_{\bar{j}_3' \bar{j}_3}}{2J+1} \ , \tag{A.23}$$

given the unitary character of the rotation matrices. Then,

$$\chi(S\ell' I)\chi(S\ell I) T_{JI}(\ell', \ell, S) = \frac{Y^0_\ell(\hat{\mathbf{z}})}{4\pi(2J+1)} \sum \int d\hat{\mathbf{P}}'' \int d\hat{\mathbf{p}}'' T^{\bar{s}_1 \bar{s}_2}_{\bar{s}_1' \bar{s}_2'}(\mathbf{p}'', p\hat{z}, \mathbf{P}'')(\bar{s}_1' \bar{s}_2' \bar{\sigma}_3' | s_1 s_2 S)$$
$$\times (\bar{s}_1 \bar{s}_2 \bar{\sigma}_3 | s_1 s_2 S)(\bar{m}' \bar{\sigma}_3' \bar{\sigma}_3 | \ell' S J)(0 \bar{\sigma}_3 \bar{\sigma}_3 | \ell S J) Y^{m'}_{\ell'}(\hat{\mathbf{p}}'')^* \ . \tag{A.24}$$

This expression reduces to the one in the vacuum, eq. (A.28), whenever the integral

$$\sum \int d\hat{\mathbf{p}}'' T^{\bar{s}_1 \bar{s}_2}_{\bar{s}_1' \bar{s}_2'}(\mathbf{p}'', p\hat{z}, \mathbf{P}'')(\bar{s}_1' \bar{s}_2' \bar{\sigma}_3' | s_1 s_2 S)(\bar{s}_1 \bar{s}_2 \bar{\sigma}_3 | s_1 s_2 S)(\bar{m}' \bar{\sigma}_3' \bar{j}_3' | \ell' S J)(0 \bar{\sigma}_3 \bar{\sigma}_3 | \ell S J) Y^{m'}_{\ell'}(\hat{\mathbf{p}}'')^* \tag{A.25}$$

does not dependent on $\hat{\mathbf{P}}$. In that case the integration over $d\hat{\mathbf{P}}''$ is simply 4π and eq. (A.22) is recovered.

Eq. (A.24) can be further simplified because for the evaluation of a nucleon-nucleon partial wave amplitude one only needs to consider the direct term in the nucleon-nucleon scattering amplitude. This follows because the operator T is Bose-symmetric so that,

$$T^{\sigma_1 \alpha_1 \sigma_2 \alpha_2}_{\sigma_1' \alpha_1' \sigma_2' \alpha_2'}(\mathbf{p}', \mathbf{p}, \mathbf{P}) = \langle \mathbf{p}', \sigma_1' \alpha_1' \sigma_2' \alpha_2' | T(\mathbf{P}) | \mathbf{p}, \sigma_1 \alpha_1 \sigma_2 \alpha_2 \rangle - \langle -\mathbf{p}', \sigma_2' \alpha_2' \sigma_1' \alpha_1' | T(\mathbf{P}) | \mathbf{p}, \sigma_1 \alpha_1 \sigma_2 \alpha_2 \rangle \ . \tag{A.26}$$

When implementing the second or exchange term in eq. (A.24), reincluding the isospin indices as well, and using the above referred symmetry properties of the Clebsch-Gordan coefficients and spherical harmonics, one is left with the same expression as for the direct term in eq. (A.26) except for the global sign $-(-1)^{S+\ell'+I}$. Summing both expressions the factor $1-(-1)^{S+\ell'+I}$ arises. Given the definition of $\chi(S\ell I)$ in eq. (A.8) and imposing the rule that $\ell+S+I = \textit{odd}$ and $\ell'+S+I = \textit{odd}$, the factor $\chi(S\ell I)\chi(S\ell' I)$ can be simplified on both sides of eq. (A.24). The latter then reads

$$\mathcal{T}^{i_3}_{JI}(\ell', \ell, S) = \frac{Y^0_\ell(\hat{\mathbf{z}})}{4\pi(2J+1)} \sum (\sigma_1' \sigma_2' s_3' | s_1 s_2 S)(\sigma_1 \sigma_2 s_3 | s_1 s_2 S)(0 s_3 s_3 | \ell S J)(m' s_3' s_3 | \ell' S J)$$
$$\times (\alpha_1' \alpha_2' i_3 | \tau_1 \tau_2 I)(\alpha_1 \alpha_2 i_3 | \tau_1 \tau_2 I) \int d\hat{\mathbf{P}} \int d\hat{\mathbf{p}}' \, \langle \mathbf{p}', \sigma_1' \alpha_1' \sigma_2' \alpha_2' | T_d(\mathbf{P}) | p\hat{\mathbf{z}}, \sigma_1 \alpha_1 \sigma_2 \alpha_2 \rangle Y^{m'}_{\ell'}(\mathbf{p}')^* \ , \tag{A.27}$$

with only the direct term, as indicated by the subscript d in the scattering operator. For the particular case of the vacuum nucleon-nucleon scattering the previous expression simplifies to

$$\mathcal{T}^{i_3}_{JI}(\ell', \ell, S) = \frac{Y^0_\ell(\hat{\mathbf{z}})}{2J+1} \sum (\sigma_1' \sigma_2' s_3' | s_1 s_2 S)(\sigma_1 \sigma_2 s_3 | s_1 s_2 S)(0 s_3 s_3 | \ell S J)(m' s_3' s_3 | \ell' S J)$$
$$\times (\alpha_1' \alpha_2' i_3 | \tau_1 \tau_2 I)(\alpha_1 \alpha_2 i_3 | \tau_1 \tau_2 I) \int d\hat{\mathbf{p}}' \, \langle \mathbf{p}', \sigma_1' \alpha_1' \sigma_2' \alpha_2' | T_d | p\hat{\mathbf{z}}, \sigma_1 \alpha_1 \sigma_2 \alpha_2 \rangle Y^{m'}_{\ell'}(\mathbf{p}')^* \ . \tag{A.28}$$

Performing the sum over the third components of spin and third components of orbital angular momenta we obtain for $S = 0$

$$\mathcal{T}^{i_3}_{\ell I}(\ell, \ell, 0) = \frac{Y^0_\ell(\hat{\mathbf{z}})}{2\ell+1} \int d\hat{\mathbf{p}}' Y^0_\ell(\hat{\mathbf{p}}')^* \mathcal{T}_d \ , \tag{A.29}$$

and for $S = 1$

$$\begin{aligned}\mathcal{T}^{i_3}_{JI}(\ell',\ell,1) = \frac{Y^0_\ell(\hat{\mathbf{z}})}{2J+1}\int d\hat{\mathbf{p}}'\Big\{ & Y^0_{\ell'}(\hat{\mathbf{p}}')\Big(\mathcal{T}_d(0,0)(000|\ell 1J)(000|\ell' 1J) \\ & + \big[\mathcal{T}_d(+1,+1)+\mathcal{T}_d(-1,-1)\big](011|\ell 1J)(011|\ell' 1J)\Big) \\ & - \big[Y^{-1}_{\ell'}(\hat{\mathbf{p}}')\mathcal{T}_d(-1,0)+Y^1_{\ell'}(\hat{\mathbf{p}}')\mathcal{T}_d(+1,0)\big](000|\ell 1J)(1-10|\ell' 1J) \\ & - \big[Y^{-1}_{\ell'}(\hat{\mathbf{p}}')\mathcal{T}_d(0,+1)+Y^1_{\ell'}(\hat{\mathbf{p}}')\mathcal{T}_d(0,-1)\big](011|\ell 1J)(101|\ell' 1J) \\ & + \big[Y^{-2}_{\ell'}(\hat{\mathbf{p}}')\mathcal{T}_d(-1,+1)+Y^2_{\ell'}(\hat{\mathbf{p}}')\mathcal{T}_d(+1,-1)\big](011|\ell 1J)(2-11|\ell' 1J)\Big\}\ . \end{aligned} \tag{A.30}$$

Let us recall that in order to apply the previous equations, the vector $\mathbf{p}$ must be taken along the $\hat{\mathbf{z}}$ axis. For the partial wave projections, we choose the reference frame with the axes

$$\begin{aligned}\hat{\mathbf{z}} &= \hat{\mathbf{p}}\ , \\ \hat{\mathbf{x}} &= \frac{\hat{\mathbf{p}}\times\hat{\mathbf{P}}}{\sin\beta}\ , \\ \hat{\mathbf{y}} &= \frac{\hat{\mathbf{p}}\times(\hat{\mathbf{p}}\times\hat{\mathbf{P}})}{\sin\beta} = \hat{\mathbf{p}}\,\mathrm{ctg}\beta - \hat{\mathbf{P}}\,\mathrm{csec}\beta\ . \end{aligned} \tag{A.31}$$

Appendix B

Lorentz transformations

An arbitrary nucleon state is defined by means of a Lorentz transformation acting on a nucleon-at-rest state with third component of spin σ,

$$|\mathbf{p},\sigma\rangle = U(L_{\mathbf{p}})|\mathbf{0},\sigma\rangle \ , \tag{B.1}$$

where $U(L_{\mathbf{p}})$ is a Lorentz boost in the direction of the three-momentum $\mathbf{p}$,

$$U(L_{\mathbf{p}}) = R(\hat{\mathbf{p}})B(v\hat{\mathbf{z}})R(\hat{\mathbf{p}})^{-1} \ . \tag{B.2}$$

In this expression $R(\hat{\mathbf{p}})$ is a rotation, such that $R(\hat{\mathbf{p}})\hat{\mathbf{z}} = \hat{\mathbf{p}}$. More specific

$$R(\hat{\mathbf{p}}) = e^{-i\phi J_3}e^{-i\theta J_2} \ , \tag{B.3}$$

with ϕ and θ the azimuthal and polar angles of $\hat{\mathbf{p}}$. On the other hand, $B(v\hat{\mathbf{z}})$ is a Lorentz boost along the z-axis and velocity $|\mathbf{p}|/E$, with $E = \sqrt{m^2+\mathbf{p}^2}$. Simple expressions can be worked out for a rotation and $B(v\hat{\mathbf{z}})$ acting on a particle of spin 1/2:

$$\begin{aligned} e^{-i\alpha\hat{\mathbf{n}}\vec{\sigma}/2} &= \cos\frac{\alpha}{2} - i\sin\frac{\alpha}{2}\hat{\mathbf{n}}\vec{\sigma} \ , \\ B(v\hat{\mathbf{z}}) = e^{\phi\gamma^3\gamma^0} &= \cosh\frac{\phi}{2} + \sinh\frac{\phi}{2}\,\gamma^3\gamma^0 \ , \end{aligned} \tag{B.4}$$

with

$$\gamma^3\gamma^0 = \begin{pmatrix} 0 & -\sigma_3 \\ -\sigma_3 & 0 \end{pmatrix} \ . \tag{B.5}$$

For the boost from the rest frame to a moving one, one has $\sinh(\phi/2) = -p/\sqrt{2m(E+m)}$ and $\cosh(\phi/2) = \sqrt{(m+E)/2m}$. It is then straightforward to obtain the Dirac spinors,

$$u_r(\mathbf{p}) = B(\mathbf{p})\begin{pmatrix} \xi_r \\ 0 \end{pmatrix} = \sqrt{\frac{E+m}{2m}}\begin{pmatrix} \xi_r \\ \frac{\vec{\sigma}\cdot\mathbf{p}}{E+m}\xi_r \end{pmatrix} \ , \tag{B.6}$$

with

$$\xi_1 = \begin{pmatrix} 1 \\ 0 \end{pmatrix} \ , \ \xi_2 = \begin{pmatrix} 0 \\ 1 \end{pmatrix} \ . \tag{B.7}$$

The behavior of $|\mathbf{p},\sigma\rangle$ under a Lorentz transformation $U(\Lambda)$ can be described in terms of a Little Wigner rotation. Let us consider the manipulation

$$U(\Lambda)|\mathbf{p},\sigma\rangle = U(\Lambda)U(L_{\mathbf{p}})|0,\sigma\rangle = U(L_{\Lambda p})U^{-1}(L_{\Lambda p})U(\Lambda)U(L_{\mathbf{p}})|0,\sigma\rangle \ . \tag{B.8}$$

The transformation

$$R = U^{-1}(L_{\Lambda p})U(\Lambda)U(L_{\mathbf{p}}) \tag{B.9}$$

is a rotation in the rest frame of the particle. Here, $L_{\Lambda p}$ is the reference Lorentz boost for the particle with four-momentum Λp. The fact that R in eq. (B.9) is a rotation follows because this transformation leaves invariant the four-vector $n = (1, \vec{0})$. Note that L_p acting on the mass m times n gives rise to the four-momentum p, then Λ transforms it to Λp and, finally, the inverse of $L_{\Lambda p}$ returns it to n.

For our studies of nucleon-nucleon interactions we are particularly interested in the rest frame of the two scattering nucleons,

$$\mathbf{P'} = \mathbf{p}_1' + \mathbf{p}_2' = \vec{0} = \gamma(\mathbf{P} - \mathbf{v}W) \rightarrow \mathbf{v} = \frac{\mathbf{P}}{W} \ , \tag{B.10}$$

with $\mathbf{P} = \mathbf{p}_1 + \mathbf{p}_2$, $W = E_1 + E_2$, $\gamma = \sqrt{1-v^2}$ and $v = |\mathbf{v}|$. The velocity for the reference boost for p is $\mathbf{w} = -\mathbf{p}/E$ and $\mathbf{w}' = -\mathbf{p}'/E'$ that for the final four-momentum Λp. We also make use of the general expression for a Lorentz boost of velocity $\mathbf{v}$,

$$\begin{aligned} \mathbf{p}' &= \mathbf{p} + [(\mathbf{p}\cdot\hat{\mathbf{v}})(\gamma - 1) - \gamma E v]\,\hat{\mathbf{v}} \ , \\ E' &= \gamma(E - \mathbf{v}\cdot\mathbf{p}) \end{aligned} \tag{B.11}$$

By definition we choose the vector $\mathbf{p}||\hat{\mathbf{x}}$ and the velocity $\mathbf{v}$ contained in the plane $\hat{xy}$. In order to obtain an expression for the angle φ of the little Wigner rotation we apply the different Lorentz transformations of eq. (B.9) to a four-vector a. This is chosen such that its transformation under L_p is

$$\begin{aligned} & a^0 - \mathbf{w}\cdot\mathbf{a} = 0 \ , \\ & \mathbf{a} + (\mathbf{a}\cdot\hat{\mathbf{w}})\hat{\mathbf{w}}(\gamma_0 - 1) - \gamma_0 a^0 \mathbf{w} = N \begin{pmatrix} \hat{v}_y \\ -\hat{v}_x \\ 0 \end{pmatrix} \ , \end{aligned} \tag{B.12}$$

where $\gamma_0 = 1/\sqrt{1-\omega^2}$ and note that the vector $(v_y, -v_x, 0)$ in this equation is orthogonal to $\mathbf{v}$. In addition, the normalization condition

$$\mathbf{a}\cdot\hat{\mathbf{w}} = 1 \tag{B.13}$$

is imposed. These conditions fix

$$\begin{aligned} a &= \left(\omega, -1, \frac{\mathrm{ctg}\theta}{\gamma_0}, 0\right) = \left(w, -\hat{\mathbf{x}} + \frac{\mathrm{ctg}\theta}{\gamma_0}\hat{\mathbf{y}}\right) \ , \\ N &= -1/\gamma_0 \sin\theta \ . \end{aligned} \tag{B.14}$$

Where θ is the polar angle of $\mathbf{v} = v(\cos\theta, \sin\theta, 0)$. We define

$$b \equiv L_p a = \begin{pmatrix} 0 \\ \frac{1}{\gamma_0}\left[-\hat{\mathbf{x}} + \mathrm{ctg}\theta\,\hat{\mathbf{y}}\right] \end{pmatrix} \ , \tag{B.15}$$

and $\mathbf{bv} = 0$, because of eq. (B.12). This makes the transformation of b under Λ trivial

$$\Lambda b = b \ , \tag{B.16}$$

the actual reason for having imposed the conditions in eq. (B.12). The last transformation is

$$\begin{aligned} c = L^{-1}_{\Lambda p} b &= \begin{pmatrix} -\gamma_2 \mathbf{b}\cdot\mathbf{u} \\ \mathbf{b} + (\mathbf{b}\cdot\hat{\mathbf{u}})(\gamma_2 - 1)\hat{\mathbf{u}} \end{pmatrix} \\ \mathbf{u} = \frac{\mathbf{p}'}{E'} &= \frac{\mathbf{p} + [(\mathbf{p}\cdot\hat{\mathbf{v}})(\gamma - 1) - \gamma E v]\,\hat{\mathbf{v}}}{\gamma(E - \mathbf{v}\cdot\mathbf{p})} \\ \mathbf{b}\cdot\mathbf{u} = \frac{\mathbf{b}\cdot\mathbf{p}}{\gamma(E - \mathbf{v}\cdot\mathbf{p})} &= -\frac{p/\gamma_0}{\gamma(E - \mathbf{v}\cdot\mathbf{p})} \ . \end{aligned} \tag{B.17}$$

It is still to check that $c^0 = a^0$ since R must be a rotation. For that let us take into account that $E' = \gamma_2 m = \gamma(E - \mathbf{v}\cdot\mathbf{p})$, so that

$$\gamma_2 = \frac{\gamma}{m}(E - \mathbf{v}\cdot\mathbf{p}) = \gamma\gamma_0(1 + \mathbf{v}\cdot\mathbf{w}) \ . \tag{B.18}$$

Then, substituting this expression in eq. (B.17),

$$c^0 = -\gamma_2 \mathbf{b}\cdot\mathbf{u} = \frac{\gamma_2 p}{\gamma_0\gamma(E - \mathbf{v}\cdot\mathbf{p})} = \frac{p}{E} = \omega = a^0 \ . \tag{B.19}$$

The expression for $\mathbf{c}$ from eq. (B.17) can be worked out straightforwardly taking into account the last two lines of eqs. (B.17)) and eq. (B.18). Then,

$$\begin{aligned} \mathbf{c} = &-\frac{\hat{\mathbf{x}}}{\gamma_0}\left[1 + \frac{w^2\gamma_0^2}{1 + \gamma\gamma_0(1 + \mathbf{v}\cdot\mathbf{w})}\left\{1 + \cos^2\theta(\gamma - 1) - \gamma\frac{v}{w}\cos\theta\right\}\right] \\ &+ \frac{\hat{\mathbf{y}}}{\gamma_0}\left[\mathrm{ctg}\theta - \frac{w^2\gamma_0^2}{1 + \gamma\gamma_0(1 + \mathbf{v}\cdot\mathbf{w})}\left\{\cos\theta(\gamma - 1) - \gamma\frac{v}{w}\right\}\sin\theta\right] \ . \end{aligned} \tag{B.20}$$

The resulting Wigner rotation is then a rotation around the z axis whose general form is

$$\begin{aligned} x'' &= x\cos\varphi - y\sin\varphi \ , \\ y'' &= x\sin\varphi + y\cos\varphi \ . \end{aligned} \tag{B.21}$$

Comparing this general expression with eq. (B.20), and keeping in mind the original vector $\mathbf{a}$ given in eq. (B.14), one has,

$$\sin\varphi = -\frac{y'' + \mathrm{ctg}\theta x''/\gamma_0}{1 + \mathrm{ctg}^2\theta/\gamma_0^2} \ . \tag{B.22}$$

Since v and w are both $\mathcal{O}(p)$ one can check straightforwardly that φ is $\mathcal{O}(p^2)$. As a result, corrections from the Lorentz boost are two orders higher in the chiral counting.

While performing the boost from the rest frame of the nuclear medium to the center of mass system of two nucleons, one introduces a dependence on the total three-momentum $\mathbf{P}$ of the two nucleons in the characterization of the Fermi seas in their rest frame. However, since a rotation of the three-momenta of the involved nucleons affects both total and relative three-momentum in the same way, the scattering operator is still invariant under rotations and one can use the previous partial wave decompositions.

Appendix C

Scalar integrals

In this appendix we present the definitions and evaluations of the scalar loop integrals comprising the reducible baryon propagators and pion propagators. Those integrals are necessary in order to perform the calculations for the nucleon-nucleon interaction.

C.1 Definitions of the scalar loop integrals

With the external (internal) momenta $p^\mu_{1/2}$ ($k^\mu_{1/2}$), we can write in relative coordinates the external relative momentum $2p^\mu = p^\mu_2 - p^\mu_1$, the total momentum $2P^\mu = p^\mu_1 + p^\mu_2 = k^\mu_1 + k^\mu_2$, with the total energy $E \doteq 2P^0$ and the loop momentum $k^\mu = (k^\mu_2 - k^\mu_1)/2$. We denote the three-momentum in units of energy as $E_{\mathbf{x}} \doteq \frac{\mathbf{x}^2}{2m}$ and abbreviate for the internal momenta $\omega_i \doteq E_{\mathbf{k}_i}$. In the definitions of the functions L_{ij} the first index indicates the number of reduced baryon propagators and the second index the number of meson propagators. Where appropriate, the third index gives the number of in-medium insertions: f(ree) stands for no insertion, m(edium) for one insertion and d(ouble) for two insertions.

The function L_{10}, with the full in-medium propagator $G_0(k)_{i_3}$, given in eq. (3.11), is given by

$$\begin{aligned}
L_{10} &\doteq i\int \frac{d^4k}{(2\pi)^4} G_0(k_1)_a G_0(k_2)_b \\
&= i\int \frac{d^4k}{(2\pi)^4}\Bigg[\frac{1}{k_1^0-\omega_1+i\epsilon}\frac{1}{k_2^0-\omega_2+i\epsilon} \\
&\quad + 2\pi i\Bigg(\delta(k_1^0-\omega_1)\theta(\xi_a-|\mathbf{k}_1|)\frac{1}{k_2^0-\omega_2+i\epsilon} + \delta(k_2^0-\omega_2)\theta(\xi_b-|\mathbf{k}_2|)\frac{1}{k_1^0-\omega_1+i\epsilon}\Bigg) \\
&\quad + (2\pi i)^2\delta(k_1^0-\omega_1)\delta(k_2^0-\omega_2)\theta(\xi_a-|\mathbf{k}_1|)\theta(\xi_b-|\mathbf{k}_2|)\Bigg] \\
&\doteq L_{10,f} + L_{10,m} + L_{10,d}\ .
\end{aligned} \tag{C.1}$$

This integration corresponds to the loop in fig. 4.4 with total incoming four-momentum $2P$. We will show the explicit evaluation of the different contributions in section C.2.

We now introduce the functions L_{11} and L_{12} defined as

$$\begin{aligned} L_{11} &\doteq i\int \frac{d^4k}{(2\pi)^4}\frac{1}{(\mathbf{k}+\mathbf{p})^2+m_\pi^2}G_0(k_1)_a G_0(k_2)_b \\ &= i\int \frac{d^4k}{(2\pi)^4}\frac{1}{(\mathbf{k}+\mathbf{p})^2+m_\pi^2}\Bigg[\frac{1}{k_1^0-\omega_1+i\epsilon}\frac{1}{k_2^0-\omega_2+i\epsilon} \\ &\quad + 2\pi i\Bigg(\delta(k_1^0-\omega_1)\theta(\xi_a-|\mathbf{k}_1|)\frac{1}{k_2^0-\omega_2+i\epsilon}+\delta(k_2^0-\omega_2)\theta(\xi_b-|\mathbf{k}_2|)\frac{1}{k_1^0-\omega_1+i\epsilon}\Bigg) \\ &\quad + (2\pi i)^2\delta(k_1^0-\omega_1)\delta(k_2^0-\omega_2)\theta(\xi_a-|\mathbf{k}_1|)\theta(\xi_b-|\mathbf{k}_2|)\Bigg] \\ &\doteq L_{11,f}+L_{11,m}+L_{11,d}\ , \end{aligned} \tag{C.2}$$

and

$$\begin{aligned} L_{12} &\doteq i\int \frac{d^4k}{(2\pi)^4}\frac{1}{(\mathbf{k}+\mathbf{p})^2+m_\pi^2}\frac{1}{(\mathbf{k}+\mathbf{p}')^2+m_\pi^2}G_0(k_1)_a G_0(k_2)_b \\ &= i\int \frac{d^4k}{(2\pi)^4}\frac{1}{(\mathbf{k}+\mathbf{p})^2+m_\pi^2}\frac{1}{(\mathbf{k}+\mathbf{p}')^2+m_\pi^2}\Bigg[\frac{1}{k_1^0-\omega_1+i\epsilon}\frac{1}{k_2^0-\omega_2+i\epsilon} \\ &\quad + 2\pi i\Bigg(\delta(k_1^0-\omega_1)\theta(\xi_a-|\mathbf{k}_1|)\frac{1}{k_2^0-\omega_2+i\epsilon}+\delta(k_2^0-\omega_2)\theta(\xi_b-|\mathbf{k}_2|)\frac{1}{k_1^0-\omega_1+i\epsilon}\Bigg) \\ &\quad + (2\pi i)^2\delta(k_1^0-\omega_1)\delta(k_2^0-\omega_2)\theta(\xi_a-|\mathbf{k}_1|)\theta(\xi_b-|\mathbf{k}_2|)\Bigg] \\ &\doteq L_{12,f}+L_{12,m}+L_{12,d}\ . \end{aligned} \tag{C.3}$$

We will also need the following additional scalar loop integrals where only pion progators are involved

$$L_{01,f} \doteq \int \frac{d^3k}{(2\pi)^3}\frac{1}{(\mathbf{k}+\mathbf{p})^2+m_\pi^2}\ , \tag{C.4}$$

$$L_{01,m} \doteq \int \frac{d^3k}{(2\pi)^3}\Big[\theta(\xi_a-|\mathbf{k}_1|)+\theta(\xi_b-|\mathbf{k}_2|)\Big]\frac{1}{(\mathbf{k}+\mathbf{p})^2+m_\pi^2}\ , \tag{C.5}$$

$$L_{02,f} \doteq \int \frac{d^3k}{(2\pi)^3}\frac{1}{(\mathbf{k}+\mathbf{p})^2+m_\pi^2}\frac{1}{(\mathbf{k}+\mathbf{p}')^2+m_\pi^2}\ , \tag{C.6}$$

$$L_{02,m} \doteq \int \frac{d^3k}{(2\pi)^3}\Big[\theta(\xi_a-|\mathbf{k}_1|)+\theta(\xi_b-|\mathbf{k}_2|)\Big]\frac{1}{(\mathbf{k}+\mathbf{p})^2+m_\pi^2}\frac{1}{(\mathbf{k}+\mathbf{p}')^2+m_\pi^2}\ . \tag{C.7}$$

Throughout this appendix, we will use the abbreviations $p=|\mathbf{p}|$, $P=|\mathbf{P}|$, $k=|\mathbf{k}|$ and $p=|\mathbf{p}|=|\mathbf{p}'|$. Furthermore, we define the angles $\cos\theta=\hat{\mathbf{P}}\cdot\hat{\mathbf{k}}$, $\cos\beta=\hat{\mathbf{P}}\cdot\hat{\mathbf{p}}$, $\cos\beta'=\hat{\mathbf{P}}\cdot\hat{\mathbf{p}}'$ and $\cos\varphi=\hat{\mathbf{p}}\cdot\hat{\mathbf{p}}'$, where the hat denotes the unit vector.

C.1.1 Auxiliary functions

On a regular basis for calculation in the medium, integration intervalls are constrained by spheres which are shifted in momentum space or by intersections of several spheres. In the following we give two examples for those Fermi sphere integrations with arbitrary integrands, which are regularly needed when performing in-medium calculations.

Shifted Fermi sphere

The integration constrained by a sphere, whose center is shifted from the origin by the vector $\pm\mathbf{P}$, of a function $f(\mathbf{k}) \doteq f(k, \cos\theta)$ with $\cos\theta = \hat{\mathbf{k}} \cdot \hat{\mathbf{P}}$ reads

$$\int \frac{d^3k}{(2\pi)^3}\theta(\xi_i - |\mathbf{k} \pm \mathbf{P}|)\, f(\mathbf{k}) = \frac{1}{(2\pi)^2}\int_0^{\xi_i+P} dk\, k^2 \int_{\max\left(-1,-\frac{\xi_i^2-P^2-k^2}{2Pk}\right)}^{-1} d\cos\theta\, f(k, \pm\cos\theta) \ , \quad \text{(C.8)}$$

where $k \doteq |\mathbf{k}|$ and $P \doteq |\mathbf{P}|$. For the trivial $f = 1$ the integration over a shifted sphere becomes the identity of the integration over an unshifted sphere $\xi_i^3/6\pi^2$.

For the evaluation of the integrals in this appendix, we usually encounter an angle-independent two-nucleon propagator and optionally additional structure from e.g. pion propagators. For the numerical evaluation of many integrals, we can perform first the angle integrations analytically and only do the momentum integration numerically. Useful is the following generic functional for one *S*hifted *F*ermi-*S*phere

$$SFS[X] = \frac{m}{4\pi^2}\left[\theta(\xi_i - P)\int_0^{\xi_i-P} dk\, X\Big|_{-1}^{1} + \int_{|\xi_i-P|}^{\xi_i+P} dk\, X\Big|_{-\frac{\xi_i^2-P^2-k^2}{2Pk}}^{1}\right] \times \frac{k^2}{k^2 - A - i\epsilon} \ . \quad \text{(C.9)}$$

We used the definition

$$A = mE - \mathbf{P}^2 \ , \quad (5.30)$$

and X is the angle-dependent part of the integrand already integrated over the angles with the boundaries of the final polar angle integration $X\big|_{x_1}^{x_2} \doteq X(\cos\theta = x_2) - X(\cos\theta = x_1)$.

Intersection of two Fermi spheres

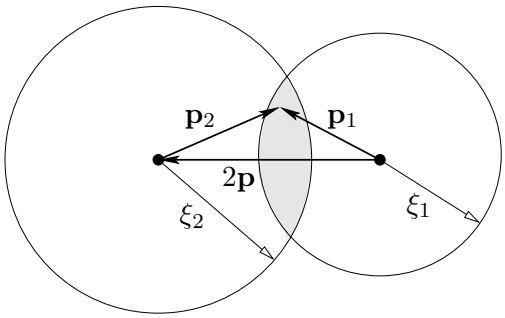

Figure C.1: Integration range constrained to the intersection of two Fermi spheres.

Now we consider the integration over the intersection of two spheres, of an arbitrary function $f(\mathbf{p}_1, \mathbf{p}_2) \doteq f(p, P, \cos\theta)$, with the angle $\cos\theta = \hat{\mathbf{P}} \cdot \hat{\mathbf{p}}$. We assume $\xi_1 \leq \xi_2$ without loss of

generality. The integration reads

$$\begin{aligned}
&\int \frac{d^3p_1}{(2\pi)^3}\theta(\xi_1-|\mathbf{p}_1|)\int \frac{d^3p_2}{(2\pi)^3}\theta(\xi_2-|\mathbf{p}_2|)\, f(\mathbf{p}_1,\mathbf{p}_2)\\
&= 8\int \frac{d^3p}{(2\pi)^3}\frac{d^3P}{(2\pi)^3}\theta(\xi_1-|\mathbf{P}-\mathbf{p}|)\theta(\xi_2-|\mathbf{P}+\mathbf{p}|)\, f(p,P,\cos\theta)\\
&= \frac{1}{\pi^4}\Bigg\{\int_0^{\frac{\xi_2-\xi_1}{2}} dp\, p^2\int_0^{\xi_1+p} dP\, P^2\int_{\max\left(-1,-\frac{\xi_1^2-P^2-p^2}{2Pp}\right)}^{1} d\cos\theta\\
&\quad+\int_{\frac{\xi_2-\xi_1}{2}}^{\frac{\xi_1+\xi_2}{2}} dp\, p^2\Bigg[\int_0^{\sqrt{\frac{\xi_1^2+\xi_2^2}{2}-p^2}} dP\, P^2\int_{\max\left(-1,-\frac{\xi_1^2-P^2-p^2}{2Pp}\right)}^{0} d\cos\theta\\
&\quad+\int_0^{\sqrt{\frac{\xi_1^2+\xi_2^2}{2}-p^2}} dP\, P^2\int_0^{\min\left(1,\frac{\xi_2^2-P^2-p^2}{2Pp}\right)} d\cos\theta\Bigg]\Bigg\} f(p,P,\cos\theta)\ ,
\end{aligned}\tag{C.10}$$

where $p \doteq |\mathbf{p}|$ and $P \doteq |\mathbf{P}|$. For two identical spheres $\xi_1 = \xi_2 \doteq \xi_F$ these expressions simplify to

$$\frac{1}{\pi^4}\int_0^{\xi_F} dp\, p^2\int_0^{\sqrt{\xi_F^2-p^2}} dP\, P^2\int_{\max\left(-1,-\frac{\xi_F^2-P^2-p^2}{2Pp}\right)}^{\min\left(1,\frac{\xi_F^2-P^2-p^2}{2Pp}\right)} d\cos\theta\, f(p,P,\cos\theta)\ . \tag{C.11}$$

These integrations correspond e.g. to closing the lines of nucleon-nucleon interactions with in-medium insertions, for example eq. (6.38). For the calculation of the two-nucleon reducible loops with two Fermi sea insertions, which we calculate in this appendix, we have only one integral over the intermediate loop momemtum with two constraining spheres and two delta-functions

$$\int \frac{d^3k}{(2\pi)^3}\theta(\xi_1-|\mathbf{k}_1|)\theta(\xi_2-|\mathbf{k}_2|)\delta(k_1^0-\omega_1)\delta(k_2^0-\omega_2)\, f(\mathbf{k}_1,\mathbf{k}_2)\ . \tag{C.12}$$

Performing the angle integration analytically and taking into account that two delta-functions make the momentum integration trivial we obtain the following generic functional for the intersection of Two Fermi-Spheres

$$\begin{aligned}
TFS[X] &= -i\frac{m\sqrt{A}}{4\pi}\theta(\xi_a^2+\xi_b^2-2mE)\Big[\theta\big(\xi_a-P-\sqrt{A}\big)\,X\Big|_{-1}^{0}+\theta\big(P+\sqrt{A}-\xi_a\big)\,X\Big|_{-\frac{\xi_a^2-P^2-A}{2P\sqrt{A}}}^{0}\\
&\quad+\theta\big(\xi_b-P-\sqrt{A}\big)\,X\Big|_{0}^{1}+\theta\big(P+\sqrt{A}-\xi_b\big)\,X\Big|_{0}^{\frac{\xi_b^2-P^2-A}{2P\sqrt{A}}}\Big]\\
&= -i\frac{m\sqrt{A}}{4\pi}\cdot\begin{cases} X\Big|_{-1}^{1} & ,\ 0\le\sqrt{A}\le\xi_m-P\ ,\\ X\Big|_{-1}^{\frac{\xi_m^2-P^2-A}{2P\sqrt{A}}} & ,\ |\xi_m-P|<\sqrt{A}\le\min(\xi_m+P,\xi_p-P)\ ,\\ X\Big|_{-\frac{\xi_p^2-P^2-A}{2P\sqrt{A}}}^{\frac{\xi_m^2-P^2-A}{2P\sqrt{A}}} & ,\ \xi_p-P<\sqrt{A}\le\xi_m+P\ \wedge\ 2mE\le\xi_m^2+\xi_p^2\ , \end{cases}
\end{aligned}\tag{C.13}$$

where X is the angle-dependent part of the integrand already integrated over the angles with the boundaries of the final polar angle integration $X\big|_{x_1}^{x_2} \doteq X(\cos\theta = x_2) - X(\cos\theta = x_1)$. The first Heaviside step function in the first representation of $TFS[\cdot]$, eq. (C.13), cuts the integral off, where

the incoming energy exceeds the sum of the two Fermi-surfaces, because holes/blocking cannot propagate/occur above the Fermi surface. In second representation of $TFS[\cdot]$, eq. (C.13), there is $\xi_m = \min(\xi_a, \xi_b)$ and $\xi_p = \max(\xi_a, \xi_b)$, but nontheless the expressions are given with the condition of $\xi_a \leq \xi_b$. If $\xi_a > \xi_b$ one has the sign switches $\cos\beta \to -\cos\beta$ and $\cos\beta' \to -\cos\beta'$ in the function X. Additionally, for tensorial reductions the reduced scalars have to be multiplied with a factor of $(-)^n$ with n equal to the count of P in the superscript.

C.2 The loop integral L_{10}

The different contributions to L_{10} are calculated according to the number of in-medium insertions in the nucleon propagators, eq. (3.11).

C.2.1 Free part $L_{10,f}$

The k^0-integration for the free part $L_{10,f}$, is performed by applying Cauchy's theorem,

$$L_{10,f} = \int \frac{d^3k}{(2\pi)^3} \frac{1}{E - \frac{\mathbf{k}^2}{m} - \frac{\mathbf{P}^2}{m} + i\epsilon} = -m \int \frac{d^3k}{(2\pi)^3} \frac{1}{\mathbf{k}^2 - A - i\epsilon} \,, \tag{C.14}$$

where A is defined in eq. (5.30). One has to keep in mind in the following the $+i\epsilon$ prescription in the definition of A. The result in eq. (C.14) corresponds to eq. (4.9) which is regularized according to the dispersion relation in

$$L_{10,f}(A) = g_0 - i\frac{m\sqrt{A}}{4\pi} \,. \tag{4.7}$$

C.2.2 One in-medium insertion $L_{10,m}$

For the contribution with one in-medium insertion $L_{10,m}$ the k^0-integration is done by making use of the energy-conserving Dirac delta-function in the in-medium part of the nucleon propagator, eq. (3.11). We are then left with

$$L_{10,m} = m \int \frac{d^3k}{(2\pi)^3} \frac{\theta(\xi_a - |\mathbf{P} - \mathbf{k}|) + \theta(\xi_b - |\mathbf{P} + \mathbf{k}|)}{\mathbf{k}^2 - A - i\epsilon} \,. \tag{C.15}$$

Evaluating the integral gives:

$$\begin{aligned} l_{10,m}(A, P, \xi_{a/b}) &= m \int \frac{d^3k}{(2\pi)^3} \frac{\theta(\xi_{a/b} - |\mathbf{P} \mp \mathbf{k}|)}{\mathbf{k}^2 - A - i\epsilon} = SFS[1] \\ &= \frac{m\sqrt{A}}{4\pi^2} \left\{ u - \operatorname{arctanh}(u+z) - \operatorname{arctanh}(u-z) + \frac{u^2 - z^2 - 1}{4z} \ln\left(\frac{(u+z)^2 - 1}{(u-z)^2 - 1} \right) \right\} \,, \end{aligned} \tag{C.16}$$

with the abbreviations $u = \xi_{a/b}/\sqrt{A}$ and $z = P/\sqrt{A}$. The Feynman prescription $A + i\epsilon$ has to be considered while evaluating the logarithm numerically. The expressions in the last line of eq. (C.16) are equal for both Fermi sea contributions because they do not depend on the angle between $\mathbf{P}$ and $\mathbf{k}$, this can also directly be seen by the substitution $\mathbf{k} \to -\mathbf{k}$. Also, there is a distinction of cases $P \geq \xi_i$ and $P < \xi_i$, however, both give rise to the same expression in eq. (C.16). In terms of the function $l_{10,m}$, eq. (C.15) reads

$$L_{10,m}(A, P, \xi_a, \xi_b) = l_{10,m}(A, P, \xi_a) + l_{10,m}(A, P, \xi_b) \,. \tag{C.17}$$

C.2.3 Two-medium insertions $L_{10,d}$

The integration of $L_{10,d}$ is done over two Fermi-spheres constrained by four-momentum conservation.

$$
\begin{aligned}
L_{10,d}(A,P,\xi_a,\xi_b) &= -im\int\frac{d^3k}{(2\pi)^2}\delta\big(\mathbf{k}^2-A\big)\,\theta(\xi_a-|\mathbf{P}-\mathbf{k}|)\,\theta(\xi_b-|\mathbf{P}+\mathbf{k}|) \qquad \text{(C.18)}\\
&= -i\frac{m\sqrt{A}}{8\pi^2}\int d\hat{\mathbf{k}}\,\theta(\xi_a-|\mathbf{P}-\hat{\mathbf{k}}\sqrt{A}|)\,\theta(\xi_b-|\mathbf{P}+\hat{\mathbf{k}}\sqrt{A}|) = TFS\big[1\big]\\
&= -i\frac{m}{8\pi P}\cdot\begin{cases} 4P\sqrt{A} & ,\ 0\le\sqrt{A}\le\xi_m-P\ ,\\ \xi_m^2-(P-\sqrt{A})^2 & ,\ |\xi_m-P|<\sqrt{A}\le\min(\xi_m+P,\xi_p-P)\ ,\\ \xi_m^2+\xi_p^2-2(P^2+A) & ,\ \xi_p-P<\sqrt{A}\le\xi_m+P\ \wedge\ 2(P^2+A)\le\xi_m^2+\xi_p^2\ . \end{cases}
\end{aligned}
$$

As a technical detail one can take directly the derivative of eq. (C.18) with respect to A for a given interval. The different intervals do not imply the appearance of delta functions of A while differentiating.

C.2.4 Particle–hole representation of L_{10}

In eq. (C.1) we have choosen the representation of the in-medium propagators with the free-space and density-dependent parts. One can also write down the integral in the particle–hole representation of eq. (3.9)

$$
\begin{aligned}
L_{10} &= i\int\frac{d^4k}{(2\pi)^4}\,G_0(P-k)_aG_0(P+k)_b\\
&= -\int\frac{d^3k}{(2\pi)^3}\left[\frac{\theta(\xi_a-|\mathbf{P}-\mathbf{k}|)\theta(\xi_b-|\mathbf{P}+\mathbf{k}|)}{2P^0-E_{\mathbf{P}-\mathbf{k}}-E_{\mathbf{P}+\mathbf{k}}-i\epsilon}-\frac{\theta(|\mathbf{P}-\mathbf{k}|-\xi_a)\theta(|\mathbf{P}+\mathbf{k}|-\xi_b)}{2P^0-E_{\mathbf{P}-\mathbf{k}}-E_{\mathbf{P}+\mathbf{k}}+i\epsilon}\right]\\
&= m\int\frac{d^3k}{(2\pi)^3}\left[\frac{\theta(\xi_a-|\mathbf{P}-\mathbf{k}|)\theta(\xi_b-|\mathbf{P}+\mathbf{k}|)}{\mathbf{k}^2-A+i\epsilon}-\frac{\theta(|\mathbf{P}-\mathbf{k}|-\xi_a)\theta(|\mathbf{P}+\mathbf{k}|-\xi_b)}{\mathbf{k}^2-A-i\epsilon}\right]\\
&\doteq L_{10,hh}+L_{10,pp}\ . \qquad \text{(C.19)}
\end{aligned}
$$

During the k^0-integration the terms with all poles on the same half plane have been avoided by closing the integration contour on the opposite half plane. In this way, the mixed terms of particles and holes give zero. For the remaining two terms we have picked up one arbitrary pole each time. Finally we made use of eq. (5.30).

Performing the three-momentum integration for $L_{10,hh}$ is straightforward

$$
\begin{aligned}
L_{10,hh}(A,P,\xi_a,\xi_b) = -\frac{m}{16\pi^2P}\Bigg\{&2P(2P-\xi_a-\xi_b)+2P\sqrt{A}\Bigg[\ln\left(\frac{\sqrt{A}-P+\xi_a}{\sqrt{A}+P-\xi_a}\right)\\
&+\ln\left(\frac{\sqrt{A}-P+\xi_b}{\sqrt{A}+P-\xi_b}\right)\Bigg]+(A+P^2-\xi_a^2)\ln\left(\frac{A+P^2-(\xi_a^2+\xi_b^2)/2}{A-(P-\xi_a)^2}\right)\\
&+(A+P^2-\xi_b^2)\ln\left(\frac{A+P^2-(\xi_a^2+\xi_b^2)/2}{A-(P-\xi_b)^2}\right)\Bigg\}\ .
\end{aligned}
$$

The Feynman prescription $A-i\epsilon$ has to be kept in mind while evaluating the logarithms numerically.

The integral $L_{10,pp}$ has to be regularized. The easiest way to handle this, is to ascribe the integration to already calculated quantities by using

$$\theta(|\mathbf{P}-\mathbf{k}|-\xi_a)\theta(|\mathbf{P}+\mathbf{k}|-\xi_b) = \big[1-\theta(\xi_a-|\mathbf{P}-\mathbf{k}|)\big]\big[1-\theta(\xi_b-|\mathbf{P}+\mathbf{k}|)\big] \ , \tag{C.20}$$

and we obtain

$$L_{10,pp}(A,P,\xi_a,\xi_b) = L_{10,f} + L_{10,m} - \mathrm{Re}L_{10,hh} + i\,\mathrm{Im}L_{10,hh} \ . \tag{C.21}$$

The sign switch of the imaginary part from $L_{10,hh}$ stems from the different position of the pole.

C.3 The loop integral L_{11}

We now consider the integrals defined in eq. (C.2) and evaluate L_{11} according to the number of in-medium insertions.

C.3.1 Free part $L_{11,f}$

After performing the k^0-integration by applying Cauchy's theorem we are left for the free part with

$$\begin{aligned} L_{11,f}(A,p) &= -m\int\frac{d^3k}{(2\pi)^3}\frac{1}{\mathbf{k}^2-A-i\epsilon}\frac{1}{(\mathbf{k}+\mathbf{p})^2+m_\pi^2} \\ &= -\frac{m}{8\pi}\int_0^1 dx\frac{1}{[\mathbf{p}^2x(1-x)+m_\pi^2x-A(1-x)-i\epsilon]^{1/2}} \\ &= -\frac{im}{8\pi p}\ln\left(\frac{A+(m_\pi-ip)^2}{m_\pi^2+(\sqrt{A}-p)^2}\right) \ . \end{aligned} \tag{C.22}$$

In the previous equation, we have introduced a Feynman integration parameter x as an intermediate step and used that $\sqrt{-a\pm i\epsilon} = \pm i\sqrt{a}$ for $a>0$.

C.3.2 One in-medium insertion $L_{11,m}$

For the case of one in-medium insertion, the k^0-integration is straightforward due to the presence of the energy Dirac delta-function

$$L_{11,m} = m\int\frac{d^3k}{(2\pi)^3}\frac{\theta(\xi_a-|\mathbf{P}-\mathbf{k}|)+\theta(\xi_b-|\mathbf{P}+\mathbf{k}|)}{\mathbf{k}^2-A-i\epsilon}\frac{1}{(\mathbf{k}+\mathbf{p})^2+m_\pi^2} \ . \tag{C.23}$$

Both terms in the sum can be obtained from the function

$$l_{11,m} = m\int\frac{d^3k}{(2\pi)^3}\frac{\theta(\xi_i-|\mathbf{P}-\mathbf{k}|)}{\mathbf{k}^2-A-i\epsilon}\frac{1}{(\mathbf{k}+\mathbf{p})^2+m_\pi^2} \ . \tag{C.24}$$

Let us work out the scalar product $\mathbf{k}\cdot\mathbf{p}$. For the integration, we introduce the reference frame

$$\begin{aligned} \hat{\mathbf{z}} &= \hat{\mathbf{P}} \ , \\ \hat{\mathbf{x}} &= \frac{\mathbf{P}\times\mathbf{p}}{|\mathbf{P}||\mathbf{p}|\sin\beta} \ , \\ \hat{\mathbf{y}} &= \hat{\mathbf{z}}\times\hat{\mathbf{x}} = \hat{\mathbf{P}}\cot\beta - \hat{\mathbf{p}}\csc\beta \ . \end{aligned} \tag{C.25}$$

From the last relation we have,

$$\begin{aligned}\hat{\mathbf{p}} &= \hat{\mathbf{P}}\,\cos\beta - \hat{\mathbf{y}}\sin\beta\ ,\\ \mathbf{k}\cdot\mathbf{p} &= |\mathbf{k}||\mathbf{p}|(\cos\theta\cos\beta - \sin\theta\sin\phi\sin\beta)\ ,\end{aligned} \tag{C.26}$$

with θ and ϕ integration variables in eq. (C.24) and $\cos\beta = \hat{\mathbf{p}}\cdot\hat{\mathbf{P}}$. Let us perform the ϕ-integration,

$$\frac{1}{2\pi}\int_0^{2\pi} d\phi \frac{1}{\mathbf{p}^2+\mathbf{k}^2+2\mathbf{k}\cdot\mathbf{p}+m_\pi^2} = \frac{1}{\sqrt{a^2-b^2}}\ . \tag{C.27}$$

In eq. (C.27) we have

$$\begin{aligned}a &= \delta + 2|\mathbf{k}||\mathbf{p}|\cos\beta\cos\theta\ ,\\ b &= -2|\mathbf{k}||\mathbf{p}|\sin\beta\sin\theta\ ,\\ \delta &= \mathbf{k}^2+\mathbf{p}^2+m_\pi^2\ ,\end{aligned} \tag{C.28}$$

where $\sin\beta = \sqrt{1-\cos^2\beta}$. Next, we move to the $\cos\theta$ integration of eq. (C.24). For this integration one has to take into account the presence of the Heaviside step function, which implies conditions on the boundaries already worked out in eq. (C.9). The latter determines an interval of integration for $\cos\theta \in [x_1(|\mathbf{k}|), x_2(|\mathbf{k}|)]$ for a given value of $|\mathbf{k}|$. Then we can write

$$\begin{aligned}\int_{x_1}^{x_2} d\cos\theta \frac{1}{\sqrt{a^2-b^2}} &= \int_{x_1}^{x_2} d\cos\theta \frac{1}{\sqrt{c+d\cos\theta+e^2\cos^2\theta}}\\ &= \frac{1}{e}\ln\Big(d+2e^2\cos\theta+2e\sqrt{\mathcal{C}}\Big)\Big|_{x_1}^{x_2}\ ,\end{aligned} \tag{C.29}$$

with

$$\begin{aligned}c &= \delta^2 - e^2\sin^2\beta\ ,\\ d &= 2e\delta\cos\beta\ ,\\ e &= 2kp\ ,\\ \mathcal{C} &= c + d\cos\theta + e^2\cos^2\theta\ .\end{aligned} \tag{C.30}$$

Now, we consider the final integration on $|\mathbf{k}|$ in eq. (C.23) and define the auxiliary function

$$f_{11}(k,p,\cos\beta) = \frac{1}{e}\ln\Big(d+2e\big(e\cos\theta+\sqrt{\mathcal{C}}\big)\Big)\ . \tag{C.31}$$

In terms of this eq. (C.24) reads

$$l_{11,m}(A,p,P,\cos\beta,\xi_i) = SFS\big[f_{11}(k,p,\cos\beta)\big]\ , \tag{C.32}$$

with $SFS[\cdot]$ defined in eq. (C.9). Then from eq. (C.23) one has

$$L_{11,m}(A,p,P,\cos\beta,\xi_a,\xi_b) = l_{11,m}(A,p,P,\cos\beta,\xi_a) + l_{11,m}(A,p,P,-\cos\beta,\xi_b)\ . \tag{C.33}$$

C.3.3 Two in-medium insertions $L_{11,d}$

If two in-medium insertions are present, the integration over $|\mathbf{k}|$ can be done straightforwardly taking into account the additional Dirac delta-function of the energy that fixes $|\mathbf{k}| = \sqrt{A}$. Then,

$$\begin{aligned} L_{11,d} &= -im \int \frac{d^3k}{(2\pi)^2} \delta\big(\mathbf{k}^2 - A\big) \frac{\theta(\xi_a - |\mathbf{P}-\mathbf{k}|)\theta(\xi_b - |\mathbf{P}+\mathbf{k}|)}{(\mathbf{k}+\mathbf{p})^2 + m_\pi^2} \\ &= -\frac{im\sqrt{A}}{8\pi^2} \int d\hat{\mathbf{k}} \frac{\theta(\xi_a - |\mathbf{P}-\hat{\mathbf{k}}\sqrt{A}|)\theta(\xi_b - |\mathbf{p}+\hat{\mathbf{k}}\sqrt{A}|)}{(\mathbf{k}+\mathbf{p})^2 + m_\pi^2} \ . \end{aligned} \tag{C.34}$$

We have the same ϕ-integration as in eq. (C.27), with the same result but now with $|\mathbf{k}| = \sqrt{A}$. The integration over $\cos\theta$ is the same as in eq. (C.29), though with a different integration interval for $\cos\theta$ that is fixed by the values of A and $|\mathbf{P}|$, according to eq. (C.13). We can use again the auxiliary function f_{11}, eq. (C.31), with $|\mathbf{k}|$ set to $\sqrt{A}$. In this way we can write

$$L_{11,d}(A, p, P, \cos\beta, \xi_a, \xi_b) = TFS\big[f_{11}(\sqrt{A}, p, \cos\beta)\big] \ , \tag{C.35}$$

with $TFS[\cdot]$ defined in eq. (C.13).

C.4 The loop integral L_{12}

Here, we wish to discuss the calculation of the basic scalar integral L_{12}. In the expressions that follow it is always assumed that the k^0-integration has been done either by using Cauchy's theorem, for the free part, or employing the energy Dirac delta-functions from the in-medium insertions. Since two pion propagators are involved we combine them introducing a Feynman parameter

$$\frac{1}{[(\mathbf{k}+\mathbf{p}')^2 + m_\pi^2][(\mathbf{k}+\mathbf{p})^2 + m_\pi^2]} = \int_0^1 dy \frac{1}{[(\mathbf{k} + \vec{\lambda}(y))^2 + \Delta^2(y)]^2} \ , \tag{C.36}$$

with

$$\vec{\lambda}(y) = y\mathbf{p} + (1-y)\mathbf{p}' \ , \tag{C.37}$$

$$\Delta^2(y) = m_\pi^2 + 2\mathbf{p}^2 y(1-y)(1-\cos\varphi) \ , \tag{C.38}$$

$$\lambda \doteq |\vec{\lambda}| = p\sqrt{1 - 2y(1-y)(1-\cos\varphi)} \ , \tag{C.39}$$

where $\cos\varphi = \hat{\mathbf{p}} \cdot \hat{\mathbf{p}}'$. In order to apply the results already derived in appendix C.3, where only one pion propagator was involved, we take into account that

$$\frac{1}{[(\mathbf{k} + \vec{\lambda}(y))^2 + \Delta^2(y)]^2} = -\frac{\partial}{\partial m_\pi^2} \frac{1}{(\mathbf{k} + \vec{\lambda}(y))^2 + \Delta^2(y)} \ , \tag{C.40}$$

as it follows from the definition of Δ^2 in eq. (C.38).

C.4.1 Free part $L_{12,f}$

For the free part

$$L_{12,f}(A, p, \cos\varphi) = m \frac{\partial}{\partial m_\pi^2} \int_0^1 dy \int \frac{d^3k}{(2\pi)^3} \frac{1}{\mathbf{k}^2 - A - i\epsilon} \frac{1}{(\mathbf{k} + \vec{\lambda}(y))^2 + \Delta^2(y)} \ . \tag{C.41}$$

The integration over $\mathbf{k}$ was already done in eq. (C.22). Making use of this result and performing the derivative with respect to the pion mass afterwards one obtains

$$L_{12,f}(A,p,\cos\varphi) = -\frac{m}{8\pi}\int_0^1 dy \frac{1}{\Delta}\frac{1}{m_\pi^2+p^2-A-2i\Delta\sqrt{A}} \ , \tag{C.42}$$

where $\Delta = \sqrt{\Delta^2(y)}$.

C.4.2 One in-medium insertion $L_{12,m}$

For the part with one in-medium insertion

$$L_{12,m} = m\int \frac{d^3k}{(2\pi)^3}\frac{\theta(\xi_a-|\mathbf{P}-\mathbf{k}|)+\theta(\xi_b-|\mathbf{P}+\mathbf{k}|)}{\mathbf{k}^2-A-i\epsilon}\frac{1}{(\mathbf{k}+\mathbf{p})^2+m_\pi^2}\frac{1}{(\mathbf{k}+\mathbf{p}')^2+m_\pi^2} \ . \tag{C.43}$$

The two terms in the sum can be obtained from the function

$$l_{12,m} = m\int_0^1 dy\int \frac{d^3k}{(2\pi)^3}\frac{\theta(\xi_i-|\mathbf{P}-\mathbf{k}|)}{\mathbf{k}^2-A-i\epsilon}\frac{1}{[(\mathbf{k}+\vec{\lambda}(y))^2+\Delta^2(y)]^2} \ . \tag{C.44}$$

This integral is analogous to $l_{11,m}$ in eq. (C.24), but with $\mathbf{p}$ and m_π replaced by $\vec{\lambda}(y)$ and $\Delta(y)$, in that order. Furthermore the second propagator appears squared. Following the calculation of $l_{11,m}$, we adopt the reference frame

$$\begin{aligned}
\hat{\mathbf{z}} &= \hat{\mathbf{P}} \ , \\
\hat{\mathbf{x}} &= \frac{\mathbf{P}\times\vec{\lambda}}{|\mathbf{P}||\vec{\lambda}|\sin\eta} \ , \\
\hat{\mathbf{y}} &= \hat{\mathbf{z}}\times\hat{\mathbf{x}} = \hat{\mathbf{P}}\cot\eta - \hat{\lambda}\csc\eta \ .
\end{aligned} \tag{C.45}$$

With

$$\cos\eta = \frac{\mathbf{P}\cdot\vec{\lambda}}{|\mathbf{P}||\vec{\lambda}|} = \frac{|\mathbf{p}|}{|\vec{\lambda}|}\left[y\cos\beta+(1-y)\cos\beta'\right] \ , \tag{C.46}$$

we obtain the scalar product

$$\mathbf{k}\cdot\vec{\lambda} = |\mathbf{k}||\vec{\lambda}|(\cos\theta\cos\eta-\sin\theta\sin\phi\sin\eta) \ , \tag{C.47}$$

where θ and ϕ are the polar and azimuthal angles of $\mathbf{k}$. Let us perform the ϕ-integration in eq. (C.43)

$$\begin{aligned}
&\frac{1}{2\pi}\int_0^{2\pi} d\phi \frac{1}{[(\mathbf{k}+\vec{\lambda})^2+\Delta^2]^2} = \frac{1}{2\pi}\int_0^{2\pi} d\phi \frac{1}{\left[\mathbf{k}^2+\vec{\lambda}^2+\Delta^2+2|\mathbf{k}||\vec{\lambda}|(\cos\theta\cos\eta-\sin\theta\sin\phi\sin\eta)\right]^2} \\
&= \frac{-1}{2|\lambda||\mathbf{k}|\cos\theta}\frac{\partial}{\partial\cos\eta}\frac{1}{2\pi}\int_0^{2\pi} d\phi \frac{1}{\mathbf{k}^2+\vec{\lambda}^2+\Delta^2+2|\mathbf{k}||\vec{\lambda}|(\cos\theta\cos\eta-\sin\theta\sin\phi\sin\eta)} \ .
\end{aligned} \tag{C.48}$$

The last integral is of the type already evaluated in eq. (C.27) where now

$$\begin{aligned}
a &= \delta + 2|\vec{\lambda}||\mathbf{k}|\cos\theta\cos\eta \ , \\
b &= -2|\vec{\lambda}||\mathbf{k}|\sin\theta\sin\eta \ , \\
\delta &= \mathbf{k}^2+\vec{\lambda}^2+\Delta^2 = \mathbf{k}^2+\mathbf{p}^2+m_\pi^2 \ ,
\end{aligned} \tag{C.49}$$

as in eq. (C.28). Then, eq. (C.48) reads

$$\frac{1}{2\pi}\int_0^{2\pi} d\phi \frac{1}{[(\mathbf{k}+\vec{\lambda})^2+\Delta^2]^2} = \frac{\delta + 2|\vec{\lambda}||\mathbf{k}|\cos\eta\cos\theta}{\Big[4\vec{\lambda}^2\mathbf{k}^2(\cos^2\theta-\sin^2\eta)+4|\vec{\lambda}||\mathbf{k}|\delta\cos\eta\cos\theta+\delta^2\Big]^{3/2}} \ . \tag{C.50}$$

The $\cos\theta$ integration of the previous result includes the Heaviside step function in eq. (C.43) that fixes the limits of integration to x_1 and x_2 given by eq. (C.9). This integration is straightforward, see e.g. the similar one of eq. (C.29). Then, our result for $l_{12,m}$ is

$$l_{12,m}(A,p,P,\cos\varphi,\cos\beta,\cos\beta',\xi_i) = SFS\big[f_{12}(k,p,\cos\varphi,\cos\beta,\cos\beta')\big] \ , \tag{C.51}$$

with $SFS[\cdot]$ defined in eq. (C.9). Here we have used the auxiliary function

$$f_{12}(k,p,\cos\varphi,\cos\beta,\cos\beta') = \int_0^1 dy \frac{e\cos\eta+\delta\cos\theta}{(\delta^2-e^2)\sqrt{\mathcal{C}}} \ , \tag{C.52}$$

where

$$\begin{aligned} c &= \delta^2 - e^2\sin^2\eta \ , \\ d &= 2e\delta\cos\eta \ , \\ e &= e = 2q|\vec{\lambda}| \ , \\ \mathcal{C} &= c + d\cos\theta + e^2\cos^2\theta \ . \end{aligned} \tag{C.53}$$

For the function $L_{12,m}$ of eq. (C.43) we have

$$\begin{aligned} L_{12,m}(A,p,P,\cos\varphi,\cos\beta,\cos\beta',\xi_a,\xi_b) &= l_{12,m}(A,p,P,\cos\varphi,\cos\beta,\cos\beta',\xi_a) \\ &\quad + l_{12,m}(A,p,P,\cos\varphi,-\cos\beta,-\cos\beta',\xi_b) \ . \end{aligned} \tag{C.54}$$

C.4.3 Two in-medium insertions $L_{12,d}$

The part with two in-medium insertions is given by

$$\begin{aligned} L_{12,d} &= -im\int \frac{d^3k}{(2\pi)^2}\delta\big(\mathbf{k}^2-A\big)\frac{\theta(\xi_a-|\mathbf{P}-\mathbf{k}|)\theta(\xi_b-|\mathbf{P}+\mathbf{k}|)}{[(\mathbf{k}+\mathbf{p}')^2+m_\pi^2][(\mathbf{k}+\mathbf{p})^2+m_\pi^2]} \\ &= -i\frac{m\sqrt{A}}{8\pi^2}\int d\hat{\mathbf{k}}\frac{\theta(\xi_a-|\mathbf{P}-\hat{\mathbf{k}}\sqrt{A}|)\theta(\xi_b-|\mathbf{P}+\hat{\mathbf{k}}\sqrt{A}|)}{[(\mathbf{k}+\mathbf{p}')^2+m_\pi^2][(\mathbf{k}+\mathbf{p})^2+m_\pi^2]} \ . \end{aligned} \tag{C.55}$$

The angular integrations are of the same type as already developed for the case of the one in-medium insertion in subsection C.4.2 whereupon the integration limits are dictated by the two Heaviside step functions. In terms of those we can write

$$L_{12,d}(A,p,P,\cos\varphi,\cos\beta,\cos\beta',\xi_a,\xi_b) = TFS\big[f_{12}(\sqrt{A},p,\cos\varphi,\cos\beta,\cos\beta')\big] \ , \tag{C.56}$$

with f_{12} given in eq. (C.52) and $TFS[\cdot]$ defined in eq. (C.13).

C.5 The loop integrals L_{01} and L_{02}

In this section we present the results from the analytic integration of the scalar loop integrals defined in eqs. (C.4)–(C.7).

C.5.1 Free scalar integral $L_{01,f}$

The integral in eq. (C.4) can be solved correspondingly to the integral $L_{10,f}$ in eq. (C.14) giving

$$L_{01,f} = -\frac{m_\pi}{4\pi} - \frac{g_0}{m} \ . \tag{C.57}$$

If $L_{01,f}$ were evaluated with Dimensional Regularization one would obtain only the first term in eq. (C.57). This result lacks physical meaning since $L_{01,f}$ would then be negative, while the integrand is positive.

C.5.2 One in-medium scalar integral $L_{01,m}$

The contribution from one in-medium insertion over a pion propagator, eq. (C.5), reads

$$\begin{aligned} L_{01,m}(p,P,\cos\beta,\xi_a,\xi_b) &= \int \frac{d^3k}{(2\pi)^3} \frac{\theta\big(\xi_a - |\mathbf{k}-\mathbf{P}|\big) + \theta\big(\xi_b - |\mathbf{k}+\mathbf{P}|\big)}{(\mathbf{k}+\mathbf{p})^2 + m_\pi^2} \\ &= l_{01,m}(p,P,\cos\beta,\xi_a) + l_{01,m}(p,P,-\cos\beta,\xi_b) \ . \end{aligned} \tag{C.58}$$

The integral can be evaluated by performing the shift $\mathbf{k} \to \mathbf{k} - \mathbf{p}$ and taking $\mathbf{p}_{2/1} = \mathbf{P} \pm \mathbf{p}$ which yields for both contributions

$$l_{01,m}(p,P,\cos\beta,\xi_i) = \frac{m_\pi}{4\pi^2}\left\{ u - \arctan(u+z) - \arctan(u-z) + \frac{1+u^2-z^2}{4z} \ln\left(\frac{(u+z)^2+1}{(u-z)^2+1}\right)\right\} , \tag{C.59}$$

with the abbreviations $u \doteq \xi_i/m_\pi$ and $z(\cos\beta) \doteq \sqrt{P^2+p^2+2Pp\cos\beta}/m_\pi$.

C.5.3 Free scalar integral $L_{02,f}$

The two pion propagators of the integral eq. (C.6) can be combined in a common expression described in the prelude of section C.4. Thus we have

$$\begin{aligned} L_{02,f}(p,\cos\varphi) &= \int_0^1 dy \, \frac{-\partial}{\partial m_\pi^2} \int \frac{d^3k}{(2\pi)^3} \frac{1}{(\mathbf{k}+\vec{\lambda}(y))^2 + \Delta(y)^2} \\ &= \frac{1}{8\pi} \int_0^1 \frac{dy}{\Delta(y)} \\ &= \frac{1}{4\pi p\sqrt{2(1-\cos\varphi)}} \arcsin\left(\frac{p\sqrt{1-\cos\varphi}}{\sqrt{2m_\pi^2 + p^2(1-\cos\varphi)}}\right) \ , \end{aligned} \tag{C.60}$$

where $\vec{\lambda}(y)$ and $\Delta(y)$ were defined in eqs. (C.37)–(C.38). Here we made use of the calculation of $L_{01,f}$ in eq. (C.57) as an intermediate step. The dependence on the subtraction constant vanishes under the assumption that the subtraction constant is independent of the pion mass.

C.5.4 One in-medium scalar integral $L_{02,m}$

For the integral with two pion propagators and one in-medium insertion, eq. (C.7), we also combine the pion propagators in one common expression according to the description in the prelude of section C.4.

$$\begin{aligned} L_{02,m}(p,P,\cos\varphi,\cos\beta,\cos\beta',\xi_a,\xi_b) &= \int_0^1 dy\,\frac{-\partial}{\partial m_\pi^2}\int\frac{d^3k}{(2\pi)^3}\frac{\theta\big(\xi_a-|\mathbf{k}-\mathbf{P}|\big)+\theta\big(\xi_b-|\mathbf{k}+\mathbf{P}|\big)}{(\mathbf{k}+\vec{\lambda}(y))^2+\Delta^2(y)} \\ &= l_{02,m}(p,P,\cos\varphi,\cos\beta,\cos\beta',\xi_a)+l_{02,m}(p,P,\cos\varphi,-\cos\beta,-\cos\beta',\xi_b)\ . \end{aligned} \tag{C.61}$$

This integral corresponds to $L_{01,m}$ evaluated in eq. (C.59), but in terms of $\vec{\lambda}(y)$ and $\Delta(y)$. Consequently, we perform the shift $\mathbf{k}\to\mathbf{k}-\vec{\lambda}(y)$ such that, defining the abbreviation $\vec{\lambda}_{2/1}(y)\doteq\mathbf{P}\pm\vec{\lambda}(y)$, we can write

$$\begin{aligned} l_{02,m}(p,P,\cos\varphi,\pm\cos\beta,\pm\cos\beta',\xi_{a/b}) &= \int_0^1 dy\,\frac{-\partial}{\partial m_\pi^2}\int\frac{d^3k}{(2\pi)^3}\frac{\theta\big(\xi_{a/b}-|\mathbf{k}\mp\vec{\lambda}_{2/1}|\big)}{\mathbf{k}^2+\Delta(y)^2} \\ &= \int_0^1 dy\,\frac{-\partial}{\partial m_\pi^2}\Big[l_{01,m}(\lambda,P,\pm\cos\eta,\xi_{a/b})\big|_{m_\pi\to\Delta}\Big] \\ &= \frac{1}{8\pi^2}\int_0^1 dy\,f_{02}(\lambda_{2/1},\Delta,\xi_{a/b})\ , \end{aligned} \tag{C.62}$$

where $\cos\eta$ has been defined in eq. (C.46). In the function $l_{01,m}$, eq. (C.59), the quantities p, $\cos\beta$ and m_π has been replaced by $\lambda(y)$, $\cos\eta(y)$ and $\Delta(y)$, respectively. Performing the derivative with respect to the pion mass squared, we can define the auxiliary function

$$f_{02}(\lambda_{2/1},\Delta,\xi_i)\doteq\frac{1}{\Delta}\left\{\arctan(u+z)+\arctan(u-z)-\frac{1}{2z}\ln\left(\frac{(u+z)^2+1}{(u-z)^2+1}\right)\right\}\ , \tag{C.63}$$

with $u\doteq\xi_i/\Delta$ and $z\doteq\lambda_{2/1}/\Delta=\sqrt{P^2+\lambda^2\pm2P\lambda\cos\eta}/\Delta$.

C.6 Derivatives of the scalar integrals

For the calculations of some in-medium corrections, i.e. for the chiral quark condensate or the pion self-energy, one needs the derivatives of all the integrals with respect to A or m_π^2. Here we only give those, which can be obtained by simple analytic calculations. All remaining derivatives have to be obtained numerically. The derivatives with respect to A read

$$\frac{m\partial}{\partial A}L_{10,f}=-\frac{im^2}{8\pi\sqrt{A}}\ , \tag{C.64}$$

$$\frac{m\partial}{\partial A}l_{10,m}=-\frac{m^2}{8\pi^2\sqrt{A}}\left\{\operatorname{arctanh}(u-z)+\operatorname{arctanh}(u+z)+\frac{1}{2z}\ln\left(\frac{(u+z)^2-1}{(u-z)^2-1}\right)\right\}\ , \tag{C.65}$$

$$\frac{m\partial}{\partial A}L_{10,d}=\frac{im^2}{8\pi P\sqrt{A}}\cdot\begin{cases}-2P & ,\ 0\le\sqrt{A}\le\xi_m-P\ , \\ \sqrt{A}-P & ,\ |\xi_m-P|<\sqrt{A}\le\min(\xi_m+P,\xi_p-P)\ , \\ 2\sqrt{A} & ,\ \xi_p-P<\sqrt{A}\le\xi_m+P\ \wedge\ 2(P^2+A)\le\xi_m^2+\xi_b^2\ , \end{cases} \tag{C.66}$$

$$\frac{m\partial}{\partial A}L_{11,f}=-\frac{im^2}{8\pi\sqrt{A}}\frac{1}{p^2+(m_\pi-i\sqrt{A})^2}\ , \tag{C.67}$$

$$\frac{m\partial}{\partial A}L_{12,f} = -\frac{m^2}{8\pi\sqrt{A}}\int_0^1 dy \frac{1}{\Delta(y)}\frac{\sqrt{A}+i\Delta(y)}{\left(m_\pi^2+p^2-A-2i\sqrt{A}\Delta(y)\right)^2} \ , \tag{C.68}$$

$$\frac{m\partial}{\partial A}L_{01} = 0 \ , \tag{C.69}$$

$$\frac{m\partial}{\partial A}L_{02} = 0 \ , \tag{C.70}$$

and the derivatives with respect to the pion mass squared read

$$\frac{\partial}{\partial m_\pi^2}L_{01,f} = -\frac{1}{8\pi m_\pi} \ , \tag{C.71}$$

$$\frac{\partial}{\partial m_\pi^2}L_{10} = 0 + \mathcal{O}(q) \ , \tag{C.72}$$

$$\frac{\partial}{\partial m_\pi^2}L_{11,f} = \frac{m}{8\pi m_\pi}\frac{1}{p^2+(m_\pi-i\sqrt{A})^2} \ , \tag{C.73}$$

$$\frac{\partial}{\partial m_\pi^2}L_{12,f} = \frac{m}{16\pi}\int_0^1 dy \frac{m_\pi^2+p^2-A+2\Delta(y)\left(\Delta(y)-2i\sqrt{A}\right)}{\Delta(y)^3\left(m_\pi^2+p^2-A-2i\sqrt{A}\Delta(y)\right)^2} \ , \tag{C.74}$$

where the pion mass dependence of the nucleon mass has not been taken into account, because it is two chiral orders higher. In case, abbreviations have to be looked up in the corresponding subsection where the basic integral has been calculated.

Appendix D

Tensor integrals

In this appendix we present the decompositions and reductions of tensor loop integrals, which are needed for our calculations of the in-medium nucleon-nucleon interactions.

D.1 Decompositions of the tensor integrals

In the following, we give the decompositions of all occuring tensorial loop integrals into a combination of kinematic structures and reduced scalar integrals. The appearing momenta are defined in the beginning of appendix C.

$$
\begin{aligned}
L_{10}^{k} &\doteq i\int \frac{d^4k}{(2\pi)^4}\,\mathbf{k}^k\, G_0(k_1)_a G_0(k_2)_b \\
&\doteq P^k\, L_{10}^{P}\ , && \text{(D.1)}\\
L_{11}^{k} &\doteq i\int \frac{d^4k}{(2\pi)^4}\,\frac{\mathbf{k}^k}{(\mathbf{k}+\mathbf{p})^2+m_\pi^2} G_0(k_1)_a G_0(k_2)_b \\
&\doteq p^k\, L_{11}^{p} + P^k\, L_{11}^{P}\ , && \text{(D.2)}\\
L_{11}^{kl} &\doteq i\int \frac{d^4k}{(2\pi)^4}\,\frac{\mathbf{k}^k\mathbf{k}^l}{(\mathbf{k}+\mathbf{p})^2+m_\pi^2} G_0(k_1)_a G_0(k_2)_b \\
&\doteq \delta^{kl}\, L_{11}^{00} + p^k p^l\, L_{11}^{pp} + P^k P^l\, L_{11}^{PP} + (P^k p^l + p^k P^l)\, L_{11}^{Pp}\ , && \text{(D.3)}\\
L_{12}^{k} &\doteq i\int \frac{d^4k}{(2\pi)^4}\,\frac{\mathbf{k}^k}{[(\mathbf{k}+\mathbf{p})^2+m_\pi^2][(\mathbf{k}+\mathbf{p}')^2+m_\pi^2]} G_0(k_1)_a G_0(k_2)_b \\
&\doteq p^k\, L_{12}^{p} + p'^k\, L_{12}^{p'} + P^k\, L_{12}^{P}\ , && \text{(D.4)}\\
L_{12}^{kl} &\doteq i\int \frac{d^4k}{(2\pi)^4}\,\frac{\mathbf{k}^k\mathbf{k}^l}{[(\mathbf{k}+\mathbf{p})^2+m_\pi^2][(\mathbf{k}+\mathbf{p}')^2+m_\pi^2]} G_0(k_1)_a G_0(k_2)_b \\
&\doteq p^k p^l\, L_{12}^{pp} + p'^k p'^l\, L_{12}^{p'p'} + (p^k p'^l + p'^k p^l)\, L_{12}^{pp'} \\
&\quad + P^k P^l\, L_{12}^{PP} + (P^k p^l + p^k P^l)\, L_{12}^{Pp} + (P^k p'^l + p'^k P^l)\, L_{12}^{Pp'}\ , && \text{(D.5)}\\
L_{12}^{(2)k} &\doteq i\int \frac{d^4k}{(2\pi)^4}\,\frac{\mathbf{k}^2\mathbf{k}^k}{[(\mathbf{k}+\mathbf{p})^2+m_\pi^2][(\mathbf{k}+\mathbf{p}')^2+m_\pi^2]} G_0(k_1)_a G_0(k_2)_b \\
&\doteq p^k\, L_{12}^{(2)p} + p'^k\, L_{12}^{(2)p'} + P^k\, L_{12}^{(2)P}\ , && \text{(D.6)}
\end{aligned}
$$

$$L_{01}^{k} \doteq \int \frac{d^3k}{(2\pi)^3} \frac{\mathbf{k}^k}{(\mathbf{k}+\mathbf{p})^2+m_\pi^2} \Big[1+\theta(\xi_a-|\mathbf{k}_1|)+\theta(\xi_b-|\mathbf{k}_2|)\Big]$$
$$\doteq p^k\, L_{01}^{p} \ , \tag{D.7}$$
$$L_{02}^{k} \doteq \int \frac{d^3k}{(2\pi)^3} \frac{\mathbf{k}^k}{[(\mathbf{k}+\mathbf{p})^2+m_\pi^2][(\mathbf{k}+\mathbf{p}')^2+m_\pi^2]} \Big[1+\theta(\xi_a-|\mathbf{k}_1|)+\theta(\xi_b-|\mathbf{k}_2|)\Big]$$
$$\doteq p^k\, L_{02}^{p} + p'^k\, L_{02}^{p'} + P^k\, L_{02}^{P} \ . \tag{D.8}$$

The procedure for obtaining the reduced scalar integrals is always the same: one multiplies each of the decompositions with every occuring kinematic structure and evaluates both sides. After that, one can solve the system of linear equations for the reduced scalar integrals.

Also there are scalar integrals with additional structures

$$L_{12}^{(2)} \doteq i \int \frac{d^4k}{(2\pi)^4} \frac{\mathbf{k}^2}{[(\mathbf{k}+\mathbf{p})^2+m_\pi^2][(\mathbf{k}+\mathbf{p}')^2+m_\pi^2]} G_0(k_1)_a G_0(k_2)_b \ , \tag{D.9}$$
$$L_{12}^{(4)} \doteq i \int \frac{d^4k}{(2\pi)^4} \frac{\mathbf{k}^4}{[(\mathbf{k}+\mathbf{p})^2+m_\pi^2][(\mathbf{k}+\mathbf{p}')^2+m_\pi^2]} G_0(k_1)_a G_0(k_2)_b \ , \tag{D.10}$$
$$L_{02}^{(2)} \doteq \int \frac{d^3k}{(2\pi)^3} \frac{\mathbf{k}^2}{[(\mathbf{k}+\mathbf{p})^2+m_\pi^2][(\mathbf{k}+\mathbf{p}')^2+m_\pi^2]} \Big[1+\theta(\xi_a-|\mathbf{k}_1|)+\theta(\xi_b-|\mathbf{k}_2|)\Big] \ . \tag{D.11}$$

These can simply be reduced to already known scalar integrals.

All scalar integrals consist of free, one and two in-medium contributions. In the following, those contributions will be denoted by a third index, where f(ree) stands for no insertion, m(edium) for one insertion and d(ouble) for two insertions. Note that the decomposition and reduction can be done separately for the three contributions. The derivation of the reduced scalar integrals will be performed in the subsequent sections. For the whole appendix we define the abbreviations $c\alpha \doteq \cos\alpha$ and $s\alpha \doteq \sqrt{1-c\alpha^2}$ for all occuring angles.

D.2 Reduced scalar integrals of L_{10}

D.2.1 Reduction of L_{10}^{k}

Free part, $L_{10,f}^{k}$

The free contribution of the decomposition in eq. (D.1) vanishes for symmetry reasons

$$L_{10,f}^{P}(A) = -\frac{m}{\mathbf{P}^2} \int \frac{d^3k}{(2\pi)^3} \frac{\mathbf{P}\cdot\mathbf{k}}{\mathbf{k}^2-A-i\epsilon} = 0 \ , \tag{D.12}$$

since the free integrals are Galilei invariant such that P can be chosen arbitrarily.

One in-medium insertion, $L_{10,m}^{k}$

The one in-medium contribution from eq. (D.1) can be expressed in terms of

$$L_{10,m}^{P}(A,P,\xi_a,\xi_b) = l_{10,m}^{P}(A,P,\xi_a) - l_{10,m}^{P}(A,P,\xi_b) \ , \tag{D.13}$$

described by the function

$$l^P_{10,m}(A,P,\xi_i) = \frac{1}{2P}\,SFS\big[k\cos^2\theta\big]$$
$$= \frac{m}{64\pi^2P^3}\left\{4P\xi_i(\xi_i^2 - A + P^2) + \big[\xi_i^4 - 2\xi_i^2(A+P^2) + (A-P^2)^2\big]\ln\left(\frac{(P-\xi_i)^2 - A}{(P+\xi_i)^2 - A}\right)\right\}, \quad \text{(D.14)}$$

where $SFS[\cdot]$ was defined in eq. (C.9).

Two in-medium insertions, $L^k_{10,d}$

Corresponding to the one in-medium case, the two in-medium contribution from eq. (D.1) can be obtained

$$L^P_{10,d}(A,P,\xi_a,\xi_b) = \frac{\sqrt{A}}{2P}\,TFS\big[\cos^2\theta\big]\,, \quad \text{(D.15)}$$

with $TFS[\cdot]$ defined in eq. (C.13).

D.3 Reduced scalar integrals of L_{11}

D.3.1 Reduction of L^k_{11}

Free part, $L^k_{11,f}$

The free contribution of eq. (D.2) can be right away expressed in terms of already known integrals, giving

$$L^p_{11,f}(A,p) = \frac{1}{2p^2}\Big[L_{10,f} + m\,L_{01,f} - (A + p^2 + m_\pi^2)\,L_{11,f}\Big]\,, \quad \text{(D.16)}$$

$$L^P_{11,f}(A,p) = 0\,. \quad \text{(D.17)}$$

The scalar of the second line vanishes due to translation invariance of the free-space integrals. Note that the integral of eq. (D.2) is convergent and therefore eq. (D.16) cannot depend on the subtraction constant. This is fulfilled because the dependence on g_0 from $L_{01,f}$ in eq. (C.57) is cancelled with that from $L_{10,f}$ in eq. (C.14). Recall that $L_{11,f}$ is also finite.

One in-medium insertion, $L^k_{11,m}$

For the one in-medium contribution of eq. (D.2) each scalar integral of the decomposition consists of contributions from both Fermi seas

$$L^p_{11,m}(A,p,P,c\beta,\xi_a,\xi_b) = l^p_{11,m}(A,p,P,c\beta,\xi_a) + l^p_{11,m}(A,p,P,-c\beta,\xi_b)\,, \quad \text{(D.18)}$$

$$L^P_{11,m}(A,p,P,c\beta,\xi_a,\xi_b) = l^P_{11,m}(A,p,P,c\beta,\xi_a) - l^P_{11,m}(A,p,P,-c\beta,\xi_b)\,, \quad \text{(D.19)}$$

where the common functions are reduced to already known integrals

$$l^p_{11,m}(A,p,P,c\beta,\xi_i) = \frac{1}{p^2\,s\beta^2}\left\{\frac{1}{2}\Big[l_{10,m} - m\,l_{01,m} - \delta_A\,l_{11,m}\Big] - p\,c\beta\,SFS\big[f^P_{11}(k,p,c\beta)\big]\right\}, \quad \text{(D.20)}$$

$$l^P_{11,m}(A,p,P,c\beta,\xi_i) = -\frac{1}{Pp\,s\beta^2}\left\{\frac{c\beta}{2}\Big[l_{10,m} - m\,l_{01,m} - \delta_A\,l_{11,m}\Big] - p\,SFS\big[f^P_{11}(k,p,c\beta)\big]\right\}, \quad \text{(D.21)}$$

with $\delta_A \doteq A + p^2 + m_\pi^2$ and $SFS[\cdot]$ defined in eq. (C.9). The auxiliary function

$$f_{11}^P(k,p,c\beta) = \frac{k}{e^2}\Big[\sqrt{\mathcal{C}} - \frac{d}{2}\, f_{11}(k,p,c\beta)\Big] \ , \tag{D.22}$$

is calculated correspondingly to the derivation of the function f_{11}, eq. (C.31) in subsection C.3.2, with the additional scalar product $\mathbf{P}\cdot\mathbf{k}$ in the integrand. The terms incorporating f_{11}^P stem from the contraction of eq. (D.2) with P^k. Abbreviations and the function f_{11} can be found in subsection C.3.2.

Two in-medium insertions, $L_{11,d}^k$

For the two in-medium insertions of eq. (D.2) recall that, because of the two energy Dirac delta distributions, one has $|\mathbf{k}| = \sqrt{A}$. The reduction yields a combination of already known scalar integrals

$$L_{11,d}^p(A,p,P,c\beta,\xi_a,\xi_b) = \frac{1}{p^2\, s\beta^2}\left\{\frac{1}{2}\Big[L_{10,d} - \delta_A\, L_{11,d}\Big] - p\, c\beta\, TFS\big[f_{11}^P(\sqrt{A},p,c\beta)\big]\right\} \tag{D.23}$$

$$L_{11,d}^P(A,p,P,c\beta,\xi_a,\xi_b) = -\frac{1}{Pp\, s\beta^2}\left\{\frac{c\beta}{2}\Big[L_{10,d} - \delta_A\, L_{11,d}\Big] - p\, TFS\big[f_{11}^P(\sqrt{A},p,c\beta)\big]\right\} \ , \tag{D.24}$$

with $\delta_A \doteq A + p^2 + m_\pi^2$. The auxiliary function f_{11}^P is defined in eq. (D.22) and $TFS[\cdot]$ in eq. (C.13).

D.3.2 Reduction of L_{11}^{kl}

Free part, $L_{11,f}^{kl}$

For the free contributions the reduced scalar integrals of the decomposition of eq. (D.3) read

$$L_{11,f}^{00}(A,p) = \frac{1}{4}\Big[2A\, L_{11,f} + (A + p^2 + m_\pi^2)\, L_{11,f}^p - m\Big(2\, L_{01,f} + L_{01,f}^p\Big)\Big] \ , \tag{D.25}$$

$$L_{11,f}^{pp}(A,p) = -\frac{1}{4p^2}\Big[2A\, L_{11,f} + 3(A + p^2 + m_\pi^2)\, L_{11,f}^p - m\Big(2\, L_{01,f} + 3\, L_{01,f}^p\Big)\Big] \ , \tag{D.26}$$

$$L_{11,f}^{PP}(A,p) = 0 \ , \tag{D.27}$$

$$L_{11,f}^{Pp}(A,p) = 0 \ . \tag{D.28}$$

The terms dependent on the total momentum do not contribute.

One in-medium insertion, $L_{11,m}^{kl}$

The one in-medium contribution of eq. (D.3) has contributions from both Fermi seas

$$L_{11,m}^{00}(A,p,P,c\beta,\xi_a,\xi_b) = l_{11,m}^{00}(A,p,P,c\beta,\xi_a) + l_{11,m}^{00}(A,p,P,-c\beta,\xi_b) \ , \tag{D.29}$$

$$L_{11,m}^{pp}(A,p,P,c\beta,\xi_a,\xi_b) = l_{11,m}^{pp}(A,p,P,c\beta,\xi_a) + l_{11,m}^{pp}(A,p,P,-c\beta,\xi_b) \ , \tag{D.30}$$

$$L_{11,m}^{PP}(A,p,P,c\beta,\xi_a,\xi_b) = l_{11,m}^{PP}(A,p,P,c\beta,\xi_a) + l_{11,m}^{PP}(A,p,P,-c\beta,\xi_b) \ , \tag{D.31}$$

$$L_{11,m}^{Pp}(A,p,P,c\beta,\xi_a,\xi_b) = l_{11,m}^{Pp}(A,p,P,c\beta,\xi_a) - l_{11,m}^{Pp}(A,p,P,-c\beta,\xi_b) \ , \tag{D.32}$$

with the common scalar functions

$$l^{00}_{11,m}(A,p,P,c\beta,\xi_i) = \frac{1}{2p\,s\beta^2}\Big\{2mp\,s\beta^2\,l_{01,m} + 2Ap\,s\beta^2\,l_{11,m} + mp(1-2c\beta^2)\,l^p_{01,m} + P\,c\beta\,l^P_{10,m} + \delta_A p(1-2c\beta^2)\,l^p_{11,m} - \delta_A P c\beta\,l^P_{11,m} - 2p\,SFS\big[f^{PP}_{11}(k,p,c\beta)\big]\Big\}\,, \tag{D.33}$$

$$l^{pp}_{11,m}(A,p,P,c\beta,\xi_i) = \frac{1}{p^3\,s\beta^4}\Big\{-mp\,s\beta^2\,l_{01,m} - Ap\,s\beta^2\,l_{11,m} + mp(2c\beta^2-1)\,l^p_{01,m} - P\,c\beta\,l^P_{10,m} + \delta_A p(2c\beta^2-1)\,l^p_{11,m} + \delta_A P c\beta\,l^P_{11,m} + p(1+c\beta^2)\,SFS\big[f^{PP}_{11}(k,p,c\beta)\big]\Big\}\,, \tag{D.34}$$

$$l^{PP}_{11,m}(A,p,P,c\beta,\xi_i) = \frac{1}{2P^2p\,s\beta^4}\Big\{-2mp\,s\beta^2\,l_{01,m} - 2Ap\,s\beta^2\,l_{11,m} + mp(3c\beta^2-1)\,l^p_{01,m} + P\,c\beta(c\beta^2-3)\,l^P_{10,m} + \delta_A p(3c\beta^2-1)\,l^p_{11,m} + \delta_A P c\beta(3-c\beta^2)\,l^P_{11,m} + 4p\,SFS\big[f^{PP}_{11}(k,p,c\beta)\big]\Big\}\,, \tag{D.35}$$

$$l^{Pp}_{11,m}(A,p,P,c\beta,\xi_i) = \frac{1}{2Pp^2\,s\beta^4}\Big\{2mp\,c\beta\,s\beta^2\,l_{01,m} + 2Ap\,c\beta\,s\beta^2\,l_{11,m} + mp\,c\beta(1-3c\beta^2)\,l^p_{01,m} + P(1+c\beta^2)\,l^P_{10,m} + \delta_A p\,c\beta(1-3c\beta^2)\,l^p_{11,m} - \delta_A P(1+c\beta^2)\,l^P_{11,m} - 4p\,c\beta\,SFS\big[f^{PP}_{11}(k,p,c\beta)\big]\Big\}\,, \tag{D.36}$$

where $\delta_A \doteq A + p^2 + m_\pi^2$ and $SFS[\cdot]$ is defined in eq. (C.9). The auxiliary function

$$f^{PP}_{11}(k,p,c\beta) = \frac{k^2}{8e^4}\Big[(4e^2\cos\theta - 6d)\sqrt{\mathcal{C}} + (3d^2 - 4ce^2)\,f_{11}(k,p,c\beta)\Big]\,, \tag{D.37}$$

is calculated correspondingly to the derivation of the function f_{11}, eq. (C.31) in subsection C.3.2, with the additional scalar product $(\mathbf{P}\cdot\mathbf{k})^2$ in the integrand. The abbreviations can also be found in subsection C.3.2. The terms incorporating f^{PP}_{11} stem from the contraction of eq. (D.3) with P^kP^l.

Two in-medium insertions, $L^{kl}_{11,d}$

For the two in-medium insertions of eq. (D.3) we have two energy Dirac delta distributions, implying $|\mathbf{k}| = \sqrt{A}$. The reduction yields, corresponding to the one in-medium insertions,

$$L^{00}_{11,d}(A,p,P,c\beta,\xi_a,\xi_b) = \frac{1}{2p\,s\beta^2}\Big\{Pc\beta\,L^P_{10,d} + 2Ap\,s\beta^2\,L_{11,d} + \delta_A p(1-2c\beta)\,L^p_{11,d} - \delta_A P\,c\beta\,L^P_{11,d} - 2p\,TFS\big[f^{PP}_{11}(\sqrt{A},p,c\beta)\big]\Big\}\,, \tag{D.38}$$

$$L^{pp}_{11,d}(A,p,P,c\beta,\xi_a,\xi_b) = \frac{1}{p^3\,s\beta^4}\Big\{-P\,c\beta\,L^P_{10,d} - Ap\,s\beta^2\,L_{11,d} + \delta_A p(2c\beta-1)\,L^p_{11,d} + \delta_A P c\beta\,L^P_{11,d} + p(1+c\beta^2)\,TFS\big[f^{PP}_{11}(\sqrt{A},p,c\beta)\big]\Big\}\,, \tag{D.39}$$

$$L^{PP}_{11,d}(A,p,P,c\beta,\xi_a,\xi_b) = \frac{1}{2P^2p\,s\beta^4}\Big\{P\,c\beta(c\beta^2-3)\,L^P_{10,d} - 2Ap\,s\beta^2\,L_{11,d} + \delta_A p(3c\beta^2-1)\,L^p_{11,d}$$

$$+ \delta_A P\, c\beta(3 - c\beta^2)\, L^P_{11,d} + 4p\, TFS\big[f^{PP}_{11}(\sqrt{A}, p, c\beta)\big] \Big\} \,, \tag{D.40}$$

$$L^{Pp}_{11,d}(A, p, P, c\beta, \xi_a, \xi_b) = \frac{1}{2Pp^2\, s\beta^4} \Big\{ P(1 + c\beta^2)\, L^P_{10,d} + 2Ap\, c\beta\, s\beta^2\, L_{11,d} + \delta_A p\, c\beta(1 - 3c\beta^2)\, L^p_{11,d}$$
$$- \delta_A P(1 + c\beta^2)\, L^P_{11,d} - 4p\, c\beta\, TFS\big[f^{PP}_{11}(\sqrt{A}, p, c\beta)\big] \Big\} \,, \tag{D.41}$$

with $\delta_A \doteq A + p^2 + m_\pi^2$. The auxiliary function f^{PP}_{11} is defined in eq. (D.37) and $TFS[\cdot]$ in eq. (C.13).

D.4 Reduced scalar integrals of L_{12}

D.4.1 Reduction of L^k_{12}

Free part, $L^k_{12,f}$

For the free contribution from eq. (D.4) the term dependent on the total momentum vanishes and the other terms can be reduced straightforwardly, with the result

$$L^p_{12,f}(A, p, c\varphi) = \frac{1}{2p^2(1 + c\varphi)} \Big[L_{11,f} - (A + p^2 + m_\pi^2)\, L_{12,f} + m\, L_{02,f} \Big] \,, \tag{D.42}$$

$$L^{p'}_{12,f}(A, p, c\varphi) = L^p_{12,f}(A, p, c\varphi) \,, \tag{D.43}$$

$$L^P_{12,f}(A, p, c\varphi) = 0 \,. \tag{D.44}$$

Note that for a free part $\mathbf{p}$ and $\mathbf{p}'$ appear only in a symmetric way and there is no vector of reference that could introduce any asymmetry between $\mathbf{p}$ and $\mathbf{p}'$. Therefore $L^p_{12,f}$ and $L^{p'}_{12,f}$ are equal.

An alternative way to obtain $L^p_{12,f}$ is to combine both pion propagators, as described in the prelude of section C.4.

$$L^k_{12,f} = \int_0^1 dy \left(\frac{\partial}{\partial m_\pi^2} \right) m \int \frac{d^3k}{(2\pi)^3} \frac{k^k}{\mathbf{k}^2 - A - i\epsilon} \frac{1}{\big(\mathbf{k} + \vec{\lambda}(y)\big)^2 + \Delta^2(y)}$$
$$\doteq (p^k + p'^k)\, L^p_{12,f} \doteq L^\lambda_{11,f} \times \lambda^k(y) \,, \tag{D.45}$$

where the circle denotes that the $\lambda(y)$ is part of the integrand for the integration in $L^\lambda_{11,f}$. Using the result of eq. (D.16), but now in terms of $\lambda(y)$ and $\Delta(y)$, we obtained

$$L^\lambda_{11,f} = \int_0^1 dy \left(\frac{-\partial}{\partial m_\pi^2} \right) \frac{1}{2\lambda^2} \big[L_{10,f} - \delta_A\, L_{11,f}(A, \lambda) + m\, L_{01,f}(\Delta) \big] \,, \tag{D.46}$$

with $\delta_A = A + \vec{\lambda}^2 + \Delta^2 = A + \mathbf{p}^2 + m_\pi^2$. It follows that

$$(p^k + p'^k)\, L^p_{12,f} = \int_0^1 dy \frac{\lambda^k}{2\lambda^2} \left(\frac{-\partial}{\partial m_\pi^2} \right) \big[m\, L_{01,f}(\Delta) - \delta_A\, L_{11,f}(A, \lambda) \big] \,. \tag{D.47}$$

Since $\lambda(y)$ and $\Delta(y)$ are symmetric under the exchange $y \leftrightarrow 1 - y$ we can replace $y\mathbf{p} + (1 - y)\mathbf{p}' \to y(\mathbf{p} + \mathbf{p}')$. This is only possible because there are no additional momenta involved. Performing the derivative with respect to the pion mass squared we obtain the final result

$$L^p_{12,f} = \frac{m}{16\pi} \int_0^1 dy \frac{y}{\lambda^2} \left\{ \frac{2}{\Delta} \frac{p^2 + m_\pi^2 - i\Delta\sqrt{A}}{p^2 + m_\pi^2 - A - 2i\Delta\sqrt{A}} - \frac{i}{\lambda} \ln \left(\frac{A - (\lambda + i\Delta)^2}{\Delta^2 + (\sqrt{A} - \lambda)^2} \right) \right\} \,. \tag{D.48}$$

One in-medium insertion, $L^k_{12,m}$

For the one in-medium contribution of eq. (D.4) each scalar integral of the decomposition consists of contributions from both Fermi seas

$$L^p_{12,m}(A,p,P,c\varphi,c\beta,c\beta',\xi_a,\xi_b) = l^p_{12,m}(A,p,P,c\varphi,c\beta,c\beta',\xi_a) + l^p_{12,m}(A,p,P,c\varphi,-c\beta,-c\beta',\xi_b)\ , \tag{D.49}$$

$$L^{p'}_{12,m}(A,p,P,c\varphi,c\beta,c\beta',\xi_a,\xi_b) = l^{p'}_{12,m}(A,p,P,c\varphi,c\beta,c\beta',\xi_a) + l^{p'}_{12,m}(A,p,P,c\varphi,-c\beta,-c\beta',\xi_b)\ , \tag{D.50}$$

$$L^P_{12,m}(A,p,P,c\varphi,c\beta,c\beta',\xi_a,\xi_b) = l^P_{12,m}(A,p,P,c\varphi,c\beta,c\beta',\xi_a) - l^P_{12,m}(A,p,P,c\varphi,-c\beta,-c\beta',\xi_b)\ , \tag{D.51}$$

where the common functions are reduced to already known integrals

$$\begin{aligned} l^p_{12,m}(A,p,P,c\varphi,c\beta,c\beta',\xi_i) = \frac{1}{2p^2(c\varphi^2+c\beta^2+c\beta'^2-2c\varphi c\beta c\beta'-1)}\Big\{&(c\varphi - c\beta c\beta')\, l_{11,m}(c\beta) \\ &- s\beta'^2\, l_{11,m}(c\beta') + \big[1+c\beta'(c\beta-c\beta')-c\varphi\big]\big[\delta_A\, l_{12,m} + m\, l_{02,m}\big] \\ &+ 2p(c\beta - c\varphi c\beta')\, SFS\big[f^P_{12}(k,p,c\varphi,c\beta,c\beta')\big]\Big\}\ , \end{aligned} \tag{D.52}$$

$$l^{p'}_{12,m}(A,p,P,c\varphi,c\beta,c\beta',\xi_i) = l^p_{12,m}(A,p,P,c\varphi,c\beta',c\beta,\xi_i)\ , \tag{D.53}$$

$$\begin{aligned} l^P_{12,m}(A,p,P,c\varphi,c\beta,c\beta',\xi_i) = \frac{1}{2Pp(c\varphi^2+c\beta^2+c\beta'^2-2c\varphi c\beta c\beta'-1)}\Big\{&(c\beta' - c\varphi c\beta)\, l_{11,m}(c\beta) \\ &+ (c\beta - c\varphi c\beta')\, l_{11,m}(c\beta') + (c\beta+c\beta')(c\varphi-1)\big[\delta_A\, l_{12,m} + m\, l_{02,m}\big] \\ &- 2p\, s\varphi^2\, SFS\big[f^P_{12}(k,p,c\varphi,c\beta,c\beta')\big]\Big\}\ , \end{aligned} \tag{D.54}$$

with $\delta_A \doteq A + p^2 + m_\pi^2$ and $SFS[\cdot]$ defined in eq. (C.9). Note the exchange $c\beta \leftrightarrow c\beta'$ for $l^{p'}_{12,m}$. The auxiliary function

$$\begin{aligned} \doteq f^P_{12}(k,p,c\varphi,c\beta,c\beta') = k\int_0^1 dy \frac{1}{e^2}\Big\{&\frac{(e^2-2\delta^2)(\delta+2e\cos\eta\cos\theta)-\delta e^2\cos(2\eta)}{2(\delta^2-e^2)\sqrt{\mathcal{C}}} \\ &+ \cos\eta\ln\big(d+2e(e\cos\theta+\sqrt{\mathcal{C}})\big)\Big\}\ , \end{aligned} \tag{D.55}$$

is calculated correspondingly to the derivation of the function f_{12}, eq. (C.52) in subsection C.4.2, with the additional scalar product $\mathbf{P}\cdot\mathbf{k}$ in the integrand. The abbreviations can also be found in that section. The terms incorporating f^P_{12} stem from the contraction of eq. (D.4) with P^k.

Two in-medium insertions, $L^k_{12,d}$

For the two in-medium insertions of eq. (D.4) we have two energy Dirac delta distributions, implying $|\mathbf{k}| = \sqrt{A}$. The reduction yields, corresponding to the contributions from one in-medium insertions,

$$\begin{aligned} L^p_{12,d}(A,p,P,c\varphi,c\beta,c\beta',\xi_a,\xi_b) = \frac{1}{2p^2(c\varphi^2+c\beta^2+c\beta'^2-2c\varphi c\beta c\beta'-1)}\Big\{&(c\varphi - c\beta c\beta')\, L_{11,d}(c\beta) \\ &- s\beta'^2\, L_{11,d}(c\beta') + \big[1+c\beta'(c\beta-c\beta')-c\varphi\big]\delta_A\, L_{12,d} \end{aligned}$$

$$+ 2p(c\beta - c\varphi c\beta')\, TFS\big[f_{12}^P(\sqrt{A}, p, c\varphi, c\beta, c\beta')\big]\Big\}\,, \tag{D.56}$$

$$L_{12,d}^{p'}(A,p,P,c\varphi,c\beta,c\beta',\xi_a,\xi_b) = L_{12,d}^{p}(A,p,P,c\varphi,c\beta',c\beta,\xi_a,\xi_b)\,, \tag{D.57}$$

$$\begin{aligned} L_{12,d}^{P}(A,p,P,c\varphi,c\beta,c\beta',\xi_a,\xi_b) = \frac{1}{2Pp(c\varphi^2 + c\beta^2 + c\beta'^2 - 2c\varphi c\beta c\beta' - 1)}\Big\{ & (c\beta' - c\varphi c\beta)\, L_{11,d}(c\beta) \\ & + (c\beta - c\varphi c\beta')\, L_{11,d}(c\beta') + (c\beta + c\beta')(c\varphi - 1)\delta_A\, L_{12,d} \\ & - 2p\, s\varphi^2\, TFS\big[f_{12}^P(\sqrt{A}, p, c\varphi, c\beta, c\beta')\big]\Big\}\,, \end{aligned} \tag{D.58}$$

with $\delta_A \doteq A + p^2 + m_\pi^2$. Note the exchange $c\beta \leftrightarrow c\beta'$ for $l_{12,m}^{p'}$. The auxiliary function f_{12}^P is defined in eq. (D.55) and $TFS[\cdot]$ in eq. (C.13).

D.4.2 Reduction of L_{12}^{kl}

Examining the decomposition of L_{12}^{kl} in eq. (D.5) one realizes that there is one more possible kinematic structure for the decomposition, namely a term proportional to δ^{kl}. However seven distinct structures would not be linear independent, because of which we skipped one term in the definition.

Free part, $L_{12,f}^{kl}$

The free contribution from the decomposition of the second rank tensor of the integral eq. (D.5) needs some additional considerations. We first start with a purely free decomposition

$$L_{12,f}^{kl} \doteq \delta^{kl}\, F_{12,f}^{00} + (p^k p^l + p'^k p'^l)\, F_{12,f}^{pp} + (p^k p'^l + p'^k p^l)\, F_{12,f}^{pp'} \tag{D.59}$$

For the free contribution $\mathbf{p}$ and $\mathbf{p}'$ appear only in a symmetric way and there is no vector of reference that could introduce any asymmetry between $\mathbf{p}$ and $\mathbf{p}'$. Therefore the scalars attending the structures $p^k p^l$ and $p'^k p'^l$ are equal.

Contracting eq. (D.59) with each of the three occuring kinematic structures, one obtains after solving the system of linear equations

$$F_{12,f}^{00}(A,p,c\varphi) = A\, L_{12,f} + \delta_A\, L_{12,f}^{p} - m\Big[L_{02,f} + L_{02,f}^{p}\Big]\,, \tag{D.60}$$

$$\begin{aligned} F_{12,f}^{pp}(A,p,c\varphi) = \frac{1}{2p^2(c\varphi^2 - 1)}\Big\{ & 2A\, L_{12,f} + m\Big[(c\varphi - 3)\, L_{02,f}^{p} - 2\, L_{02,f}\Big] + c\varphi\, L_{11,f}^{p} \\ & + \delta_A(3 - c\varphi)\, L_{12,f}^{p}\Big\}\,, \end{aligned} \tag{D.61}$$

$$\begin{aligned} F_{12,f}^{pp'}(A,p,c\varphi) = \frac{1}{2p^2(c\varphi^2 - 1)}\Big\{ & -2Ac\varphi\, L_{12,f} + m\Big[(3c\varphi - 1)\, L_{02,f}^{p} + 2c\varphi\, L_{02,f}\Big] \\ & - L_{11,f}^{p} + \delta_A(1 - 3c\varphi)\, L_{12,f}^{p}\Big\}\,, \end{aligned} \tag{D.62}$$

with $\delta_A = A + p^2 + m_\pi^2$.

As it was done for the case of the vector integrals, subsection D.4.1, we wish to give here an alternative derivation of the rank-two reduced scalar integrals. Using the prescription in the prelude of section C.4, the rank-two tensor integral can be written in the form

$$L^{kl}_{12,f} = \int_0^1 dy \frac{\partial}{\partial m_\pi^2} m \int \frac{d^3k}{(2\pi)^3} \frac{k^k k^l}{\mathbf{k}^2 - A - i\epsilon} \frac{1}{\left(\mathbf{k} + \vec{\lambda}(y)\right)^2 + \Delta^2} ,$$
$$= -\int_0^1 dy \left(\frac{\partial L^{00}_{11,f}}{\partial m_\pi^2}(A,\lambda)\, \delta^{kl} + \frac{\partial L^{\lambda\lambda}_{11,f}}{\partial m_\pi^2}(A,\lambda) \times \lambda^k(y)\lambda^l(y) \right) , \tag{D.63}$$

with $L^{00}_{11,f}$ and $L^{\lambda\lambda}_{11,f}$ given in eqs. (D.25) and (D.26), where m_π and $|\mathbf{p}|$ are replaced now by $\Delta(y)$ and $|\vec{\lambda}(y)|$, respectively. The $\times$ denotes that the integration with respect to y in $L^{\lambda\lambda}_{11,f}$ also includes $\lambda^k(y)\lambda^l(y)$. It is

$$\lambda^k\lambda^l = y^2 p^k p^l + (1-y)^2 p'^k p'^l + y(1-y)(p^k p'^l + p^l p'^k) . \tag{D.64}$$

Taking into account that in the integral of eq. (D.63) we can exchange $y \leftrightarrow (1-y)$ without changing the result, because $|\vec{\lambda}|$ and Δ depend only on the product $y(1-y)$, we can rewrite eq. (D.63) as

$$L^{kl}_{12,f} = -\delta^{kl} \int_0^1 dy \frac{\partial L^{00}_{11,f}}{\partial m_\pi^2} - (p^k p^l + p'^k p'^l) \int_0^1 dy\, y^2 \frac{\partial L^{\lambda\lambda}_{11,f}}{\partial m_\pi^2} - (p^k p'^l + p^l p'^k) \int_0^1 dy\, y(1-y) \frac{\partial L^{\lambda\lambda'}_{11,f}}{\partial m_\pi^2} . \tag{D.65}$$

Comparing coefficients with eq. (D.59) we find

$$F^{00}_{12,f}(A,p,c\varphi) = -\int_0^1 dy \frac{\partial}{\partial m_\pi^2} \left(L^{00}_{11,f}(A,\lambda)|_{m_\pi \to \Delta} \right) , \tag{D.66}$$

$$F^{pp}_{12,f}(A,p,c\varphi) = -\int_0^1 dy\, y^2 \frac{\partial}{\partial m_\pi^2} \left(L^{\lambda\lambda}_{11,f}(A,\lambda)|_{m_\pi \to \Delta} \right) , \tag{D.67}$$

$$F^{pp'}_{12,f}(A,p,c\varphi) = -\int_0^1 dy\, y(1-y) \frac{\partial}{\partial m_\pi^2} \left(L^{\lambda\lambda'}_{11,f}(A,\lambda)|_{m_\pi \to \Delta} \right) . \tag{D.68}$$

We still have to convert the free part of the reduced scalar integrals from our tensor basis defined in eq. (D.59) to the one employed in eq. (D.5), we have to rewrite the tensor δ^{kl} in terms of the tensor basis eq. (D.5). For that we express the Kronecker delta in terms of the cartesian basis vectors $\hat{\mathbf{e}}_1$, $\hat{\mathbf{e}}_2$ and $\hat{\mathbf{e}}_3$

$$\delta^{kl} = \hat{\mathbf{e}}_1^k \hat{\mathbf{e}}_1^l + \hat{\mathbf{e}}_2^k \hat{\mathbf{e}}_2^l + \hat{\mathbf{e}}_3^k \hat{\mathbf{e}}_3^l . \tag{D.69}$$

We choose the orientation of the reference frame in the following way:

$$\begin{aligned} \hat{\mathbf{e}}_1 &= \hat{\mathbf{p}} , \\ \hat{\mathbf{e}}_2 &= \mathcal{N}_2(\hat{\mathbf{P}} - \hat{\mathbf{P}} \cdot \hat{\mathbf{e}}_1\, \hat{\mathbf{e}}_1) , \\ \hat{\mathbf{e}}_3 &= \mathcal{N}_3(\hat{\mathbf{p}}' - \hat{\mathbf{p}}' \cdot \hat{\mathbf{e}}_1\, \hat{\mathbf{e}}_1 - \hat{\mathbf{p}}' \cdot \hat{\mathbf{e}}_2\, \hat{\mathbf{e}}_2) , \end{aligned} \tag{D.70}$$

with the normalization constants $\mathcal{N}_2$ and $\mathcal{N}_3$ fixed such that $\hat{\mathbf{e}}_1^2 = \hat{\mathbf{e}}_2^2 = 1$, giving

$$\mathcal{N}_2 = \frac{1}{\sin\beta} , \tag{D.71}$$

$$\mathcal{N}_3 = \frac{\sin\beta}{\sqrt{-n_3}} , \tag{D.72}$$

$$n_3 = c\varphi^2 + c\beta^2 + c\beta'^2 - 2c\varphi c\beta c\beta' - 1 . \tag{D.73}$$

With these expressions it is straightforward to rewrite eq. (D.59) in the basis of eq. (D.5)

$$L^{pp}_{12,f}(A,p,P,c\varphi,c\beta,c\beta') = \frac{c\beta'^2-1}{p^2\,n_3}\,F^{00}_{12,f}(A,p,c\varphi) + F^{pp}_{12,f}(A,p,c\varphi)\ , \tag{D.74}$$

$$L^{p'p'}_{12,f}(A,p,P,c\varphi,c\beta,c\beta') = \frac{c\beta^2-1}{p^2\,n_3}\,F^{00}_{12,f}(A,p,c\varphi) + F^{pp}_{12,f}(A,p,c\varphi)\ , \tag{D.75}$$

$$L^{pp'}_{12,f}(A,p,P,c\varphi,c\beta,c\beta') = \frac{c\varphi-c\beta c\beta'}{p^2\,n_3}\,F^{00}_{12,f}(A,p,c\varphi) + F^{pp'}_{12,f}(A,p,c\varphi)\ , \tag{D.76}$$

$$L^{PP}_{12,f}(A,p,P,c\varphi,c\beta,c\beta') = \frac{c\varphi^2-1}{P^2\,n_3}\,F^{00}_{12,f}(A,p,c\varphi)\ , \tag{D.77}$$

$$L^{Pp}_{12,f}(A,p,P,c\varphi,c\beta,c\beta') = \frac{c\beta-c\varphi c\beta'}{Pp\,n_3}\,F^{00}_{12,f}(A,p,c\varphi)\ , \tag{D.78}$$

$$L^{Pp'}_{12,f}(A,p,P,c\varphi,c\beta,c\beta') = \frac{c\beta'-c\varphi c\beta}{Pp\,n_3}\,F^{00}_{12,f}(A,p,c\varphi)\ . \tag{D.79}$$

One in-medium insertion, $L^{kl}_{12,m}$

For the one in-medium contribution of eq. (D.5) each scalar integral of the decomposition consists of contributions from both Fermi seas

$$L^{pp}_{12,m}(A,p,P,c\varphi,c\beta,c\beta',\xi_a,\xi_b) = l^{pp}_{12,m}(A,p,P,c\varphi,c\beta,c\beta',\xi_a) + l^{pp}_{12,m}(A,p,P,c\varphi,-c\beta,-c\beta',\xi_b)\ , \tag{D.80}$$

$$L^{p'p'}_{12,m}(A,p,P,c\varphi,c\beta,c\beta',\xi_a,\xi_b) = l^{p'p'}_{12,m}(A,p,P,c\varphi,c\beta,c\beta',\xi_a) + l^{p'p'}_{12,m}(A,p,P,c\varphi,-c\beta,-c\beta',\xi_b)\ , \tag{D.81}$$

$$L^{pp'}_{12,m}(A,p,P,c\varphi,c\beta,c\beta',\xi_a,\xi_b) = l^{pp'}_{12,m}(A,p,P,c\varphi,c\beta,c\beta',\xi_a) + l^{pp'}_{12,m}(A,p,P,c\varphi,-c\beta,-c\beta',\xi_b)\ , \tag{D.82}$$

$$L^{PP}_{12,m}(A,p,P,c\varphi,c\beta,c\beta',\xi_a,\xi_b) = l^{PP}_{12,m}(A,p,P,c\varphi,c\beta,c\beta',\xi_a) + l^{PP}_{12,m}(A,p,P,c\varphi,-c\beta,-c\beta',\xi_b)\ , \tag{D.83}$$

$$L^{Pp}_{12,m}(A,p,P,c\varphi,c\beta,c\beta',\xi_a,\xi_b) = l^{Pp}_{12,m}(A,p,P,c\varphi,c\beta,c\beta',\xi_a) - l^{Pp}_{12,m}(A,p,P,c\varphi,-c\beta,-c\beta',\xi_b)\ , \tag{D.84}$$

$$L^{Pp'}_{12,m}(A,p,P,c\varphi,c\beta,c\beta',\xi_a,\xi_b) = l^{Pp'}_{12,m}(A,p,P,c\varphi,c\beta,c\beta',\xi_a) - l^{Pp'}_{12,m}(A,p,P,c\varphi,-c\beta,-c\beta',\xi_b)\ . \tag{D.85}$$

The expressions for the reduced scalar integrals are far too large to be listed here, so we restrict ourselves to present just the system of linear equations that have to be solved with respect to the desired scalars. It is given by:

$$\begin{pmatrix} p^2 & p^2 & 2p^2c\varphi & P^2 & 2Ppc\beta & 2Ppc\beta' \\ p^4 & p^4c\varphi^2 & 2p^4c\varphi & P^2p^2c\beta^2 & 2Pp^3c\beta & 2Pp^3c\beta c\varphi \\ p^4c\varphi^2 & p^4 & 2p^4c\varphi & P^2p^2c\beta'^2 & 2Pp^3c\beta' c\varphi & 2Pp^3c\beta' \\ p^4c\varphi & p^4c\varphi & p^4(1+c\varphi) & P^2p^2c\beta c\beta' & Pp^3(c\beta'+c\beta c\varphi) & Pp^3(c\beta+c\beta' c\varphi) \\ P^2p^2c\beta^2 & P^2p^2c\beta'^2 & 2P^2p^2c\beta c\beta' & P^4 & 2P^3pc\beta & 2P^2pc\beta' \\ Pp^3c\beta & Pp^3c\beta' c\varphi & Pp^3(c\beta'+c\beta c\varphi) & P^3pc\beta & P^2p^2(1+c\beta^2) & P^2p^2(c\varphi+c\beta c\beta') \\ Pp^3c\beta c\varphi & Pp^3c\beta' & Pp^3(c\beta+c\beta' c\varphi) & P^3pc\beta' & P^2p^2(c\varphi+c\beta c\beta') & P^2p^2(1+c\beta'^2) \end{pmatrix} \cdot \begin{pmatrix} l^{pp}_{12,m} \\ l^{p'p'}_{12,m} \\ l^{pp'}_{12,m} \\ l^{PP}_{12,m} \\ l^{Pp}_{12,m} \\ l^{Pp'}_{12,m} \end{pmatrix} = \begin{pmatrix} A^{00}_m \\ A^{pp}_m \\ A^{p'p'}_m \\ A^{pp'}_m \\ A^{PP}_m \\ A^{Pp}_m \\ A^{Pp'}_m \end{pmatrix} \tag{D.86}$$

where the functions in the vector on the right hand side are given by

$$A^{00}_m = m\, l_{02,m} + A\, l_{12,m} \ , \tag{D.87}$$

$$A^{pp}_m = \frac{1}{4}\Big\{ 2p^2\, c\varphi\, l^p_{11,m}(c\beta') + 2Pp\, c\beta\, l^P_{11,m}(c\beta') + m\big[(\delta_A + p^2 + m^2)\, l_{02,m} + l^{(2)}_{02,m} - l_{01,m}(c\beta')\big] - \delta_A\, l_{11,m}(c\beta') + \delta_A^2\, l_{12,m} \Big\} \ , \tag{D.88}$$

$$A^{p'p'}_m = \frac{1}{4}\Big\{ 2p^2\, c\varphi\, l^p_{11,m}(c\beta) + 2Pp\, c\beta'\, l^P_{11,m}(c\beta) + m\big[(\delta_A + p^2 + m^2)\, l_{02,m} + l^{(2)}_{02,m} - l_{01,m}(c\beta)\big] - \delta_A\, l_{11,m}(c\beta) + \delta_A^2\, l_{12,m} \Big\} \ , \tag{D.89}$$

$$A^{pp'}_m = \frac{1}{4}\Big\{ l_{10,m} + m\big[(\delta_A + p^2 + m_\pi^2)\, l_{02,m} + l^{(2)}_{02,m} - l_{01,m}(c\beta) - l_{01,m}(c\beta')\big] - \delta_A\big[l_{11,m}(c\beta) + l_{11,m}(c\beta')\big] + \delta_A^2\, l_{12,m} \Big\} \ , \tag{D.90}$$

$$A^{PP}_m = P^2\, SFS\big[f^{PP}_{12}(k,p,c\varphi,c\beta,c\beta')\big] \ , \tag{D.91}$$

$$A^{Pp}_m = \frac{P}{2}\Big\{ SFS\big[f^P_{11}(k,p,c\beta')\big] - \delta_A\, SFS\big[f^P_{12}(k,p,c\varphi,c\beta,c\beta')\big] - m f^P_{02}(\lambda_2,\Delta) \Big\} \ , \tag{D.92}$$

$$A^{Pp'}_m = \frac{P}{2}\Big\{ SFS\big[f^P_{11}(k,p,c\beta)\big] - \delta_A\, SFS\big[f^P_{12}(k,p,c\varphi,c\beta,c\beta')\big] - m f^P_{02}(\lambda_2,\Delta) \Big\} \ , \tag{D.93}$$

with $\delta_A \doteq A + p^2 + m_\pi^2$ and $SFS[\cdot]$ defined in eq. (C.9). The lines in eq. (D.86) correspond to contracting the composition eq. (D.5) with δ_{kl}, $p_k p_l$, $p'_k p'_l$, $p_k p'_l$, $P_k P_l$, $P_k p_l$ and $P_k p'_l$, in that order. However, since that system of linear equation is overdetermined, we should drop one arbitrary line. With the wish to reduce the numerical load one might choose one of the last three lines, because they contain the most exclusively needed numerical integrations. The auxiliary function

$$\begin{aligned} f^{PP}_{12}(k,p,c\varphi,c\beta,c\beta') = k^2 \int_0^1 dy \frac{1}{e^3}\Big\{ & \frac{1}{(4ce^2-d^2)\sqrt{\mathcal{C}}}\Big[2e\delta\big[d^2\cos\theta + c(d-2e^2\cos\theta)\big] + \big[8c^2e^2 - d^2\cos\theta(3d+e^2\cos\theta) \\ & + c(-3d^2 + 10de^2\cos\theta + 4e^4\cos^2\theta)\big]\cos\eta\Big] + \frac{2e\delta - 3d\cos\eta}{2e}\ln\big(d + 2e(e\cos\theta + \sqrt{\mathcal{C}})\big)\Big\} \ , \end{aligned} \tag{D.94}$$

is calculated correspondingly to the derivation of the function f_{12}, eq. (C.52) in subsection C.4.2, with the additional scalar product $(\mathbf{P}\cdot\mathbf{k})^2$ in the integrand. The abbreviations can also be found in subsection C.4.2.

Two in-medium insertions, $L^{kl}_{12,d}$

For the two in-medium insertions of eq. (D.5) we have two energy Dirac delta distributions, implying $|\mathbf{k}| = \sqrt{A}$. We do not list the explicit solution but merely outline the way to obtain them. We employ the system of linear equation of eq. (D.86) but replace all $l^{\cdots}_{12,m}$ by $L^{\cdots}_{12,d}$ in the vector on the left hand side and all $A^{\cdots}_{m}$ by $A^{\cdots}_{d}$ on the right hand side. The latter are given by

$$A^{00}_d = A\,L_{12,d}\;, \tag{D.95}$$

$$A^{pp}_d = \frac{1}{4}\Big\{2p^2\,c\varphi\,L^{p}_{11,d}(c\beta') + 2Pp\,c\beta\,L^{P}_{11,d}(c\beta') - \delta_A\,L_{11,d}(c\beta') + \delta_A^2\,L_{12,d}\Big\}\;, \tag{D.96}$$

$$A^{p'p'}_d = \frac{1}{4}\Big\{2p^2\,c\varphi\,L^{p}_{11,d}(c\beta) + 2Pp\,c\beta'\,L^{P}_{11,d}(c\beta) - \delta_A\,L_{11,d}(c\beta) + \delta_A^2\,L_{12,d}\Big\}\;, \tag{D.97}$$

$$A^{pp'}_d = \frac{1}{4}\Big\{L_{10,d} - \delta_A\big[L_{11,d}(c\beta) + L_{11,d}(c\beta')\big] + \delta_A^2\,L_{12,d}\Big\}\;, \tag{D.98}$$

$$A^{PP}_d = P^2\,TFS\big[f^{PP}_{12}(\sqrt{A},p,c\varphi,c\beta,c\beta')\big]\;, \tag{D.99}$$

$$A^{Pp}_d = \frac{P}{2}\Big\{TFS\big[f^{P}_{11}(\sqrt{A},p,c\beta')\big] - \delta_A\,TFS\big[f^{P}_{12}(\sqrt{A},p,c\varphi,c\beta,c\beta')\big]\Big\}\;, \tag{D.100}$$

$$A^{Pp'}_d = \frac{P}{2}\Big\{TFS\big[f^{P}_{11}(\sqrt{A},p,c\beta)\big] - \delta_A\,TFS\big[f^{P}_{12}(\sqrt{A},p,c\varphi,c\beta,c\beta')\big]\Big\}\;, \tag{D.101}$$

with $\delta_A \doteq A + p^2 + m_\pi^2$. One arbitrary line in should be dropped eq. (D.86), because the system of linear equations is overdetermined. The auxiliary function f^{PP}_{12} is defined in eq. (D.94) and $TFS[\cdot]$ in eq. (C.13). The abbreviations are defined in subsection C.4.2.

D.4.3 Reduction of $L^{(2)}_{12}$

The integral eq. (D.9) can straightforwardly be reduced to basic scalar integrals. The free part reads

$$\begin{aligned} L^{(2)}_{12,f}(A,p,c\varphi) &= -m\int\frac{d^3k}{(2\pi)^3}\frac{\mathbf{k}^2}{\mathbf{k}^2-A-i\epsilon}\frac{1}{(\mathbf{k}+\mathbf{p})^2+m_\pi^2}\frac{1}{(\mathbf{k}+\mathbf{p}')^2+m_\pi^2} \\ &= A\,L_{12,f} - m\,L_{02,f}\;. \end{aligned} \tag{D.102}$$

Whereas the one in-medium contribution consists of two pieces

$$\begin{aligned} &L^{(2)}_{12,m}(A,p,P,c\varphi,c\beta,c\beta',\xi_a,\xi_b) \\ &\quad= m\int\frac{d^3k}{(2\pi)^3}\Big[\theta(\xi_a-|\mathbf{P}-\mathbf{k}|)+\theta(\xi_b-|\mathbf{P}+\mathbf{k}|)\Big]\frac{\mathbf{k}^2}{\mathbf{k}^2-A-i\epsilon}\frac{1}{(\mathbf{k}+\mathbf{p})^2+m_\pi^2}\frac{1}{(\mathbf{k}+\mathbf{p}')^2+m_\pi^2} \\ &\qquad= l^{(2)}_{12,m}(A,p,P,c\varphi,c\beta,c\beta',\xi_a) + l^{(2)}_{12,m}(A,p,P,c\varphi,-c\beta,-c\beta',\xi_b)\;, \end{aligned} \tag{D.103}$$

with

$$l^{(2)}_{12,m}(A,p,P,c\varphi,c\beta,c\beta',\xi_i) = SFS\big[k^2 f_{12}(k,p,c\varphi,c\beta,c\beta')\big] \ , \tag{D.104}$$

where the auxiliary function f_{12} is given in eq. (C.52).

Finally, the two in-medium part is given by

$$\begin{aligned} &L^{(2)}_{12,d}(A,p,P,c\varphi,c\beta,c\beta',\xi_a,\xi_b) \\ &\qquad = -im\int\frac{d^3k}{(2\pi)^2}\,\mathbf{k}^2\,\delta\big(\mathbf{k}^2-A\big)\frac{\theta(\xi_a-|\mathbf{P}-\mathbf{k}|)}{(\mathbf{k}+\mathbf{p})^2+m_\pi^2}\frac{\theta(\xi_b-|\mathbf{P}+\mathbf{k}|)}{(\mathbf{k}+\mathbf{p}')^2+m_\pi^2} = A\,L_{12,d} \ . \end{aligned} \tag{D.105}$$

D.4.4 Reduction of $L^{(2)k}_{12}$

The reduction of the scalars from the decomposition of $L^{(2)k}_{12}$, eq. (D.6), is trivial, as soon as one has derived the scalars from the decomposition of L^{k}_{12}, eq. (D.4). In the following we just give the results:

Free part, $L^{(2)k}_{12,f}$

$$L^{(2)p}_{12,f}(A,p,c\varphi) = A\,L^{p}_{12,f} - m\,L^{p}_{02,f} \ , \tag{D.106}$$

$$L^{(2)p'}_{12,f}(A,p,c\varphi) = A\,L^{p'}_{12,f} - m\,L^{p'}_{02,f} \ , \tag{D.107}$$

$$L^{(2)P}_{12,f}(A,p,c\varphi) = 0 \ , \tag{D.108}$$

One in-medium insertion, $L^{(2)k}_{12,m}$

$$L^{(2)p}_{12,m}(A,p,P,c\varphi,c\beta,c\beta',\xi_a,\xi_b) = A\,L^{p}_{12,m} + m\,L^{p}_{02,m} \ , \tag{D.109}$$

$$L^{(2)p'}_{12,m}(A,p,P,c\varphi,c\beta,c\beta',\xi_a,\xi_b) = A\,L^{p'}_{12,m} + m\,L^{p'}_{02,m} \ , \tag{D.110}$$

$$L^{(2)P}_{12,m}(A,p,P,c\varphi,c\beta,c\beta',\xi_a,\xi_b) = A\,L^{P}_{12,m} + m\,L^{P}_{02,m} \ , \tag{D.111}$$

Two in-medium insertions, $L^{(2)k}_{12,d}$

$$L^{(2)p}_{12,d}(A,p,P,c\varphi,c\beta,c\beta',\xi_a,\xi_b) = A\,L^{p}_{12,d} \ , \tag{D.112}$$

$$L^{(2)p'}_{12,d}(A,p,P,c\varphi,c\beta,c\beta',\xi_a,\xi_b) = A\,L^{p'}_{12,d} \ , \tag{D.113}$$

$$L^{(2)P}_{12,d}(A,p,P,c\varphi,c\beta,c\beta',\xi_a,\xi_b) = A\,L^{P}_{12,d} \ . \tag{D.114}$$

D.4.5 Reduction of $L_{12}^{(4)}$

The integral eq. (D.10) can straightforwardly be reduced to basic scalar integrals. The free part reads

$$\begin{aligned} L_{12,f}^{(4)}(A,p,c\varphi) &= -m\int\frac{d^3k}{(2\pi)^3}\frac{\mathbf{k}^4}{\mathbf{k}^2-A-i\epsilon}\frac{1}{(\mathbf{k}+\mathbf{p})^2+m_\pi^2}\frac{1}{(\mathbf{k}+\mathbf{p}')^2+m_\pi^2} \\ &= A^2\,L_{12,f} - m\Big[A\,L_{02,f}+L_{02,f}^{(2)}\Big]\ . \end{aligned} \tag{D.115}$$

Whereas the one in-medium contribution consists of two pieces

$$\begin{aligned} &L_{12,m}^{(4)}(A,p,P,c\varphi,c\beta,c\beta',\xi_a,\xi_b) \\ &\quad= m\int\frac{d^3k}{(2\pi)^3}\Big[\theta(\xi_a-|\mathbf{P}-\mathbf{k}|)+\theta(\xi_b-|\mathbf{P}+\mathbf{k}|)\Big]\frac{\mathbf{k}^4}{\mathbf{k}^2-A-i\epsilon}\frac{1}{(\mathbf{k}+\mathbf{p})^2+m_\pi^2}\frac{1}{(\mathbf{k}+\mathbf{p}')^2+m_\pi^2} \\ &\qquad= l_{12,m}^{(4)}(A,p,P,c\varphi,c\beta,c\beta',\xi_a)+l_{12,m}^{(4)}(A,p,P,c\varphi,-c\beta,-c\beta',\xi_b)\ , \end{aligned} \tag{D.116}$$

with

$$l_{12,m}^{(4)}(A,p,P,c\varphi,c\beta,c\beta',\xi_i) = SFS\big[k^4 f_{12}(k,p,c\varphi,c\beta,c\beta')\big]\ , \tag{D.117}$$

where the auxiliary function f_{12} is given in eq. (C.52).

Finally, the two in-medium part is given by

$$\begin{aligned} &L_{12,d}^{(4)}(A,p,P,c\varphi,c\beta,c\beta',\xi_a,\xi_b) \\ &\qquad= -im\int\frac{d^3k}{(2\pi)^2}\,\mathbf{k}^4\,\delta\big(\mathbf{k}^2-A\big)\frac{\theta(\xi_a-|\mathbf{P}-\mathbf{k}|)}{(\mathbf{k}+\mathbf{p})^2+m_\pi^2}\frac{\theta(\xi_b-|\mathbf{P}+\mathbf{k}|)}{(\mathbf{k}+\mathbf{p}')^2+m_\pi^2} = A^2\,L_{12,d}\ . \end{aligned} \tag{D.118}$$

D.5 Reduced scalar integrals of L_{01} and L_{02}

D.5.1 Reduction of L_{01}^k

Free part, $L_{01,f}$

The first term in eq. (D.7) corresponds to the integral

$$L_{01,f}^p = \frac{1}{\mathbf{p}^2}\int\frac{d^3k}{(2\pi)^3}\frac{\mathbf{k}\cdot\mathbf{p}}{(\mathbf{k}+\mathbf{p})^2+m_\pi^2} = \frac{m_\pi}{4\pi}-\frac{\Lambda}{3\pi^2}\ . \tag{D.119}$$

Note that the result for $L_{01,f}^p$ is not the same as one would obtain by performing the shift of variables $\mathbf{k}+\mathbf{p}\to\mathbf{k}$ in the previous integral, which yields $L_{01,f}^p = -L_{01,f}$. We have performed the integral for $L_{01,f}^p$ exactly. Analyzing the resulting terms with respect to their behavior for $\Lambda\to\infty$, with cut-off Λ, we only keep those terms that do not vanish in that limit. Employing the regularization method which involves the subtraction constant g_0, we obtain

$$L_{01,f}^p = \frac{1}{\mathbf{p}^2}\int\frac{d^3k}{(2\pi)^3}\frac{\mathbf{k}\cdot\mathbf{p}}{(\mathbf{k}+\mathbf{p})^2+m_\pi^2} = \frac{m_\pi}{4\pi}+\frac{2g_0}{3m}\ . \tag{D.120}$$

One in-medium insertion, $L_{01,m}$

The one in-medium contributions of eq. (D.7) are quoted in the usual way

$$L^p_{01,m}(p,P,c\beta,\xi_a,\xi_b) = l^p_{01,m}(p,P,c\beta,\xi_a) + l^p_{01,m}(p,P,-c\beta,\xi_b)\ . \tag{D.121}$$

We perform the shift $\mathbf{k}+\mathbf{p}\to\mathbf{k}$ and the integration results in

$$l^p_{01,m}(p,P,c\beta,\xi_i) = \left(1+\frac{P}{p}c\beta\right) f^p_{01}\big(p_2,m_\pi,\xi_i\big) - l_{01,m}\ , \tag{D.122}$$

with $p_2(c\beta) = |\mathbf{P}+\mathbf{p}| = \sqrt{P^2+p^2+2pP\,c\beta}$ and the auxiliary function

$$\begin{aligned} f^p_{01}(q,m_\pi,\xi_i) \doteq \frac{1}{64\pi^2 q^3}\Bigg\{ & 4q\xi_i(q^2+m_\pi^2+\xi_i^2) \\ & + \Big[(q^2+m_\pi^2+\xi_i^2)^2 - 4q^2\xi_i^2\Big]\ln\left(\frac{(\xi_i-q)^2+m_\pi^2}{(\xi_i+q)^2+m_\pi^2}\right)\Bigg\}\ . \end{aligned} \tag{D.123}$$

D.5.2 Reduction of L^k_{02}

Free part, $L_{02,f}$

For the free contributions of the decompositions of L^k_{02}, eq. (D.8), we obtain

$$\begin{aligned} L^p_{02,f}(p,c\varphi) &= \frac{1}{2p^2(1+c\varphi)}\Big[L_{01,f} - (p^2+m_\pi^2)L_{02,f} - L^{(2)}_{02,f}\Big] \\ &= -\frac{1}{\pi p\sqrt{128(1-c\varphi)}}\arcsin\left(\frac{p\sqrt{1-c\varphi}}{\sqrt{2m_\pi^2+p^2(1-c\varphi)}}\right)\ , \end{aligned} \tag{D.124}$$

$$L^{p'}_{02,f}(p,c\varphi) = L^p_{02,f}(p,c\varphi)\ , \tag{D.125}$$

$$L^P_{02,f}(p,c\varphi) = 0\ . \tag{D.126}$$

The part $L^p_{02,f}$ can either be reduced to other scalar integrals, first line of eq. (D.124) or it can be solved using the derivation of eq. (C.57), second line of eq. (D.124). The part $L^{p'}_{02,f}$ is equal to $L^p_{02,f}$ due to translation invariance. For the same reason $L^P_{02,f}$ vanishes.

One in-medium insertion, $L_{02,m}$

The one in-medium contribution of eq. (D.8) consists as usual of two parts which can each be expressed in terms of the same function

$$L^p_{02,m}(p,P,c\varphi,c\beta,c\beta',\xi_a,\xi_b) = l^p_{02,m}(p,P,c\varphi,c\beta,c\beta',\xi_a) + l^p_{02,m}(p,P,c\varphi,-c\beta,-c\beta',\xi_b)\ , \tag{D.127}$$

$$L^{p'}_{02,m}(p,P,c\varphi,c\beta,c\beta',\xi_a,\xi_b) = l^{p'}_{02,m}(p,P,c\varphi,c\beta,c\beta',\xi_a) + l^{p'}_{02,m}(p,P,c\varphi,-c\beta,-c\beta',\xi_b)\ , \tag{D.128}$$

$$L^P_{02,m}(p,P,c\varphi,c\beta,c\beta',\xi_a,\xi_b) = l^P_{02,m}(p,P,c\varphi,c\beta,c\beta',\xi_a) - l^P_{02,m}(p,P,c\varphi,-c\beta,-c\beta',\xi_b)\ . \tag{D.129}$$

Solving the system of linear equations yields

$$l^{p}_{02,m}(p,P,c\varphi,c\beta,c\beta',\xi_i) = \frac{1}{2p^2(c\varphi^2+c\beta^2+c\beta'^2-2c\varphi c\beta c\beta'-1)}\Big\{(c\varphi - c\beta c\beta')\, l_{01,m}(c\beta) \\ - s\beta'^2\, l_{01,m}(c\beta') + \big[1+c\beta'(c\beta-c\beta')-c\varphi\big]\big[(m_\pi^2+p^2)\, l_{02,m} + l^{(2)}_{02,m}\big] \\ + 2p(c\beta - c\varphi c\beta')\, f^{P}_{02}\Big\}\,, \tag{D.130}$$

$$l^{p'}_{02,m}(p,P,c\varphi,c\beta,c\beta',\xi_i) = l^{p}_{02,m}(p,P,c\varphi,c\beta',c\beta,\xi_i)\,, \tag{D.131}$$

$$l^{P}_{02,m}(p,P,c\varphi,c\beta,c\beta',\xi_i) = \frac{1}{2Pp(c\varphi^2+c\beta^2+c\beta'^2-2c\varphi c\beta c\beta'-1)}\Big\{(c\beta' - c\varphi c\beta)\, l_{01,m}(c\beta) \\ + (c\beta - c\varphi c\beta')\, l_{01,m}(c\beta') + (c\beta+c\beta')(c\varphi-1)\big[(m_\pi^2+p^2)\, l_{02,m} + l^{(2)}_{02,m}\big] \\ - 2p\, s\varphi^2\, f^{P}_{02}\Big\}\,. \tag{D.132}$$

Note that $l^{p'}_{02,m}$ corresponds to $l^{p}_{02,m}$ with $c\beta \leftrightarrow c\beta'$.

$$f^{P}_{02}(p,P,c\varphi,c\beta,c\beta',\xi_i) = -\int_0^1 dy\,\Big\{[P-\lambda\cos\eta]\,\frac{\partial f^{p}_{01}}{\partial m_\pi^2}(\lambda_2,\Delta,\xi_i) + \lambda\cos\eta\, f_{02}(\lambda_2,\Delta,\xi_i)\Big\}\,, \tag{D.133}$$

where $\lambda(y)$, $\Delta(y)$, $\cos\eta(y)$ have been defined in eqs. (C.39), (C.38), (C.46), respectively, and $\lambda_2(\cos\eta, y) = |\mathbf{P}+\vec{\lambda}(y)|$. The pion mass derivative of f^{p}_{01} with the $m_\pi \to \Delta$ beforehand reads

$$\frac{\partial f^{p}_{01}}{\partial m_\pi^2}(q,\Delta,\xi_i) \doteq -\frac{1}{32\pi^2 q^3}\Big\{4q\xi_i + \big(q^2+m_\pi^2+\xi_i^2\big)\ln\left(\frac{(\xi_i-q)^2+m_\pi^2}{(\xi_i+q)^2+m_\pi^2}\right)\Big\}\,. \tag{D.134}$$

D.5.3 Reduction of $L^{(2)}_{02}$

As described in the prelude of section C.4, two pion propagators can be combined using a Feynman parameter. The free part of eq. (D.11) with two pion propagators and the additional structure of the loop momentum squared then reads

$$L^{(2)}_{02,f}(p,\cos\varphi) = \int_0^1 dy\,\frac{-\partial}{\partial m_\pi^2}\int\frac{d^3k}{(2\pi)^3}\frac{\mathbf{k}^2}{(\mathbf{k}+\vec{\lambda}(y))^2+\Delta^2(y)} \\ = \frac{1}{8\pi}\int_0^1 dy\left[\frac{\lambda^2(y)}{\Delta(y)} - 3\Delta(y)\right] - \frac{g_0}{m}\,, \tag{D.135}$$

with $\vec{\lambda}(y)$ and $\Delta(y)$ defined in eq. (C.37) and (C.38), respectively. g_0 is the subtraction constant introduced in section 4.2.

For the contributions from one in-medium insertions of eq. (D.11) we proceed correspondingly to $L_{02,m}$, eq. (C.61),

$$L^{(2)}_{02,m}(p,P,\cos\varphi,\cos\beta,\cos\beta',\xi_a,\xi_b) = \int_0^1 dy\,\frac{-\partial}{\partial m_\pi^2}\int\frac{d^3k}{(2\pi)^3}\,\mathbf{k}^2\,\frac{\theta\big(\xi_a-|\mathbf{k}-\mathbf{P}|\big)+\theta\big(\xi_b-|\mathbf{k}+\mathbf{P}|\big)}{(\mathbf{k}+\vec{\lambda}(y))^2+\Delta^2(y)} \\ = l^{(2)}_{02,m}(p,P,\cos\varphi,\cos\beta,\cos\beta',\xi_a) + l^{(2)}_{02,m}(p,P,\cos\varphi,-\cos\beta,-\cos\beta',\xi_b)\,. \tag{D.136}$$

Applying the shift $\mathbf{k} \to \mathbf{k} - \vec{\lambda}(y)$ we can perform the momentum integration without further problems and obtain for both pieces

$$l^{(2)}_{02,m}(p, P, \cos\varphi, \pm\cos\beta, \pm\cos\beta', \xi_{a/b}) = \int_0^1 dy\, \frac{-\partial}{\partial m_\pi^2} \int \frac{d^3k}{(2\pi)^3}\, \mathbf{k}^2\, \frac{\theta\big(\xi_{a/b} - |\mathbf{k} \mp \vec{\lambda}_{2/1}|\big)}{\mathbf{k}^2 + \Delta(y)^2}$$
$$= \frac{1}{8\pi^2} \int_0^1 dy\, \Delta \Bigg\{ 2u - 3\arctan(u+z) - 3\arctan(u-z) + \frac{2 + u^2 - z^2}{2z} \ln\Big(\frac{(u+z)^2+1}{(u-z)^2+1}\Big) \Bigg\}\,, \tag{D.137}$$

with $u \doteq \xi_{a/b}/\Delta$ and $z \doteq \lambda_{2/1}/\Delta = \sqrt{P^2 + \lambda^2 \pm 2P\lambda\cos\eta}/\Delta$, where $\cos\eta(y)$ was defined in eq. (C.46).

Appendix E

Nucleon-nucleon interaction kernels

E.1 LO interaction kernel

In this section we give the partial waves of the interaction kernel at leading order $N^{(0)}_{JI}(\ell',\ell,S)$ with total spin S, in- and out-going orbital angular momentum ℓ and ℓ', total angular momentum J and total isospin I. The basic amplitude is depicted in figure 4.1 and is given in eqs. (4.2) and (4.3) and its partial wave projection is to be obtained from eq. (4.4). The partial waves up to F–wave read

$$
\begin{aligned}
N^{(0)}_{01}(0,0,0) &= -(C_S - 3C_T) - \frac{g_A^2}{4f_\pi^2}\frac{1}{4p^2}\left[4p^2 + m_\pi^2 \ln\frac{m_\pi^2}{m_\pi^2+4p^2}\right] , \\
N^{(0)}_{10}(0,0,1) &= -(C_S + C_T) - \frac{g_A^2}{4f_\pi^2}\frac{1}{4p^2}\left[4p^2 + m_\pi^2 \ln\frac{m_\pi^2}{m_\pi^2+4p^2}\right] , \\
N^{(0)}_{10}(1,1,0) &= \frac{g_A^2}{4f_\pi^2}\frac{3m_\pi^2}{8p^4}\left[4p^2 + (m_\pi^2+2p^2) \ln\frac{m_\pi^2}{m_\pi^2+4p^2}\right] , \\
N^{(0)}_{01}(1,1,1) &= \frac{g_A^2}{4f_\pi^2}\frac{1}{4p^2}\left[4p^2 + m_\pi^2 \ln\frac{m_\pi^2}{m_\pi^2+4p^2}\right] , \\
N^{(0)}_{11}(1,1,1) &= \frac{g_A^2}{4f_\pi^2}\frac{1}{16p^4}\left[4p^2(m_\pi^2-2p^2) + m_\pi^4 \ln\frac{m_\pi^2}{m_\pi^2+4p^2}\right] , \\
N^{(0)}_{21}(1,1,1) &= \frac{g_A^2}{4f_\pi^2}\frac{1}{80p^4}\left[4p^2(3m_\pi^2+2p^2) + m_\pi^2(3m_\pi^2+8p^2) \ln\frac{m_\pi^2}{m_\pi^2+4p^2}\right] , \\
N^{(0)}_{21}(2,2,0) &= -\frac{g_A^2}{4f_\pi^2}\frac{m_\pi^2}{32p^6}\left[12p^2(m_\pi^2+2p^2) + (3m_\pi^4+12m_\pi^2p^2+8p^4) \ln\frac{m_\pi^2}{m_\pi^2+4p^2}\right] , \\
N^{(0)}_{10}(2,2,1) &= -\frac{g_A^2}{4f_\pi^2}\frac{1}{16p^4}\left[4p^2(3m_\pi^2+2p^2) + m_\pi^2(3m_\pi^2+8p^2) \ln\frac{m_\pi^2}{m_\pi^2+4p^2}\right] , \\
N^{(0)}_{20}(2,2,1) &= -\frac{g_A^2}{4f_\pi^2}\frac{1}{16p^6}\left[4p^2(3m_\pi^4+3m_\pi^2p^2-2p^4) + 3(m_\pi^6+3m_\pi^4p^2) \ln\frac{m_\pi^2}{m_\pi^2+4p^2}\right] , \\
N^{(0)}_{30}(2,2,1) &= -\frac{g_A^2}{4f_\pi^2}\frac{1}{224p^6}\Big[4p^2(15m_\pi^4+42m_\pi^2p^2+8p^4) \\
&\qquad + 3m_\pi^2(5m_\pi^4+24m_\pi^2p^2+24p^4) \ln\frac{m_\pi^2}{m_\pi^2+4p^2}\Big] ,
\end{aligned}
$$

$$
\begin{aligned}
N_{30}^{(0)}(3,3,0) &= \frac{g_A^2}{4f_\pi^2}\frac{m_\pi^2}{64p^8}\Big[4p^2(15m_\pi^4+60m_\pi^2p^2+44p^4) \\
&\quad + 3(5m_\pi^6+30m_\pi^4p^2+48m_\pi^2p^4+16p^4)\ln\frac{m_\pi^2}{m_\pi^2+4p^2}\Big]\,, \\
N_{21}^{(0)}(3,3,1) &= \frac{g_A^2}{4f_\pi^2}\frac{1}{480p^6}\Big[4p^2(15m_\pi^4+42m_\pi^2p^2+8p^4) \\
&\quad + 3m_\pi^2(5m_\pi^4+24m_\pi^2p^2+24p^4)\ln\frac{m_\pi^2}{m_\pi^2+4p^2}\Big]\,, \\
N_{31}^{(0)}(3,3,1) &= \frac{g_A^2}{4f_\pi^2}\frac{1}{768p^8}\Big[4p^2(45m_\pi^6+150m_\pi^4p^2+48m_\pi^2p^4-16p^6) \\
&\quad + 3m_\pi^4(15m_\pi^4+80m_\pi^2p^2+96p^4)\ln\frac{m_\pi^2}{m_\pi^2+4p^2}\Big]\,, \\
N_{41}^{(0)}(3,3,1) &= \frac{g_A^2}{4f_\pi^2}\frac{1}{6912p^8}\Big[4p^2(105m_\pi^6+510m_\pi^4p^2+560m_\pi^2p^4+48p^6) \\
&\quad + 3m_\pi^2(35m_\pi^6+240m_\pi^4p^2+480m_\pi^2p^4+256p^6)\ln\frac{m_\pi^2}{m_\pi^2+4p^2}\Big]\,, \\
N_{30}^{(0)}(4,4,1) &= -\frac{g_A^2}{4f_\pi^2}\frac{1}{1792p^8}\Big[4p^2(105m_\pi^6+510m_\pi^4p^2+560m_\pi^2p^4+48p^6) \\
&\quad + 3m_\pi^2(35m_\pi^6+240m_\pi^4p^2+480m_\pi^2p^4+256p^6)\ln\frac{m_\pi^2}{m_\pi^2+4p^2}\Big] \\
N_{10}^{(0)}(0,2,1) &= N_{10}^{(0)}(2,0,1) \\
&= -\frac{g_A^2}{4f_\pi^2}\frac{\sqrt{2}}{16p^4}\Big[4p^2(3m_\pi^2-2p^2)+m_\pi^2(3m_\pi^2+4p^2)\ln\frac{m_\pi^2}{m_\pi^2+4p^2}\Big]\,, \\
N_{21}^{(0)}(1,3,1) &= N_{21}^{(0)}(3,1,1) \\
&= \frac{g_A^2}{4f_\pi^2}\frac{\sqrt{6}}{480p^6}\Big[4p^2(15m_\pi^4+24m_\pi^2p^2-4p^4) \\
&\quad + 3m_\pi^2(5m_\pi^4+18m_\pi^2p^2+8p^4)\ln\frac{m_\pi^2}{m_\pi^2+4p^2}\Big]\,, \\
N_{30}^{(0)}(2,4,1) &= N_{30}^{(0)}(4,2,1) \\
&= -\frac{g_A^2}{4f_\pi^2}\frac{\sqrt{3}}{896p^8}\Big[4p^2(105m_\pi^6+390m_\pi^4p^2+224m_\pi^2p^4-16p^6) \\
&\quad + 3m_\pi^2(35m_\pi^6+200m_\pi^4p^2+288m_\pi^2p^4+64p^6)\ln\frac{m_\pi^2}{m_\pi^2+4p^2}\Big]\,,
\end{aligned}
\tag{E.1}
$$

including those amplitudes coupling different ℓ and $\bar{\ell}$.

E.2 NLO contributions to in-medium NN interactions

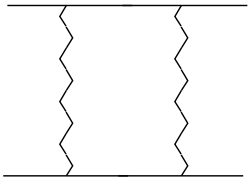

Figure E.1: The two-nucleon reducible loop corresponding to $L_{JI}^{(1)}$. The exchange of a wiggly line, the basic interaction, corresponds to local plus one-pion exchange terms, fig. 4.1. Taking into account that a wiggle exchange always has a crossed part, the twice iterated wiggle exchange has a symmetry factor of 1/2.

In this section we evaluate explicitly $L_{JI}^{(1)}$, since it enters for fixing the interaction kernel at NLO $N_{JI}^{(1)}$, which is necessary for calculations in chapters 4–7. When the two-nucleon reducible loop, includes only nucleon-nucleon local vertices, we have $\mathcal{T}_1$. At the same order, when one of the wiggly lines corresponds to a one-pion exchange, $\mathcal{T}_2$ results. Finally, when both lines are due to one-pion exchange, one has $\mathcal{T}_3$. As explained in section 4.2 only the direct terms of diagrams are used to evaluate the different partial waves and we can write

$$L_{JI}^{(1)}(\ell', \ell, S) = \mathcal{T}_{1,d} + \mathcal{T}_{2,d} + \mathcal{T}_{3,d} \ . \tag{E.2}$$

E.2.1 Spin and isospin projections

Beforehand, let us consider the projection onto certain spin oder isospin states. Since both obey the same calculus, we give here a general treatment. Be $(\alpha\beta q|ABQ)$ the Clebsch-Gordan coefficient of two quantum numbers A, B coupling to a quantum number Q with z-components α, β and q, respectively. Given below is a table for the matrix elements $\langle Q, q'|\mathcal{Q}|Q, q\rangle$ with several operators $\mathcal{Q}$, where Q can take the values 0 or 1, according to A and B being 1/2.

$\mathcal{Q}$	$Q=0$	$Q=1$
$\delta_{\alpha'\alpha}\delta_{\beta'\beta}$	1	$\mathbb{I}$
$\delta_{\alpha'\beta}\delta_{\beta'\alpha}$	-1	$\mathbb{I}$
$\vec{\sigma}_{\alpha'\alpha}\cdot\vec{\sigma}_{\beta'\beta}$	-3	$\mathbb{I}$
$\vec{\sigma}_{\alpha'\beta}\cdot\vec{\sigma}_{\beta'\alpha}$	3	$\mathbb{I}$
$\left(\vec{\sigma}_{\alpha'\gamma}\cdot\vec{\sigma}_{\beta'\delta}\right)\left(\vec{\sigma}_{\gamma\alpha}\cdot\vec{\sigma}_{\delta\beta}\right)$	9	$\mathbb{I}$
$\left(\vec{\sigma}_{\alpha'\delta}\cdot\vec{\sigma}_{\beta'\gamma}\right)\left(\vec{\sigma}_{\gamma\alpha}\cdot\vec{\sigma}_{\delta\beta}\right)$	-9	$\mathbb{I}$
$\delta_{\alpha'\alpha}\sigma^i_{\beta'\beta}+\sigma^i_{\alpha'\alpha}\delta_{\beta'\beta}$	0	$\mathbb{B}^i_{\alpha'+\beta',\alpha+\beta}$
$\delta_{\alpha'\beta}\sigma^i_{\beta'\alpha}+\sigma^i_{\alpha'\beta}\delta_{\beta'\alpha}$	0	$\mathbb{B}^i_{\alpha'+\beta',\alpha+\beta}$
$\sigma^i_{\alpha'\alpha}\sigma^j_{\beta'\beta}$	$-\delta^{ij}$	$\mathbb{B}^{ij}_{\alpha'+\beta',\alpha+\beta}$
$\sigma^i_{\alpha'\beta}\sigma^j_{\beta'\alpha}$	δ^{ij}	$\mathbb{B}^{ij}_{\alpha'+\beta',\alpha+\beta}$

Table E.1: Operators projected onto states with well defined quantum numbers. Here σ^i are the Pauli matrices and $\mathbb{I}$ is the unity matrix. The vector and the rank-two-tensor operators $\mathbb{B}^i$ and $\mathbb{B}^{ij}$ are given in eqs. (E.3) and (E.4), respectively. The indices represent the z-components of the quantum states, with α, β corresponding to the initial and α', β' to the final states.

We introduce the abbreviation $\delta^{i\pm} \doteq \delta^{i1} \pm i\delta^{i2}$. Then the matrix of the vector operator is

$$\mathbb{B}^{i}_{q',q} = \left(\begin{array}{c|ccc} & +1 & 0 & -1 \\ \hline +1 & 2\delta^{i3} & \sqrt{2}\delta^{i+} & 0 \\ 0 & \sqrt{2}\delta^{i-} & 0 & \sqrt{2}\delta^{i+} \\ -1 & 0 & \sqrt{2}\delta^{i-} & -2\delta^{i3} \end{array}\right) . \tag{E.3}$$

and the matrix of the tensor operator of rank two is given by

$$\mathbb{B}^{ij}_{q',q} = \left(\begin{array}{c|ccc} & +1 & 0 & -1 \\ \hline +1 & \delta^{i3}\delta^{j3} & \frac{\delta^{i3}\delta^{j-}+\delta^{i-}\delta^{j3}}{\sqrt{2}} & \delta^{i-}\delta^{j-} \\ 0 & \frac{\delta^{i3}\delta^{j+}+\delta^{i+}\delta^{j3}}{\sqrt{2}} & \delta^{ij} - 2\delta^{i3}\delta^{j3} & -\frac{\delta^{i3}\delta^{j-}+\delta^{i-}\delta^{j3}}{\sqrt{2}} \\ -1 & \delta^{i+}\delta^{j+} & -\frac{\delta^{i3}\delta^{j+}+\delta^{i+}\delta^{j3}}{\sqrt{2}} & \delta^{i3}\delta^{j3} \end{array}\right) . \tag{E.4}$$

Now, we can proceed calculating the box diagram fig. E.1.

E.2.2 Explicit calculation of $\mathcal{T}_1$

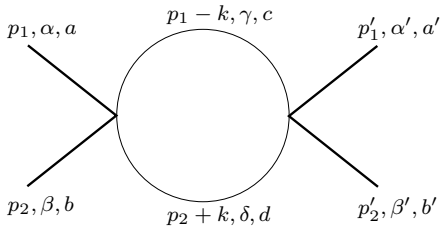

Figure E.2: The four-momenta, spin and isospin indices are shown on this figure contributing to $\mathcal{T}_1$. The symmetry factor of the diagram is 1/2.

We first consider the two-nucleon reducible loop with only local vertices, fig. E.2. With the four nucleon local vertex of eq. (4.2) we have for $\mathcal{T}_1$

$$\begin{aligned}\mathcal{T}_1 = -\frac{1}{2}\Big\{ & C_S\left(\delta_{\alpha'\gamma}\delta_{\beta'\delta}\delta_{a'c}\delta_{b'd} - \delta_{\alpha'\delta}\delta_{\beta'\gamma}\delta_{a'd}\delta_{b'c}\right) + C_T\left(\vec{\sigma}_{\alpha'\gamma}\cdot\vec{\sigma}_{\beta'\delta}\delta_{a'c}\delta_{b'd} - \vec{\sigma}_{\alpha'\delta}\cdot\vec{\sigma}_{\beta'\gamma}\delta_{a'd}\delta_{b'c}\right)\Big\} \\ & \times i\int\frac{d^4k}{(2\pi)^4}G_0(p_1-k)_c G_0(p_2+k)_d\Big\{C_S\left(\delta_{\gamma\alpha}\delta_{\delta\beta}\delta_{ca}\delta_{db} - \delta_{\gamma\beta}\delta_{\delta\alpha}\delta_{cb}\delta_{da}\right) \\ & + C_T\left(\vec{\sigma}_{\gamma\alpha}\cdot\vec{\sigma}_{\delta\beta}\delta_{ca}\delta_{db} - \vec{\sigma}_{\gamma\beta}\cdot\vec{\sigma}_{\delta\alpha}\delta_{cb}\delta_{da}\right)\Big\} .\end{aligned} \tag{E.5}$$

The spin indices are indicated with greek and the isospin with latin letters. The momentum integration in the previous equation is the same as for the function L_{10}. In this way, after some straightforward algebra one can write

$$\begin{aligned}\mathcal{T}_1 = -L^{i_3}_{10}\Big\{ & \Big[C_S^2\delta_{\alpha'\alpha}\delta_{\beta'\beta} + 2C_SC_T\vec{\sigma}_{\alpha'\alpha}\cdot\vec{\sigma}_{\beta'\beta} + C_T^2(\vec{\sigma}_{\alpha'\gamma}\cdot\vec{\sigma}_{\beta'\delta})(\vec{\sigma}_{\gamma\alpha}\cdot\vec{\sigma}_{\delta\beta})\Big]\delta_{a'a}\delta_{b'b} \\ & - \Big[C_S^2\delta_{\alpha'\beta}\delta_{\beta'\alpha} + 2C_SC_T\vec{\sigma}_{\alpha'\beta}\cdot\vec{\sigma}_{\beta'\alpha} + C_T^2(\vec{\sigma}_{\alpha'\gamma}\cdot\vec{\sigma}_{\beta'\delta})(\vec{\sigma}_{\gamma\beta}\cdot\vec{\sigma}_{\delta\alpha})\Big]\delta_{a'b}\delta_{b'a}\Big\}\end{aligned} \tag{E.6}$$

This equation contains both the direct and exchange terms, the latter corresponding to the last contribution between squared brackets preceded by a minus sign. However, as explained in eq. (A.28)

the direct term is the only one needed to evaluate the different partial waves. Working out the spin and isospin projections of the direct term we obtain the result

$$\mathcal{T}_{1,d} = -f_I f_S \, L_{10}^{i_3} \ . \tag{E.7}$$

In this equation the subscript d indicates that we are keeping only the direct contribution. The isospin factor f_I and the spin factor f_S are given by

$$f_I = 1 \ , \qquad f_S = (C_S + (4S-3)C_T)^2 \ . \tag{E.8}$$

Notice that since $L_{10}^{i_3}$ is pure S-wave – because it only depends on A and P^2 – $\mathcal{T}_1$ only contributes to the partial waves ${}^1S_0$ and ${}^3S_1$.

E.2.3 Explicit calculation of $\mathcal{T}_2$

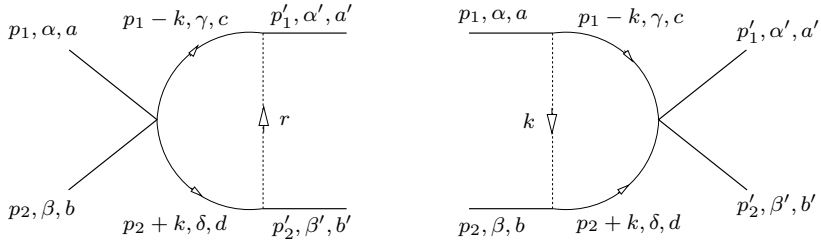

Figure E.3: The four-momenta, spin and isospin indices are shown on this figure contributing to $\mathcal{T}_2^f$ (left hand side) and $\mathcal{T}_2^i$ (right hand side). With the crossed channels of the pion exchange, the symmetry factor of each diagram is 1/2.

We now consider $\mathcal{T}_2$, with a local and a one-pion exchange vertex. The contribution corresponds to the left and side of fig. E.3, T_2^f, and the right hand side, T_2^i, depending on whether the one-pion exchange is between the final or initial two nucleons, respectively. Taking into account that the direct and crossed channels of the pion exchange cancels the symmetry factor, one has for the final state pion exchange

$$\begin{aligned}\mathcal{T}_2^f = \left(\frac{g_A}{2f_\pi}\right)^2 i \int \frac{d^4k}{(2\pi)^4} \Big\{ &\left[C_S(\vec{\sigma}_{\alpha'\alpha}\cdot\mathbf{r})(\vec{\sigma}_{\beta'\beta}\cdot\mathbf{r}) + C_T(\vec{\sigma}_{\alpha'\gamma}\cdot\mathbf{r})(\vec{\sigma}_{\beta'\delta}\cdot\mathbf{r})(\vec{\sigma}_{\gamma\alpha}\cdot\vec{\sigma}_{\delta\beta})\right]\tau^i_{a'a}\tau^i_{b'b} \\ &- \left[C_S(\vec{\sigma}_{\alpha'\beta}\cdot\mathbf{r})(\vec{\sigma}_{\beta'\alpha}\cdot\mathbf{r}) + C_T(\vec{\sigma}_{\alpha'\gamma}\cdot\mathbf{r})(\vec{\sigma}_{\beta'\delta}\cdot\mathbf{r})(\vec{\sigma}_{\gamma\beta}\cdot\vec{\sigma}_{\delta\alpha})\right]\tau^i_{a'b}\tau^i_{b'a}\Big\} \\ &\times G_0(p_1-q)_a G_0(p_2+q)_b \frac{1}{\mathbf{r}^2+m_\pi^2} \ , \end{aligned} \tag{E.9}$$

where the repeated indices are summed and $r = p_1' - p_1 + k$. For the pion propagator we neglect its dependence on r_0^2, since it is $\mathcal{O}(p^4)$, while $\mathbf{r}^2$ is $\mathcal{O}(p^2)$. Let us consider the isospin and spin projections for the direct term, given by the first term in the previous equation. The spin operator, after some algebraic manipulation in the term proportional to C_T, reads

$$(C_S + C_T)(\vec{\sigma}_{\alpha'\alpha}\cdot\mathbf{r})(\vec{\sigma}_{\beta'\beta}\cdot\mathbf{r}) + C_T\,\mathbf{r}^2\left(\delta_{\alpha'\alpha}\delta_{\beta'\beta} - \vec{\sigma}_{\alpha'\alpha}\cdot\vec{\sigma}_{\beta'\beta}\right) \ . \tag{E.10}$$

Those spin structures are already projected in tab. E.1 for the different states. The same for the isospin operator $\tau^i_{a'a}\tau^i_{b'b}$, whose projection between states of well defined isospin is given by $4I-3$. Then, we can write for the direct term with total spin $S=0$

$$\mathcal{T}_{2,d}^f = (C_S - 3C_T)(4I-3)\left(\frac{g_A}{2f_\pi}\right)^2 i\int\frac{d^4k}{(2\pi)^4} G_0(p_1-k)_a G_0(p_2+k)_b \frac{-\mathbf{r}^2}{\mathbf{r}^2+m_\pi^2} \ , \tag{E.11}$$

and with total spin $S = 1$

$$\mathcal{T}^f_{2,d}(s'_3, s_3) = (C_S + C_T)(4I - 3)\left(\frac{g_A}{2f_\pi}\right)^2 i \int \frac{d^4k}{(2\pi)^4} G_0(p_1 - k)_a G_0(p_2 + k)_b \frac{r^i r^i}{\mathbf{r}^2 + m_\pi^2} B^{ij}_{s'_3\, s_3} \ . \quad \text{(E.12)}$$

For the integrals it is convenient to perform the shift of the integration variable

$$k \ \rightarrow \ k + \frac{p_1 - p_2}{2} = k + p \ , \quad \text{(E.13)}$$

which implies with $2P = p_1 + p_2$ and $2p' = p'_1 - p'_2$ that

$$\begin{aligned} p_1 - k \ &\rightarrow \ P - k \ , \\ p_2 + k \ &\rightarrow \ P + k \ , \\ r = p'_1 - p_1 + k \ &\rightarrow \ k + p' \ . \end{aligned} \quad \text{(E.14)}$$

From eqs. (E.11) and (E.12) can be read off that we have to project the integration on states with well defined quantum numbers. We can express the different matrix elements of $\mathcal{T}^f_2$ in terms of the scalar integrals defined and evaluated in app. C and the reduced tensorial integrals of app. D. The direct term of the amplitude for spin $S = 0$ is

$$\mathcal{T}^f_{2,d} = f_I f_S \left\{ m_\pi^2 \widetilde{L}_{11} - \widetilde{L}_{10} \right\} , \quad \text{(E.15)}$$

and for $S = 1$ the matrix reads

$$\begin{aligned}
\mathcal{T}^f_{2,d}(+,+) &= f_I f_S \left\{ \widetilde{L}^{00}_{11} + {p'_z}^2 \Big[\widetilde{L}_{11} + 2\widetilde{L}^p_{11} + \widetilde{L}^{pp}_{11} \Big] + 2p'_z P_z \Big[\widetilde{L}^P_{11} + \widetilde{L}^{Pp}_{11} \Big] + P_z^2 \widetilde{L}^{PP}_{11} \right\} , \\
\mathcal{T}^f_{2,d}(+,-) &= f_I f_S \left\{ (p'_x - ip'_y)^2 \Big[\widetilde{L}_{11} + 2\widetilde{L}^p_{11} + \widetilde{L}^{pp}_{11} \Big] + 2(p'_x - ip'_y)(P_x - iP_y) \Big[\widetilde{L}^P_{11} + \widetilde{L}^{Pp}_{11} \Big] \right. \\
&\quad \left. + (P_x - iP_y)^2 \widetilde{L}^{PP}_{11} \right\} , \\
\mathcal{T}^f_{2,d}(-,+) &= f_I f_S \left\{ (p'_x + ip'_y)^2 \Big[\widetilde{L}_{11} + 2\widetilde{L}^p_{11} + \widetilde{L}^{pp}_{11} \Big] + 2(p'_x + ip'_y)(P_x + iP_y) \Big[\widetilde{L}^P_{11} + \widetilde{L}^{Pp}_{11} \Big] \right. \\
&\quad \left. + (P_x + iP_y)^2 \widetilde{L}^{PP}_{11} \right\} , \\
\mathcal{T}^f_{2,d}(+,0) &= f_I f_S \sqrt{2} \Big\{ (p'_x - ip'_y) \Big[p'_z \big(\widetilde{L}_{11} + 2\widetilde{L}^p_{11} + \widetilde{L}^{pp}_{11} \big) + P_z \big(\widetilde{L}^P_{11} + \widetilde{L}^{Pp}_{11} \big) \Big] \\
&\quad + (P_x - iP_y) \Big[p'_z \big(\widetilde{L}^P_{11} + \widetilde{L}^{Pp}_{11} \big) + P_z \widetilde{L}^{PP}_{11} \Big] \Big\} , \\
\mathcal{T}^f_{2,d}(0,+) &= f_I f_S \sqrt{2} \Big\{ (p'_x + ip'_y) \Big[p'_z \big(\widetilde{L}_{11} + 2\widetilde{L}^p_{11} + \widetilde{L}^{pp}_{11} \big) + P_z \big(\widetilde{L}^P_{11} + L^{Pp}_{11} \big) \Big] \\
&\quad + (P_x + iP_y) \Big[p'_z \big(\widetilde{L}^P_{11} + \widetilde{L}^{Pp}_{11} \big) + P_z \widetilde{L}^{PP}_{11} \Big] \Big\} , \\
\mathcal{T}^f_{2,d}(-,-) &= \mathcal{T}^f_{2,d}(+,+) \ , \\
\mathcal{T}^f_{2,d}(0,0) &= -2\, \mathcal{T}^f_{2,d}(+,+) - \mathcal{T}^f_{2,d} \ , \\
\mathcal{T}^f_{2,d}(0,-) &= -\mathcal{T}^f_{2,d}(+,0) \ , \\
\mathcal{T}^f_{2,d}(-,0) &= -\mathcal{T}^f_{2,d}(0,+) \ .
\end{aligned} \quad \text{(E.16)}$$

The tilde indicates the symmetric form

$$\widetilde{L}^{ij\cdots}_{1x} = \frac{1}{2}\left(L^{ij\cdots}_{1x}(a,b) + L^{ij\cdots}_{1x}(b,a)\right) \ , \tag{E.17}$$

where the superscript $ij\ldots$ outlines a tensor structure and the isospin labels a, b obey $i_z = a + b$. The isospin factor f_I and the spin factor f_S are given by

$$f_I = (4I-3)\left(\frac{g_A}{2f_\pi}\right)^2 \ , \qquad f_S = C_S + (4S-3)C_T \ . \tag{E.18}$$

For the one-pion exchange between the initial nucleons $\mathcal{T}_2^i$, right hand side of fig. E.3, we perform the same transformation in the integration variable as in eq. (E.13) and proceed in the same way as followed for the calculation of $\mathcal{T}_2^f$ above. We obtain, that the expressions for $\mathcal{T}_2^f$ can be used for $\mathcal{T}_2^i$ under the replacement $\mathbf{p}' \to \mathbf{p}$.

Let us now consider the partial wave projection of the $\mathcal{T}_2$. As discussed at the end of app. A, we can still use eq. (A.28), valid in the vacuum, if the integral in eq. (A.25) does not depend on $\hat{P}$. For $\mathcal{T}_2^f$, with the one-pion exchange between the final nucleons, this is clearly the case, because it only depends on $\hat{P}$ through its scalar product with $\mathbf{p}'$. Thus, there is no angular dependence left on $\mathbf{P}$ once the integration over $d\hat{\mathbf{p}}'$ is performed. For the case when the pion is exchanged between the initial nucleons, the resulting $\mathcal{T}_2^i$ do not depend on the final three-momentum $\hat{\mathbf{p}}'$. In this way, the integration over $d\hat{\mathbf{p}}'$ cannot remove the dependence on $\hat{P}$. This also implies that this diagram only can contribute to partial waves with $\ell' = 0$, that is ${}^3S_1$ and ${}^3D_1 \to {}^3S_1$. However, the exchange $\mathbf{p}' \leftrightarrow \mathbf{p}$ transforms $\mathcal{T}_2^f$ into $\mathcal{T}_2^i$ and vice versa. In addition, one has to notice the symmetry between $\mathbf{p}$ and $\mathbf{p}'$ for the partial wave decomposition in eq. (A.10). From this it is clear, that the same partial waves result for both diagrams of fig. E.3 with the exchange $\ell' \leftrightarrow \ell$. Thus, we can still use eq. (A.28) but using the diagrams with the pion exchanged between the final nucleons. The elastic partial wave ${}^3S_1$ is exactly the same for both diagrams and the transition matrix element ${}^3D_1 \to {}^3S_1$ is equal to ${}^3S_1 \to {}^3D_1$. We denote the corresponding partial waves by $\mathcal{T}^f_{2;JI}(\ell',\ell,S)$. Then one has the partial waves $\mathcal{T}_{2;01}(0,0,0) = \mathcal{T}^f_{2;01}(0,0,0) + \mathcal{T}^i_{2;01}(0,0,0) = 2\mathcal{T}^f_{2;01}(0,0,0)$, $\mathcal{T}_{2;10}(0,0,1) = \mathcal{T}^f_{2;10}(0,0,1) + \mathcal{T}^i_{2;10}(0,0,1) = 2\mathcal{T}^f_{2;10}(0,0,1)$, $\mathcal{T}_{2;10}(2,0,1) = \mathcal{T}^f_{2;10}(2,0,1)$ and $\mathcal{T}_{2;10}(0,2,1) = \mathcal{T}^i_{2;10}(0,2,1) = \mathcal{T}^f_{2;10}(2,0,1)$.

E.2.4 Explicit calculation of $\mathcal{T}_3$

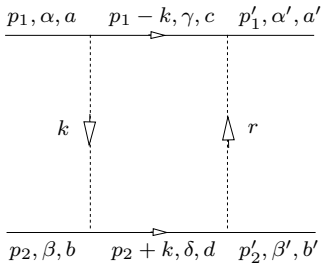

Figure E.4: The four-momenta, spin and isospin indices are shown on this figure contributing to $\mathcal{T}_3$. With the crossed channels of the pion exchanges, the symmetry factor of the diagram is 1/2.

Let us move now to the evaluation of $\mathcal{T}_3$ where both interactions in the two-nucleon reducible loop correspond to a one-pion exchange. The crossed channel of the first pion exchange cancels the

symmetry factor and we can write for the contribution from the diagram in fig. E.4

$$\mathcal{T}_3 = -\left(\frac{g_A}{2f_\pi}\right)^4 \tau^s_{ca}\tau^s_{db}\, i \int \frac{d^4k}{(2\pi)^4}(\vec\sigma_{\gamma\alpha}\cdot\mathbf{k})(\vec\sigma_{\delta\beta}\cdot\mathbf{k})\Big[\tau^t_{a'c}\tau^t_{b'd}(\vec\sigma_{\alpha'\gamma}\cdot\mathbf{r})(\vec\sigma_{\beta'\delta}\cdot\mathbf{r}) + \tau^t_{b'c}\tau^t_{a'd}(\vec\sigma_{\beta'\gamma}\cdot\mathbf{r})(\vec\sigma_{\alpha'\delta}\cdot\mathbf{r})\Big]\frac{1}{\mathbf{r}^2+m_\pi^2}\frac{1}{\mathbf{k}^2+m_\pi^2}G_0(p_1-k)_c G_0(p_2+k)_d\ . \quad \text{(E.19)}$$

The first summand corresponds again to the direct term which we will consider exclusively in following. The diagonal matrix elements of the isospin operator $\tau^t_{a'c}\tau^s_{ca}\tau^t_{b'd}\tau^s_{db}$ between states with well defined isospin is given as $9-8I$, according to tab. E.1. With respect to spin we can rewrite,

$$(\vec\sigma_{\alpha'\gamma}\cdot\mathbf{r})(\vec\sigma_{\beta'\delta}\cdot\mathbf{r})(\vec\sigma_{\gamma\alpha}\cdot\mathbf{k})(\vec\sigma_{\delta\beta}\cdot\mathbf{k}) = (\mathbf{r}\cdot\mathbf{k})^2\delta_{\alpha'\alpha}\delta_{\beta'\beta} + i\left[(\mathbf{r}\times\mathbf{k})\cdot\vec\sigma_{\alpha'\alpha}\right](\mathbf{r}\cdot\mathbf{k})\delta_{\beta'\beta} + (\mathbf{r}\cdot\mathbf{k})\delta_{\alpha'\alpha} i\left[(\mathbf{r}\times\mathbf{k})\cdot\vec\sigma_{\beta'\beta}\right] - \left[(\mathbf{r}\times\mathbf{k})\cdot\vec\sigma_{\alpha'\alpha}\right]\left[(\mathbf{r}\times\mathbf{k})\cdot\vec\sigma_{\beta'\beta}\right]\ . \quad \text{(E.20)}$$

The matrix elements of the spin operators between states with well defined total spin were already worked out in tab. E.1. Applying those one has for the operator of eq. (E.20):

$$\begin{aligned}
&S=0\to S=0\ : \mathbf{r}^2\,\mathbf{k}^2\ ,\\
&S=1\to S=1\ :\\
&\quad +1\to+1\ :\ [\mathbf{r}\cdot\mathbf{k}+i\,(\mathbf{r}\times\mathbf{k})_z]^2\ ,\\
&\quad -1\to-1\ :\ [\mathbf{r}\cdot\mathbf{k}-i\,(\mathbf{r}\times\mathbf{k})_z]^2\ ,\\
&\quad\ \ 0\to 0\ : 2(\mathbf{r}\cdot\mathbf{k})^2+2[(\mathbf{r}\times\mathbf{k})_z]^2-\mathbf{r}^2\mathbf{k}^2\ ,\\
&\quad +1\to-1\ :\ -[(\mathbf{r}\times\mathbf{k})_x+i\,(\mathbf{r}\times\mathbf{k})_y]^2\ ,\\
&\quad -1\to+1\ :\ -[(\mathbf{r}\times\mathbf{k})_x-i\,(\mathbf{r}\times\mathbf{k})_y]^2\ ,\\
&\quad\ +1\to 0\ :\sqrt{2}\,[(\mathbf{r}\times\mathbf{k})_x+i\,(\mathbf{r}\times\mathbf{k})_y]\,[i\,\mathbf{r}\cdot\mathbf{k}-(\mathbf{r}\times\mathbf{k})_z]\ ,\\
&\quad\ \ 0\to+1\ :\sqrt{2}\,[(\mathbf{r}\times\mathbf{k})_x-i\,(\mathbf{r}\times\mathbf{k})_y]\,[i\,\mathbf{r}\cdot\mathbf{k}-(\mathbf{r}\times\mathbf{k})_z]\ ,\\
&\quad\ \ 0\to-1\ :\sqrt{2}\,[(\mathbf{r}\times\mathbf{k})_x+i\,(\mathbf{r}\times\mathbf{k})_y]\,[i\,\mathbf{r}\cdot\mathbf{k}+(\mathbf{r}\times\mathbf{k})_z]\ ,\\
&\quad\ -1\to 0\ :\sqrt{2}\,[(\mathbf{r}\times\mathbf{k})_x-i\,(\mathbf{r}\times\mathbf{k})_y]\,[i\,\mathbf{r}\cdot\mathbf{k}+(\mathbf{r}\times\mathbf{k})_z]\ ,
\end{aligned} \quad \text{(E.21)}$$

where the Cartesian coordinates of $\mathbf{r}\times\mathbf{k}$ are indicated with subscripts. Performing the shift of eq. (E.13) we have $\mathbf{k}\to\mathbf{k}+\mathbf{p}$ and $\mathbf{r}\to\mathbf{k}+\mathbf{p}'$. Inserting into eq. (E.19) the matrix elements of eqs. (E.21) for spin and $9-8I$ for the isospin operator, the amplitudes $\mathcal{T}_{3,d}$ for $S=0$ and $T_{3,d}(s'_3,s_3)$ for $S=1$ can be determined. We choose the orientation of our reference frame such that $\mathbf{p}=p\hat e_z$ and $\cos\vartheta=\hat p\cdot\hat p'$ and define the abbreviations

$$\begin{aligned}
a_* &= p(p+p'_z)\ ,\\
a_\pm &= p(p'_x\pm ip'_y)\ ,\\
a^P_{++} &= (P_x+iP_y)(p'_x-ip'_y)+P_z(p+p'_z)\ ,\\
a^P_{--} &= (P_x-iP_y)(p'_x+ip'_y)+P_z(p+p'_z)\ ,\\
a^P_{00} &= P_xp'_x+P_yp'_y+P_z(p+p'_z)\ ,\\
a^P_{-+} &= (P_x+iP_y)(p-p'_z)+P_z(p'_x+ip'_y)\ ,\\
a^P_{+-} &= (P_x-iP_y)(p-p'_z)+P_z('p_x-ip'_y)\ .
\end{aligned} \quad \text{(E.22)}$$

There is still one choice left with respect to the orientation of the coordinate frame. Generally one would choose something like $P_x = 0$. We obtain for $S = 0$

$$\mathcal{T}_{3,d} = -f_I f_S \left\{ L_{10} - m_\pi^2 \left[L_{11}(\cos\beta) + L_{11}(\cos\beta') \right] + m_\pi^4 \, L_{12} \right\} , \tag{E.23}$$

with $\cos\beta = \hat{P}\cdot\hat{p}$ and $\cos\beta' = \hat{P}\cdot\hat{p}'$ and for $S = 1$

$$\begin{aligned}
\mathcal{T}_{3,d}(+,+) = -f_I f_S \Big\{ & p^4 \cos^2\vartheta \, L_{12} + 2p^2 \cos\vartheta \Big[a_* \, L_{12}^{p} + a_* \, L_{12}^{p'} + a_{++}^P \, L_{12}^P \Big] + 2p^2 \cos\vartheta \, L_{12}^{(2)} \\
& + a_*^2 L_{12}^{pp} + a_*^2 L_{12}^{p'p'} + (a_{++}^P)^2 L_{12}^{PP} + 2a_*^2 \, L_{12}^{pp'} + 2a_* a_{++}^P \, L_{12}^{Pp} + 2a_* a_{++}^P L_{12}^{Pp'} \\
& + 2\Big[a_* \, L_{12}^{(2)p} + a_* \, L_{12}^{(2)p'} + a_{++}^P \, L_{12}^{(2)P} \Big] + L_{12}^{(4)} \Big\} , \\
\mathcal{T}_{3,d}(-,-) = -f_I f_S \Big\{ & p^4 \cos^2\vartheta \, L_{12} + 2p^2 \cos\vartheta \Big[a_* \, L_{12}^{p} + a_* \, L_{12}^{p'} + a_{--}^P \, L_{12}^P \Big] + 2p^2 \cos\vartheta \, L_{12}^{(2)} \\
& + a_*^2 L_{12}^{pp} + a_*^2 L_{12}^{p'p'} + (a_{--}^P)^2 L_{12}^{PP} + 2a_*^2 \, L_{12}^{pp'} + 2a_* a_{--}^P \, L_{12}^{Pp} + 2a_* a_{--}^P L_{12}^{Pp'} \\
& + 2\Big[a_* \, L_{12}^{(2)p} + a_* \, L_{12}^{(2)p'} + a_{--}^P \, L_{12}^{(2)P} \Big] + L_{12}^{(4)} \Big\} , \\
\mathcal{T}_{3,d}(0,0) = -f_I f_S \, 2 \Big\{ & p^4 \cos^2\vartheta \, L_{12} + 2p^2 \cos\vartheta \Big[a_* \, L_{12}^{p} + a_* \, L_{12}^{p'} + a_{00}^P \, L_{12}^P \Big] + 2p^2 \cos\vartheta \, L_{12}^{(2)} \\
& + a_*^2 L_{12}^{pp} + a_*^2 \, L_{12}^{p'p'} + a_{++}^P a_{--}^P \, L_{12}^{PP} + 2a_*^2 \, L_{12}^{pp'} + 2a_* a_{00}^P \, L_{12}^{Pp} + 2a_* a_{00}^P \, L_{12}^{Pp'} \\
& + 2\Big[a_* \, L_{12}^{(2)p} + a_* \, L_{12}^{(2)p'} + a_{00}^P \, L_{12}^{(2)P} \Big] + L_{12}^{(4)} \Big\} - \mathcal{T}_{3,d} , \\
\mathcal{T}_{3,d}(-,+) = -f_I f_S \Big\{ & a_+^2 \Big[L_{12} + 2\, L_{12}^{p} + 2\, L_{12}^{p'} + L_{12}^{pp} + L_{12}^{p'p'} + 2\, L_{12}^{pp'} \Big] \\
& + 2a_+ a_{-+}^P \Big[L_{12}^P + L_{12}^{Pp} + L_{12}^{Pp'} \Big] + (a_{-+}^P)^2 L_{12}^{PP} \Big\} , \\
\mathcal{T}_{3,d}(+,-) = -f_I f_S \Big\{ & a_-^2 \Big[L_{12} + 2\, L_{12}^{p} + 2\, L_{12}^{p'} + L_{12}^{pp} + L_{12}^{p'p'} + 2\, L_{12}^{pp'} \Big] \\
& + 2a_- a_{+-}^P \Big[L_{12}^P + L_{12}^{Pp} + L_{12}^{Pp'} \Big] + (a_{+-}^P)^2 L_{12}^{PP} \Big\} , \\
\mathcal{T}_{3,d}(0,+) = -f_I f_S \sqrt{2} \Big\{ & a_+ p^2 \cos\vartheta \, L_{12} + a_+ \big(p^2 \cos\vartheta + a_* \big) \Big[L_{12}^{p} + L_{12}^{p'} \Big] + \big(a_+ a_{++}^P + a_{-+}^P p^2 \cos\vartheta \big) L_{12}^P \\
& + a_+ \, L_{12}^{(2)} + a_* a_+ \Big[L_{12}^{pp} + L_{12}^{p'p'} + 2L_{12}^{pp'} \Big] + a_{++}^P a_{-+}^P L_{12}^{PP} + \big(a_+ a_{++}^P + a_* a_{-+}^P \big) \, L_{12}^{Pp} \\
& + \big(a_+ a_{++}^P + a_* a_{-+}^P \big) \, L_{12}^{Pp'} + a_+ \Big[L_{12}^{(2)p} + L_{12}^{(2)p'} \Big] + a_{-+}^P \, L_{12}^{(2)P} \Big\} , \\
\mathcal{T}_{3,d}(+,0) = +f_I f_S \sqrt{2} \Big\{ & a_- p^2 \cos\vartheta \, L_{12} + a_- \big(p^2 \cos\vartheta + a_* \big) \Big[L_{12}^{p} + L_{12}^{p'} \Big] + \big(a_- a_{++}^P + a_{+-}^P p^2 \cos\vartheta \big) L_{12}^P \\
& + a_- \, L_{12}^{(2)} + a_* a_- \Big[L_{12}^{pp} + L_{12}^{p'p'} + 2L_{12}^{pp'} \Big] + a_{++}^P a_{+-}^P L_{12}^{PP} + \big(a_- a_{++}^P + a_* a_{+-}^P \big) \, L_{12}^{Pp} \\
& + \big(a_- a_{++}^P + a_* a_{+-}^P \big) \, L_{12}^{Pp'} + a_- \Big[L_{12}^{(2)p} + L_{12}^{(2)p'} \Big] + a_{+-}^P \, L_{12}^{(2)P} \Big\} , \\
\mathcal{T}_{3,d}(-,0) = -f_I f_S \sqrt{2} \Big\{ & a_+ p^2 \cos\vartheta \, L_{12} + a_+ \big(p^2 \cos\vartheta + a_* \big) \Big[L_{12}^{p} + L_{12}^{p'} \Big] + \big(a_+ a_{--}^P + a_{-+}^P p^2 \cos\vartheta \big) L_{12}^P
\end{aligned}$$

$$
\begin{aligned}
&+ a_+ L_{12}^{(2)} + a_* a_+ \Big[L_{12}^{pp} + L_{12}^{p'p'} + 2L_{12}^{pp'} \Big] + a_{--}^P a_{-+}^P L_{12}^{PP} + \big(a_+ a_{--}^P + a_* a_{-+}^P \big) L_{12}^{Pp} \\
&+ \big(a_+ a_{--}^P + a_* a_{-+}^P \big) L_{12}^{Pp'} + a_+ \Big[L_{12}^{(2)p} + L_{12}^{(2)p'} \Big] + a_{-+}^P L_{12}^{(2)P} \Big\} \,, \\
\mathcal{T}_{3,d}(0,-) = &+ f_I f_S \sqrt{2} \Big\{ a_- p^2 \cos\vartheta \, L_{12} + a_- \big(p^2 \cos\vartheta + a_* \big) \Big[L_{12}^{p} + L_{12}^{p'} \Big] + \big(a_- a_{--}^P + a_{+-}^P p^2 \cos\vartheta \big) L_{12}^{P} \\
&+ a_- L_{12}^{(2)} + a_* a_- \Big[L_{12}^{pp} + L_{12}^{p'p'} + 2L_{12}^{pp'} \Big] + a_{--}^P a_{+-}^P L_{12}^{PP} + \big(a_- a_{--}^P + a_* a_{+-}^P \big) L_{12}^{Pp} \\
&+ \big(a_- a_{--}^P + a_* a_{+-}^P \big) L_{12}^{Pp'} + a_- \Big[L_{12}^{(2)p} + L_{12}^{(2)p'} \Big] + a_{+-}^P L_{12}^{(2)P} \Big\} \,. \qquad \text{(E.24)}
\end{aligned}
$$

The isospin factor f_I and the spin factor f_S are given by

$$
f_I = (9 - 8I) \left(\frac{g_A}{2 f_\pi} \right)^4 \,, \qquad f_S = 1 \,. \qquad \text{(E.25)}
$$

E.3 NLO contributions to free NN interactions

It is convenient for calculations of nucleon-nucleon scattering in the vacuum to choose the reference frame identical with the center-of-mass system of the two interacting nucleons. Given the total momentum P equals zero, the expressions presented in the last section simplify extraordinary. Here we wish to give, in short, the contributions for the simplified case of vacuum calculations from nucleon-nucleon interactions at $\mathcal{O}(p)$. The calculations of section E.2 still holds, but the spin projections are simpler.

Contribution T_1 of fig. E.2 in the vacuum reads

$$T_{1,d} = -f_I f_S \, L_{10,f} \ , \tag{E.26}$$

with isospin and isospin factors f_I, f_S given in eq. (E.8).

The contributions of T_2 of fig. E.3 simplify to

$$\begin{aligned}
T^f_{2,d} &= f_I f_S \left\{ m_\pi^2 L_{11,f} - L_{10,f} \right\} \ , \\
T^f_{2,d}(+,+) &= f_I f_S \left\{ L^{00}_{11,f} + {p'_z}^2 \big(L_{11,f} + 2L^p_{11,f} + L^{pp}_{11,f} \big) \right\} \ , \\
T^f_{2,d}(+,-) &= f_I f_S \, (p'_x - i p'_y)^2 \big(L_{11,f} + 2L^p_{11,f} + L^{pp}_{11,f} \big) \\
T^f_{2,d}(-,+) &= f_I f_S \, (p'_x + i p'_y)^2 \big(L_{11,f} + 2L^p_{11,f} + L^{pp}_{11,f} \big) \\
T^f_{2,d}(+,0) &= f_I f_S \, \sqrt{2} (p'_x - i p'_y) p'_z \big(L_{11,f} + 2L^p_{11,f} + L^{pp}_{11,f} \big) \ , \\
T^f_{2,d}(0,+) &= f_I f_S \, \sqrt{2} (p'_x + i p'_y) p'_z \big(L_{11,f} + 2L^p_{11,f} + L^{pp}_{11,f} \big) \ , \\
T^f_{2,d}(-,-) &= T^f_{2,d}(+,+) \ , \\
T^f_{2,d}(0,0) &= -2 \, T^f_{2,d}(+,+) - T^f_{2,d} \ , \\
T^f_{2,d}(0,-) &= -T^f_{2,d}(+,0) \ , \\
T^f_{2,d}(-,0) &= -T^f_{2,d}(0,+) \ ,
\end{aligned} \tag{E.27}$$

with isospin and isospin factors f_I, f_S given in eq. (E.18).

For the case of T_3 of fig. E.4 with the abbreviations $a_* = p(p + p'_z)$, $a'_* = p(3p - p'_z)$ and $a_\pm = p(p'_x \pm i p'_y)$ the expressions of the spin projections simplify to

$$\begin{aligned}
T_{3,d} &= -f_I f_S \left\{ L_{10,f} - 2m_\pi^2 \, L_{11,f} + m_\pi^4 \, L_{12,f} \right\} \ , \\
T_{3,d}(+,+) &= -f_I f_S \Big\{ p^4 \cos^2\vartheta \, L_{12,f} + 4a_* p^2 \cos\vartheta \, L^p_{12,f} + 2p^2 \cos\vartheta \, L^{(2)}_{12,f} \\
&\qquad + a_*^2 \, L^{00}_{12,f}/p^2 + 2a_*^2 \Big[L^{pp}_{12,f} + L^{pp'}_{12,f} \Big] + 4a_* \, L^{(2)p}_{12,f} + L^{(4)}_{12,f} \Big\} \ , \\
T_{3,d}(-,-) &= T_{3,d}(+,+) \ , \\
T_{3,d}(0,0) &= -f_I f_S \, 2 \Big\{ p^4 \cos^2\vartheta \, L_{12,f} + 4a_* p^2 \cos\vartheta \, L^p_{12,f} + 2p^2 \cos\vartheta \, L^{(2)}_{12,f} \\
&\qquad + a_* a'_* \, L^{00}_{12,f}/p^2 + 2a_*^2 \Big[L^{pp}_{12,f} + L^{pp'}_{12,f} \Big] + 4a_* \, L^{(2)p}_{12,f} + L^{(4)}_{12,f} \Big\} - T_{3,d} \ ,
\end{aligned}$$

$$
\begin{aligned}
T_{3,d}(-,+) &= -f_I f_S\, a_+^2 \Big\{ L_{12,f} + 4\, L^{p}_{12,f} + L^{00}_{12,f}/p^2 + 2\, L^{pp}_{12,f} + 2\, L^{pp'}_{12,f} \Big\} \,, \\
T_{3,d}(+,-) &= -f_I f_S\, a_-^2 \Big\{ L_{12,f} + 4\, L^{p}_{12,f} + L^{00}_{12,f}/p^2 + 2\, L^{pp}_{12,f} + 2\, L^{pp'}_{12,f} \Big\} \,, \\
T_{3,d}(0,+) &= -f_I f_S\, \sqrt{2}\, a_+ \Big\{ p^2 \cos\vartheta\, L_{12,f} + 2(p^2\cos\vartheta + a_*)\, L^{p}_{12,f} + L^{(2)}_{12,f} \\
&\quad + a_*\, L^{00}_{12,f}/p^2 + 2a_* \Big[L^{pp}_{12,f} + L^{pp'}_{12,f} \Big] + 2\, L^{(2)p}_{12,f} \Big\} \,, \\
T_{3,d}(+,0) &= +f_I f_S\, \sqrt{2}\, a_- \Big\{ p^2 \cos\vartheta\, L_{12,f} + 2(p^2\cos\vartheta + a_*)\, L^{p}_{12,f} + L^{(2)}_{12,f} \\
&\quad + a'_*\, L^{00}_{12,f}/p^2 + 2a_* \Big[L^{pp}_{12,f} + L^{pp'}_{12,f} \Big] + 2\, L^{(2)p}_{12,f} \Big\} \,, \\
T_{3,d}(-,0) &= -f_I f_S\, \sqrt{2}\, a_+ \Big\{ p^2 \cos\vartheta\, L_{12,f} + 2(p^2\cos\vartheta + a_*)\, L^{p}_{12,f} + L^{(2)}_{12,f} \\
&\quad + a'_*\, L^{00}_{12,f}/p^2 + 2a_* \Big[L^{pp}_{12,f} + L^{pp'}_{12,f} \Big] + 2\, L^{(2)p}_{12,f} \Big\} \,, \\
T_{3,d}(0,-) &= +f_I f_S\, \sqrt{2}\, a_- \Big\{ p^2 \cos\vartheta\, L_{12,f} + 2(p^2\cos\vartheta + a_*)\, L^{p}_{12,f} + L^{(2)}_{12,f} \\
&\quad + a_*\, L^{00}_{12,f}/p^2 + 2a_* \Big[L^{pp}_{12,f} + L^{pp'}_{12,f} \Big] + 2\, L^{(2)p}_{12,f} \Big\} \,.
\end{aligned}
\tag{E.28}
$$

with isospin and isospin factors f_I, f_S given in eq. (E.25). Note, that the basis transformation described in eq. (D.69) et seqq. is not performed here, that is why the reduced scalar $L^{00}_{12,f}$ is not absorbed into the other reduced scalars of rank two and it occurs here explicitely.

E.4 LO contributions to in-medium NN interactions with scalar source

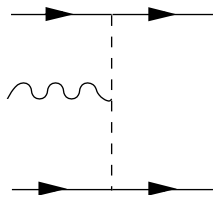

Figure E.5: The scalar source coupling to the one-pion exchange. Only the direct term is shown. Note, that a coupling of the scalar source coupling to a local four-nucleon vertex is two chiral orders higher.

The amplitude where the scalar source couples to the one-pion exchange, see fig. E.5, reads

$$T^{1\pi}_{NN\chi} = -B\delta_{ij}\left(\frac{g_A}{2f_\pi}\right)^2\left[\frac{\vec{\tau}_{a'a}\cdot\vec{\tau}_{b'b}(\vec{\sigma}_{\alpha'\alpha}\cdot\mathbf{q})(\vec{\sigma}_{\beta'\beta}\cdot\mathbf{q})}{(\mathbf{q}^2+m_\pi^2-i\epsilon)^2} - \frac{\vec{\tau}_{a'b}\cdot\vec{\tau}_{b'a}(\vec{\sigma}_{\alpha'\beta}\cdot\mathbf{q}')(\vec{\sigma}_{\beta'\alpha}\cdot\mathbf{q}')}{(\mathbf{q}'^2+m_\pi^2-i\epsilon)^2}\right] , \quad \text{(E.29)}$$

where α,β are a spin and a,b are isospin labels. The first terms corresponds to the direct term and the second to the crossed term. This can be rewritten as the derivative of the one-pion exchange amplitude with respect to the pion mass squared

$$T^{1\pi}_{NN\chi} = B\delta_{ij}\frac{\partial}{\partial m_\pi^2}T^{1\pi}_{NN} \ . \quad \text{(E.30)}$$

The amplitude can be partial wave projected according to eq. (4.4). Now we give the partial waves of the derivative with respect to the pion mass of the leading order interaction kernel $\frac{\partial N^{(0)}_{IJ}}{\partial m_\pi^2}(\ell',\ell,S)$ with total spin S, in- and out-going orbital angular momentum ℓ and ℓ', total angular momentum J and total isospin I. The partial waves up to D–wave read

$$\frac{\partial N^{(0)}_{01}}{\partial m_\pi^2}(0,0,0) = -\frac{g_A^2}{4f_\pi^2}\frac{1}{4p^2}\left[\frac{4p^2}{m_\pi^2+4p^2}+\ln\frac{m_\pi^2}{m_\pi^2+4p^2}\right] ,$$
$$\frac{\partial N^{(0)}_{10}}{\partial m_\pi^2}(0,0,1) = -\frac{g_A^2}{4f_\pi^2}\frac{1}{4p^2}\left[\frac{4p^2}{m_\pi^2+4p^2}+\ln\frac{m_\pi^2}{m_\pi^2+4p^2}\right] ,$$
$$\frac{\partial N^{(0)}_{10}}{\partial m_\pi^2}(1,1,0) = \frac{g_A^2}{4f_\pi^2}\frac{3}{4p^4}\left[\frac{4p^2(m_\pi^2+3p^2)}{m_\pi^2+4p^2}+(m_\pi^2+p^2)\ln\frac{m_\pi^2}{m_\pi^2+4p^2}\right] ,$$
$$\frac{\partial N^{(0)}_{01}}{\partial m_\pi^2}(1,1,1) = \frac{g_A^2}{4f_\pi^2}\frac{1}{4p^2}\left[\frac{4p^2}{m_\pi^2+4p^2}+\ln\frac{m_\pi^2}{m_\pi^2+4p^2}\right] ,$$
$$\frac{\partial N^{(0)}_{11}}{\partial m_\pi^2}(1,1,1) = \frac{g_A^2}{4f_\pi^2}\frac{1}{8p^4}\left[\frac{4p^2(m_\pi^2+2p^2)}{m_\pi^2+4p^2}+m_\pi^2\ln\frac{m_\pi^2}{m_\pi^2+4p^2}\right] ,$$
$$\frac{\partial N^{(0)}_{21}}{\partial m_\pi^2}(1,1,1) = \frac{g_A^2}{4f_\pi^2}\frac{1}{40p^4}\left[\frac{4p^2(3m_\pi^2+10p^2)}{m_\pi^2+4p^2}+(3m_\pi^2+4p^2)\ln\frac{m_\pi^2}{m_\pi^2+4p^2}\right] ,$$
$$\frac{\partial N^{(0)}_{21}}{\partial m_\pi^2}(2,2,0) = -\frac{g_A^2}{4f_\pi^2}\frac{1}{32p^6}\left[\frac{4p^2(9m_\pi^4+42m_\pi^2p^2+32p^4)}{m_\pi^2+4p^2}+(9m_\pi^4+24m_\pi^2p^2+8p^4)\ln\frac{m_\pi^2}{m_\pi^2+4p^2}\right] ,$$
$$\frac{\partial N^{(0)}_{10}}{\partial m_\pi^2}(2,2,1) = -\frac{g_A^2}{4f_\pi^2}\frac{1}{8p^4}\left[\frac{4p^2(3m_\pi^2+10p^2)}{m_\pi^2+4p^2}+(3m_\pi^2+4p^2)\ln\frac{m_\pi^2}{m_\pi^2+4p^2}\right] ,$$

$$
\begin{aligned}
\frac{\partial N_{20}^{(0)}}{\partial m_\pi^2}(2,2,1) &= -\frac{g_A^2}{4f_\pi^2}\frac{3}{16p^6}\left[\frac{4p^2(3m_\pi^4+12m_\pi^2p^2+4p^4)}{m_\pi^2+4p^2}+3m_\pi^2(m_\pi^2+2p^2)\ln\frac{m_\pi^2}{m_\pi^2+4p^2}\right], \\
\frac{\partial N_{30}^{(0)}}{\partial m_\pi^2}(2,2,1) &= -\frac{g_A^2}{4f_\pi^2}\frac{3}{224p^6}\left[\frac{4p^2(15m_\pi^4+78m_\pi^2p^2+80p^4)}{m_\pi^2+4p^2}+3(5m_\pi^4+16m_\pi^2p^2+8p^4)\ln\frac{m_\pi^2}{m_\pi^2+4p^2}\right], \\
\frac{\partial N_{21}^{(0)}}{\partial m_\pi^2}(3,3,1) &= \frac{g_A^2}{4f_\pi^2}\frac{1}{160p^6}\left[\frac{4p^2(15m_\pi^4+78m_\pi^2p^2+80p^4)}{m_\pi^2+4p^2}+3(5m_\pi^4+16m_\pi^2p^2+8p^4)\ln\frac{m_\pi^2}{m_\pi^2+4p^2}\right], \\
\frac{\partial N_{30}^{(0)}}{\partial m_\pi^2}(4,4,1) &= -\frac{g_A^2}{4f_\pi^2}\frac{1}{448p^8}\left[\frac{4p^2(105m_\pi^6+750m_\pi^4p^2+1520m_\pi^2p^4+752p^6)}{m_\pi^2+4p^2}\right. \\
&\quad \left.+3(35m_\pi^6+180m_\pi^4p^2+240m_\pi^2p^4+64p^6)\ln\frac{m_\pi^2}{m_\pi^2+4p^2}\right] \\
\frac{\partial N_{10}^{(0)}}{\partial m_\pi^2}(0,2,1) &= \frac{\partial N_{10}^{(0)}}{\partial m_\pi^2}(2,0,1) \\
&= \frac{g_A^2}{4f_\pi^2}\frac{\sqrt{2}}{8p^4}\left[\frac{4p^2(3m_\pi^2+8p^2)}{m_\pi^2+4p^2}+(3m_\pi^2+2p^2)\ln\frac{m_\pi^2}{m_\pi^2+4p^2}\right], \\
\frac{\partial N_{21}^{(0)}}{\partial m_\pi^2}(1,3,1) &= \frac{\partial N_{21}^{(0)}}{\partial m_\pi^2}(3,1,1) \\
&= -\frac{g_A^2}{4f_\pi^2}\frac{\sqrt{6}}{160p^6}\left[\frac{4p^2(15m_\pi^4+66m_\pi^2p^2+40p^4)}{m_\pi^2+4p^2}+(15m_\pi^4+36m_\pi^2p^2+8p^4)\ln\frac{m_\pi^2}{m_\pi^2+4p^2}\right], \\
\frac{\partial N_{30}^{(0)}}{\partial m_\pi^2}(2,4,1) &= \frac{\partial N_{30}^{(0)}}{\partial m_\pi^2}(4,2,1) \\
&= \frac{g_A^2}{4f_\pi^2}\frac{\sqrt{3}}{224p^8}\left[\frac{4p^2(105m_\pi^6+660m_\pi^4p^2+1052m_\pi^2p^4+272p^6)}{m_\pi^2+4p^2}\right. \\
&\quad \left.+3(35m_\pi^6+150m_\pi^4p^2+144m_\pi^2p^4+16p^6)\ln\frac{m_\pi^2}{m_\pi^2+4p^2}\right], \qquad \text{(E.31)}
\end{aligned}
$$

including those amplitudes coupling different ℓ and $\bar{\ell}$.

E.5 NLO contributions to in-medium NN interactions with scalar source

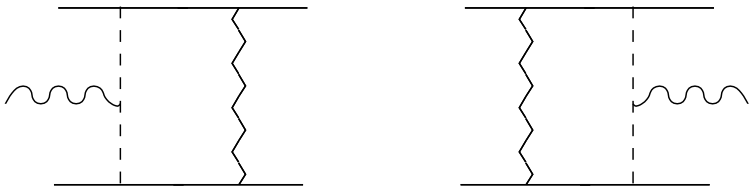

Figure E.6: The two-nucleon reducible loops, where the scalar source couples into, that contribute to $DL_{JI}^{(1)}$. Keeping in mind the crossed channels, the contributions have a symmetry factor of 1/2.

In this section we evaluate explicitly $DL_{JI}^{(1)}$ for the case of the chiral quark condensate since it enters for fixing the interaction kernel at NLO, $\xi_{JI}^{(1)}$. For this contribution the scalar source is coupling into the interaction kernel. The coupling to the contact interaction is of higher order so we are left with the coupling to the pion exchange. When the second wiggle exchange is a local vertex, we call the contribution $\mathcal{T}_{\Xi 1}$. If it corresponds to a one-pion exchange one has $\mathcal{T}_{\Xi 2}$. As explained in section 4.2 only the direct terms of diagrams are used to evaluate the different partial waves and we can write

$$DL_{JI}^{(1)}(\ell', \ell, S) = \mathcal{T}_{\Xi 1,d} + \mathcal{T}_{\Xi 2,d} \ . \tag{E.32}$$

E.5.1 Explicit calculation of $\mathcal{T}_{\Xi 1}$

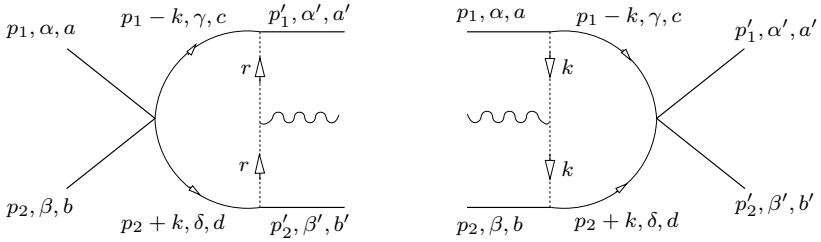

Figure E.7: The four-momenta, spin and isospin indices are shown on this figure contributing to $\mathcal{T}_{\Xi 1}^{f}$ (left hand side) and $\mathcal{T}_{\Xi 1}^{i}$ (right hand side). With the crossed channels of the pion exchange, the symmetry factor of each diagram is 1/2.

$\mathcal{T}_{\Xi 1}$ can straightforwardly be obtained from the amplitude $\mathcal{T}_2$, subsection E.2.3, considering the fact that all structures are the same except for the additional vertex of the scalar source coupling to pions, eq. (8.8), and the pion propagator squared. One has for the final-state pion exchange, whose diagram is shown in fig. E.7 on the left hand side

$$\begin{aligned}\mathcal{T}_{\Xi 1}^{f} = -\delta_{ij} B_0 \left(\frac{g_A}{2f_\pi}\right)^2 i \int \frac{d^4k}{(2\pi)^4} \Big\{ &\left[C_S(\vec{\sigma}_{\alpha'\alpha}\cdot\mathbf{r})(\vec{\sigma}_{\beta'\beta}\cdot\mathbf{r}) + C_T(\vec{\sigma}_{\alpha'\gamma}\cdot\mathbf{r})(\vec{\sigma}_{\beta'\delta}\cdot\mathbf{r})(\vec{\sigma}_{\gamma\alpha}\cdot\vec{\sigma}_{\delta\beta})\right]\tau^s_{a'a}\tau^s_{b'b} \\ &- \left[C_S(\vec{\sigma}_{\alpha'\beta}\cdot\mathbf{r})(\vec{\sigma}_{\beta'\alpha}\cdot\mathbf{r}) + C_T(\vec{\sigma}_{\alpha'\gamma}\cdot\mathbf{r})(\vec{\sigma}_{\beta'\delta}\cdot\mathbf{r})(\vec{\sigma}_{\gamma\beta}\cdot\vec{\sigma}_{\delta\alpha})\right]\tau^s_{a'b}\tau^s_{b'a}\Big\} \\ &\times G_0(p_1 - q)_a G_0(p_2 + q)_b \left[\frac{1}{\mathbf{r}^2 + m_\pi^2}\right]^2 . \end{aligned} \tag{E.33}$$

One obtains corresponding expressions for the source coupling to the pion in the inital state, $\mathcal{T}^i_{\Xi 1}$, that is shown fig. E.7 on the right hand side. Putting both contributions together $\mathcal{T}_{\Xi 1} = \mathcal{T}^i_{\Xi 1} + \mathcal{T}^f_{\Xi 1}$ we find that the amplitude is related to the one of the plain box

$$\mathcal{T}_{\Xi 1,d} = \delta_{ij} B_0 \frac{\partial}{\partial m_\pi^2} \mathcal{T}_{2,d} \ . \tag{E.34}$$

E.5.2 Explicit calculation of $\mathcal{T}_{\Xi 2}$

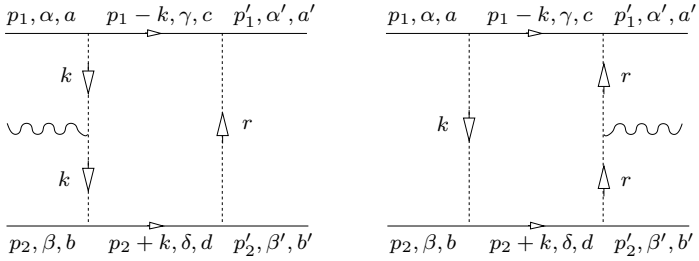

Figure E.8: The four-momenta, spin and isospin indices are shown on this figure contributing to $\mathcal{T}^f_{\Xi 2}$ (left hand side) and $\mathcal{T}^i_{\Xi 2}$ (right hand side). With the crossed channels of the pion exchange, the symmetry factor of each diagram is 1/2.

Correspondingly to the case in the last subsection, $\mathcal{T}_{\Xi 2}$ can straightforwardly be obtained from the amplitude $\mathcal{T}_3$, subsection E.2.4. Here again it has to be taken into account, that the scalar source can couple into both initial- and final-state pion exchange. Consequently, we have two contributions which can be combined in the following way

$$\begin{aligned}\mathcal{T}_{\Xi 2} = \delta_{ij} B_0 \left(\frac{g_A}{2 f_\pi}\right)^4 \tau^s_{ca} \tau^s_{db}\, i \int \frac{d^4k}{(2\pi)^4} (\vec{\sigma}_{\gamma\alpha} \cdot \mathbf{k})(\vec{\sigma}_{\delta\beta} \cdot \mathbf{k}) \Big[\tau^r_{a'c} \tau^r_{b'd} (\vec{\sigma}_{\alpha'\gamma} \cdot \mathbf{r})(\vec{\sigma}_{\beta'\delta} \cdot \mathbf{r}) + \tau^r_{b'c} \tau^r_{a'd} \\ (\vec{\sigma}_{\beta'\gamma} \cdot \mathbf{r})(\vec{\sigma}_{\alpha'\delta} \cdot \mathbf{r}) \Big] \frac{1}{\mathbf{r}^2 + m_\pi^2} \frac{1}{\mathbf{k}^2 + m_\pi^2} \left[\frac{1}{\mathbf{r}^2 + m_\pi^2} + \frac{1}{\mathbf{k}^2 + m_\pi^2} \right] G_0(p_1 - k)_c G_0(p_2 + k)_d \ ,\end{aligned} \tag{E.35}$$

where the first summand in the first square bracket corresponds to the direct term, as usual. Comparing these expressions with the amplitude of the plain box with two exchanged pions, eq. (E.19), we can write

$$\mathcal{T}_{\Xi 2,d} = \delta_{ij} B_0 \frac{\partial}{\partial m_\pi^2} \mathcal{T}_{3,d} \ . \tag{E.36}$$

E.6 NLO contributions to in-medium NN interactions with 2-pion source

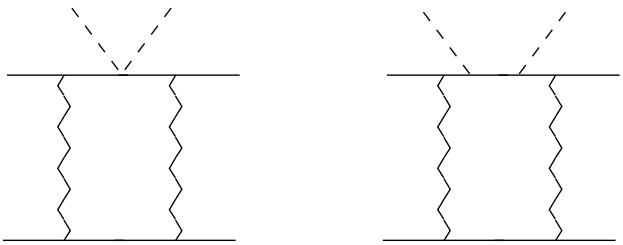

Figure E.9: The two-nucleon reducible loops contributing to $DL^{(1)}_{JI}$ of the pion-production. The figure on the left hand side with the Weinberg-Tomozawa (WT) vertex is an isovector contribution $DL^{(1)}_{JI;iv}$. For the diagram with the Born term, on the right hand side, the external pion lines have to be understood as entering and leaving the diagram; it contributes to both isovector $DL^{(1)}_{JI;iv}$ and isoscalar $DL^{(1)}_{JI;is}$.

In this section we evaluate explicitly $DL^{(1)}_{JI}$ for the case of the pion self-energy since it enters for fixing the interaction kernel at NLO, $\xi^{(1)}_{JI}$. For the problem of the in-medium pion self-energy there are two contributions namely an isovector part $\xi^{(1)}_{JI;iv}$ and an isoscalar $\xi^{(1)}_{JI;is}$, with their contributions from the NLO box diagrams $DL^{(1)}_{JI;iv}$ and $DL^{(1)}_{JI;is}$, respectively. When the two-nucleon reducible loop includes only nucleon-nucleon local vertices, we have $\mathcal{T}_{\Pi 1}$. At the same order, when one of the wiggly lines corresponds to a one-pion exchange $\mathcal{T}_{\Pi 2}$ results. Finally, when both lines are due to one-pion exchange one has $T_{\Pi 3}$. As explained in section 4.2 only the direct terms of diagrams are used to evaluate the different partial waves and we can write

$$DL^{(1)}_{JI;iv}(\ell',\ell,S) = \mathcal{T}^{iv}_{\Pi 1,d} + \mathcal{T}^{iv}_{\Pi 2,d} + \mathcal{T}^{iv}_{\Pi 3,d} \ , \tag{E.37}$$

$$DL^{(1)}_{JI;is}(\ell',\ell,S) = \mathcal{T}^{is}_{\Pi 1,d} + \mathcal{T}^{is}_{\Pi 2,d} + \mathcal{T}^{is}_{\Pi 3,d} \ . \tag{E.38}$$

We define the abbreviations for the pion self-energy isovector and isoscalar factors as

$$\kappa_{iv} = \frac{q_0}{2f_\pi^2}\left(\frac{g_A^2\mathbf{q}^2}{q_0^2} - 1\right) \ , \qquad \kappa_{is} = -\frac{g_A^2\mathbf{q}^2}{2f_\pi^2 q_0^2} \ . \tag{E.39}$$

Compared to the calculations of $L^{(1)}_{JI}$, section E.2, the diagrams considered here have no symmetry factor, because the external sources can couple both to the direct and to the crossed part of the first wiggle exchange.

E.6.1 Explicit calculation of $\mathcal{T}^{iv}_{\Pi 1}$ and $\mathcal{T}^{is}_{\Pi 1}$

The coupling of the WT vertex and isovector part of the Born term to the loop with only local nucleon-nucleon vertices reads

$$\begin{aligned}\mathcal{T}^{iv}_{\Pi 1} = i\varepsilon_{ijk}\,\kappa_{iv}\Big\{ & C_S\big(\delta_{\alpha'\gamma}\delta_{\beta'\delta}\delta_{a'c}\delta_{b'd} - \delta_{\alpha'\delta}\delta_{\beta'\gamma}\delta_{a'd}\delta_{b'c}\big) + C_T\big(\vec{\sigma}_{\alpha'\gamma}\cdot\vec{\sigma}_{\beta'\delta}\delta_{a'c}\delta_{b'd} \\ & - \vec{\sigma}_{\alpha'\delta}\cdot\vec{\sigma}_{\beta'\gamma}\delta_{a'd}\delta_{b'c}\big)\Big\} i\int\frac{d^4k}{(2\pi)^4}G_0(p_1-k)_c G_0(p_2+k)_d\Big\{\tau^k_{cc}G_0(p_1-k)_c\big[C_S\delta_{\gamma\alpha}\delta_{\delta\beta} \\ & + C_T\vec{\sigma}_{\gamma\alpha}\cdot\vec{\sigma}_{\delta\beta}\big]\delta_{ca}\delta_{db} - \tau^k_{dd}G_0(p_2+k)_d\big[C_S\delta_{\gamma\beta}\delta_{\delta\alpha} + C_T\vec{\sigma}_{\gamma\beta}\cdot\vec{\sigma}_{\delta\alpha}\big]\delta_{cb}\delta_{da}\Big\} \ . \end{aligned} \tag{E.40}$$

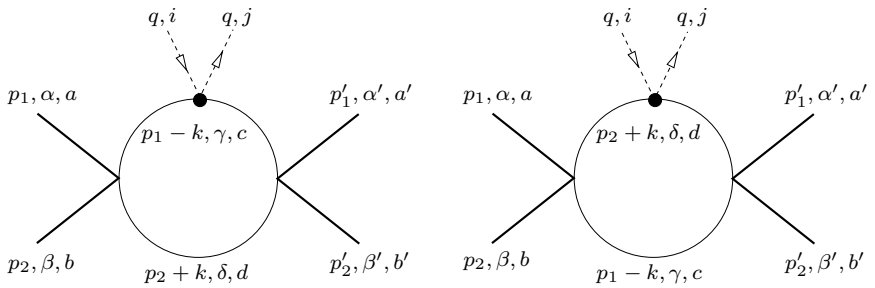

Figure E.10: The four-momenta, spin (greek letters) and isospin (latin letters) indices are shown on this figures whose sum determines $\mathcal{T}_{\Pi 1}$. The dot symbolizes that the diagram has contributions from a WT vertex and a Born term.

Making use of eqs. (7.13) and (7.42) we can write

$$\mathcal{T}^{iv}_{\Pi 1,d} = -i\varepsilon_{ij3}\,\kappa_{iv}\frac{m\partial}{\partial A}L^{i_3}_{10}\Big[C_S^2\delta_{\alpha'\alpha}\delta_{\beta'\beta} + 2C_SC_T\vec{\sigma}_{\alpha'\alpha}\cdot\vec{\sigma}_{\beta'\beta} + C_T^2(\vec{\sigma}_{\alpha'\gamma}\cdot\vec{\sigma}_{\beta'\delta})(\vec{\sigma}_{\gamma\alpha}\cdot\vec{\sigma}_{\delta\beta})\Big]\Big(\delta_{a'a}\tau^3_{b'b} + \tau^3_{a'a}\delta_{b'b}\Big)\ , \quad \text{(E.41)}$$

restricting ourselves to the direct contribution. Perfoming the projections on definite spin and isospin states given in tab. E.1 we can sum up

$$\mathcal{T}^{iv}_{\Pi 1,d} = i\varepsilon_{ij3}\,\kappa_{iv}\,\frac{m\partial}{\partial A}\mathcal{T}_{1,d}\ . \quad \text{(E.42)}$$

where $i_3 = a + b$. The isospin and spin factors incorporated in $\mathcal{T}_{1,d}$, eq. (E.7), are given this time by

$$f_I = 2i_3\ , \qquad f_S = (C_S + (4S-3)C_T)^2\ . \quad \text{(E.43)}$$

For the isoscalar part of the Born term the square of the propagator drops out and the vertex $i\varepsilon_{ij3}\tau^3\kappa_{iv}$ is replaced by $\delta_{ij}\kappa_{is}$ and we can write

$$\mathcal{T}^{is}_{\Pi 1,d} = -\delta_{ij}\,\kappa_{is}L^{i_3}_{10}\Big[C_S^2\delta_{\alpha'\alpha}\delta_{\beta'\beta} + 2C_SC_T\vec{\sigma}_{\alpha'\alpha}\cdot\vec{\sigma}_{\beta'\beta} + C_T^2(\vec{\sigma}_{\alpha'\gamma}\cdot\vec{\sigma}_{\beta'\delta})(\vec{\sigma}_{\gamma\alpha}\cdot\vec{\sigma}_{\delta\beta})\Big]2\delta_{a'a}\delta_{b'b}\ , \quad \text{(E.44)}$$

which leads to

$$\mathcal{T}^{is}_{\Pi 1,d} = \delta_{ij}\,\kappa_{is}\,\mathcal{T}_{1,d}\ . \quad \text{(E.45)}$$

with

$$f_I = 2\ , \qquad f_S = (C_S + (4S-3)C_T)^2\ . \quad \text{(E.46)}$$

E.6.2 Explicit calculation of $\mathcal{T}^{iv}_{\Pi 2}$ and $\mathcal{T}^{is}_{\Pi 2}$

We now consider $\mathcal{T}^{iv}_{\Pi 2}$ and $\mathcal{T}^{is}_{\Pi 2}$ with a local vertex and a one-pion exchange. The contributions correspond to fig. E.11 for $\mathcal{T}^{f}_{\Pi 2}$ and fig. E.12 for $\mathcal{T}^{i}_{\Pi 2}$, depending on whether the one-pion echange is between the final or the inital two nucleons, respectively. For the sum of the diagrams in fig. E.11

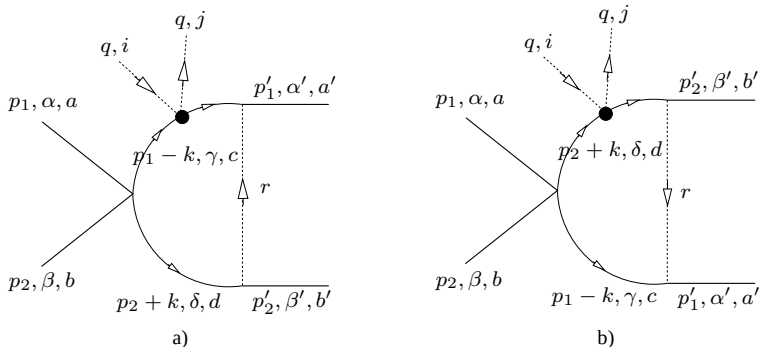

Figure E.11: The four-momenta, spin (greek letters) and isospin (latin letters) indices are shown on this figures whose sum determines the contribution from the final state pion exchange part $\mathcal{T}^f_{\Pi 2}$. The dot symbolizes that the diagram has contributions from a WT vertex and a Born term. The diagram on the right hand side should be understood as the crossed part of the pion exchange.

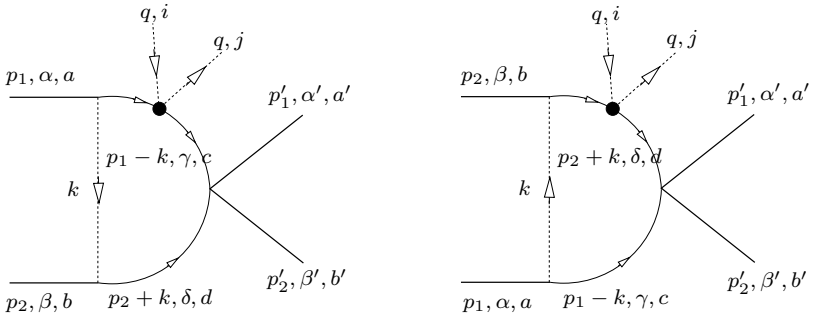

Figure E.12: Contribution from the initial state pion exchange part $\mathcal{T}^i_{\Pi 2}$. The diagram on the right hand side should be understood as the crossed part of the pion exchange, where the twist is not drawn explicitely for reasons of lucidity.

one has for the isovector part

$$\mathcal{T}^{iv,f}_{\Pi 2} = -i\varepsilon_{ijk}\,\kappa_{iv}\left(\frac{g_A}{2f_\pi}\right)^2 i\int\frac{d^4k}{(2\pi)^4}\Big\{(\vec\tau_{a'c}\cdot\vec\tau_{b'd})(\vec\sigma_{\alpha'\gamma}\cdot\mathbf{r})(\vec\sigma_{\beta'\delta}\cdot\mathbf{r}) - (\vec\tau_{a'd}\cdot\vec\tau_{b'a})(\vec\sigma_{\alpha'\delta}\cdot\mathbf{r})(\vec\sigma_{\beta'\gamma}\cdot\mathbf{r})\Big\}$$
$$\times\, G_0(p_1-k)_c G_0(p_2+k)_d\frac{1}{\mathbf{r}^2+m_\pi^2}\Big\{\tau^k_{cc}G_0(p_1-k)_c\big[C_S\delta_{\gamma\alpha}\delta_{\delta\beta}+C_T\vec\sigma_{\gamma\alpha}\cdot\vec\sigma_{\delta\beta}\big]\delta_{ca}\delta_{db}$$
$$-\,\tau^k_{dd}G_0(p_2+k)_d\big[C_S\delta_{\gamma\beta}\delta_{\delta\alpha}+C_T\vec\sigma_{\gamma\beta}\cdot\vec\sigma_{\delta\alpha}\big]\delta_{cb}\delta_{da}\Big\}\ . \quad \text{(E.47)}$$

The energy dependence enters in $\mathcal{T}^f_{\Pi 2}$ similarly as in L_{10} and the derivative can be taken with respect to the variable A, eq. (7.47), with $A\to\mathbf{p}^2$ after the derivative is performed. Restricting to the direct term we end up with

$$\mathcal{T}^{iv,f}_{\Pi 2,d} = i\varepsilon_{ij3}\,\kappa_{iv}\left(\frac{g_A}{2f_\pi}\right)^2\frac{m\partial}{\partial A}i\int\frac{d^4k}{(2\pi)^4}G_0(p_1-k)_c G_0(p_2+k)_d\frac{1}{\mathbf{r}^2+m_\pi^2}\Big[C_S(\vec\sigma_{\alpha'\alpha}\cdot\mathbf{r})(\vec\sigma_{\beta'\beta}\cdot\mathbf{r})$$
$$+\,C_T(\vec\sigma_{\alpha'\gamma}\cdot\mathbf{r})(\vec\sigma_{\beta'\delta}\cdot\mathbf{r})(\vec\sigma_{\gamma\alpha}\cdot\vec\sigma_{\delta\beta})\Big]\tau^s_{a'a}\tau^s_{b'b}\big(\tau^3_{aa}+\tau^3_{bb}\big)\ . \quad \text{(E.48)}$$

The spin operator was already evaluated in eq. (E.10) and the isospin operator $\tau^s_{a'a}\tau^s_{b'b}(\tau^3_{aa}+\tau^3_{bb})$ gives $2i_3$, with $i_3 = a+b$. So we may sum up

$$\mathcal{T}^{iv,f}_{\Pi 2,d} = i\varepsilon_{ij3}\,\kappa_{iv}\frac{m\partial}{\partial A}\mathcal{T}^f_{2,d}\ , \tag{E.49}$$

where $\mathcal{T}^f_{2,d}$ is given in eqs. (E.15) and (E.16) and the isospin and spin factors incorporated therein are

$$f_I = 2i_3\left(\frac{g_A}{2f_\pi}\right)^2\ , \qquad f_S = C_S + (4S-3)C_T\ . \tag{E.50}$$

For the isoscalar part of the Born term we obtain for the direct term

$$\mathcal{T}^{is,f}_{\Pi 2,d} = \delta_{ij}\,\kappa_{is}\left(\frac{g_A}{2f_\pi}\right)^2 i\int\frac{d^4k}{(2\pi)^4}G_0(p_1-k)_c G_0(p_2+k)_d\frac{1}{\mathbf{r}^2+m_\pi^2}\Big[C_S(\vec\sigma_{\alpha'\alpha}\cdot\mathbf{r})(\vec\sigma_{\beta'\beta}\cdot\mathbf{r}) + C_T(\vec\sigma_{\alpha'\gamma}\cdot\mathbf{r})(\vec\sigma_{\beta'\delta}\cdot\mathbf{r})(\vec\sigma_{\gamma\alpha}\cdot\vec\sigma_{\delta\beta})\Big]2\tau^s_{a'a}\tau^s_{b'b}\ , \tag{E.51}$$

and obtain

$$\mathcal{T}^{is,f}_{\Pi 2,d} = \delta_{ij}\,\kappa_{is}\mathcal{T}^f_{2,d}\ , \tag{E.52}$$

with

$$f_I = 2(4I-3)\left(\frac{g_A}{2f_\pi}\right)^2\ , \qquad f_S = C_S + (4S-3)C_T\ . \tag{E.53}$$

For the one-pion exchange between the initial nucleons $\mathcal{T}^i_{\Pi 2}$, fig. E.12 the calculation can be performed straightforwardly. We perform the transformation given in eq. (E.13) and obtain the same expressions for $\mathcal{T}^i_{\Pi 2}$ as for $\mathcal{T}^f_{\Pi 2}$ under the replacement $\mathbf{p}' \to \mathbf{p}$, respectively for isovector and isoscalar part.

The whole discussion given at the end of subsection E.2.3 also holds for the expressions derived here. Note that $I = 1$ is required for $\mathcal{T}^{iv}_{\Pi 2}$, so only the partial wave $\mathcal{T}_{2;01}(0,0,0) = \mathcal{T}^f_{2;01}(0,0,0) + \mathcal{T}^i_{2;01}(0,0,0) = 2\mathcal{T}^f_{2;01}(0,0,0)$ is not zero.

E.6.3 Explicit calculation of $\mathcal{T}^{iv}_{\Pi 3}$ and $\mathcal{T}^{is}_{\Pi 3}$

Let us move now to the evaluation of $\mathcal{T}^{iv}_{\Pi 3}$ and $\mathcal{T}^{is}_{\Pi 3}$ where both vertices in the two-nucleon reducible loop, to which the two pions are attached, correspond to a one-pion exchange. As in the previous cases we start by calculating the isovector case. We restrict ourselves from the beginning to the direct contribution, corresponding to the diagrams in fig. E.13, whose sum is

$$\mathcal{T}^{iv}_{\Pi 3,d} = -i\varepsilon_{ijk}\,\kappa_{iv}\left(\frac{g_A}{2f_\pi}\right)^4\tau^s_{a'c}\tau^t_{ca}\tau^s_{b'd}\tau^t_{db}\big(\tau^3_{cc}+\tau^3_{dd}\big)\frac{m\partial}{\partial A}\int\frac{d^4k}{(2\pi)^4}(\vec\sigma_{\alpha'\gamma}\cdot\mathbf{r})(\vec\sigma_{\beta'\delta}\cdot\mathbf{r}) \times(\vec\sigma_{\gamma\alpha}\cdot\mathbf{k})(\vec\sigma_{\delta\beta}\cdot\mathbf{k})\frac{1}{\mathbf{r}^2+m_\pi^2}\frac{1}{\mathbf{k}^2+m_\pi^2}G_0(p_1-k)_c G_0(p_2+k)_d\ . \tag{E.54}$$

The spin operator was already evaluated in eq. (E.20) and the isospin operator $\tau^s_{a'c}\tau^t_{ca}\tau^s_{b'd}\tau^t_{db}(\tau^3_{cc}+\tau^3_{dd})$ gives $2i_3$, with $i_3 = a+b$. So we may sum up

$$\mathcal{T}^{iv}_{\Pi 3,d} = i\varepsilon_{ij3}\,\kappa_{iv}\frac{m\partial}{\partial A}\mathcal{T}_{3,d}\ , \tag{E.55}$$

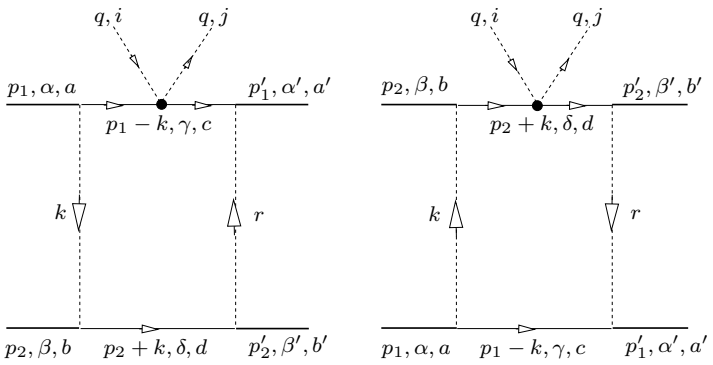

Figure E.13: The four-momenta, spin (greek letters) and isospin (latin letters) indices are shown on this figures whose sum determines $\mathcal{T}_{\Pi 3}$. The dot symbolizes that the diagram has contributions from a WT vertex and a Born term. The diagram on the right hand side corresponds to the crossed channels of both pion exchanges.

with

$$f_I = 2i_3 \left(\frac{g_A}{2f_\pi}\right)^4 , \qquad f_S = 1 . \tag{E.56}$$

Proceeding correspondingly for the isovector part we keep in touch with

$$\mathcal{T}^{is}_{\Pi 3,d} = -\delta_{ij}\,\kappa_{is} \left(\frac{g_A}{2f_\pi}\right)^4 2\tau^s_{a'c}\tau^t_{ca}\tau^s_{b'd}\tau^t_{db} \int \frac{d^4k}{(2\pi)^4} (\vec{\sigma}_{\alpha'\gamma}\cdot\mathbf{r})(\vec{\sigma}_{\beta'\delta}\cdot\mathbf{r}) \\ \times (\vec{\sigma}_{\gamma\alpha}\cdot\mathbf{k})(\vec{\sigma}_{\delta\beta}\cdot\mathbf{k}) \frac{1}{\mathbf{r}^2+m_\pi^2}\frac{1}{\mathbf{k}^2+m_\pi^2} G_0(p_1-k)_c G_0(p_2+k)_d . \tag{E.57}$$

With the isospin operator $2\tau^s_{a'c}\tau^t_{ca}\tau^s_{b'd}\tau^t_{db}$ sandwiched giving 2, we sum up

$$\mathcal{T}^{is}_{\Pi 3,d} = \delta_{ij}\,\kappa_{is}\mathcal{T}_{3,d} , \tag{E.58}$$

and

$$f_I = 2(9-8I) \left(\frac{g_A}{2f_\pi}\right)^4 , \qquad f_S = 1 . \tag{E.59}$$

Acknowledgements

At the end of this thesis, I would like to express my gratitude towards all those, who in one way or another, were involved in my scientific work during the last three and a half years.

First of all, I would very much like to thank my thesis advisors Prof. Ulf-G. Meißner und Prof. José Antonio Oller! On the one hand for giving me the opportunity to work on such an interesting topic on the other hand for their continuous support, for the collaboration on various publications that emerged from this research and for their encouragement and enthusiasm during the inevitable difficult period of a long PhD work.

Special thanks also to Priv. Doz. Andreas Wirzba for sharing his insights into physics with me during the period of familiarization with the topic of in-medium physics. I also wish to thank my former diploma mentor Dr. Bastian Kubis for teaching me low-energy hadron physics and for the continuous work beyond my diploma thesis which culminated in a first publication, and for always having an open ear for questions.

I am very grateful to Matthias Frink and Priv. Doz. Akaki Rusetsky for careful proof-reading of and fruitful comments on the manuscript of this thesis.

My thanks go also to my office colleagues Matthias Frink, Mark Lenkewitz and Shahin B. Bour for the relaxed and casual atmosphere in the office, for many interesting discussions and help on all sorts of questions.

Furthermore, my thanks go to all the past and current members of our theory department at the "Helmholtz-Institut für Strahlen- und Kernphysik" who made the work at the institute comfortable and entertaining and who regularly extended discussions including beer and TV–shows late into the evenings.

For inviting me twice to the University of Murcia for scientific stays I want to thank Prof. Jose Antonio Oller. I also want to thank the local group for hospitality and making the stay comfortable.

This thesis would not have been possible without the financial support of the "Bundesministerium für Bildung und Forschung". In particular, I would like to thank Prof. Hans-Werner Hammer for sharing the BMBF grants to realize this work.

Darüber hinaus möchte ich meinen Freunden und den Capoeristas der Grupo Capoeira Equilíbrio in Bonn danken, die einfach zu viele sind um sie namentlich zu nennen, dafür daß sie mir regelmässig zeigen daß es auch ein Leben außerhalb der Physik gibt und dafür daß sie für den notwendigen Ausgleich sorgen, ohne den sich eine solche Arbeit nicht verwirklichen ließe. Besonderer Dank geht hierbei an Tatjana und Simone, ohne die ich niemals so weit gekommen wäre.

Schließlich danke ich meiner Familie, meinen Eltern und meiner Schwester, für die Unterstützung, den Rückhalt und die Sicherheit, ohne die mein ganzes Studium mit anschließender Promotion nicht zu verwirklichen gewesen wäre.

Ruth, danke für alles.

Bibliography

[ACS81] M. R. Anastasio, L. S. Celenza and C. M. Shakin, "Boson Exchange Potentials And The Nucleon Selfenergy In Nuclear Matter," Phys. Rev. C **23** (1981) 569.

[AFCO96] L. Alvarez-Ruso, P. Fernandez de Cordoba and E. Oset, "The imaginary part of the nucleon self-energy in hot nuclear matter," Nucl. Phys. A **606** (1996) 407 [arXiv:nucl-th/9610003].

[APR98] A. Akmal, V. R. Pandharipande and D. G. Ravenhall, "The equation of state for nucleon matter and neutron star structure," Phys. Rev. C **58** (1998) 1804 [arXiv:nucl-th/9804027].

[Ao06] Y. Aoki, Z. Fodor, S. D. Katz and K. K. Szabo, "The QCD transition temperature: Results with physical masses in the continuum limit," Phys. Lett. B **643** (2006) 46 [arXiv:hep-lat/0609068].

[AO08] M. Albaladejo and J. A. Oller, "Identification of a Scalar Glueball," Phys. Rev. Lett. **101** (2008) 252002 [arXiv:hep-ph/0801.4929].

[Ar04] R. A. Arndt, W. J. Briscoe, I. I. Strakovsky, R. L. Workman and M. M. Pavan, "Dispersion Relation Constrained Partial Wave Analysis of πN Elastic and $\pi N \to \eta N$ Scattering Data: The Baryon Spectrum," Phys. Rev. C **69** (2004) 035213 [arXiv:nucl-th/0311089].

[Ba65] G. Bargon, "Introduction to Dispersion Techniques in Field Theory", W. A. Benjamin, Inc, New York, Amsterdam, 1965.

[BBSK02] S. R. Beane, P. F. Bedaque, M. J. Savage and U. van Kolck, "Towards a perturbative theory of nuclear forces," Nucl. Phys. A **700** (2002) 377 [arXiv:nucl-th/0104030].

[BGF97] C. J. Batty, E. Friedman and A. Gal, "Strong interaction physics from hadronic atoms," Phys. Rept. **287** (1997) 385.

[BFS05] S. K. Bogner, A. Schwenk, R. J. Furnstahl and A. Nogga, "Is nuclear matter perturbative with low-momentum interactions?," Nucl. Phys. A **763** (2005) 59 [arXiv:nucl-th/0504043].

[BFS06] S. K. Bogner, R. J. Furnstahl, S. Ramanan and A. Schwenk, "Convergence of the Born Series with Low-Momentum Interactions," Nucl. Phys. A **773** (2006) 203 [arXiv:nucl-th/0602060].

[BFS09] S. K. Bogner, R. J. Furnstahl, A. Nogga and A. Schwenk, "Nuclear matter from chiral low-momentum interactions," arXiv:nucl-th/0903.3366.

[BGKT60] R. Blankenbecler, M. L. Goldberger, N. N. Khuri and S. B. Treiman, "Mandelstam representation for potential scattering," Annals Phys. **10** (1960) 62.

[BKKM92] V. Bernard, N. Kaiser, J. Kambor and U.-G. Meißner, "Chiral structure of the nucleon," Nucl. Phys. B **388** (1992) 315.

[BKM95] V. Bernard, N. Kaiser and U.-G. Meißner, "Chiral Dynamics In Nucleons And Nuclei," Int. J. Mod. Phys. E **4**, 193 (1995) [arXiv:hep-ph/9501384].

[BKM97] V. Bernard, N. Kaiser and U.-G. Meißner, "Aspects of chiral pion-nucleon physics," aka "Determination of the low-energy constants of the next-to-leading order chiral pion nucleon Lagrangian," Nucl. Phys. A **615** (1997) 483 [arXiv:hep-ph/9611253].

[Bl80] J. P. Blaizot, "Nuclear Compressibilities," Phys. Rept. **64** (1980) 171.

[BL99] T. Becher and H. Leutwyler, "Baryon chiral perturbation theory in manifestly Lorentz invariant form," Eur. Phys. J. C **9** (1999) 643 [arXiv:hep-ph/9901384].

[BM90] R. Brockmann and R. Machleidt, "Relativistic nuclear structure. 1: Nuclear matter," Phys. Rev. C **42** (1990) 1965.

[BM94] G. E. Brown and R. Machleidt, "Strength of the rho meson coupling to nucleons," Phys. Rev. C **50** (1994) 1731.

[BM96] B. Borasoy and U.-G. Meißner, "Chiral expansion of baryon masses and sigma-terms," Annals Phys. **254** (1997) 192 [arXiv:hep-ph/9607432].

[BM00] P. Buettiker and U.-G. Meißner, "Pion nucleon scattering inside the Mandelstam triangle," Nucl. Phys. A **668** (2000) 97 [arXiv:hep-ph/9908247].

[BM07] V. Bernard and U.-G. Meißner, "Chiral perturbation theory," Ann. Rev. Nucl. Part. Sci. **57** (2007) 33 [arXiv:hep-ph/0611231].

[BMN06] B. Borasoy, U.-G. Meißner and R. Nißler, "K-p scattering length from scattering experiments," Phys. Rev. C **74** (2006) 055201 [arXiv:hep-ph/0606108].

[BMZ87] V. Bernard, U.-G. Meißner and I. Zahed, "Decoupling of the Pion at Finite Temperature and Density," Phys. Rev. D **36** (1987) 819.

[BNW05] B. Borasoy, R. Nißler and W. Weise, "Kaonic hydrogen and K- p scattering," Phys. Rev. Lett. **94** (2005) 213401 [arXiv:hep-ph/0410305]; [Erratum-ibid. **96** (2006) 199201].

[Bo07] B. Borasoy, E. Epelbaum, H. Krebs, D. Lee and U.-G. Meißner, "Lattice simulations for light nuclei: Chiral effective field theory at leading order," Eur. Phys. J. A **31**, 105 (2007) [arXiv:nucl-th/0611087].

[BW96] R. Brockmann and W. Weise, "The Chiral condensate in nuclear matter," Phys. Lett. B **367** (1996) 40.

[CCWZ69] C. G. Callan, S. R. Coleman, J. Wess and B. Zumino, "Structure of phenomenological Lagrangians. 2," Phys. Rev. **177**, 2247 (1969).

[CDD56] L. Castillejo, R. H. Dalitz and F. J. Dyson, "Low's scattering equation for the charged and neutral scalar theories," Phys. Rev. **101** (1956) 453.

[CEO03] G. Chanfray, M. Ericson and M. Oertel, "In-Medium Modification Of The Isovector Pion Nucleon Amplitude," Phys. Lett. B **563** (2003) 61.

[CFG91] T. D. Cohen, R. J. Furnstahl and D. K. Griegel, "From QCD sum rules to relativistic nuclear physics," Phys. Rev. Lett. **67** (1991) 961.

[CFG92] T. D. Cohen, R. J. Furnstahl and D. K. Griegel, "Quark And Gluon Condensates In Nuclear Matter," Phys. Rev. C **45** (1992) 1881.

[CGL01] G. Colangelo, J. Gasser and H. Leutwyler, "The quark condensate from K(e4) decays," Phys. Rev. Lett. **86** (2001) 5008 [arXiv:hep-ph/0103063].

[Cl83] B. C. Clark, S. Hama, R. L. Mercer, L. Ray and B. d. Serot, "Dirac Equation Impulse Approximation For Intermediate-Energy Nucleon Nucleus Scattering," Phys. Rev. Lett. **50** (1983) 1644.

[Cu60] R. E. Cutkosky, "Singularities and discontinuities of Feynman amplitudes," J. Math. Phys. **1** (1960) 429.

[CWZ69] S. R. Coleman, J. Wess and B. Zumino, "Structure of phenomenological Lagrangians. 1," Phys. Rev. **177**, 2239 (1969).

[Da81] B. D. Day, "Three-body correlations in nuclear matter," Phys. Rev. C **24** (1981) 1203.

[DHL71] C. B. Dover, J. Hüfner and R. H. Lemmer, "Pions In Nuclear Matter - An Approach To The Pion-Nucleus Optical Potential," Annals Phys. **66** (1971) 248.

[DL91] E. G. Drukarev and E. M. Levin, "Structure of nuclear matter and QCD sum rules," Prog. Part. Nucl. Phys. **27**, 77 (1991).

[DM10] E. N. E. van Dalen and H. Muther, "Off-Shell Behavior of Nucleon Self-Energy in Asymmetric Nuclear Matter," arXiv:1004.1570 [nucl-th].

[DO08] M. Döring and E. Oset, "The s-wave pion-nucleus optical potential," Phys. Rev. C **77** (2008) 024602 [arXiv:nucl-th/0705.3027].

[EE66] M. Ericson and T. E. O. Ericson, "Optical properties of low-energy pions in nuclei," Annals Phys. **36** (1966) 323.

[EGM00] E. Epelbaum, W. Gloeckle and U.-G. Meißner, "Nuclear forces from chiral Lagrangians using the method of unitary transformation. II: The two-nucleon system," Nucl. Phys. A **671** (2000) 295 [arXiv:nucl-th/9910064];

[EGM04] E. Epelbaum, W. Gloeckle and U. G. Meißner, "Improving the convergence of the chiral expansion for nuclear forces. II: Low phases and the deuteron," Eur. Phys. J. A **19** (2004) 401 [arXiv:nucl-th/0308010].

[EGM05] E. Epelbaum, W. Gloeckle and U.-G. Meißner, "The two-nucleon system at next-to-next-to-next-to-leading order," Nucl. Phys. A **747** (2005) 362 [arXiv:nucl-th/0405048].

[EG09] E. Epelbaum and J. Gegelia, "Regularization, renormalization and 'peratization' in effective field theory for two nucleons," Eur. Phys. J. A **41** (2009) 341 [arXiv:nucl-th/0906.3822].

[EHM09] E. Epelbaum, H. W. Hammer and U.-G. Meißner, "Modern Theory of Nuclear Forces," Rev. Mod. Phys. **81** (2009) 1773 [arXiv:nucl-th/0811.1338].

[EM03] D. R. Entem and R. Machleidt, "Accurate Charge-Dependent Nucleon-Nucleon Potential at Fourth Order of Chiral Perturbation Theory," Phys. Rev. C **68** (2003) 041001 [arXiv:nucl-th/0304018].

[EM06] E. Epelbaum and U.-G. Meißner, "On the renormalization of the one-pion exchange potential and the consistency of Weinberg's power counting," arXiv:nucl-th/0609037.

[En97] L. Engvik, M. Hjorth-Jensen, R. Machleidt, H. Müther and A. Polls, "Modern nucleon nucleon potentials and symmetry energy in infinite matter," Nucl. Phys. A **627** (1997) 85 [arXiv:nucl-th/9707002].

[Ep01] E. Epelbaum, H. Kamada, A. Nogga, H. Witala, W. Glöeckle and U.-G. Meißner, "The three- and four-nucleon systems from chiral effective field theory," Phys. Rev. Lett. **86** (2001) 4787 [arXiv:nucl-th/0007057].

[Ep06] E. Epelbaum, "Few-nucleon forces and systems in chiral effective field theory," Prog. Part. Nucl. Phys. **57** (2006) 654 [arXiv:nucl-th/0509032].

[ET82] T. E. O. Ericson and L. Tauscher, "A New Effect In Pionic Atoms," Phys. Lett. B **112** (1982) 425.

[FG07] E. Friedman and A. Gal, "In-medium nuclear interactions of low-energy hadrons," Phys. Rept. **452** (2007) 89 [arXiv:nucl-th/0705.3965].

[FGC92] R. J. Furnstahl, D. K. Griegel and T. D. Cohen, "QCD sum rules for nucleons in nuclear matter," Phys. Rev. C **46** (1992) 1507;
X. m. Jin, T. D. Cohen, R. J. Furnstahl and D. K. Griegel, "QCD sum rules for nucleons in nuclear matter. 2," Phys. Rev. C **47** (1993) 2882;
X. m. Jin, M. Nielsen, T. D. Cohen, R. J. Furnstahl and D. K. Griegel, Phys. Rev. C **49** (1994) 464.

[FGJS03] T. Fuchs, J. Gegelia, G. Japaridze and S. Scherer, "Renormalization of relativistic baryon chiral perturbation theory and power counting," Phys. Rev. D **68** (2003) 056005 [arXiv:hep-ph/0302117].

[FGL73] H. Fritzsch, M. Gell-Mann and H. Leutwyler, "Advantages Of The Color Octet Gluon Picture," Phys. Lett. B **47** (1973) 365.

[FM00] N. Fettes and U. G. Meißner, "Pion nucleon scattering in chiral perturbation theory. II: Fourth order calculation," Nucl. Phys. A **676** (2000) 311 [arXiv:hep-ph/0002162].

[FM04] M. Frink and U.-G. Meißner, "Chiral extrapolations of baryon masses for unquenched three-flavor lattice simulations," JHEP **0407** (2004) 028 [arXiv:hep-lat/0404018].

[FM06] M. Frink and U. G. Meißner, "On the chiral effective meson-baryon Lagrangian at third order," Eur. Phys. J. A **29** (2006) 255 [arXiv:hep-ph/0609256].

[FMS05] M. Frink, U.-G. Meißner and I. Scheller, "Baryon masses, chiral extrapolations, and all that," Eur. Phys. J. A **24** (2005) 395 [arXiv:hep-lat/0501024].

[FMMS00] N. Fettes, U.-G. Meißner, M. Mojžiš and S. Steininger, "The chiral effective pion nucleon Lagrangian of order p^4," Annals Phys. **283**, 273 (2000) [arXiv:hep-ph/0001308]; [Erratum-ibid. **288**, 249 (2001)].

[FMS98] N. Fettes, U.-G. Meißner and S. Steininger, "Pion nucleon scattering in chiral perturbation theory I: Isospin-symmetric case," Nucl. Phys. A **640** (1998) 199 [arXiv:hep-ph/9803266].

[FMS00a] S. Fleming, T. Mehen and I. W. Stewart, "NNLO corrections to nucleon nucleon scattering and perturbative pions," Nucl. Phys. A **677** (2000) 313 [arXiv:nucl-th/9911001].

[FMS00b] S. Fleming, T. Mehen and I. W. Stewart, "The NN scattering $^3S_1$ - $^3D_1$ mixing angle at NNLO," Phys. Rev. C **61** (2000) 044005 [arXiv:nucl-th/9906056].

[FRS08] R. J. Furnstahl, G. Rupak and T. Schäfer, "Effective Field Theory and Finite Density Systems," Ann. Rev. Nucl. Part. Sci. **58** (2008) 1 [arXiv:nucl-th/0801.0729].

[FS00] R. J. Furnstahl and B. D. Serot, "Quantum hadrodynamics: Evolution and revolution," Comments Nucl. Part. Phys. **2** (2000) A23 [arXiv:nucl-th/0005072].

[FSS91] N. H. Fuchs, H. Sazdjian and J. Stern, "How to probe the scale of $(\bar{q}q)$ in chiral perturbation theory," Phys. Lett. B **269** (1991) 183;

[FSS93] N. H. Fuchs, H. Sazdjian and J. Stern, "What π-π scattering tells us about chiral perturbation theory," Phys. Rev. D **47** (1993) 3814.

[FW03] A. L. Fetter and J. D. Walecka, "Quantum Theory of Many-Particle Systems" 2003 edition. Dover Publications, Inc., 31 East 2nd Street, Mineolan N.Y 11501. ISBN 0-486-42827-3.

[Ge90] H. Georgi, "An effective field theory for heavy quarks at low-energies," Phys. Lett. B **240** (1990) 447.

[Ge02] H. Geissel *et al.*, "Deeply bound 1s and 2p pionic states in Pb-205 and determination of the S-wave part of the pion nucleus interaction," Phys. Rev. Lett. **88** (2002) 122301.

[Ge09] H. Georgi, "Weak interactions and modern particle theory", Dover Publications, Inc., Mineola, New York, 2009.

[Gi00] H. Gilg *et al.*, "Deeply Bound π-States In Pb-207 Formed In The Pb-208(D,He-3) Reaction Part I: Experimental Method And Results," Phys. Rev. C **62** (2000) 025201.

[GL84] J. Gasser and H. Leutwyler, "Chiral Perturbation Theory To One Loop," Annals Phys. **158** (1984) 142.

[GL85] J. Gasser and H. Leutwyler, "Chiral Perturbation Theory: Expansions In The Mass Of The Strange Quark," Nucl. Phys. B **250**, 465 (1985).

[GL88] P. Gerber and H. Leutwyler, "Hadrons Below the Chiral Phase Transition," Nucl. Phys. B **321** (1989) 387.

[GLS91] J. Gasser, H. Leutwyler and M. E. Sainio, "Form-factor of the sigma term," Phys. Lett. B **253**, 260 (1991).

[GOR68] M. Gell-Mann, R. J. Oakes and B. Renner, "Behavior of current divergences under SU(3) x SU(3)," Phys. Rev. **175** (1968) 2195.

[Gr64] O. W. Greenberg, "Spin And Unitary Spin Independence In A Paraquark Model Of Baryons And Mesons," Phys. Rev. Lett. **13** (1964) 598.

[GRW04] L. Girlanda, A. Rusetsky and W. Weise, "Chiral perturbation theory in a nuclear background," Annals Phys. **312** (2004) 92 [arXiv:hep-ph/0311128].

[GRW05] L. Girlanda, A. Rusetsky and W. Weise, "The π-nucleus optical potential to $\mathcal{O}(p^5)$ in Chiral Perturbation Theory," Nucl. Phys. A **755** (2005) 653.

[GSS88] J. Gasser, M. E. Sainio and A. Svarc, "Nucleons With Chiral Loops," Nucl. Phys. B **307**, 779 (1988).

[GSW62] J. Goldstone, A. Salam and S. Weinberg, "Broken Symmetries," Phys. Rev. **127** (1962) 965.

[HK85] T. Hatsuda and T. Kunihiro, "Critical Phenomena Associated With Chiral Symmetry Breaking And Restoration In QCD," Prog. Theor. Phys. **74**, 765 (1985).

[HZC02] M. Huang, P. Zhuang and W. Chao, "Meson effects on chiral condensate at finite density," Commun. Theor. Phys. **38**, 181 (2002).

[It00] K. Itahashi *et al.*, "Deeply Bound Pi- States In Pb-207 Formed In The Pb-208(D, He-3) Reaction Part II: Deduced Binding Energies And Widths And The Pion-Nucleus Interaction," Phys. Rev. C **62** (2000) 025202.

[Ja51] R. Jastrow, "On the Nucleon-Nucleon Interaction," Phys. Rev. 81, (1951) 165.

[Ji03] D. Jido, J. A. Oller, E. Oset, A. Ramos and U. G. Meissner, "Chiral dynamics of the two Lambda(1405) states," Nucl. Phys. A **725** (2003) 181 [arXiv:nucl-th/0303062].

[JM91] E. Jenkins and A. V. Manohar, "Baryon chiral perturbation theory using a heavy fermion Lagrangian," Phys. Lett. B **255**, 558 (1991).

[JMi91] H. Jung and G. A. Miller, "Nucleon selfenergy in relativistic nuclear matter with pion ring series," Phys. Rev. C **43** (1991) 1958.

[Ka00] N. Kaiser, "Chiral 3π exchange NN potentials: Results for representation-invariant classes of diagrams," Phys. Rev. C **61** (2000) 014003 [arXiv:nucl-th/9910044].
N. Kaiser, "Chiral 3π exchange NN potentials: Results for diagrams proportional to $g(A)^4$ and $g(A)^6$," Phys. Rev. C **62** (2000) 024001 [arXiv:nucl-th/9912054].
N. Kaiser, "Chiral 3π-exchange NN potentials: Results for dominant next-to-leading order contributions," Phys. Rev. C **63** (2001) 044010 [arXiv:nucl-th/0101052].
N. Kaiser, "Chiral 2π exchange NN potentials: Two-loop contributions," Phys. Rev. C **64** (2001) 057001 [arXiv:nucl-th/0107064].

N. Kaiser, "Chiral 2π-exchange NN potentials: Relativistic $1/M^2$-corrections," Phys. Rev. C **65** (2002) 017001 [arXiv:nucl-th/0109071].

[Ka06] N. Kaiser, "Twice-iterated boson exchange scattering amplitudes," Phys. Rev. C **74** (2006) 014002 [arXiv:nucl-th/0606016].

[KBW97] N. Kaiser, R. Brockmann and W. Weise, "Peripheral nucleon nucleon phase shifts and chiral symmetry," Nucl. Phys. A **625** (1997) 758 [arXiv:nucl-th/9706045].

[KEM07] H. Krebs, E. Epelbaum and U.-G. Meißner, "Nuclear forces with Delta-excitations up to next-to-next-to-leading order I: peripheral nucleon-nucleon waves," Eur. Phys. J. A **32** (2007) 127 [arXiv:nucl-th/0703087].

[KEM08] E. Epelbaum, H. Krebs and U.-G. Meißner, "Delta-excitations and the three-nucleon force," Nucl. Phys. A **806** (2008) 65 [arXiv:nucl-th/0712.1969].

[KFW02] N. Kaiser, S. Fritsch and W. Weise, "Chiral dynamics and nuclear matter," Nucl. Phys. A **697** (2002) 255 [arXiv:nucl-th/0105057].

[KFW03] N. Kaiser, S. Fritsch and W. Weise, "Nuclear energy density functional from chiral pion nucleon dynamics," Nucl. Phys. A **724** (2003) 47 [arXiv:nucl-th/0212049].

[KFW05] N. Kaiser, S. Fritsch and W. Weise, "Chiral approach to nuclear matter: Role of two-pion exchange with virtual Delta-isobar excitation," Nucl. Phys. A **750** (2005) 259 [arXiv:nucl-th/0406038].

[KHW08] N. Kaiser, P. de Homont and W. Weise, "In-medium chiral condensate beyond linear density approximation," Phys. Rev. C **77** (2008) 025204 [arXiv:nucl-th/0711.3154].

[Ki02] H. c. Kim, "In-medium pion weak decay constants," Phys. Rev. C **65** (2002) 055201 [arXiv:hep-ph/0105085].

[KKW03] E. E. Kolomeitsev, N. Kaiser and W. Weise, "Chiral dynamics of deeply bound pionic atoms," Phys. Rev. Lett. **90** (2003) 092501 [arXiv:nucl-th/0207090].

[KM01] B. Kubis and U.-G. Meißner, "Baryon form factors in chiral perturbation theory," Eur. Phys. J. C **18** (2001) 747 [arXiv:hep-ph/0010283].

[KMW07] N. Kaiser, M. Muhlbauer and W. Weise, "Scales in nuclear matter: Chiral dynamics with pion nucleon form factors," Eur. Phys. J. A **31** (2007) 53 [arXiv:nucl-th/0610060].

[KN86] D. B. Kaplan and A. E. Nelson, "Strange Goings on in Dense Nucleonic Matter," Phys. Lett. B **175** (1986) 57.

[KN88] D. B. Kaplan and A. E. Nelson, "Kaon Condensation In Dense Matter," Nucl. Phys. A **479** (1988) 273.

[Ko82] R. Koch, "A New Determination Of The πN Sigma Term Using Hyperbolic Dispersion Relations In The (ν^2, T) Plane," Z. Phys. C **15** (1982) 161.

[Ko99] U. van Kolck, "Effective field theory of nuclear forces," Prog. Part. Nucl. Phys. **43** (1999) 337 [arXiv:nucl-th/9902015].

[KOV06] M. M. Kaskulov, E. Oset and M. J. Vicente Vacas, "Two pion mediated scalar isoscalar N N interaction in the nuclear medium," Phys. Rev. C **73** (2006) 014004 [arXiv:nucl-th/0506031].

[KR93] M. Kirchbach and D. O. Riska, "The Effective induced pseudoscalar coupling constant," Nucl. Phys. A **578** (1994) 511.

[KSW98a] D. B. Kaplan, M. J. Savage and M. B. Wise, "Two-nucleon systems from effective field theory," Nucl. Phys. B **534** (1998) 329 [arXiv:nucl-th/9802075].

[KSW98b] D. B. Kaplan, M. J. Savage and M. B. Wise, "A new expansion for nucleon nucleon interactions," Phys. Lett. B **424** (1998) 390 [arXiv:nucl-th/9801034].

[KW96] M. Kirchbach and A. Wirzba, "Deriving the quark condensate within a finite Fermi system from the generating functional of chiral perturbation theory," Nucl. Phys. A **604** (1996) 395 [arXiv:nucl-th/9603017].

[KW97] M. Kirchbach and A. Wirzba, "In-medium chiral perturbation theory and pion weak decay in the presence of background matter," Nucl. Phys. A **616** (1997) 648 [arXiv:hep-ph/9701237].

[KW01] N. Kaiser and W. Weise, "Systematic calculation of s-wave pion and kaon self-energies in asymmetric nuclear matter," Phys. Lett. B **512** (2001) 283 [arXiv:nucl-th/0102062].

[KW09] N. Kaiser and W. Weise, "Chiral condensate in neutron matter," Phys. Lett. B **671** (2009) 25 [arXiv:nucl-th/0808.0856.

[La59] L. D. Landau, "On analytic properties of vertex parts in quantum field theory," Nucl. Phys. **13** (1959) 181.

[La07] A. Lacour, "Chiral analysis of hyperon decay vector form factors," Diploma thesis, University of Bonn (2007), HISKP-TH-07/02.

[Le94] H. Leutwyler, "Nonrelativistic effective Lagrangians," Phys. Rev. D **49** (1994) 3033 [arXiv:hep-ph/9311264].

[LFA00] M. Lutz, B. Friman and C. Appel, "Saturation from nuclear pion dynamics," Phys. Lett. B **474** (2000) 7 [arXiv:nucl-th/9907078].

[LKM07] A. Lacour, B. Kubis and U.-G. Meißner, "Hyperon decay form factors in chiral perturbation theory," JHEP **0710** (2007) 083 [arXiv:hep-ph/0708.3957].

[LOMa] J. A. Oller, A. Lacour and U.-G. Meißner, "Chiral Effective Field Theory for Nuclear Matter with long- and short-range Multi-Nucleon Interactions," J. Phys. G **37** (2010) 015106 [arXiv:nucl-th/0902.1986].

[LOMb] A. Lacour, J. A. Oller and U.-G. Meißner, "Non-perturbative methods for a chiral effective field theory of finite density nuclear systems," Annals of Physics (2010), in press [arXiv:nucl-th/0906.2349].

[LOMc] A. Lacour, J. A. Oller and U.-G. Meißner, "Chiral effective field theory for nuclear matter including long- and short-range multi-nucleon interactions," EPJ Web Conf. **3** (2010) 06003.

[LOMd] A. Lacour, J. A. Oller and U.-G. Meißner, "The chiral quark condensate and pion decay constant in nuclear matter at next-to-leading order," [arXiv:nucl-th/1007.2574].

[LOMe] A. Lacour, U.-G. Meißner and J. A. Oller, "Chiral effective field theory for nuclear matter," Proceedings of the Chiral10 Workshop, Valencia, Spain, 21 - 24 June 2010. [arXiv:nucl-th/1009.2957].

[Ma58] S. Mandelstam, "Determination Of The Pion - Nucleon Scattering Amplitude From Dispersion Relations And Unitarity. General Theory," Phys. Rev. **112** (1958) 1344.

[Ma96] A. V. Manohar, "Effective field theories," arXiv:hep-ph/9606222.

[Ma01] R. Machleidt, "The high-precision, charge-dependent Bonn nucleon-nucleon potential (CD-Bonn)," Phys. Rev. C **63** (2001) 024001 [arXiv:nucl-th/0006014].

[MBKM09] M. Mai, P. C. Bruns, B. Kubis and U.-G. Meißner, "Aspects of meson-baryon scattering in three- and two-flavor chiral perturbation theory," Phys. Rev. D **80** (2009) 094006 [arXiv:0905.2810 [hep-ph]].

[MS01] R. Machleidt and I. Slaus, "The nucleon nucleon interaction," J. Phys. G **27** (2001) R69 [arXiv:nucl-th/0101056].

[Me93] U.-G. Meißner, "Recent developments in chiral perturbation theory," Rept. Prog. Phys. **56** (1993) 903 [arXiv:hep-ph/9302247].

[Mi71] A. B. Migdal, "Stability of vacuum and limiting fields," Zh. Eksp. Teor. Fiz. **61** (1971) 2209.

[Mi78] A. B. Migdal, "Pion Fields In Nuclear Matter," Rev. Mod. Phys. **50** (1978) 107.

[MLEA10] R. Machleidt, P. Liu, D. R. Entem and E. R. Arriola, "Renormalization of the leading-order chiral nucleon-nucleon interaction and bulk properties of nuclear matter," Phys. Rev. C **81** (2010) 024001 [arXiv:nucl-th/0910.3942].

[MNRS04] S. Mallik, A. Nyffeler, M. C. M. Rentmeester and S. Sarkar, "On the nucleon self-energy in nuclear matter," Eur. Phys. J. A **22** (2004) 371 [arXiv:nucl-th/0407038].

[MOW02] U.-G. Meißner, J. A. Oller and A. Wirzba, "In-medium chiral perturbation theory beyond the mean-field approximation," Annals Phys. **297** (2002) 27 [arXiv:nucl-th/0109026].

[MRR92] T. Mannel, W. Roberts and Z. Ryzak, "A Derivation of the heavy quark effective Lagrangian from QCD," Nucl. Phys. B **368** (1992) 204.

[MRR06] U.-G. Meißner, U. Raha and A. Rusetsky, "Isospin-breaking corrections in the pion deuteron scattering length," Phys. Lett. B **639** (2006) 478 [arXiv:nucl-th/0512035].

[MS70] A. D. Martin and T. D. Spearman, "Elementary Particle Theory", North-Holland Publishing Company, Amsterdam. 1970.

[MSW83] J. A. McNeil, J. R. Shepard and S. J. Wallace, "Impulse Approximation Dirac Optical Potential," Phys. Rev. Lett. **50** (1983) 1439;

[Na60a] Y. Nambu, "Quasi-particles and gauge invariance in the theory of superconductivity," Phys. Rev. **117** (1960) 648.

[Na60b] Y. Nambu, "Axial vector current conservation in weak interactions," Phys. Rev. Lett. **4** (1960) 380.

[Na07] P. Navratil, V. G. Gueorguiev, J. P. Vary, W. E. Ormand and A. Nogga, "Structure of A=10-13 nuclei with two- plus three-nucleon interactions from chiral effective field theory," Phys. Rev. Lett. **99** (2007) 042501 [arXiv:nucl-th/0701038].

[NNO] NN-Online program, M. C. M. Rentmeester *et al.*, http://nn-online.org/

[NOG93] J. Nieves, E. Oset and C. Garcia-Recio, "A Theoretical approach to pionic atoms and the problem of anomalies," Nucl. Phys. A **554** (1993) 509.

[NTK05] A. Nogga, R. G. E. Timmermans and U. van Kolck, "Renormalization of One-Pion Exchange and Power Counting," Phys. Rev. C **72** (2005) 054006 [arXiv:nucl-th/0506005].

[OGN95] E. Oset, C. Garcia-Recio and J. Nieves, "Pion cloud contribution to the S-wave repulsion in pionic atoms," Nucl. Phys. A **584** (1995) 653.

[Ol00] J. A. Oller, "The Case of a WW dynamical scalar resonance within a chiral effective description of the strongly interacting Higgs sector," Phys. Lett. B **477** (2000) 187 [arXiv:hep-ph/9908493].

[Ol02] J. A. Oller, "Chiral Lagrangians at finite density," Phys. Rev. C **65** (2002) 025204 [arXiv:hep-ph/0101204].

[Ol03] J. A. Oller, "Nucleon nucleon interactions from effective field theory," Nucl. Phys. A **725** (2003) 85.

[Ol06] J. A. Oller, "On the strangeness -1 S-wave meson baryon scattering," Eur. Phys. J. A **28** (2006) 63 [arXiv:hep-ph/0603134].

[OM01] J. A. Oller and U.-G. Meißner, "Chiral dynamics in the presence of bound states: Kaon nucleon interactions revisited," Phys. Lett. B **500** (2001) 263 [arXiv:hep-ph/0011146].

[OO97] J. A. Oller and E. Oset, "Chiral Symmetry Amplitudes in the S-Wave Isoscalar and Isovector Channels and the σ, $f_0(980)$, $a_0(980)$ Scalar Mesons," Nucl. Phys. A **620** (1997) 438 [Erratum-ibid. A **652** (1999) 407] [arXiv:hep-ph/9702314].

[OO99] J. A. Oller and E. Oset, "N/D Description of Two Meson Amplitudes and Chiral Symmetry," Phys. Rev. D **60** (1999) 074023 [arXiv:hep-ph/9809337].

[OOR00] J. A. Oller, E. Oset and A. Ramos, "Chiral unitary approach to meson meson and meson baryon interactions and nuclear applications," Prog. Part. Nucl. Phys. **45** (2000) 157 [arXiv:hep-ph/0002193].

[OPV05] J. A. Oller, J. Prades and M. Verbeni, "Surprises in threshold antikaon nucleon physics," Phys. Rev. Lett. **95** (2005) 172502 [Erratum-ibid. **96** (2006) 199202]; [arXiv:hep-ph/0508081].

[OR98] E. Oset and A. Ramos, "Non perturbative chiral approach to s-wave anti-K N interactions," Nucl. Phys. A **635** (1998) 99 [arXiv:nucl-th/9711022].

[ORK96] C. Ordonez, L. Ray and U. van Kolck, "The Two-Nucleon Potential from Chiral Lagrangians," Phys. Rev. C **53** (1996) 2086 [arXiv:hep-ph/9511380].

[OFT86] E. Oset, Y. Futami and H. Toki, "Pion absorption in the resonance region," Nucl. Phys. A **448** (1986) 597.

[OTW82] E. Oset, H. Toki and W. Weise, "Pionic modes of excitation in nuclei," Phys. Rept. **83** (1982) 281.

[PDG06] W. M. Yao *et al.* [Particle Data Group], "Review of particle physics," J. Phys. G **33** (2006) 1.

[PDG08] C. Amsler *et al.* [Particle Data Group], "Review of particle physics," Phys. Lett. B **667**, (2008) 1.

[PF07] O. Plohl and C. Fuchs, "Nuclear matter in the chiral limit and the in-medium chiral condensate," Nucl. Phys. A **798** (2008) 75 [arXiv:0710.3700 [nucl-th]].

[PFF06] O. Plohl, C. Fuchs and A. Faessler, "Model independent study of the nucleon self-energy in matter," arXiv:nucl-th/0603070.

[PT96] R. D. Pisarski and M. Tytgat, "Propagation of Cool Pions," Phys. Rev. D **54** (1996) 2989 [arXiv:hep-ph/9604404].

[Pi97] R. D. Pisarski and M. Tytgat, "Scattering of soft, cool pions," Phys. Rev. Lett. **78** (1997) 3622 [arXiv:hep-ph/9611206].

[PJM02] T. S. Park, H. Jung and D. P. Min, "In-medium effective pion mass from heavy-baryon chiral perturbation theory," J. Korean Phys. Soc. **41** (2002) 195 [arXiv:nucl-th/0101064].

[PR04] M. Pavon Valderrama and E. Ruiz Arriola, "Renormalization of NN-Scattering with One Pion Exchange and Boundary Conditions," Phys. Rev. C **70** (2004) 044006 [arXiv:nucl-th/0405057].

[PSWA02] M. M. Pavan, I. I. Strakovsky, R. L. Workman and R. A. Arndt, "The pion nucleon Sigma term is definitely large: Results from a GWU analysis of pi N scattering data," PiN Newslett. **16**, 110 (2002) [arXiv:hep-ph/0111066].

[PW79] V. R. Pandharipande and R. B. Wiringa, "Variations on a theme of nuclear matter," Rev. Mod. Phys. **51** (1979) 821.

[RD87] H. Reinhardt and B. V. Dang, "Restoration of chiral symmetry at finite temperature and baryon density in the Nambu-Jona-Lasinio model," J. Phys. G **13**, 1179 (1987).

[RDP89] A. Ramos, W. H. Dickhoff and A. Polls, "Hole-hole propagation and saturation," Phys. Lett. B **219** (1989) 15;

[RPD89] A. Ramos, A. Polls and W. H. Dickhoff, "Single-particle properties and short-range correlations in nuclear matter," Nucl. Phys. A **503** (1989) 1.

[Ro89] R. Rockmore, "Chiral repulsion in the pion nucleus optical potential," Phys. Rev. C **40** (1989) 13.

[Ro95] M. E. Rose, "Elementary Theory of Angular Momentum", New York, Dover, 1995.

[Sa72] R. F. Sawyer, "Condensed pi^- phase in neutron star matter," Phys. Rev. Lett. **29** (1972) 382.

[Sc72] D. J. Scalapino, "π^- condensate in dense nuclear matter," Phys. Rev. Lett. **29** (1972) 386.

[Se92] B. D. Serot, "Quantum hadrodynamics," Rept. Prog. Phys. **55**, 1855 (1992).

[SKEM08] P. Saviankou, S. Krewald, E. Epelbaum and U.-G. Meißner, "Saturation of nuclear matter in effective field theory," arXiv:nucl-th/0802.3782.

[SKRS93] V. G. J. Stoks, R. A. M. Kompl, M. C. M. Rentmeester and J. J. de Swart, "Partial wave analysis of all nucleon-nucleon scattering data below 350-MeV," Phys. Rev. C **48** (1993) 792.

[SKTS94] V. G. J. Stoks, R. A. M. Klomp, C. P. F. Terheggen and J. J. de Swart, "Construction of high quality N N potential models," Phys. Rev. C **49** (1994) 2950.

[St00] H. Stöcker, "Taschenbuch der Physik". Verlag Harri Deutsch, Thun und Frankfurt am Main, 2000. ISBN 3-8171-1627-6.

[ST08] J. Soto and J. Tarrus, "Effective Field Theory With Dibaryon Degrees Of Freedom," Phys. Rev. C **78** (2008) 024003 [arXiv:nucl-th/0712.3404].

[Su04] K. Suzuki *et al.*, "Precision spectroscopy of pionic 1s states of Sn nuclei and evidence for partial restoration of chiral symmetry in the nuclear medium," Phys. Rev. Lett. **92** (2004) 072302 [arXiv:nucl-ex/0211023].

[SW86] B. D. Serot and J. D. Walecka, "The Relativistic Nuclear Many Body Problem," Adv. Nucl. Phys. **16** (1986) 1.

[SW00] B. D. Serot and J. D. Walecka, "Effective field theory in nuclear many-body physics," arXiv:nucl-th/0010031.

[tHo76] G. 't Hooft, "Symmetry breaking through Bell-Jackiw anomalies," Phys. Rev. Lett. **37** (1976) 8.

[TPRM98] A. Trasobares, A. Polls, A. Ramos and H. Muther, "On the Dirac structure of the nucleon selfenergy in nuclear matter," Nucl. Phys. A **640** (1998) 471 [arXiv:nucl-th/9703020].

[TSTV07] K. Tsushima, K. Saito, A. W. Thomas and A. Valcarce, "Nucleon sigma term and quark condensate in nuclear matter," Eur. Phys. J. A **31** (2007) 626 [arXiv:nucl-th/0608062].

[TW95] V. Thorsson and A. Wirzba, "S-wave Meson-Nucleon Interactions and the Meson Mass in Nuclear Matter from Chiral Effective Lagrangians," Nucl. Phys. A **589** (1995) 633 [arXiv:nucl-th/9502003].

[Vr97] D. Vretenar, G. A. Lalazissis, R. Behnsch, W. Pöschl, P. Ring, "Monopole giant resonances and nuclear compressibility in relativistic mean field theory," Nucl. Phys. A **621** (1997) 853.

[Wa74] J. D. Walecka, "A Theory of highly condensed matter," Annals Phys. **83** (1974) 491.

[We35] C. F. V. Weizsäcker, "Zur Theorie Der Kernmassen," Z. Phys. **96** (1935) 431.

[We79] S. Weinberg, "Phenomenological Lagrangians," Physica A **96**, 327 (1979).

[We90] S. Weinberg, "Nuclear forces from chiral Lagrangians," Phys. Lett. B **251** (1990) 288.

[We91] S. Weinberg, "Effective Chiral Lagrangians For Nucleon - Pion Interactions And Nuclear Forces," Nucl. Phys. B **363** (1991) 3.

[Wey90] H. J. Weyer, "Pion absorption in light nuclei," Phys. Rept. **195** (1990) 295.

[WSS95] R. B. Wiringa, V. G. J. Stoks and R. Schiavilla, "An Accurate nucleon-nucleon potential with charge independence breaking," Phys. Rev. C **51** (1995) 38 [arXiv:nucl-th/9408016].

[WT95] A. Wirzba and V. Thorsson, "In-Medium Effective Chiral Lagrangians And The Pion Mass In Nuclear Matter," Hirschegg '95: Dynamical Properties of Hadrons in Nuclear Matter, pp. 31-43, GSI-print, Darmstadt, 1995; arXiv:hep-ph/9502314.